Production, purification and characterization of siderophores from marine bacteria and their application in heavy metal chelation and silver nano particles synthesis

THESIS

Submitted in the partial fulfilment of the requirements

for the award of the degree of

DOCTOR OF PHILOSOPHY

in

Biotechnology

by

SARVEPALLI MOUNIKA

(Reg. No. 717157)

Under the Guidance of

Dr. NARASIMHULU K

DEPARTMENT OF BIOTECHNOLOGY

NATIONAL INSTITUTE OF TECHNOLOGY

WARANGAL-506 004, TELANGANA, INDIA

December - 2023

NATIONAL INSTITUTE OF TECHNOLOGY
WARANGAL
DEPARTMENT OF BIOTECHNOLOGY

CERTIFICATE

This is to certify that the thesis entitled **"Production, purification and characterization of siderophores from marine bacteria and their application in heavy metal chelation and silver nano particles synthesis"** isbeing submitted by **Ms. Sarvepalli Mounika** (Reg. No. 717157) in partial fulfilment for the award of the degree of Doctor of Philosophy (**Ph.D.**) in the Department of Biotechnology, National Institute of Technology, Warangal, is a record of bonafide work carried out by him under my guidance and supervision. The results embodied in this thesis have not beensubmitted to any other Universities or Institutes for the award of any degree or diploma.

Dr. Narasimhulu K

(Supervisor)

Professor
Department of Biotechnology

NATIONAL INSTITUTE OF TECHNOLOGY
WARANGAL
DEPARTMENT OF BIOTECHNOLOGY

DECLARATION

This is to certify that the work presented in the thesis entitled **"Production, purification and characterization of siderophores from marine bacteria and their application in heavy metal chelation and silver nano particles synthesis"**, is a bonafide work done by me under the supervision of **Dr. Narasimhulu K** and was not submitted elsewhere for the award of any degree.

I declare that this written submission represents my idea in my own words and where other's ideas or words have been included, I have adequately cited and referenced the sources. I also declare that I have adhered to all principles of academic honesty and integrity and have not misinterpreted or fabricated or falsified any idea/data/fact/source in my submission. I understand that any violation of the above will be a cause for disciplinary action by the Institute and can also evoke penal action from the sources which have thus not been properly cited or from whom proper permission has not taken when needed.

Date: 29.12.2023

Place: Warangal

S. Mounika

(Sarvepalli Mounika)

Ph.D. Scholar
Reg. No. 717157

ACKNOWLEDGMENTS

I would like to express my deepest gratitude to my supervisor **Dr. Narasimhulu K** (Professor, Department of Biotechnology) and Doctoral scrutiny committee: **Dr. Sreenivasa Rao P**, (Professor, Department of Biotechnology), **Dr. Rama Raju B** (Associate Professor, Department of Biotechnology) and **Dr. Srinath S** (Professor, Department of Chemical Engineering) National Institute of Technology, Warangal for their insightful comments and encouragement.

I sincerely thank, **Prof. Bidyadhar Subudhi**, Director, National Institute of Technology, Warangal and other authorities who gave me this opportunity to carry out my research work.

I wish to extend my heartfelt thanks to **Dr. Prakash Saudagar**, Head and Professor, Department of Biotechnology for providing infrastructure facilities required for my study.

I would like to extend my thanks to all the **faculty members** and **research scholars** in the **Department of Biotechnology** who has directly or indirectly helped me during my work. I also acknowledge all the **supporting and technical staff** of the **Department of Biotechnology,** for providing research environment and necessary facilities when required.

Sarvepalli Mounika

CONTENTS

ABSTRACT

Iron (Fe) is one of the most essential micronutrients for all the existing life systems. However, at biological pH, Fe gets oxidized to insoluble oxyhydroxide polymers. In low Fe conditions, microbes secrete specialized molecules called Siderophores, which are high affinity and low molecular weight chelating agents that increase iron availability for microbial usage. In marine water, the concentration of Fe is as low as nanomolar. Very little light has been shed on marine bacterial siderophores compared to terrestrial ones. In this study, marine bacteria were isolated from different locations in the Bay of Bengal in Visakhapatnam, India. All the isolates were screened for siderophore production using CAS (Chrome Azurol S) assay, and the most efficient four isolates were selected for further work. 16S rRNA molecular characterization of isolates showed the nearest similarity of SMI_1 with *Bacillus taeanensis,* AABM_9 with *Enterobacter* sp., SVU_3 with *Marinobacter sp*. SVU_3 and AMPPS_5 with *Pseudomonas mendocina*. The production parameters of the succinate medium were optimized to enhance the siderophore production. The optimum production of siderophores for SMI_1 was *93.57 %SU* (Siderophore Units) (after 48 h of incubation at 30 °C, pH 8, sucrose as carbon source, sodium nitrate as nitrogen source, 0.4% of succinic acid) and for AABM_9 was *87.18 %SU* (after 36 h of incubation period at 30 °C and pH 8 in the presence of sucrose, ammonium sulfate and 0.4% succinic acid). The maximum production of siderophores for SVU_3 was *83.15 %SU* (after 48 h of incubation at 35 °C and pH 8.5 in the presence of glucose, sodium nitrate and 0.6 % succinic acid) and for AMPPS_5 was *91.17 %SU* (after 36 h of incubation at 35 °C, pH 8.5, glucose as carbon source, ammonium sulfate as nitrogen source, and 0.4% of citric acid). Effects of Copper, Manganese and Zinc metal ions on siderophore production were studied. The siderophore was separated using an Amberlite XAD-2 column followed by Sephadex LH-20. The

fractions were concentrated by rotary evaporation and lyophilized, purified by Thin-layer chromatography solvent system n-butanol:acetic acid:dH2O (12:3:5). Wine-coloured spots confirmed presence of hydroxamate type of siderophore on spraying 0.1 M $FeCl_3$ solution. The λmax was observed at 421 nm on UV- spectral analysis which reflects the trihydroxamate siderophores. The chemical nature was identified by Fourier Transformation Infrared analysis (FTIR), Liquid Chromatography – Mass Spectroscopy (LC-MS) and Nuclear Magnetic Resonance (NMR) spectroscopy. The siderophore was identified at R_T 3.95 min on using acetonitrile and water as mobile phase and identified mass of siderophore $[M+H]^+$ m/z 561.3. The heavy metal chelation of siderophore-producing marine bacterial isolates was investigated on Ag^{+2}, Al^{+2}, Cd^{+2}, Co^{+2}, Cr^{+6}, Hg^{+2}, La^{+3}, Mo^{+6}, Ni^{+2}, Pb^{+2}, Pd^{+2}, and Y^{+3} metal ions (1mM, 5mM) by spotting method. All four isolates showed chelation activity on heavy metals except Ag^{+2}, Cd^{+2} and Mo^{+6} due to species-specific trait. Seed germination studies were performed on seeds Brown chickpea (*Cicer arietinum* L.), Peanut (*Arachis hypogaea*), Green gram (*Vigna radiata*), and Kabul chana (*Cicer arietinum*) using siderophore supernatant. As the siderophores have multiple advantages, the siderophore-based silver nanoparticles (AgNP's) were synthesized and characterized for their optical, physicochemical, crystalline, and elemental composition properties. The antimicrobial activity of these nanoparticles against gram positive-bacteria *Escherichia coli, Klebsiella pneumoniae*, *Pseudomonas aeruginosa* and gram-negative bacteria *Bacillus subtilis*, Coagulase-negative *Staphylococci*, *Staphylococcus aureus* was reported in this study. In summary, four siderophore producing marine bacteria was isolated and characterized. The significant process parameters were optimized for maximum siderophore production and purified using high-throughput techniques. Marine bacterial isolates were screened for chelation activity on different heavy metals at 1mM and 5mM concentration as well as seed

germination potential also investigated. The as-synthesized siderophore AgNP's were characterized and anti-bacterial activity was explored.

Keywords: Heavy metal chelation, Marine bacteria, Nanoparticles, Optimization, Purification, Siderophores.

List of Symbols and Abbreviations

°C	degree Celsius
%SU	Siderophore units
%GP	Germination percentage
µl	Microlitre
µm	Micrometre
µM	Micromolar
ACN	Acetonitrile
Ag	Silver
$AgNO_3$	Silver nitrate
AgNPs	Silver nanoparticles
A. hypogaea	*Arachis hypogaea*
ANOVA	Analysis of variance
a.u.	Absorbance units
Bio-AgNPs	Biological silver nanoparticles
BLAST	Basic local alignment search tool
B. subtilis	*Bacillus subtilis*
B. taeanensis	*Bacillus taeanensis*
C. arietinum	*Cicer arietinum*
CAS	Chrome azurol sulphate
CCD	Central composite design
Che-AgNPs	Chemical silver nanoparticles
CoNS	Coagulase-negative *Staphylococci*
Da	Daltons
DFO	Desferrioxamine
DH_2O	Sterile double distilled water
DNA	Deoxyribonucleic acid
E. coli	*Escherichia coli*
EDX	Energy dispersive X-ray spectroscopy

E. hormaechei	*Enterobacter hormaechei*
ESI	Electrospray ionization
Fe	Iron
Fe^{+2}	Ferric
Fe^{+3}	Ferrous
FTIR	Fourier Transform Infrared spectroscopy
FWHM	Full width at half-maximum
HDTMA	Hexadecyl trimethylammonium bromide
HPLC	High performance liquid chromatography
HRMS	High resolution mass spectrometry
ID	Internal diameter
K. pneumoniae	*Klebsiella pneumoniae*
LC	Liquid chromatography
M	Molar
mg/ml	Milligram per millilitre
M. hydrocarbonoclausticus	*Marinobacter hydrocarbonoclausticus*
mm	Millimetre
mM	Millimolar
MS	Mass spectrophotometry
N	Normal
NCBI	National centre for biotechnology information
NJ	Neighbor-Joining
NMR	Nuclear magnetic resonance
NPs	Nanoparticles
NaOH	Sodium hydroxide
nm	Nanometre
OD	Optical density
OFAT	One factor at a time
P. aeruginosa	*Pseudomonas aeruginosa*
PDI	Polydispersity index
pH	Potential of hydrogen
PSA	Particle size analyser
P. mendocina	*Pseudomonas mendocina*
PSD	Particle size distribution

PVD	Pyoverdin
PVDF	Polyvinylidene fluoride
P. vulgaris	*Proteus vulgaris*
RP-HPLC	Reverse phase-high performance liquid chromatography
rRNA	Ribosomal ribonucleic acid
RNA	Ribonucleic acid
rpm	Rotations per minute
RSM	Response surface methodology
S. aureus	*Staphylococcus aureus*
SEM	Scanning electron microscope
SPR	Surface Plasmon Resonance
TFA	Trifluoroacetic acid
TOF	Time of flight
USD	United States Dollar
UV-Vis spec	Ultraviolet-Visible spectrophotometer
V/V	Volume/volume
V. radiata	*Vigna radiata*
Wt.%	Weight percentage
w/v	Weight by volume
XRD	X-ray diffraction
ZOI	Zone of inhibition
ZMA	Zobell marine agar 2216
ZP	Zeta potential

List of Figures

List of Tables

List of Equations

Eq. 3.1 ***050***

$$\% \text{ SU (siderophore units)} = \left(\frac{A_r - A_s}{Ar}\right) \times 100$$

Where, *"A_r"* is the reference absorbance and *"A_s"* is the sample absorbance at 630 nm.

Eq. 3.2 ***052***

$$\boldsymbol{Yi} = \beta 0 + \sum \beta i Xi + \sum \beta ii Xi^2 + \sum \beta ij Xi Xj$$

Where, Yi = predicted response, XiXj=independent variables which effect the dependent variable Yi, β0 = offset term, βi = i^{th} linear variable, βii = quadratic coefficient and βij = ij^{th} interaction coefficient.

Eq. 3.3 ***057***

$$Germination\ Percentage\ (\%GP) = \left(\frac{Seeds\ germinated}{Total\ number\ of\ seeds}\right) x\ 100$$

Eq. 3.4 ***058***

$$D\ (nm) = \frac{k\lambda}{\beta cos\theta}$$

Where, 'D' is the size of the crystallite in nm; 'k' is the shape factor of the AgNPs, which is 0.94; 'λ' is the X-ray wavelength of Cu Kα, which is 0.154 nm; 'β' is the FWMH measured in radians and 'θ' is the Bragg angle of the peaks measured in radians.

Eq. 4.1 ***088***

$$Y = +93.83 + 1.06\ (A) + 2.03\ (B) + 2.85\ (C) - 0.4987\ (AB) - 1.36\ (AC) + 0.8138\ (BC) - 4.05\ (A)^2 - 8.05\ (B)^2 - 3.41\ (C)^2$$

Where, Y = Siderophore units (%SU), A = Sucrose, B = Initial pH, and C = Succinic acid.

Chapter I:
INTRODUCTION

INTRODUCTION

1.1. Importance of iron in living ecosystem

Among the micronutrients, iron (Fe) as a metal ion, is a much needed trace element which is irreplaceable because of its role in several fundamental biochemical processes associated with the development and growth of all the living organisms (microbes, animals and plants) [1]. Compared to other metal ions, Fe has a unique redox chemistry and coordination [1]. In virtue of its oxidative states (ferric (Fe^{+2}) and ferrous (Fe^{+3})), Fe is a part of various biochemical systems such as transcriptional regulation, chemical transitions, providing protection against reactive oxygen species, as a cofactor in DNA synthesis, electron transport chain, biocatalysis, biosynthetic, biodegradation, and cellular respiration pathways [1–4].

At acidic pH (pH<7), Fe^{+2} is the most prevalent species in anaerobic conditions, whereas it is comparatively more soluble and accessible to living organisms in aerobic conditions, however, in the aerobic conditions it is easily oxidized into Fe^{+3}, which subsequently precipitates [5]. On the other hand, at physiological pH (7.0-7.4), Fe^{+3} (10^{-18} M) is predominantly seen but it is not readily accessible in the absence of a chelating agent [6]. Thus Fe^{+3} is considered as a primary growth limiting factor for the majority of the living organisms at physiological pH [4,7,8].

At pH ~8, in oxygenated seawater inorganic dissolved iron is most thermodynamically stable by forming Fe^{+3}-hydroxide complexes, which in turn reduces the iron (10^{-36} M) bioavailability [8,9]. Additionally, Fe^{+3}-hydroxide complexes are present in equilibrium with Fe^{+3}-oxyhydroxide complexes, which are considered to be poorly soluble. However, Fe^{+3}-hydroxide complexes have the propensity to be scavenged by sinking particulate matter [9]. In comparison with their terrestrial counterparts, marine bacterial siderophores demonstrate

different characteristics [10,11]. In virtue of its unique chemical composition, dissolubility kinetics, low bioavailability, and low solubility makes iron absorption/uptake challenging [7].

1.2. Siderophores and their purpose

As a part of coping mechanisms, microbes have developed several unique strategies to absorb iron from the surrounding habitats; among them is the production and secretion of Fe^{+3}-chelating molecules, widely known as "siderophores" [6]. Siderophores are iron-scavenging low-molecular-weight ligand (secondary metabolites) molecules (500 - 1500 Da), endowed with and named after their specific and high affinity for Fe^{+3} (Kf >1030) [2,12,13]. Excreted siderophores can chelate even minute concentrations of Fe^{+3} from the habitat in order to facilitate uptake by microbes, thus preventing their precipitation and loss of its bioavailable forms [14]. In general, Fe^{+3} can be reversibly bound by siderophores thus their transport, uptake, reactivity, and bioavailability can be closely regulated [14,15].

During Fe^{+3}-deficient growth conditions, the hydrophobicity of microbial surface is greatly decreased leading to changes in the composition of surface proteins followed by limiting biofilm formation, which then ultimately results in microbial death [16]. Therefore, during the low bioavailability of Fe^{+3} in the surrounding habitat, siderophores are produced and secreted by the microbes, to this date it is one of the evolutionary coping mechanism developed by the microbes to survive in iron deficient habitat [16]. With the help of siderophores, microbes can uptake iron in the form of Fe^{+3}-siderophore complexes and then in the cytosol, iron is reduced and released as Fe^{+3} [3]. Fe^{+3} forms a hexadentate octahedral complex with the siderophores during their transportation inside the microbes [2]. Upon the disassociation of Fe^{+3}-siderophore complexes, siderophores are recycled and excreted again for Fe^{+3} acquisition [5].

Since siderophores can greatly increase the amount of dissolved Fe^{+3} by solubilizing the iron particulates (insoluble), this in turn will affect the bioavailability of iron in the environment thus shaping the composition and structure of the microbial ecosystem [17]. Additionally, this will greatly affect the bioavailability of Fe^{+3} to non-siderophore producing microbes, thus acting as a key regulator in the bioavailability of iron and other biogeochemical cycles [18]. The transportation of siderophores in bacteria represented in Figure1.1. Compared to terrestrial siderophores, most of the marine siderophores show unique structural properties [11]. In view of that, they show photochemical and amphipathic properties in Fe^{+3} complexes [16].

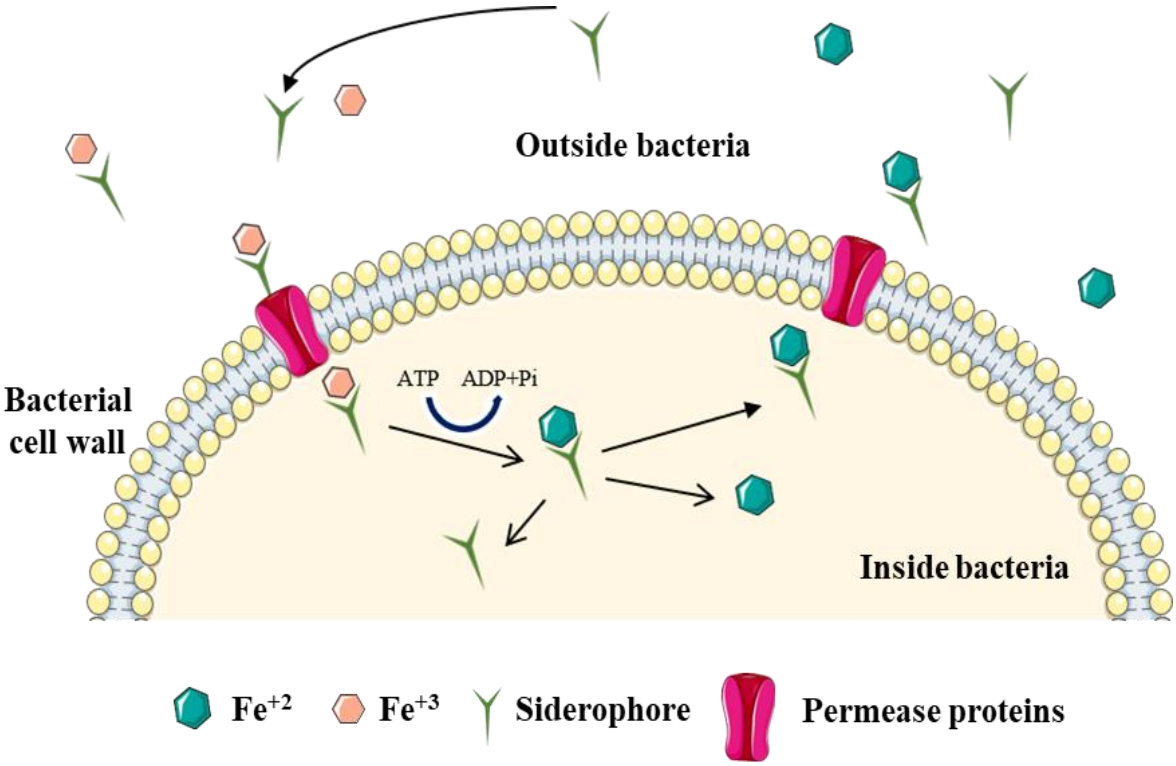

Figure 1.1: Schematic representation of transportation of Siderophore-Iron in Gram-Positive bacteria [19].

Depending on membrane affinity and length, siderophores could anchor a particular gradient outside the microbial membrane, thereby increasing the efficiency of siderophores in chelating Fe^{+3} from the environment [16]. On the other hand, Fe^{+3} acquisition is closely

regulated by the microbes, as occurrence of intracellular Fe^{+3} in excess amounts will result in oxidative stress leading to microbial death. In this regard, siderophores also act as key regulators in microbial iron homeostasis [8]. In comparison with other metal ions, Fe^{+3} is preferentially chelated by siderophores [16,20]. Siderophores can be further classified into: carboxylates, catecholates, hydroxamates, and mixed-types siderophores depending upon the primary oxygen-donating ligands which bind with Fe^{+3} [2].

1.3. Siderophores and their discovery

Initially, siderophores were identified as Growth factors i.e., myobactin, ferrichrome and coprogen in 1949 - 1952 [21–23]. Garibaldi and Neilands (1956) observed the mode of action of above growth factors and improved the production of Ferrichrome A by inoculating the siderophore producing organism in Fe^{+3} deficient media was reported. In 1960's, the Neiland's laboratory scientists formed a natural product group from ETH, Zurich and ciba, identified the ferrioxamines, ferrimycin and reported the structural explanation of desferrioxamine B. Emery and Neilands elucidated the structures of ferrichrome and ferrichrome A. Presently, more than 500 siderophores are known among them 270 are structurally characterized [25,26].

1.4. Types of siderophores

Based on (i) nature of backbone i.e., peptide or nonpeptide and open or close chain, (ii) nature of the chelating group, (iii) producing organism, and (iv) Depending on the oxygen ligands for Fe^{+3} coordination [27], siderophores can be classified into three main categories, namely, hydroxamates, catecholates, and α-Hydroxycarboxylates **(**Figure 1.2).

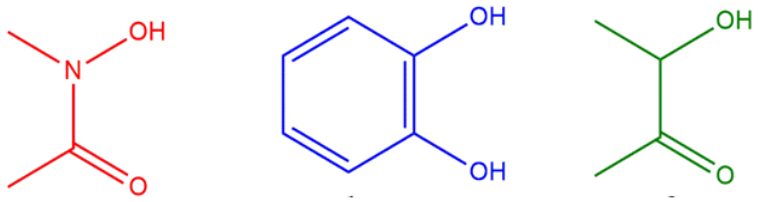

(a) (b) (c)

Figure 1.2: Chelating units of siderophore that form Fe^{+3} coordination complex [19].

1.4.1. Hydroxymates

Hydroxymate is commonly found in a group of siderophores an environment that consists of hydroxylated and acylated alkylamines includes N6-acyl-N6-Hydroxy lysine or N5acyl-N5-Hydroxy ornithine in bacteria. This type of siderophore contains C (=O) N-(OH) R, (R = an amino acid or a derivative of it). Marine bacteria were reported to produce suits of amphiphilic siderophores from different genera of bacteria but unique peptide head group to coordinate with Fe^{+3} are amphibactins and marinobactins [28]. *Vibrio* sp. R-10 produced amphibactins having long fatty acid appendages (C-14 to C-18) which are unsaturated, saturated, hydroxylated, and short peptide head group. Alike mycobactins, these are cell-associated [29].

The marine bacterium *Marinobacter* sp. DS40M6 produced a group of marinobactins A-E comprise the same six amino acid peptidic head group but differs in the length of the fatty acid appendage (C12-C16) at N terminus [30]. The marinobactins differ from amphibactins in peptide head (six vs four) and fatty acid tails [29]. Each hydroxymate group of peptide head forms a hexadentate octahedral complex with iron with binding constants in the range of 10^{22} to 10^{32} M^{-1} [31]. The hydroxymates can be detected by using several methods, initially Neilands assay (spectroscopic) used for finding the production of siderophores. Csaky's assay also widely used to characterize the siderophores. To detect the

structure of hydroxamate siderophore Electrospray ionization mass spectrometry (ESI-MS) has been used [32].

1.4.2. Catecholates

Catecholates are produced by certain bacteria [33]. The catecholate and the hydroxyl group of siderophore coordinate with Fe^{+3} to form a hexadentate octahedral complex. Complex stability, resistance to natural pH, and lipophilicity are catecholate unique properties. Nigribactin is a novel siderophore produced from marine bacteria *Vibrio nigripulchritudo*. Structural elucidation reveals the similarity with siderophores vibriobactin and fluvibactin. Nigribactin increases the expression of *spa* encoding protein A by inducing *spa* transcription [34]. This type of siderophore can be detected by Neilands assay, forms wine-coloured complex when siderophore binds $FeCl_3$ and shows maximum absorbance at 495nm.

O-CAS assay is another method to detect catechol siderophore [35]. High-performance liquid chromatography (HPLC) analysis with diode array detection (DAD) and ESI-MS assay can be used to detect catecholate siderophore [32].

1.4.3. α-Hydroxycarboxylates

This type of siderophore has both hydroxyl and carboxyl groups that coordinate with iron. A unique property of hydroxycarboxylates is their amphiphilic nature. The aquachelins produced by *Halomonas aquamarina* strain DS40M3, consists of peptide head group and hydrophobic fatty acid tails, forms self-assembled structures because of their amphiphilic and surface active nature [36]. Loihichelins A-F, were derived from the marine *Halomonas* sp. LOB-5 consists of a hydrophilic head group (an octapeptide) and joined by a series of fatty acids ranging from decanoic acid to tetra-decanoic acid.

An interesting characteristic of the loihichelins is photoreactive, which relates to the presence of β-hydroxy aspartic acid, which when coordinated to Fe^{+3} [37]. Carboxylates can be detected by spectrophotometric test in the range of 190 - 280nm [38]. O-CAS assay can be used for the detection of siderophore [35]. In recent times, it has been reported that HPLC and MS are used for structural analysis.

1.4.4. Mixed siderophores

In this type of siderophores, the compound will have a combination of hydroxy, carboxy and catecholates groups in side chains. Petrobactin, a bis-catechol α-hydroxy acid siderophore produced from *Marinobacter hydrocarbonoclasticus* oil-degrading marine bacteria. It is the first report that demonstrates structural characterization and photo decarboxylation when siderophores bound to Fe^{+3}. The citryl moiety of petrobactin binds to iron and found to be quickly photolyzed under sunlight and near-surface sea water. This results in the decarboxylation of α-hydroxy acids and oxidation of Petrobactin-Iron ligand [39,40].

Hickford et al. reported a novel siderophore; Petrobactin sulfonate isolated from *M. hydrocarbonoclasticus* contains sulfonated 3, 4-dihydroxy aromatic ring. The structure appears in the form of double zwitterion involving N-2 and N-2’ and the carboxylate and sulfonate moieties Hickford et al., (2004). Petrobactin sulfonate is more hydrophilic than petrobactin due to the presence of sulfonate, which resulted in the short retention times in HPLC. Few structures of different siderophores are shown in Figure 1.3.

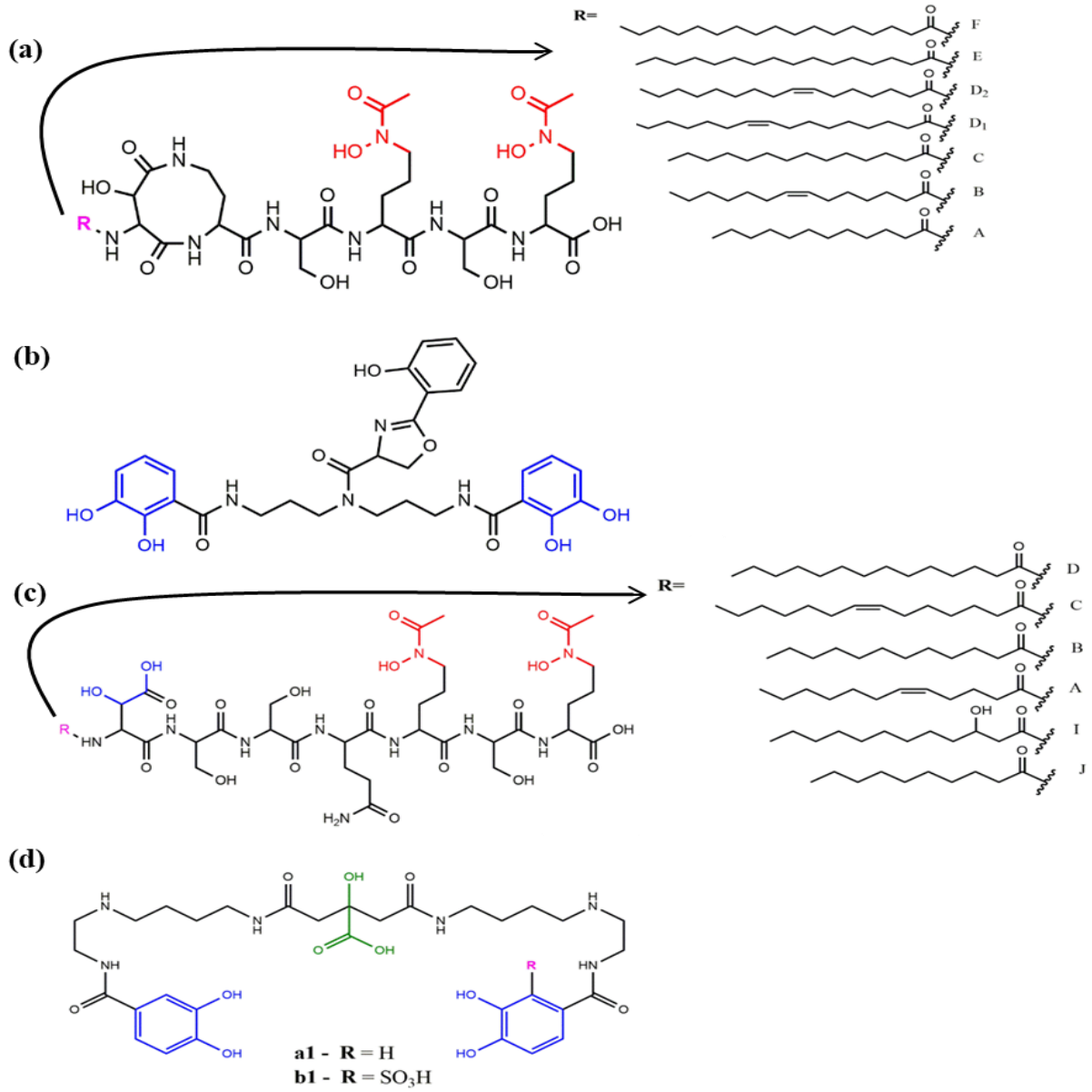

Figure 1.3: Structures of siderophores. **(a)** Marinobactin [29], **(b)** Nigribactin [34], **(c)** Aquachelins [36], and **(d)** Petrobactin (al) and Petrobactin sulfonate (b1) [39,41].

Marine *Pseudoalteromonas* sp. KP20-4 bacterium isolated from the Republic of Palau reported producing new siderophores, Pseudoalterobactin A and B. The structure of these compounds is similar to alterobactins, that have a catechol and two β-hydroxy-Asp residues which have a high affinity towards Fe^{+2} (affinity constant of 10^{49} - 10^{53}). Pseudoalterobactins showed high activity like enterobactin and desferrioxamine B by CAS assay that exhibited

20µM under assay conditions whereas, enterobactin and desferrioxamine B showed ED50 values of 500 µM and 60 µM, respectively [42].

1.5. Applications of siderophores

Siderophores, small and unique biological organic molecules produced under iron-limited conditions by microorganisms, have insightful applications in the following topics.

1.5.1. Biosensors

Recently, Siderophores were used as biosensing platforms to detect metal ions because of their high selectivity and sensitivity, cost-effectiveness, the suitability of handling, rapid response, and non-toxicity [43]. Biosensor is an analytical device capable of generating specific quantitative and semi-quantitative information using a biomolecule coupled to an electrical device (transducer), an amplifier to enhance the signal to noise ratio [44–46]. Siderophores have high affinity and specificity towards numerous metals and their receptors supply the basis for using them as sensors or probes [47].

Currently, some siderophores based biosensors and nanosensors have initiated with substantial success for different metal ions detection such as copper [48], iron [49–53], aluminium [54,55] and molybdate [56–58]. Several siderophore based techniques developed to detect and estimate metal ions, especially iron. Among them, fluorescent siderophores were considered as highly sensitive, because they are capable to detect low concentrations of analyte and shows rapid response rates. Biosensors utilize various electrochemical properties of siderophores to detect metals. Figure 1.4 represents the schematic diagram of siderophore based biosensor.

Fluorephore molecules are developed by using fluorescence siderophores which are dynamic receptors for iron ions detection [59]. Pyoverdins (PVD) are natural fluorescent

siderophores mostly used for the detection of Fe. These molecules are yellow green fluorescent siderophores which are produced by *Pseudomonas fluorescenes, P.aeruginosa* and other fluorescent Pseudomonads [60]. The hydroxymate and catecholate groups of PVDs reacts with Fe and form hexa-coordinate complexes, because of their high stability constants (10^{22} to 10^{32} M^{-1}) it protects against hydrolysis and enzymatic degradation [61]. Azobactin is another PVD type siderophore produced by nitrogen fixing soil bacteria *Azobacter vinelendii.* The selective sensors were identified iron in tap water and human serum (FI system) successfully [62,63].

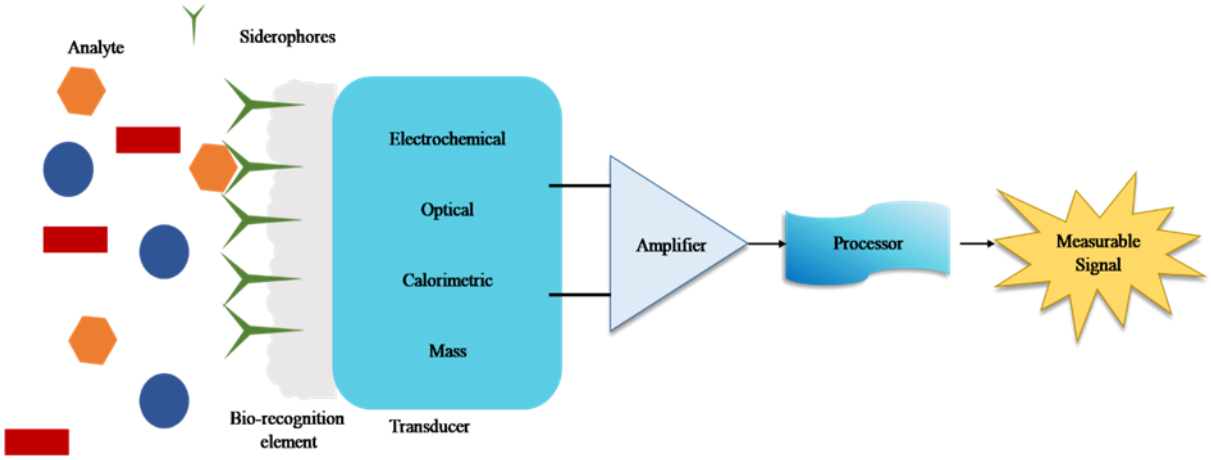

Figure 1.4: Representation of siderophore biosensor [19].

In recent times, several studies have been reported on the usage of siderophores in microbial pathogen detection. It depends on the high affinity of siderophores towards cell surface receptors of bacteria, which identifies and facilitates the Siderophore-Iron complex and Immobilization of siderophores. Doorneweerd et al., (2010) introduced the method to detect siderophore by immobilizing pyoverdine on gold-plated glass chips to identify the pathogen like *P. aeruginosa*. A treated polydimethylsiloxane stamp with pyoverdine-BSA conjugate was used as pattern for gold-plated glass surface. This technique is significantly faster than PCR for pathogen detection because it takes only fifteen minutes for maximum binding of *P. aeruginosa* to pyoverdine.

The biosensors were designed to detect pathogens by developing new methodologies, discovering siderophore binding proteins from pathogen cell extracts. Petrobactin is a biscatecholate, α-hydroxy acid siderophore isolated from marine bacteria and other human pathogens *Bacillus anthracis, B. subtilis, B. Cereus* [65,66]. Siderophore-based piezoelectric biosensor was developed by Inomata research group for the detection of several microorganisms using gold NPs [67–69]. They considered as mass measurement devices that depend on detecting the change of resonance frequency on a Quartz Crystal Microbalance, this change proportional to the mass binding to the electrode [47].

1.5.2. Siderotyping

Siderotyping or siderophore typing is a method to characterize the microbes based on the type of siderophores they produce [70,71]. It can be done in both analytical and biological methods. In the analytical method, the physicochemical properties of siderophores were studied using HPLC-MS and in biological method, using molecular biology techniques like immunoblot detection directly measure the siderophore mediated iron in microbial cells [72]. In siderotyping, major classification based on siderophore producers group and non-siderophore producers group.

400 strains of fluorescent and non-fluorescent *Pseudomonas* spp. are investigated and depending on siderophore type they classified into 28 taxa and using mass spectrometry analysis, 68 fluorescent Pseudomonas were identified by studying their pyoverdines [72–74]. Siderotyping can also be used as a chemotaxonomic marker to identify other types of bacteria for example *Mycobacterium* sp. and *Burkholderia* sp. depending on the difference in chemical structures of mycobactin and ornibactins respectively [75,76].

1.5.3. Growth of uncultivable bacteria

Kaeberlein et al., (2002) reported that siderophores can be acted as a growth factor to promote the growth of uncultivable microorganisms by co-culture of microorganisms [77,78]. Certain siderophores produced by actinobacteria can mediate actinomycete interactions. The Inter specific stimulatory events mediated by putative diffusible metabolites for the antibiotic production and morphological differentiation from *Streptomyces* species occur at a high rate. *Streptomyces griseus* produces desferrioxamine E that shows identical stimulatory effects on the growth and development of *S. tanashiensis*. Ferrichrome and nocobactin produced by microorganisms do not show any impact on the growth of uncultivatable microbes. But desferrioxamine E promotes secondary metabolites production and morphological differentiation in several actinomycete strain [79]. The siderophore genes of amychelin produced by *Amycolatopsis* sp. A4 were down-regulated when they grow nearby *S. coelicolor* because it inhibits the aerial hyphae formation (development arrest). But *Amycolatopsis* sp.AA4 utilizes desferrioxamine E produced by *S. coelicolor* [80]. Therefore, the species specific siderophores can modify the morphological differentiation and patterns of gene expression in actinomycete interactions and several uncultivable organisms can be cultivated and purified as pure culture. The pure cultures of uncultivatable microorganisms can be investigated for potential applications in various fields [32].

1.5.4. Medicine

1.5.4.1. Trojan horse strategy

The efficacy of therapy can be improved by developing various promising drug delivery methods [81]. For delivering drug molecules of less size Trojan horse therapy is the most promising one. This therapy works by transporting drug molecules through membranes, which act as barriers and thereby enhancing the in-take of drug molecules by cells. The

practical application of this method has failed *in vivo* due to its toxic side-effects. These effects are due to the unregulated transport of drug molecules into the cells [81].

The Trojan horse strategy can be applied to antibody conjugated siderophores called sideromycins. The intake of drugs will be efficient and easy as the cells take up iron part of sideromycins through the cell gates and along with iron they also carry the conjugated antibiotic into the cell. In most of the bacteria, the outer membrane is very selectively permeable; by applying this strategy the permeability issue of drug molecule can be resolved with ease. The main parts of drug-siderophore conjoint are three and they are linker, siderophore and the drug (Figure 1.5). The key role players in this conjoint are siderophore and drug molecule, Siderophore has to bind the iron whereas drug has the antibacterial activity when it is released from the complex.

The role of the linker is not only to connect the drug molecule and siderophore but also to regulate the drug release from the siderophore-drug molecule conjoint [82–85]. When this conjoint reach the bacterial cytoplasm with the help of a siderophore, it slowly releases the drug which starts microbial extermination. This action of the conjoint can trigger an equal and opposite reaction which blocks the further transport of iron into the cell [86].

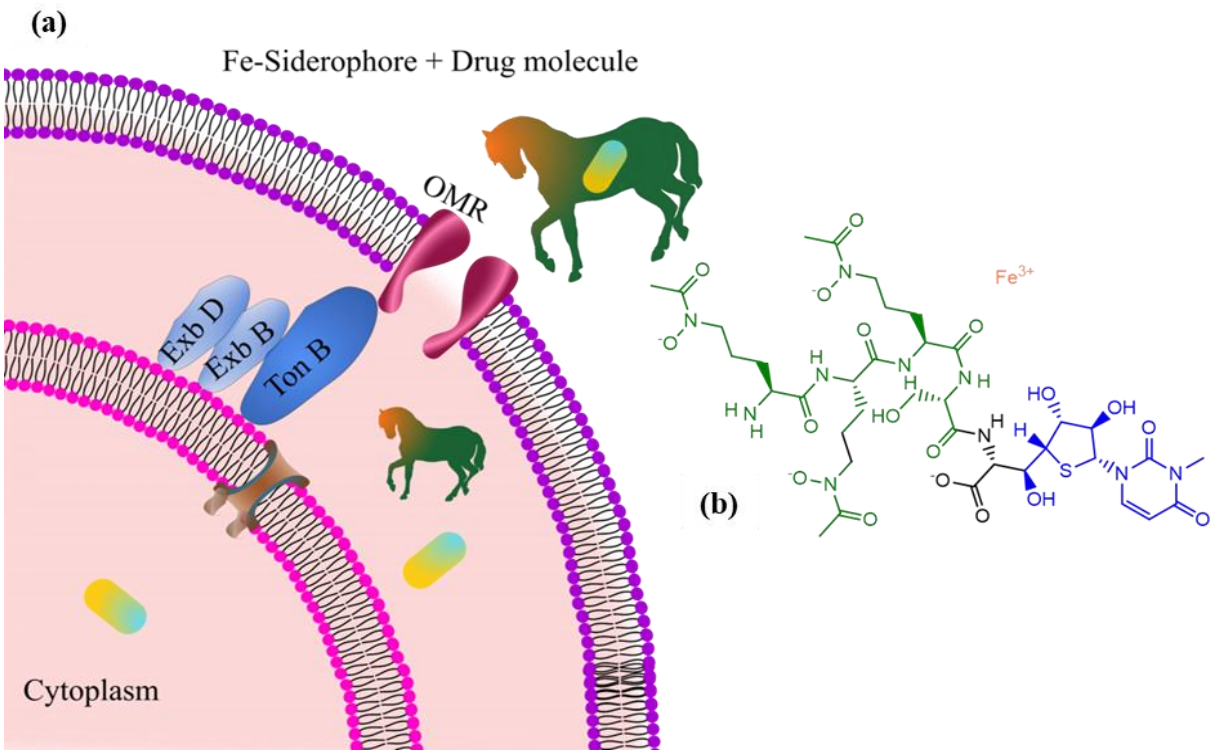

Figure 1.5: Schematic diagram of drug molecule linked to siderophore (Trojan horse strategy). Iron-siderophore-drug complex enters the cell outer membrane (OM) through specific outer membrane receptors (OMRs). After entering the cell, drug molecule gets released into periplasm or cytoplasm depends on target. Ton B complex provides energy in active transportation [19].

1.5.4.2. Iron overload therapy

There are a few diseases which are caused due to the overload of iron and siderophores have the potential to be used as a treatment for those. For treating disorders like sickle cell anaemia, beta-thalassemia, blood transfusion is a must [94]. The red blood cells reach their graveyard, spleen at the end of their life span and die. This is the only mechanism of iron removal in the human body and no other mechanism exists. Consecutive blood transfusions result in an elevated level of iron in the body which is very harmful to the vital body parts and especially the liver. So this iron overload should be minimized to reduce the risk of damaging vitals. Siderophore associated drugs have the potential to minimize iron overload in the body and can be used in treating many disorders [95]. One such siderophore

associated drug is Desferal [96]. It contains deferoxamine mesylate, which is an iron chelating siderophore, primarily used for treating disorders like sickle cell anaemia and thalassemia major [97–99]. The representation of chelation therapy is shown in Figure 1.6.

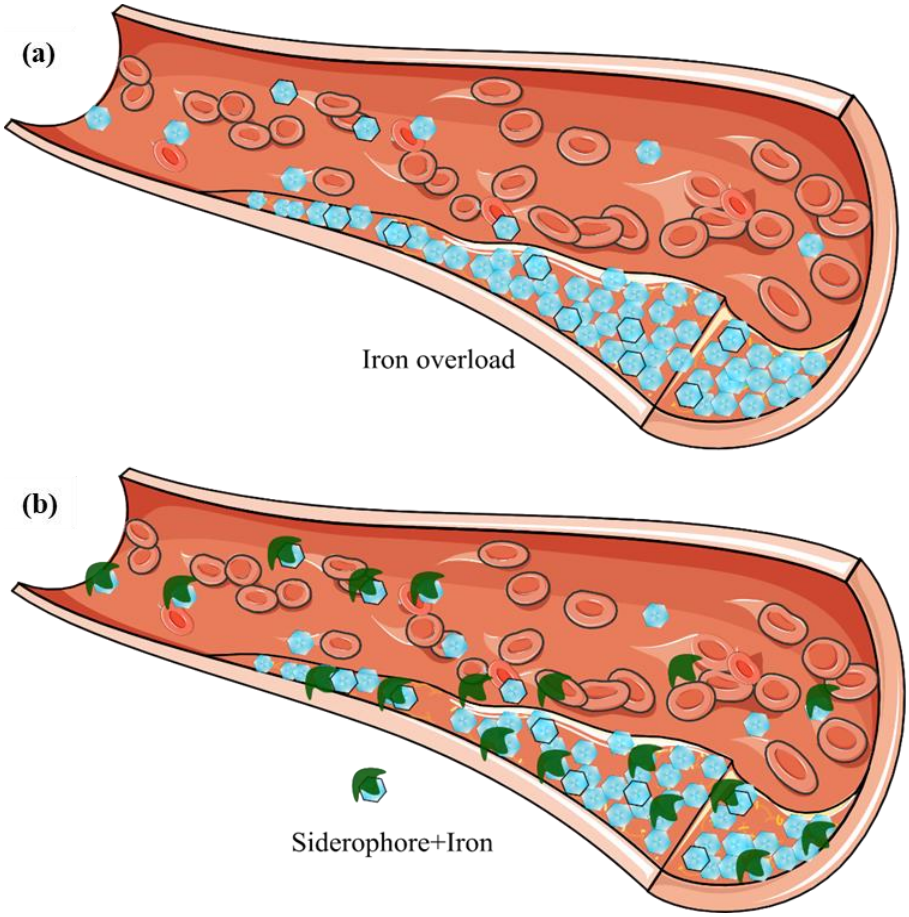

Figure 1.6: Schematic representation of chelation therapy. Repetitive blood transfusions resulted in iron overload in the body. Chelation is required to remove iron, because excess iron levels in blood leads to organ damage or failure and cardiac death. Desferrioxamine is used as a chelator, Iron- desferrioxamine (Siderophore) complex is water soluble and excreted through urine and faeces [19].

1.5.4.3. Antimicrobial activity

Nowadays, multi-drug resistant microbes are evolving very rapidly and the old antibiotics have significantly reduced showing effect towards them. For this reason, researchers have started exploring new horizons for effectively handling this issue and came up with many discoveries and one among them is usage of siderophores [100].

In order to stay alive, few parasites require an iron source and *P. falciparum*, *Leishmania* spp. and *Trypanosoma cruzi* are some among them. For most of the parasites, life cycle begins in insects and later on, they infect mammals for completing their life cycle, in the parasite's life cycle (especially in mammals) they depend on iron taken in by the hosts [101]. Lytton et al., in 1993 experimented and reported a curative effect on parasites in mice. A Swiss mice was administered 370 mg/Kg hydrophobic chelator of iron dose in combination with coconut oil subcutaneously 3 - 4 times with a time interval of 8 hours. The results were surprising with two to three fold decreases in parasite concentration in its body and the infected mice had an increased survival time. According to Loyevsky et al., (1999), desferrioxamine B is a potent drug used for malaria disease and action of it might be based on its ability to chelate iron lying in the cytoplasm of plasmodium parasite. The anti-malarial effect of desferrioxamine B has been proved in both *in vitro* and *in vivo* studies but the drawback is its limited time of action. Despite continuous exposure of drug, the suppression of parasite is too slow to develop the anti-malarial activity.

According to Pradines et al., 2006, desferrioxamine has very less absorption into the blood when administered orally and even if administered as intravenous it has a very short half-life. *Crassostrea virginica*, an oyster amasses large amounts of iron in its body leading to more parasitic attacks and easy proliferation of parasites like *Perkinsus marinus.* Desferrioxamine works effectively for *Crassostrea virginica* when given in a proper continuous dosage [105].

1.5.4.4. Removal of transuranic elements

With depleting energy reserves scientists are working on new reliable technologies for energy generation to meet day to day increasing human needs and one such technology is the generation of electricity through nuclear energy. This has paved a way for the increase of

vanadium, aluminium, etc., which are transuranic elements [93]. The increasing levels of these transuranic elements are not good for life in any form. Apart from the environmental issues, patients who undergo dialysis for a very long period accumulate aluminium in brain, which is called encephalopathy due to dialysis. Aluminium overload is also observed in patients with end-stage renal failure. To treat these aluminium overload related disorders, siderophores like desferal is being employed [93]. Desferol forms aluminoxamine complex in the presence of aluminium (Figure 1.7). This complex is easily dissolved in water and gets excreted along with faeces and urine [93,106–109]. It's been already reported that desferal has the potential to reduce the amount of vanadium from the body. According to Nagoba and Vedpathak, 2011 its been reported that usage of desferal removes vanadium by 25% in lungs, 26% in liver, and 20% in kidneys.

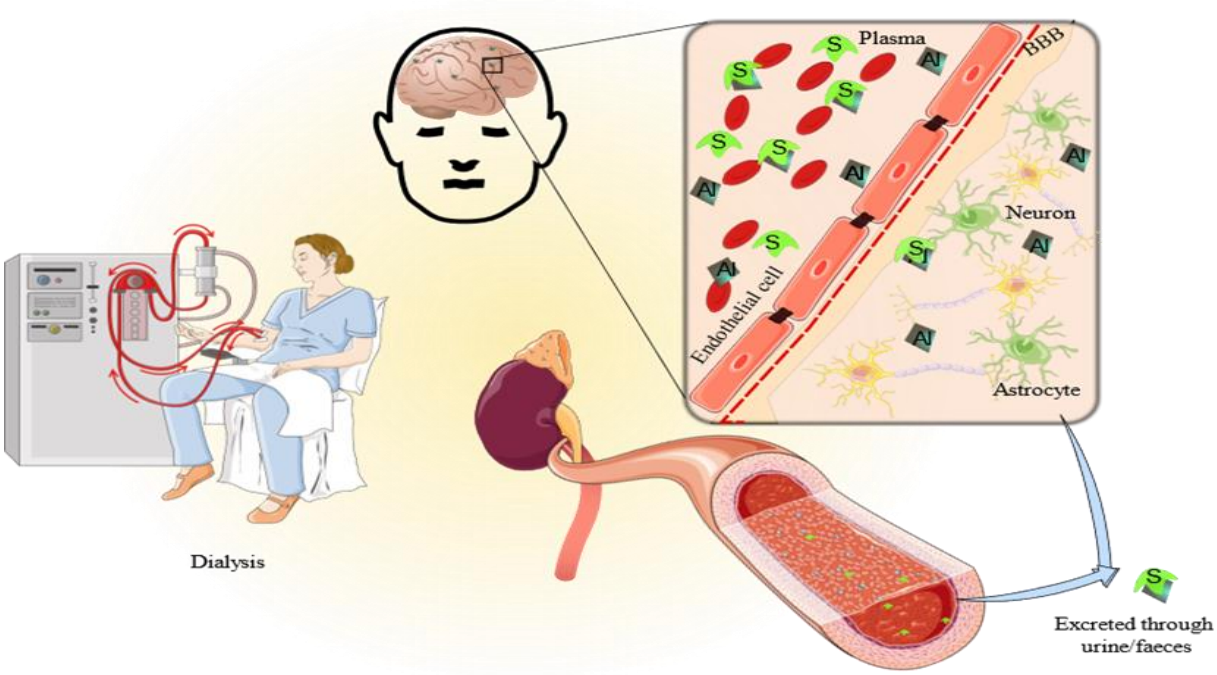

Figure 1.7: Representation of removal of transuranic elements from body. Due to long term dialysis, aluminium gets accumulated in brain and kidneys. Desferal or desferrioxamine reacts with aluminium and form water soluble Aluminoxamine complex which is rapidly excreted through urine and faeces [19].

1.5.4.5. Cancer therapy

Cancerous cells divide unrestingly to form tumors. For this uninterrupted cell division, continuous growth & development, these cells must have high concentrations of iron. So, cancerous cells require more iron than the normal non-cancerous cells. The relationship between cancer development and iron overload has been under continuous review ever since the fact of their dependency has been established [110]. According to Nakouti et al., (2013), siderophores, especially iron chelators are being employed as they are restricting the growth of cancer cells. For instance, patients suffering from neuroblastoma were administered with desferrioxamines and there was a significant reduction in development of belligerent cancer cells. Out of the available desferrioxamines, desferrioxamine E has been reported to have cytotoxicity effect through induced apoptosis towards malignant melanoma cancers [31].

1.5.5. Toxic and heavy metal bioremediation

Though heavy metals (Pb, Cd, Hg, Cu, Cr, Fe, Zn, Al, Co, Mn, Ar) are present naturally in soil and water. Due to rapid industrialization and other activates like mining, usage of pesticides and fertilizers, the concentration of heavy metals increased and disposal of these metals without treatment poses a persistent risk to human health and environment. The bioremediation of heavy metals became a challenging task because these metals cannot be degraded completely but can transform from one organic complex to another [96,100]. Presently, the investigation on the usage of siderophores for bioremediation potentially increased. Neubauer et al., (2000) reported that desferrioxamine B, a siderophore can chelate Co^{+3} at high pH conditions than Fe^{+3}. Azotobactin and azotochelin siderophores produced from *Azotobacter vinelandii* used for the acquisition of Mo and V [62].

Raoultella sp. strain X13 cadmium resistant microbe absorbs cadmium that present in the soil by ion exchange and chelation enhances the production of indole acetic acid and

siderophores for plant growth. The siderophores produced by *strain X13* reduces the bioavailability of cadmium in cadmium stressed soils [113]**.** Some siderophores isolated from *Actinobacteria* reduces the cadmium uptake by bacteria. Under Ni contamination, *S. acidiscabies* E13 secreted hydroxymate type of siderophores. It promoted the growth of cowpea by binding nickel and iron, inhibited uptake of Ni and supplied Fe for the plant growth [114]. *P. azotoformans* produced the mixed type of siderophore (catecholate and hydroxymate) showed a high affinity towards several metals Cd, Pb, Ni, Ar, Al, Mg, Zn, Cu, Co, Sn other than Fe. Among them, Ar removed 92.8% by five washes using siderophore and 77.3% by EDTA, 70.0% by citric acid [115].

Vibrio parahaemolyticus, marine estuarine enteropathogen reported to produce Vibrioferrin a citrate-based siderophore that shows less affinity towards Fe when compared to other marine siderophores. *Marinobacter* sp. also produced the vibrioferrrin siderophore but observed as borate complex, though borate was not added to isolating media. Authors proposed that siderophore forming a complex with Boron from borosilicate glassware used during experimentation [116–118]. Shinozaki et al., (2019) reported that *Pandoraea* sp. HCo-4B produced thermostable siderophore chelated Co^{+2}, when organism grown in Co^{+2} supplemented medium. The siderophore binds to Co^{+2} in 1:1 ratio, it gets absorbed to C18 column and eluted with ethanol.

In the marine environment, petroleum hydrocarbons are one of the major problems. For the bioremediation of petroleum hydrocarbons in marine ecosystems, microorganisms play a significant role [120]. Under Fe starvation, the marine microbes produce siderophores, by facilitating the Fe acquisition the siderophore participate in the degradation of petroleum hydrocarbons [39]. *Marinobacter hydrocarbonoclasticus* oil-degrading micro bacterium secreted Petrobactin siderophore and structurally characterized. *M. Hydrocarbonoclasticus* reported to produce another sulfonated siderophore called Petrobactin sulfonate, catecholate

type [41]. Gauglitz et al., (2012) reported that amphiphilic siderophores called ochrobactins were produced from marine bacterium *Vibrio* sp. that isolated from the Gulf of Mexico after the Deepwater Horizon oil spill in 2010. Ochrobactins, may contribute to the degradation of petroleum hydrocarbons.

1.5.6. Agriculture

1.5.6.1. Plant growth promoter

Plant Growth Promoting Bacteria are a different set of bacteria which aren't harmful and can increase the tolerance to stresses, growth rate, resistance towards diseases in plants. They are wide range of bacteria and exist in different habitats like soil especially the phyllosphere and rhizosphere of plants. Some bacteria exist as symbionts and especially as endophytes that live in the interior tissues of plants [114,122–124]. According to Omidvari et al., (2010), at neutral pH the level of available iron required for microbial growth is 0.006-0.01 m.mol/mL, whereas plants require more concentration of iron than microbes i.e., 0.010-0.017 m.mol/mL. The fact that pyoverdine siderophores produced by various *Pseudomonas* species can boost the growth of plants is proved beyond doubt [126,127]. So, all these bacteria which boost the plant growth are referred to as Plant Growth Promoting Bacteria [128]. In 2000, Masalha et al., experimented on plants to know the importance of microbes in the plants iron takes up. For this, plants were grown on soil with loess loam texture and care was taken to maintain asepsis in the soil for one plant and microbes were allowed to grow in another. After some time, it was observed that plant roots in soil with microbial growth were observed to have more iron than the plant roots with aseptic soil.

On the other hand, the plants are grown on aseptic soil were observed to have iron malnutrition and even didn't have a proper vegetative growth. They have concluded that the siderophores produced by soil microbes can be an effective iron source for plants. According

to Rungin et al., (2012) *Streptomyces* sp., an endophytic bacterium in Thai jasmine rice plant enhanced the roots and shoots remarkably. In 2013, Qi and Zhao have reported enhanced salt stress tolerance in cucumber by siderophore produced by *Trichoderma asperellum*. Apart from siderophores of microbial origin, there are some siderophores which are produced by the plant itself. They are called phyto-siderophore, whose working is similar to microbial siderophores. When an iron malnutrition plant was supplemented with phyto-siderophore, plant showed better growth and the symptoms related to iron shortage were significantly reduced. For enhanced iron uptake of plant and its growth, siderophores of both microbial and plant origin play a very vital role [129,132].

1.5.6.2. Potential biocontrol agent

Siderophores have an important role in controlling pathogens affecting plants (Figure 1.8). Siderophores hold large amounts of iron leading to the reduced accessibility of iron for other microbes in the habitat, which even include the plant pathogenic bacteria. With this strategy, they are helping plants in combating their pathogens [133,134]. Many researchers have reported the biocontrol agent application of siderophores. The usage of chemical fertilizer and synthetic fungicides can the minimised, as siderophores are natural nontoxic products of bacteria [128].

In 1980, Kloepper et al., raised the curtain unveiling the potential of siderophore for being used as a biological application. Kloepper et al. used different strains of *Pseudomonas fluorescens* (like TL3B1, A1, B10, BK1) for confronting *Erwinia carotovora* infection. *Fusarium oxysporum* causes wilt disease in potato, which can be controlled by Pyoverdine, a siderophore produced by Pseudomonads sp. Bacteria [135]. *Gaeumannomyces graminis* is a pathogenic fungus that causes damages barley and wheat crops mainly [136]. The siderophore Pyoverdine is very much active against it and shields the plant from its pathogenic effects.

Not only in barley and wheat Pyoverdines are capable of shielding other crops like maize and peanuts [137].

Apart from Pseudomonads, even *Bacillus subtilis* is also a producer of siderophores and plays a key role in controlling *F.oxysporum* caused Fusarium wilt in pepper [138]. Many fungi, mostly pathogenic to plants depend on Fe^{+3} in the soil for their survival. *Azadirachtaindica* produces a cocktail of siderophores which chelate Fe^{+3} and thereby restricting the growth of several pathogenic fungi [139]. In the literature its already been reported by many researchers that siderophores have a capability in inhibiting the plant pathogenic fungi like *Sclerotinia sclerotiorum*, *Phytophthora parasitica*, and *Pythium ultimum* [140,141]. According to the available and reported literature, siderophores can be considered as potential alternates for biocontrol agents against many plant pathogens.

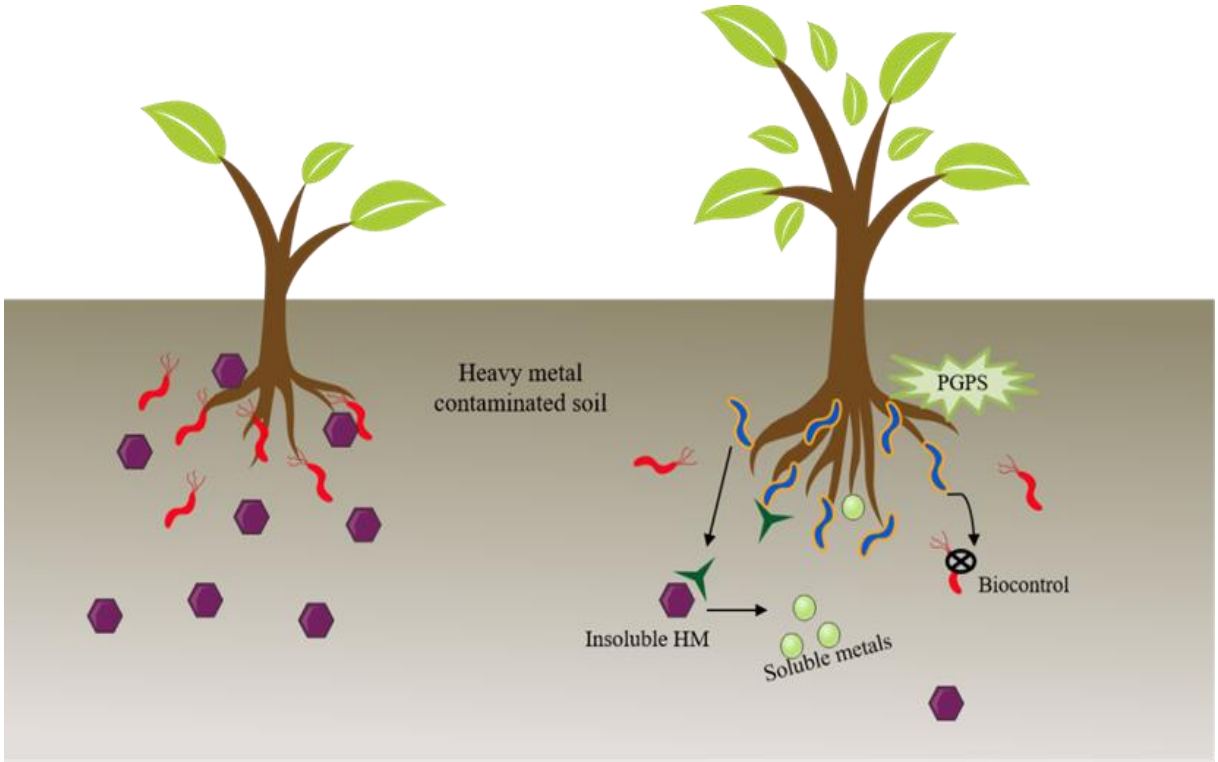

Figure 1.8: Application of siderophore in agriculture and heavy metal remediation. Soil contains pathogens and heavy metal contamination due to extensive industrialization. Siderophores released by the PGP bacteria, bind to the Iron present in the soil. Due to iron sequestration, pathogens cannot survive as iron is one of the growth limiting factors. PGP

bacteria chelate the insoluble heavy metals to soluble form quickly taken up by plants for their growth and microorganisms for their metabolic processes as cofactors [19].

Depending upon the proficiency of siderophores-mediated Fe^{+3} acquisition mechanisms, marine bacterial siderophores can be used as novel antimicrobial agents through covalently bonding with commercial antibiotics or as novel Fe^{+3}-chelating desferals. Additionally, siderophores extracted from marine bacteria have also demonstrated several unconventional biological properties, for example, as agents which can negatively affect the regulation of quorum sensing, as intermediaries for mutualistic associations by swamping into bacteria and can be secreted as signalling molecules to regulate factors associated with virulence in pathogenic microbes. Based on these diverse properties, marine siderophores have significant potential in medicine [142,143]. To date, several industrial and research groups have shifted their interest towards marine bacteria because they have become a primary source in the production of unique and biologically active secondary metabolites with diverse biological applications [144–146]. Siderophores are also employed in optical biosensors, biodegradation of petroleum hydrocarbons, biogeochemical cycling of Fe in oceans, bioremediation of pollutants such as heavy metals and in pharmaceutical industry [32,147].

1.5.7. Biological significance of siderophores in pathogenicity

Siderophores are pivotal in the pathogenicity of numerous bacteria, especially those affecting humans. Within the human body, iron is typically bound to proteins like transferrin and lactoferrin, rendering it inaccessible to bacteria. Siderophores, small molecules produced by bacteria, exhibit a strong affinity for iron. They scavenge iron from host proteins or environments with low iron levels, enabling bacteria to obtain the iron necessary for growth and replication within the host [83]. Often regarded as virulence factors, siderophores enhance bacterial pathogenicity by facilitating iron acquisition from the host, thereby circumventing

the host immune system's iron-limiting defences. This fosters bacterial growth and colonization in host tissues, facilitating infection establishment and progression [148]. Iron regulation is tightly controlled in the human body, and siderophore-mediated iron sequestration can disrupt host iron homeostasis. This disruption may impede the function of immune cells, such as macrophages, which rely on iron for antimicrobial activities. Through manipulation of iron availability, bacteria can evade immune responses and establish persistent infections [149]. Additionally, certain bacteria produce siderophores to outcompete other bacteria for scarce iron resources in their environment. This competitive advantage may contribute to the dominance of specific bacterial species within particular niches, including host-associated microbiomes [150].

This chapter highlights the importance of siderophores, vital low molecular weight molecules synthesized in environments deficient in iron. It explores their significance and mechanisms of transportation, often categorized based on chelating group nature and coordination with Fe^{+3} via oxygen ligands. With their versatility, siderophores find applications in biosensors, siderotyping, medicine, bioremediation of toxic metals, and agriculture. Subsequently, the following chapter provides an extensive literature review on marine siderophores, offering insights into their multifaceted roles and attributes. This comprehensive exploration will shed further light on the diverse roles and characteristics of these molecules within marine environments.

The thesis was organized into five chapters.

CHAPTER I: Presents the general introduction, scope, contents and the aim of the present work. This chapter presents the information about the iron requirement, siderophores importance, types of siderophore, transportation mechanism and applications.

CHAPTER II: Briefly reported the review literature related to the doctoral thesis work. In this section, details of the siderophores from marine source and studies so far reported on siderophores production from marine microbes, applications and siderophore based nanoparticles.

CHAPTER III: Gives a detailed description of the materials and methods employed for the work carried out in four parts. The first part includes the sample collection and isolation of siderophore-producing marine bacteria from different locations in the Bay of Bengal and the detection of siderophore production from them. In the second part, the optimization of production parameters (Incubation time, temperature, initial pH, carbon source, nitrogen source and organic acids) of siderophore production medium, purification, concentration and characterization of extracted siderophores. In the third part, the heavy metal chelation and seed germination activity were tested using marine bacteria and supernatant, respectively. The fourth part includes the synthesis of siderophore-based silver nanoparticles, their characterization, and antibacterial activity against Gram-positive and Gram-negative bacteria.

CHAPTER IV: Presents the results and discussion related to the work done in four parts. In first part the collection of marine water and sediments samples from marine estuary regions and isolated the fast-growing bacteria. All the isolates were screened for siderophore production using CAS (Chrome Azurol S) assay, and the most efficient four isolates were selected for further work. 16S rRNA molecular characterization of isolates showed the nearest similarity of SMI_1 with *Bacillus taeanensis*, AABM_9 with *Enterobacter* sp., SVU_3

with *Marinobacter sp.* SVU_3 and AMPPS_5 with *Pseudomonas mendocina*. In the second part the production parameters of the succinate medium were optimized to enhance the siderophore production. The optimum production of siderophores for SMI_1 was *93.57 %SU* (Siderophore Units) (after 48 h of incubation at 30 °C, pH 8, sucrose as carbon source, sodium nitrate as nitrogen source, 0.4% of succinic acid) and for AABM_9 was *87.18 %SU* (after 36 h of incubation period at 30 °C and pH 8 in the presence of sucrose, ammonium sulfate and 0.4% succinic acid). The maximum production of siderophores for SVU_3 was *83.15 %SU* (after 48 h of incubation at 35 °C and pH 8.5 in the presence of glucose, sodium nitrate and 0.6% succinic acid) and for AMPPS_5 was *91.17 %SU* (after 36 h of incubation at 35 °C, pH 8.5, glucose as carbon source, ammonium sulfate as nitrogen source, and 0.4% of citric acid). Effects of Copper, Manganese and Zinc metal ions on siderophore production were studied. The siderophore was separated using an Amberlite XAD-2 column followed by Sephadex LH-20. The fractions were concentrated by removing methanol using rotary evaporator and lyophilized samples stored. The chemical nature was identified by Thin-layer chromatography, Fourier Transformation Infrared analysis (FTIR), High Resolution – Mass Spectroscopy (HR-MS) and Nuclear Magnetic Resonance (NMR) spectroscopy. In the third part the heavy metal chelation of siderophore-producing marine bacterial isolates was investigated on Ag^{+2}, Al^{+2}, Cd^{+2}, Co^{+2}, Cr^{+6}, Hg^{+2}, La^{+3}, Mo^{+6}, Ni^{+2}, Pb^{+2}, Pd^{+2}, and Y^{+3} metal ions (1 mM, 5 mM) by spotting method. All four isolates showed chelation activity on heavy metals except Ag^{+2}, Cd^{+2} and Mo^{+6} due to species-specific trait. Seed germination studies were performed on seeds Brown chickpea (*Cicer arietinum* L.), Peanut (*Arachis hypogaea*), Green gram (*Vigna radiata*), and Kabul chana (*Cicer arietinum*) using siderophore supernatant. Finally, in the fourth part the as-synthesized silver nanoparticles (AgNPs) via chemical (Che-AgNPs) and biological (Bio-AgNPs) methods were characterized for their optical, physicochemical, crystalline, and elemental composition properties. Che-AgNPs and

Bio-AgNPs showed a peak at 455 nm and 415 nm with average particle size of 198.73 nm and 135.19 nm, whereas surface charge was found to be -21.94 mV and -32.67 mV, respectively. Che-AgNPs have shown better zone of inhibition (ZOI) against Gram- bacteria such as *Escherichia coli* (10.57 mm), *Klebsiella pneumoniae* (11.25 mm), *Pseudomonas aeruginosa* (15.43 mm), whereas Bio-AgNPs showed better ZOI against Gram+ bacteria such as *Bacillus subtilis* (13.31 mm), Coagulase-negative *staphylococci* (12.28 mm), *Staphylococcus aureus* (12.03 mm) at 50 µg per well concentration.

CHAPTER V: Presents the conclusions drawn from the isolation of siderophore-producing marine bacteria, optimization of production parameters and purification of siderophores. It includes heavy metal chelation, seed germination ability of siderophore-producing bacteria, and synthesis of siderophore-based AgNPs. Future research scope was also presented in this chapter.

Chapter II: LITERATURE REVIEW

2.1. Siderophores from marine source

Recently, many siderophores have been isolated from marine bacteria including *Actinomycetes*. Marine microbes well known for its production of numerous siderophores, which act contingently and regulated independently to compete efficiently in the environment. *Streptomycetes* are highly available and important group of actinomycetes in the marine environment [100]. You et al. (2005) isolated 94 different strains of actinomycetes from the marine sediments, among them 87.2% are *Streptomycetes* and most of the strains having siderophore producing ability on CAS agar plates and influence the growth of pathogenic *Vibro* sp. Strains *in vitro Streptomyces* can form desiccation-heat resistant spores and probiotic products will be stable under preservation. Streptobactin, a novel catecholate type of siderophore was isolated from actinomycetes *Streptomyces* sp. YM5-799 by chromatography under acidic conditions using porous-polymer resin Diaion HP20 column. Streptobactin ($C_{51}H_{69}N_{15}O_{18}$) is a colourless gum, having catechol bonded arginine-substituted siderophore framed on a cyclic triester backbone of threonine (-Thr-Arg-DHBA). Along with Streptobactin, dibenarthin, tribenarthin, and benarthin were also obtained. When the compounds screened for iron-chelating activity, results showed slightly stronger activity than desferrioxamine mesylate. Under iron limited conditions, these siderophores might play a significant role in the existence of *Streptomyces* sp. strain YM5-799 [151].

Nocardamine, a cyclic siderophore isolated from novel marine *Citricoccus* sp. KMM3890 from bottom sediments of Sakhalin seashore. It contains three units of 5-succinylated-1-amino- ydroxyamino-pentane which is similar to bisucaberin- symmetric cyclic dihydroxamate, which was isolated from a marine *Alteromonas haloplanktis*. Initially, Nocardamine reported as an antibiotic [152]. Nocardamine was examined for its cytotoxicity

to melanoma SK-Mel-5, RPMI-7951, SK-Mel-28 and breast cancer T-47D cell lines *in vitro* using MTS assay and inhibition of colony formation using soft agar clonogenic assay. Results showed no cytotoxicity was observed but nocardamine inhibited colony formation of cancer cells [153].

In silico analysis of marine *Salinispora arenicola* and *S. tropica* proposed that they have several phenolate and hydroxamate type siderophore biosynthetic loci, desferrioxamine (DFO) B and E are produced from *Salinispora* in the laboratory. Ejje et al. reported possibility of the biosynthesis of siderophores by genome analysis of marine actinomycete *S. tropica* CNB-440 but unable to predict the siderophore of hydroxymate and phenolate-thia(oxa)zol(id)ine class are produced [154]. Ni^{+2}-based immobilized metal ion affinity chromatography used to pre-fractionate the metabolome of *S. tropica* CNB-440 and identified DFOA1a, DFOA1b, DFOA2, DFOB, DFOD1, DFOE, DFOD2, DFON compounds, among these DFON was a new siderophore. Based on these studies, the focus on marine actinomycetes is growing for drug discovery. Siderophore metabolome of *S. tropica* CNB-440 was modulated by culture conditions intended to mimic the changeable marine environment. At constant pH and increase in temperature resulted in the increase of DFOA2 and DFOA1 and decreases of DFOB and DFOE, at constant temperature and an increase in pH showed increase in DFOB, DFON, and DFOE decrease in the levels of DFOA2 and DFOA1. DFOB has been used as an iron chelator for iron overload diseases in humans.

Streptomyces olivaceus FXJ8.012 was isolated from the deep seawater samples of south West Indian Ocean, reported to produce two novel oxazole/thiazole siderophores entitled as Tetroazolemycins A and B. The structures of these compounds are similar to Pyochelin and Spoxazomicins. It is difficult to decide the absolute configuration of Pyochelin type of siderophore because of their multi chiral centers and isomerization on ring C. So, Liu et al., (2013) failed to crystallize the Tetroazolemycins A and B, as the structures contain

neither hydroxyl groups nor amino acids and CD spectra were not recorded from reference samples. Compounds A&B were screened for heavy metal ion binding ability, results showed that Cu^{+2}, Zn^{+2}, and Fe^{+3} have high affinity and Pb^{+2}, Cr^{+3}, and Mn^{+2} showed no affinity. Compounds were inactive against *Klebsiella pneumonia* but their Zn^{+2} complexes weakly inhibited this pathogen with minimum inhibition concentrations of 125 - 250 µg/ml and 125 µg/ml.

Using LC-HRESI-MS based non- targeted metabolomics, a novel hydroxymate type siderophore Fradiamine A and B were isolated from marine *Streptomyces fradiae* MM456M-mF7 from deep-sea sediments of Sagami Bay, Japan. Compounds were purified by Diaion CHP-20P, Sephadex LH-20 column chromatography and eluted with 50% MeOH and further purified by HPLC. Fradiamine A, a new siderophore having two alkyl diamines asymmetrically bound to citric acid core. Fradiamine A&B showed modest antimicrobial activity against *Clostridium difficile* with IC_{50} values of 32 and 8µg ml^{-1}, respectively. Despite the antibacterial activity, under the presence of Fe^{+3} cancelled dose-dependently [156].

Yang et al., (2019) studied the antagonistic activity of *Streptomyces* sp. isolate S073 towards pathogenic *Vibrio parahaemolyticus* using the agar diffusion method. *Streptomyces* sp. S073 produced carboxylate type of siderophore which was confirmed by Vogets test (disappearance of pink color). The antagonistic activity of S073 was mostly attributed to the siderophore mediated Iron competition because most of its life cycle S073 produce siderophores. *Amycolatopsis albispora* WP1T reported to produce a new siderophore, designated as albisporachelin, isolated from samples collected in the Indian Ocean at a water depth of 2945m. Albisporachelin, has a cyclized hydroxyl ornithine at the C-terminus, at least one N-δ-OH-N-δ-formyl-Orn and includes serine as the only other amino acid residue. The discovery of albisporachelin adds to the diversity of marine-derived

siderophores and shows its impact on marine ecology, marine chemistry, and biogeochemistry. Deep-sea derived siderophores are few explored and this study represented one of the few examples to date [158]. The structures of siderophores from marine actinomycetes are represented in Figure 2.1 and listed in Table 2.1.

Yan et al., (2019) reported isolation of two noval siderophores Madurastatin D1 and D2 which have unusual 4-imidazolidinone cyclic moiety in their structures. To identify the biosynthetic origins of this structure, sequenced the genome of *Actinomadura* sp. WMMA-1423 and found *mad* biosynthetic gene cluster. The genome sequencing allowed them to propose a hypothesis, but needed further studies to clearly understand the biosynthesis of madurastatins.

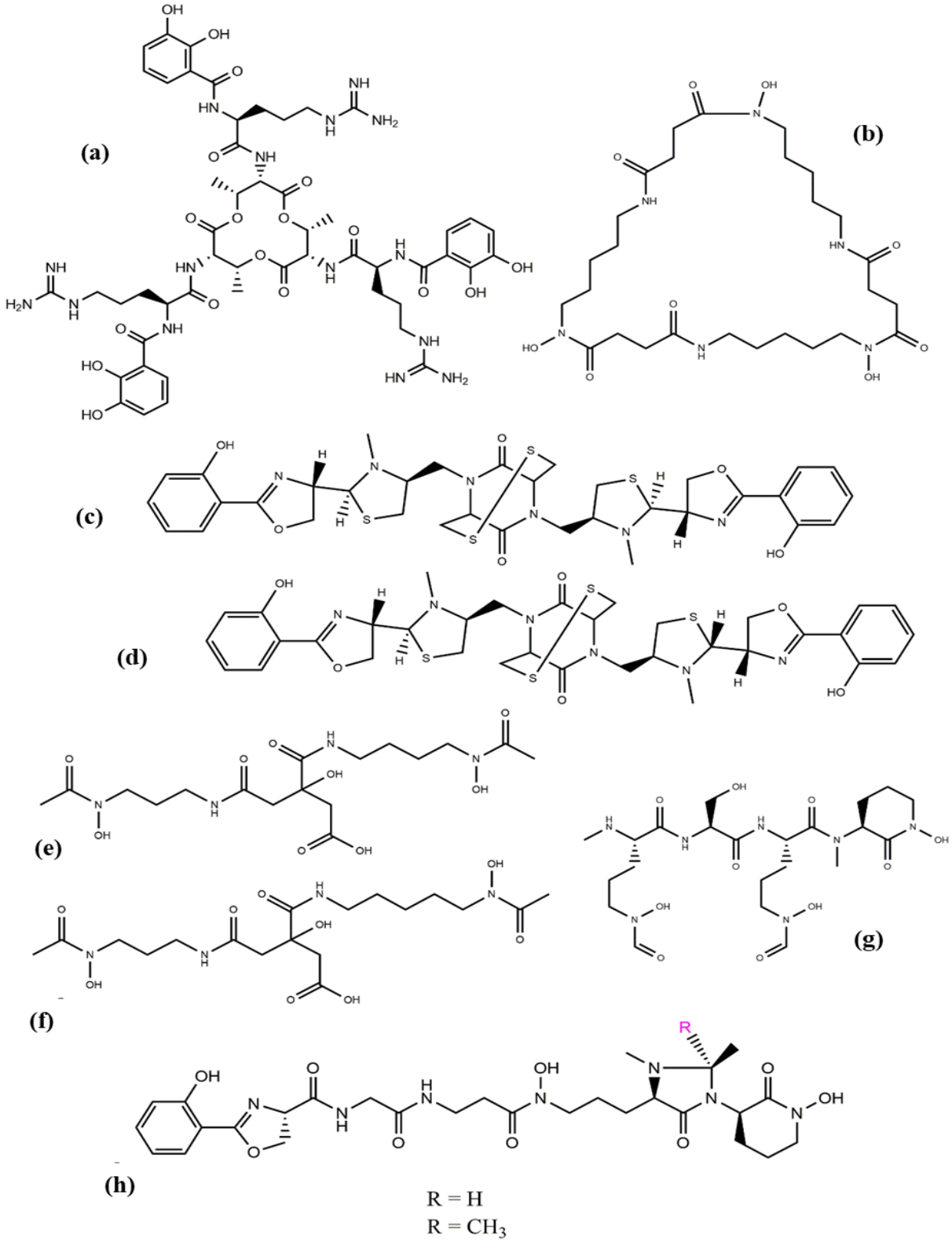

Figure 2.1: Structures of Siderophores from marine bacteria. Structures of siderophores from marine Actinomycetes. **(a)** Streptobactin [151], **(b)** Nocardamine [153], **(c)** Tetroazolemycin A [155], **(d)** Tetroazolemycin B [155], **(e)** Fradiamine A [156], **(f)** Fradiamine B [156], **(g)** Albisporachelin [158], and **(h)** Madurastatins [159].

Table 2.1: List of Siderophores from marine source.

Siderophore	Microorganism	Type	Remarks on siderophore activity and structural data	Ref.
Madurastatin D1 Madurastatin D2	*Actinomadura* sp. WMMA-1423	Phenolate-Hydroxamate	Both siderophores contain unusual 4-imidazolidinone cyclic moiety. Moderately active in antimicrobial assays with *M. luteus*	[157]
Unknown	*Streptomyces* sp. S073	Carboxylate	Studied excretion of antagonistic substances and impact of siderophore production against pathogenic bacteria.	[155]
Albisporachelin	*Amycolatopsis albispora* WP1	Hydroxymate	Structure of noval siderophore was determined by 1D & 2D NMR and MS-MS experiments.	[156]
Fradiamine A	*Streptomyces fradiae* MM456M-mF7	Hydroxymate	Novel siderophore, showed anti-microbial activity against *C. difficile.*	[154]
Tetroazolemycin A Tetroazolemycin B	*Streptomyces olivaceus* FXJ8.012	Mixed type	Sulfur containing siderophores and binds to several metal ions other than iron.	[153]
Desferrioxamine A1 Desferrioxamine A2 Desferrioxamine B Desferrioxamine D1 Desferrioxamine D2 Desferrioxamine E Desferrioxamine N	*Salinispora tropica* CNB-440	Hydroxymate	The LC-MS analysis revealed 8 siderophores of desferrioxamine class from *S. tropica* CNB-440. The siderophore metabolome was dynamic and modulated by optimizing micro environment.	[152]
Streptobactin Dibernarthin Tribenarthin	*Streptomyces* sp. YM5-799	Catecholate	All three siderophores were novel and showed iron chelating activity slightly more than desferrioxamine mesylate.	[149]
Nocardamine	*Citricoccus* sp. KMM 3890	Hydroxymate	Novel actinobacteria was isolated and screened for nocardamine. And it was showing anti-tumor activity.	[151]

2.2. Characterization of siderophores using modern techniques

Intricate tiny compound compositions can be easily analyzed through liquid chromatography-mass spectrometry (LC-MS) technique. Due to the above-stated application, LC-MS has got importance in different research expenses such as medicine and biology like metabolomics, in combinatorial and environmental chemistries for characterization of molecules [160–163]. Many novel iron-holding proteins namely polypeptide siderophores are also being discovered with the help of LC-MS/MS. In this process, the obtained MS/MS spectrum of newly identified siderophore is compared with the database which has the data of known siderophores to interpret the characteristics of the new siderophore. The salient feature of LC-MS is the concoction of both the mass-to-charge ratio and retention time. Table 2.2 summarizes HPLC protocol, which includes columns and methods of marine siderophores. In LC-MS, out of all the soft ionization procedures, Electrospray Ionization (ESI) is the regularly employed procedure. ESI can develop the mass spectrum of the compound with its minimum amount of fragmentation. It also can assist and mine LC-MS characteristics without disturbing the ions at the molecular level.

Table 2.2: HPLC column and method employed in the purification of marine siderophores based on literature.

Compounds (Yield)	**Instrument**	**Column**	**Method**			**Ref.**
			Gradient system	**Mobile phase**	**Flow rate**	
Woodybactin	HPLC	YMC 20 x 250 mm C18-AQ column	5% to 100% methanol	Methanol, Water	-	[162]
Myxochelin B (3.7 mg/L)	LC/MS	Nucleodur 100-5 C18 ec VarioPrep column (125 x 21 mm, 5 µm; Macherey-Nagel)	37% to 53% methanol over 63 min, 63% to 100% over 2 min, and 100% methanol for 7 min	Methanol, Water	4 ml/min	[163]
Massiliachelin	RP-HPLC	Nucleodur 18 PAH column (250 x 8.0 mm, 3 µm, Macherey Nagel)	10% methanol for 5 min, from 10% to 100% over 35 min, 100% for 10 min, followed by 10% for 10 min	Methanol, Water	-	[164]

Pacifibactin	RP-HPLC	YMC 20 x 250 mm C18-AQ Column	10% methanol in H_2O to 30% methanol in H_2O 10/90% H_2O/methanol over 40 min	Methanol, Water	-	[165]
Imaqobactin (11.6 mg)	LC-HRMS	C18 column (Phenomenex, Kinetex, 1.7 µm 50 x 2.1 mm)	95% H_2O/0.1% formic acid and 5% ACN/0.1% formic acid over 4.8 min	ACN, Formic acid	500 µl/min	[166]
Albisporachelin	HPLC-MS	C18 column (Waters Xbridge, 4.6 mm x 50 mm)	5 to 25% ACN in H_2O (each with 0.05% TFA) over 60 min	ACN, Water	1 ml/min.	[156]
Fradiamines A and B	HRESI-MS	SPELCO Ascentis Express C18 column (2.1 mm ID x 50 mm	95% A to 0% A (5 min), 0% A (5 - 8.5 min), 95% A (8.5 - 12 min); 0.1% formic acid aq. (A) and 0.1% formic acid-ACN (B)	Formic acid, Formic acid-ACN	0.4 ml/min	[154]
Pseudochelin A (6.3 mg)	LC-MS/MS	Reverse phase C18	0 - 100% methanol	Methanol	2 ml/min	[167]
Thalassosamide (60 mg)	LC-MS	Phenomenex Luna C18 reversed-phase column (250 x 4.6 mm, 5 µm)	10 - 40% CAN - H_2O with H_2O containing 0.1% acetic acid over 25 min, 4.0 mg/ml	ACN-Water, Acetic acid	1.0 ml/min	[168]
Variochelins	LC-MS	C18 column (Betasil C18, 150 x 2.1 mm, 3 µm; Thermo Scientific)	Methanol-H_2O gradient from 50% to 100% over 20 min	Methanol, Water	0.2 ml/min	[169]
Avaroferrin (6.9 mg)	LC-MS	C18 Inertsil ODS-3, 2 x 100 mm	20% - 60% methanol	Methanol	0.2 ml/min	[170]
Moanachelins	RP-HPLC	C4 column (250 mm length x 20 mm diameter, Higgins)	100 % A [0.05 % TFA in H_2O] to 100 % B [0.05 % TFA in 80 % methanol, 20 % H_2O] over 37 min	Methanol, Water	-	[171]
Tetroazolemycin A (19.1 mg)	HPLC	Waters Xbridge ODS (10 x 150 mm, 5 µm) column	Methanol:H_2O = 70:30, v/v	Methanol	-	[153]
Ochrobactin	RP-HPLC	preparative C4 column (250 mm x 20 mm Higgins)	50% A (0.05% TFA in H_2O), 100% B (0.05%TFA in 80% methanol, 20% H_2O) over 15 min	Methanol, Water		[121]

Nocardamine (298 mg)	HPLC	C-18 column 10.0 mm x 250 mm, 5 µm, Supelco	(30 - 60%) of methanol:H_2O over 25 min	52% Methanol or in 27% ACN	2 ml/min	[151]
Aquachelin	(RP-HPLC)	C4 column (250 mm length x 20 mm diameter	50% A [0.05% TFA in H_2O] to 100% B (0.05% TFA in 80% Methanol) over 15 min	Methanol, Water	-	[35]
Streptobactin (18.8 mg)	RP-HPLC	TSK gel ODS 80Ts, ϕ2.0 x 25 cm,	20% to 50% aqueous ACN containing 0.1% TFA in 30 min	ACN	10 ml/ min	[149]
Loihichelins	RP-HPLC	C4 column (250 mm length x 22 mm diameter)	80% A (0.05% TFA) and 20% B (0.05% TFA) in 19.95% water and 80% ACN over 45 min	ACN, Water	-	[36]
Marinobactin	HPLC	C4 reversed-phase column (Vydac, 5 mm ID· 250 mm length).	100/0 (% A/B) for 7 min to 0/100 over 25 min; and a hold at 0/100 for 3 min [A = 99.95% $H_2O$and 0.05% TFA; B = 19.95% H_2O, 0.05% TFA, and 80% ACN]	ACN, Water	-	[27]
Synechobactin A–C (7.5, 1.5, 0.3 mg)	HPLC	C18 reversed-phase column (Vydac 10 mm ID 3 250 mm length).	20% to 50%ACN with 0.05% TFA	ACN	100 ml/min	[172]
Petrobactin sulfonate (0.55 mg/L)	RP-HPLC	(Vydac C4 column (10 ím, 22 mm ID x 250 mm)	ACN/H_2O gradient (0% to 60%) over 35 min	ACN, Water	-	[40]
Amphibactin	HPLC	C4 reversed-phase column (Vydac)	100/0 (% A/B) to 0/100 (% A/B) over 37 min A = 99.95% H_2O and 0.05% TFA B = 19.95% H_2O, 0.05% TFA, and 80% methanol	Methanol, Water	-	[28]
Desferroxiamine G	HPLC	C18 or C4 reversed phase column (Vydac 10 mm ID 3 250 mm length)	100/0 (% A/B) to 0/100 over 35 min A = 99.95% H_2O and 0.05% TFA B = 39.95% H_2O, 0.05%	Methanol, Water	-	[173]

			TFA, and 60% methanol			

Imaqobactin is a siderophore with amphiphilicity extracted from a bacterium (*Variovorax sp*. RKJM285) isolated from the Arctic region. In this study, the core-shell 100 Å C18 column of Phenomenex was used for accomplishing chromatography. The injection volume was 10 µl and the flow rate for the entire process was maintained at 500 µl/min. Two mobile phases were used in this process, one was 0.1% formic acid with H_2O which acts as solvent A and the other was 0.1% formic acid with CH_3CN which acts as solvent B. A gradient of these two solvents ranging from 95% of solvent A, 5% of solvent B to 100% solvent B for 4.8 mins trailed by a 3.2 min hold with the above-mentioned flow rate and injection volume. UV 200−600 nm, ELSD, and ESI-MS were the detectors used. Sample analysis of Liquid Chromatography (LC) High-Resolution Mass Spectrometry (HRMS) revealed the two ions which are eluting at the same time. One of them has mass/charge ratio of 934.5038 $[M + H]^+$ and the other has 987.4168 $[M + H]^+$, based on these ratios their suggested molecular formulas are $C_{41}H_{71}N_7O_{17}$ and $C_{41}H_{68}FeN_7O_{17}$, respectively. The first one, $C_{41}H_{71}N_7O_{17}$ has 53 units less mass/charge ratio when compared to $C_{41}H_{68}FeN_7O_{17}$. This loss of mass might be related to the Fe^{+3} loss, which is typical for siderophores that bind iron [168].

Characterizing structures of compounds using MS/MS is a challenging task due to the complex melange of tiny molecular structures [121]. A marine bacterium namely *Shewanella woodyi* MS32 produced a set of novel siderophores (Woodybactins A, B, C, D) with fatty acyl group. Waters Xevo G2-XS QT of Mass Spectrometry was used to determine the molecular multitudes. This instrument possesses Waters BEH C18 column and positive mode Electrospray Ionization attached to an ACQUITY UPLC-H-Class system. Mobile phase used was CH_3CH with 0.1% formic acid in double-distilled H_2O with 0.1% formic acid and a

gradient of 0 - 100% was applied linearly. The Woodybactins (A, D) molecular ion peaks of mass/charge ratio were determined as 463 and 491 respectively, whereas both Woodybactins B and C had peaks as 477. Peculiarly, the difference in mass between Woodybactins A & B is the same as Woodybactins C & D which is 14 units. This indicates the difference between a CH_2 groups. The available data suggests that the fatty acid chains of woodybactins A-D might most probably vary in length [164].

For identification of an unknown compound and to identify its structural aspects, MS/MS is the most suitable technique. The m/z ratio of selected siderophores and type of ionization are listed in Table 2.3. In 2005 Owen et al., identified a set of siderophores with amphiphilicity from *Marinobacter* sp. Strain DS40M6 & Strain DS40M8 and named them marinobactins A to E. For these marinobactins, the head group is made of protein, which manages the fatty acid chain and Fe^{+3}. A few years later in 2007, Martinez et al., identified another marinobactin with C18 fatty acid and having a single double bond, namely marinobactin F. The hydrophilicity of marinobactin F is much higher than the other A to E marinobactins. All these marinobactins are established with the help of electrospray mass spectrometry and HPLC (analytical). A VG-Fisons Platform II (Micromass) with quadrupole mass spectrometer was used and which was coupled with Michrom BioResources HPLC unit, for injecting directly. For marinobactins A, B, C, D, E the source temperature and a cone voltage are 70 °C and 65 V, respectively, whereas for marinobactin F the source temperature and a cone voltage are 90 °C and 80 V, respectively are enough for fragmenting. The marinobactin F molecular ion peaks of mass/charge ratio were determined as 1014 $(M + H)^+$. In 2000, Martinez et al., identified two new members of the aquachelins family, namely aquachelins J and I, which were identified from *Vibrio* sp. HC0601C5 and *Halomonas meridiana* str. HC4321C1 with the help of reverse phase HPLC. Electrospray ionization mass spectrometry (ESI-MS) and tandem mass spectrometry were executed on Micromass Q-TOF2

with collision gas as Argon to determine the structural aspects of the above mentioned aquachelins.

Table 2.3: Mass spectrometry data of marine siderophores.

Instrument	Ionization	m/z Ratio	Mode	Compounds	Ref.
HRESI-MS	ESI	513.3655 $(M+H)^+$	-	Fw0622	[175]
HRESI-MS	ESI	467.2033 $(M+H)^+$	-	Massiliachelin	[164]
HRESI-MS (Q-TOF)	ESI	372.1919-408.1747	Positive	Myxochelin B(1-9)	[163]
HRESI-MS (Q-TOF)	ESI	370.1759-390.1647	Positive	Pseudochelin A(4-9)	[163]
HR-ESIMS	ESI	923.4081 $(M+H)^+$	Positive	Pacifibactin	[165]
HRESI-MS (Q-TOF)	ESI	463, 477,477,and491	positive	Woodybactins A-D	[162]
HR-ESI-MS	ESI	560.2712$(M-H)^-$	Negative	Albisporachelin	[156]
LC-HRMS, MS/MS	ESI	934.5038 $(M+H)^+$	-	Imaqobactin	[166]
FTICR MS	ESI	895.3995	Negative	Amphibactin Ua	[176]
LC-HRESI-MS	ESI	435.2086 $(M+H)^+$	Positive	Fradiamine A	[154]
LC-HRESI-MS	ESI	449.2242 $(M+H)^+$	Positive	Fradiamine B	[154]
HR-ESI-MS(MALDI-TOF/TOF)	ESI	1074.604 $(M+H)^+$	-	Variochelin A	[169]
LCMS-8040	ESI	419, 405, 401, 391,387,373	-	Avaroferrin	[170]
HR-ESI-MS	ESI	757.1971, 757.1965 $(M+H)^+$	-	Tetroazolemycins A And B	[153]
HRESI-MS (Q-TOF II)	ESI	778, 788, 800, 802, 816, 828 $(M+H)^+$	-	Moanachelins	[171]
LC-MS	-	628.29 $(M+H)^+$	-	Desferroxiamine N	[152]
ESI-MS (Q-TOF2)	ESI	793, 821, 849	-	Ochrobactin-OH A-C	[121]
HRESIMS (Q-TOF)	ESI	5909.3407 $(M-H)^-$	-	Nocardamine	[151]
ESI-MS (Q-TOF2)	ESI	830.54 $(M+H)^+$	-	Amphibactin S	[35]
ESI-MS (Q-TOF2)	ESI	804.55 $(M+H)^+$	-	Amphibactin T	[35]
HR-FABMS	ESI	1180.5004	-	Streptobactin	[149]
GC-MS	ESI	930, 974, 956, 958, 984, 986	-	Loihichelins A-F	[36]
HR-ESI-MS (Q-TOF)	ESI	614.261, 586.23, 558.198	-	Synechobactins A-C	[172]
HRESI-MS	ESI	799.3199 $(M+H)^+$	Negative	Petrobactin Sulfonate	[40]
ESI-MS	-	1078.4, 1106.5 $(M+H)^+$	-	Pseudoalterobactin A, B	[41]
ESI-MS	ESI	719.3614 $(M+H)^+$	Positive	Petrobactin	[38]
ESI-MS	ESI	619.3647 $(M+H)^+$	-	Desferrioxamine G	[173]
FAB-CI-MS	CI	373.21 $(M+H)^+$	-	Putrebactin	[177]
VG ZAB-E FAB MS	-	349.0944 $(M+H)^+$	-	Anguibactin	[178]
SI-MS	SI	401 $(M+H)^+$	-	Bisucaberin	[179]

To identify the siderophores in marine water, the samples were pre-treated with Solid-phase extraction and coupled with LC-tandem MS. ZORBAX SB-C18 reversed phase column (50 mm x 2.1 mm, 1.8 µm, Agilent, USA) was used to separate the sample using formic acid 0.1% (V/V) and methanol as mobile phase A and B at a flow rate of 0.25 ml/min. Mass spectrometry performed under multiple reaction monitoring and ESI-positive mode. This method is used in analyzing siderophores under HNLC regions and exhibited advantages such as high enrichment factor, matrix effect, in accurate quantification of ability and good recovery [181].

Matrix-assisted laser desorption/ionization time-of-flight mass spectrometry (MALDI-TOF MS) is a rapid and economical technique used to identify several biomolecules and bacteria based on ribosomal MS data. Successive developments in the instrumentation resulted in better-resolved spectra of perfectly folded proteins. Total acquisition and analysis of intact proteins and rare metabolites of 384 bacterial colonies can be completed in less than four hours by using MALDI-TOF-MS but it requires basic expertise for sample preparation and to operate in comparison with regular instrumentation like Orbitrap, quadruple TOF, Fourier transform ion cyclotron resonance mass spectrometers [182].

Variovorax boronicumulans produces variochelins, lipopeptide siderophores differ in biosynthesis when compared with most of the other lipopeptide siderophores where polyketide synthase is involved. The head group of variochelin A and connectivity of constituents were analyzed by tandem MS. The three bidentate ligand groups include two hydroxamate functions and hydroxy carboxylate (i.e., the β-hydroxyaspartate residue) were identified by MALDI-TOF/TOF (Bruker Ultraflex spectrometer) fragmentation [171]. Desferrioxamine E (DFO-E) is an ideal siderophore used for iron chelation therapy, isolated

from *Streptomycetes* bacteria. It requires cost effective industrial production for *in vitro* and animal studies. Approximately, 97% of pure DFO-E was analyzed by two-step purification process using HPLC. MALDI-TOF MS analysis demonstrated the purified Desferrioxamine E always contains traces of Desferrioxamine D2 [183].

Guerrero-garzón et al., (2020) isolated ten strains of *Streptomyces* from marine environment for secondary metabolites Biosynthetic gene cluster analysis. LC-MS analysis of strain ADI96- 02, led to detection of several different metabolites. Among them, one of the main compounds identified as nocardamine (desferrioxamine E).

2.3. Nanoparticles synthesis

Metallic NPs presence has increased in several areas of human applications because of its diverse nature and potential as biosensors, solar cell technology, cryogenic superconducting material, cancer therapy, drug delivery and safety control, cosmetic industry, pollution control, pharmaceutical ingredients, antimicrobial agents, biomarkers, and primarily in biomedicine and bioscience as biological tagging agents [185,186]. Among them, AgNPs or nano-Ag has garnered a lot of attention or been in the spotlight for long due to tis characteristic or unique features such as superior catalytic activity, chemical resistance, higher conductivity, superior chemical stability, enhanced magnetic, electrical, and optical properties, surface area, shape, and importantly its size [186–188]. These unique characteristic features of AgNPs have made them indispensable and superior compared to other metallic NPs [189]. Due to its innovative use in the energy industry, where stability and strong catalytic performance of Ag-based NPs make it a promising substitute for platinum in dye-sensitized solar cell technology, AgNPs have also received a lot of attention recently [190–192] In current nanotech research, the synthesis of AgNPs is of essential importance in

addition to its diverse applications [193]. AgNPs' market size is anticipated to grow as well, from more than 2 billion USD in 2020 to more than 5.5 billion USD by 2027 [194].

The biological process for synthesizing AgNPs depends on the methodical use of plant extracts and microbes such as fungi, yeast, and bacteria which are environmentally friendly [187,195]. Microbes reduce metal ions in response to environmental stress conditions [196]. Additionally, bacteria are simple to handle, proliferate quickly and affordable, and allow for simple control of growth factors including incubation time, oxygen, and temperature [197]. Compared to physical and chemical processes, the biological synthesis of NPs is thought to be non-toxic, more affordable, and more environmentally benign [198,199]. However, a revolutionary change in the biological synthesis of NPs is envisaged by the use of extracellularly produced secondary metabolites with little interference of the toxic nature of the NPs on the biological system in order to avoid destruction of the biological resources for the synthesis of nanoparticles [197,200,201]. In addition, synthesis of NPs extracellularly is more affordable, viable, and simpler [197]. The surface of the AgNPs is covered by these biological substances, which improves their biocompatibility and stability [202]. AgNPs can have their size, shape, and morphology altered by changing the reaction conditions, such as using a reducing agent, stabilizing agent, or capping agent through various biological processes [185,187]. Furthermore, the requirement for the use of reducing agents will be eliminated if the capping agent can reduce the metal ions which produce the AgNPs [194].

2.4. Siderophores in synthesis of nanoparticles

The present study's utilization of marine bacterial secondary metabolites for the biological synthesis of AgNPs is predicted to provide a wide range of advantages, including the following: (a) the presence or toxicity of Ag^+ ions would never affect the growth of bacteria or production (different bacteria have varying tolerances for Ag^+ ions [203]), (b) NPs

segregation won't go through a pointless purification process where bacteria's siderophore tends to chelate the NPs, and (c) The synthesis of NPs does not involve the use of hazardous substances [203]. For the purpose of mass-producing NPs, the same metabolite can be synthesized unimpeded from continuous or batch culturing of bacteria [203].

Low molecular weight ligands known as "siderophores" are produced as a result of the absence of soluble iron in the environment [204]. The stability constants (β) of different siderophores range from 10^{10} to 10^{49} for their iron complexation [204]. Siderophores have the potential to chelate several metal ions such as Zn^{2+}, Tl^{+}, Tb^{3+}, Sn^{2+}, Pb^{2+}, Ni^{2+}, Mn^{2+}, Hg^{2+}, Ga^{3+}, Eu^{3+}, Cu^{2+}, Cr^{2+}, Co^{2+}, Cd^{2+}, Al^{3+}, and Ag^{+} apart from Fe^{3+} [204]. These secondary metabolites' metal ion redox potential may be crucial for the production of metal NPs [185,204]. Bioleaching, biomineralization, and bioremediation all depend on metal-microbe interactions, or more precisely, metal-chelator interactions [204]. Therefore, based on the above stated information, the presented work focused on the comparative analysis of AgNPs synthesized through chemical and biological approaches. Throughout the literature, only a few papers have highlighted the use of siderophores in the NPs synthesis (Table 2.4).

Table 2.4: Use of siderophores in the synthesis of various NPs as per the existing literature available.

NPs	Siderophore(s)	Source	Feature(s)	Remark(s)	Ref.
Ag	Pyoverdine	Purified from *Pseudomonas aeruginosa* DM1	415 nm (SPR), FCC, spherical or pseudo-spherical, 45 to 100 nm	Anti-algal effect on *Chlorella pyrenoidosa* and *C. vulgaris*	[184]
TiO_2	Enterobactin	Commercial	386 nm (SPR)	Promote surface solubilization of TiO_2 NPs	[204]
Au	Catechol	Synthesized	532 nm (SPR), 40 nm	Selective detection of Fe^{3+} ions in aqueous solution	[51]
Fe_3O_4 @SiO_2	Feroxamine	Synthesized	Crystalline, 22.14 mV, ~10 nm	Electrostatic surface interactions between NP	[205]

@NH_2				conjugate and feroxamine receptor for pathogen (*Yersinia enterocolitica* wild type) detection	
Ag	Pyoverdine	Isolated from *P. aeruginosa* 25W	425 nm (SPR), FCC, irregular shape, 50 to 100 nm	NPs showed potent anticancer activity against metastatic A549 lung cancer cells	[206]
Au			550 nm (SPR), FCC, triangular and hexagonal, 50 nm and 2 µm		
Fe_3O_4	2,3-dihydroxybenzoylglycine	Synthesized	Crystalline, 9.8 ± 1.8 nm (DLS), ~7.2 ± 1 nm	Showed highly selective and sensitive fluorimetric detection of Al^{3+} in water at physiological pH	[55]
ZnO	Pyoverdine	Extracted from *P. aeruginosa* DM1	362 nm (SPR), polycrystalline wurtzite, 50 to 100 nm	Their Broad-Spectrum Antimicrobial Effects	[207]
Au	Delftibactin, Enterobactin, Aerobactin, and Yersiniabactin	Isolated from *Escherichia coli* Nissle 1917	600 nm (SPR)	NPs formation by microbial metallophores (hydroxamates, catechols, citrates, mixed ligands)	[208]
Ag	Desferrioxamine B	Synthesized	450 nm (SPR)	Ag NPs functionalized with desferrioxamine b derived ligand for Fe^{3+} binding and sensing	[209]
ZnO	Tripodal catecholates	Synthesized	Spherical, 25 nm	Immobilization of tripodal PEG-catecholates on ZnO NPs	[210]

This chapter offers a comprehensive review of bacterial siderophore production and the molecular structures of these compounds originating from marine sources. It thoroughly examines the processes involved in synthesizing siderophores by bacteria residing in marine environments. Moreover, the chapter provides detailed insights into the characterization of

siderophores, employing modern high-throughput techniques to elucidate their properties and attributes.

In addition to characterization, the chapter explores the synthesis of nanoparticles, particularly those derived from siderophores. It investigates novel methods of nanoparticle synthesis using siderophore-based approaches, capitalizing on the unique characteristics of these molecules to facilitate nanoparticle formation. Such innovative methods hold significant promise for applications across diverse fields, including biomedicine, environmental remediation, and materials science.

By presenting a comprehensive analysis of siderophore production, molecular structures, and nanoparticle synthesis, this chapter advances our understanding of these processes and their potential applications. It serves as a bridge between fundamental research and practical applications, laying the groundwork for future developments in siderophore-based technologies. In the coming chapter the detailed methodology employed for the planned work was described.

2.5. Research gaps

1. Knowledge on identifying and exploring the siderophores produced by marine bacteria was limited.
2. Marine bacterial siderophores are less explored for their potential to chelate wide range of heavy metals.
3. The marine siderophore-based nanoparticles and their activity have not yet been investigated.

2.6. Objectives of the work

1. Isolation, screening and characterization of siderophore producing marine bacteria from marine environment.
2. Siderophore production and optimization of process parameters.
3. Separation, purification and concentration of siderophores.
4. Heavy metal chelation and seed germination studies of siderophore producing bacteria.
5. Synthesis, characterization and antibacterial activity of siderophore-AgNPs.

Complete Work Flow chart

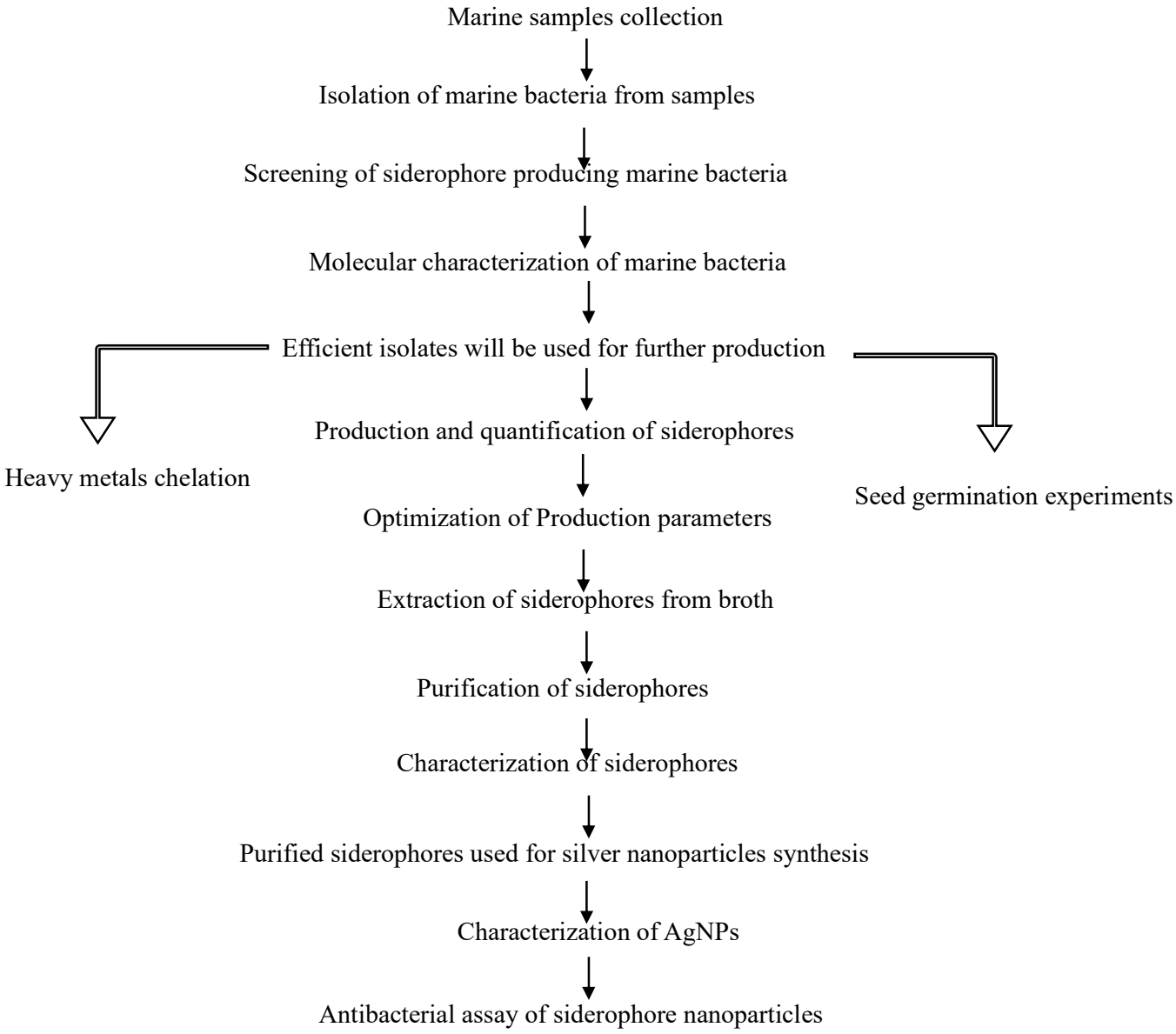

Chapter III: MATERIALS and METHODS

3.1. Materials

3.1.1. Chemicals used

All the media and chemicals were purchased from HI-Media Laboratories Pvt. Ltd., and Sigma-Aldrich, India. Sterile double distilled water (DH_2O) was used for the work. pH of solutions was adjusted by using 1 M NaOH and 1 N HCl, accordingly wherever required. Preparation of media, stock solutions, reagents, buffers, and necessary dilutions were made using DH_2O. Non-ionic detergent was used to wash the glassware, later rinsed with DH_2O several times, and then dried in a hot air oven before use. All the glassware was washed with 6 M HCl prior to siderophore production. Amberlite XAD-2 and Sephadex LH-20 (Sigma, Germany), TLC Silica Gel Plates 20 x 20 cm (Merck, India).

3.1.2. Instrument details

Instruments such as Ultraviolet-Visible spectroscopy (UV-Vis spec; Model: UV-1800; Manufacturer: Shimadzu; Japan), Particle size analyzer (PSA; Model: LiteSeizer 500; Manufacturer: Anton Paar, Austria), Scanning electron microscope (SEM; Tescan, Vega 3 LMU, Czech Republic) coupled with energy dispersive X-ray (EDX) spectroscopy, and X-ray diffraction (XRD; Model: X'Pert Pro; Manufacturer: Malvern PANalytical, UK) were used. The as-synthesized AgNPs were separated from the solutions by centrifugation for 5 min at 15,000 rpm (RCF: 20,630xg) (KUBOTA 3300; Table-top Micro Centrifuge; RA-2024). Liquid chromatography Mass Spectroscopy (Maker: Waters; Model: 2695 Alliance, Milford, Massachusetts), Fourier Transform Infrared Spectroscopy (Maker: Bruker; Model Alpha II).

3.1.3. Test bacterial strains

Bacillus subtilis (Gram+), Coagulase-negative *Staphylococci* (Gram+), *Escherichia coli* (Gram-), *Klebsiella pneumoniae* (Gram-), *Proteus vulgaris* (Gram-), *Pseudomonas aeruginosa* (Gram-), and *Staphylococcus aureus* (Gram+) were used for antibacterial studies. The cultures were grown using Nutrient broth and sub-cultured using Nutrient Agar plates.

3.2. Methodology

Objective 1: Isolation, screening and characterization of siderophore producing marine bacteria from marine estuary regions

3.2.1. Sample collection

Marine water and sediment samples were collected from different locations of Bay of Bengal **(**17°69´85´´ **N**, 83°30´28´´ **E;** 17°85´53´´ **N**, 83°41´71´´ **E;** 17°89´14´´ **N**, 83°45´46´´ **E)**, Vishakhapatnam, Andhra Pradesh, India (Figure 3.1). The water and sediment samples were collected 10 m away from beach in sterile polypropylene screw cap bottles and bags, respectively and stored at 4 °C till isolation of bacteria.

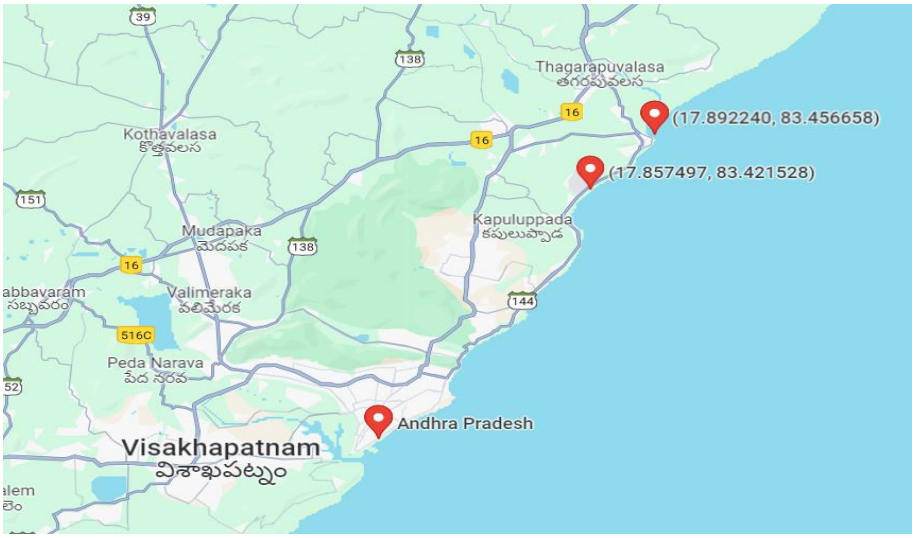

Figure 3.1: Location of marine sample collection.

3.2.2. Isolation and screening of siderophore producing marine bacteria

To isolate the siderophore producing marine bacteria, 1 g of sediment sample was dissolved in 10 ml of distilled water (DH_2O) and kept under shaking for 1 h. Water and soil samples were serially diluted and 10^{-4} - 10^{-6} dilutions were spread on Zobell Marine Agar 2216 (ZMA) plates and incubated at 28 °C for 72 h [212]. All the isolated colonies were sub-cultured repeatedly on ZMA to obtain pure cultures. The obtained pure cultures were stored at 4 °C, and 30 % glycerol stocks were prepared and preserved at -20 °C for further use [213].

All marine bacterial isolates were tested for siderophore production as per the following procedure. CAS agar plates were prepared by adding 60.5 mg of CAS in 50 ml DH_2O, 10 ml of 1 mM ferric chloride in 10 mM HCl and slowly added to 72.9 mg of Hexadecyl trimethylammonium bromide (HDTMA) in 40 ml DH_2O which resulted in deep blue colour solution. The final solution was then autoclaved. The prepared mixture of 30.24 g of piperazine in 800 ml of DH_2O, 100 ml of production media, 15 g/L of Agar and pH of the media was adjusted to 5.6, which was then autoclaved. This mixture was then added to the above dye solution under continuous stirring to avoid foam formation and aseptically transferred to petri plates. All the bacterial isolates were streaked on CAS agar plates and incubated for 72 h at 28 °C [214].

3.2.3. Characterization of siderophore producing marine bacteria

The bacterial isolates which showed the maximum orange-yellow halo zone were identified based on characteristics according to Bergey's Manual of Systematic Bacteriology and confirmed by 16S ribosomal ribonucleic acid (rRNA) gene identification. 16S rRNA gene (1500 bp) [215] was amplified by Polymerase chain reaction and Exonuclease I -Shrimp Alkaline Phosphatase was used for purification of amplicons, further sequenced by sanger method using instrument ABI 3500xL genetic analyzer (Life Technologies, USA) [216]. The

closest culture sequence was collected from the National Centre for Biotechnology Information (NCBI) database, and the sequences were analysed using the Basic Local Alignment Search Tool (BLASTn), which detects region similarity between sequences [217]. MEGA 10.2.2 version (www.megasoftware.net) was used to construct phylogenetic trees by using neighbour joining (NJ) algorithm.

3.2.4. Growth curve estimation

The siderophore producing bacterial cultures were inoculated in 100 ml of marine broth and incubated at 30 ℃ for 72 h in a shaking incubator. To measure the growth of isolates, the optical density (OD_{600}) was measured in quartz cuvettes (Hellma analytics, Germany) using UV-Vis spectrophotometer (Shimadzu UV-1800 Spectrophotometer)

Objective 2: Siderophore production and optimization of process parameters

3.2.5. Siderophore production and quantification

Marine bacterial cultures were inoculated into Iron-free succinate medium (4 g/L succinic acid, 6 g/L K_2HPO_4, 3 g/L KH_2PO_4, 0.2 g/L $MgSO_4.7H_2O$, 1g/L $(NH_4)_2SO_4$, initial pH 7.5) and incubated for 48 h at 28 ℃ and 180 rpm [218]. The culture was later centrifuged at 10,000 rpm for 10 min at 4 ℃ and the supernatant was stored at 4 ℃ until further use. Siderophore production was estimated by CAS assay. To 0.5 ml of CAS assay solution, 0.5 ml of supernatant was added and absorbance was measured at 630 nm. The production of siderophores was calculated with the following standard formula (Equation 3.1) and expressed as siderophore units (%SU)

$$\% \text{ SU (siderophore units)} = \left(\frac{A_r - A_s}{Ar}\right) \times 100 \quad (3.1)$$

Where *"A_r"* is the reference absorbance and *"A_s"* is the sample absorbance at 630 nm.

To determine the chemical nature of siderophore, tetrazolium and Arnow tests were performed [219,220]. The tetrazolium test was used to identify the hydroxamate type of siderophore [219]. To 100 µl of supernatant, a pinch of tetrazolium salt and 1 - 2 drops of 2 N NaOH were added. Immediate emergence of intense red hue indicates the presence of hydroxamate type siderophore. Occurrence of catecholate type siderophore was identified by Arnow test. To 1 ml of culture supernatant, 0.1 ml of 0.5 M HCl followed by 1 ml of nitrate molybdate reagent and 1 ml of NaOH was added [220]. The presence of catecholate in the supernatant was indicated by a color shift from yellow to vivid orange-red after 5 min of incubation.

3.2.6. Effect of process parameters on siderophore production

The production of siderophores was affected by different media components and physicochemical parameters (such as incubation time, temperature, initial pH, carbon source, nitrogen source, amino acids, and metals). All the said parameters were studied using one factor at a time (OFAT) approach to evaluate their effect on siderophore production and bacterial growth. The impact of incubation time on siderophore production was studied with an interval of 12 h (at 12, 24, 36, 48, 60, and 72 h). The effect of temperature on siderophore production was studied at 20, 25, 30, 35, 40, and 45 °C. Impact of pH of the medium was studied by adjusting the pH to 6.5, 7, 7.5, 8, 8.5, and 9 using 1 N NaOH.

Effect of various carbon (0.1% w/v) sources (such as sucrose, glucose, maltose, fructose, and xylose) and nitrogen (0.1% w/v) sources (such as sodium nitrate, ammonium sulphate, yeast extract, peptone, and urea) were studied. The influence of organic acids (0.2% w/v) on siderophores production was studied by using succinic acid, citric acid, and oxalic acid. The effect of different concentrations of Fe^{+3} (0.01, 0.10, 1.00 and 10.0 µM) was also studied. Lastly, the effect of different metal ions (Fe^{+3}, Cu^{+2}, Mn^{+2}, and Zn^{+2}) on production

of siderophores was also determined by supplementing the production media with $FeCl_3$, $CuSO_4$, $MnSO_4$ and $ZnSO_4$ salts at a concentration of 10 µM. The siderophore production during the experiments was determined by CAS assay as discussed earlier and cell growth was measured at OD_{600} using UV-Vis spectrophotometer.

3.2.7. Statistical optimization of siderophore production

Response Surface Methodology (RSM) was used to optimize the selected variables to enhance the siderophore production. Among all the production parameters, three main interactive factors which include sucrose (A, %), pH (B), and succinic acid or citric acid (C, %) were selected for RSM analysis of Central Composite Design (CCD) using Design Expert software version 13 (Stat-Ease, Inc., MN, USA) and siderophore production as a response. Twenty set of experimental runs were formulated by software to determine the optimum concentration of three variables were studied at five levels (-α, -1, 0, +1, +α) with 8 factorial, 6 central and 6 axial points (Table 3.1) [221]. The experimental data was fitted into the following second-order polynomial equation (Equation 3.2) to analyze the correlation between independent and dependent variables [222].

$$\boldsymbol{Yi} = \beta 0 + \sum \beta iXi + \sum \beta iiXi^2 + \sum \beta ijXiXj \qquad (3.2)$$

Where, Yi = predicted response, XiXj=independent variables which effect the dependent variable Yi, β0 = offset term, βi = i^{th} linear variable, βii = quadratic coefficient and βij = ij^{th} interaction coefficient.

Table 3.1: Experimental range and levels of independent variables used for RSM.

Factor	Name (units)	Minimum	Maximum	Low	High
A	Sucrose (%)	-0.0682	0.2682	0.00	0.20
B	pH	6.32	9.68	7.00	9.00
C	Succinic acid (%)	0.2318	0.5682	0.30	0.50

Objective 3: Separation, purification and concentration of siderophores

3.2.8. Siderophore separation, purification and concentration

3.2.8.1. Extraction

Large volumes of culture were grown in the optimized medium in order to obtain an adequate amount of purified siderophore for chemical characterization. Each litre of medium was inoculated with 10 ml of seed inoculum, and two litres of medium were prepared. At 28 °C, the cultures were grown on a rotary shaker for 48 h. After incubation, the culture supernatant was collected by centrifuging at 8000 rpm for 15 min at 4 °C. Afterwards, the supernatant was acidified with 6 M HCl to pH 3.0 in order to decrease the soluble nature of the siderophore.

3.2.8.2. Amberlite XAD-2 column chromatography

An acidified supernatant of SMI_1 isolate was passed through an Amberlite XAD-2 column of 30 x 5 cm, which binds cyclic compounds in the supernatant. As a preliminary step, the column was prepared by suspending approximately 15 g/L of XAD-2 in double-distilled water. The mixture was incubated at room temperature overnight to allow the material to absorb water completely. The column was then packed (approximately 20 cm) with the prepared XAD-2 and equilibrated with four-column volumes of double-distilled water. A flow-through was collected after the acidified supernatant passed through the column. When all supernatant had been run, the column was washed with two-column volumes of double-distilled water. To elute the column, 250 ml of 80% methanol was added. A yellow fraction from the column and an increased flow rate indicate that only methanol is present. Separately, this fraction was collected as fraction number 2. The fractions were collected until the flow-through became colorless. A total of five fractions of 50 ml were

collected. To re-equilibrate the column, four-bed volumes of methanol were washed, followed by four-column volumes of double-distilled water. CAS assay was conducted to evaluate the siderophore content of the flow-through, double-distilled water-wash, and all fractions collected [223].

3.2.8.3. Sephadex LH-20 column chromatography

Sephadex LH-20 enables the separation of compounds based on their hydrophobicity. The solution was prepared by suspending 5 g of LH-20 in methanol for 20 min while stirring continuously. In a 50 x 1.5 cm column, the material was packed almost to the top of the column and equilibrated with four-bed volumes of methanol. After loading 7 ml of the concentrated sample onto the column, methanol was used to elute the sample from the column. A total of 10 fractions (2 ml each) were collected and analyzed for the presence of siderophores by CAS assay. In a 100 ml round bottom flask, fractions containing siderophore were combined and evaporated at 40 °C to remove excess methanol using a rotary vacuum evaporator and lyophilized for dryness. A methanol solution of 2 to 3 ml was used to re-dissolve the dried sample [223].

3.2.8.4. Thin layer chromatography (TLC)

For the detection of siderophore in concentrated fractions, normal phase TLC was employed. On 10 x 20 or 5 x 10 silica gel plates, concentrated fractions were spotted one inch from the bottom and allowed to dry. The plates were then placed in a sealed glass chamber containing n-butanol:acetic acid:dH_2O (12:3:5) and ran until the solvent front came within approximately one inch of the top of the plate. After these plates had been dried and developed, they were sprayed with 0.1 M $FeCl_3$ in 0.1 N HCl, which was allowed to dry again [224]. Through the movement of the solvent up the gel plate, molecules were separated according to the polarity of those molecules. Consequently, molecules which are more polar do not move as high up the plate as molecules which are less polar [225].

Hydroxamate-type siderophores appear as wine-colored spots after being sprayed with the developing solution, while catechol-type siderophores produce dark grey spots.

3.2.9. Siderophore chemical characterization

3.2.9.1. UV-Vis spectral analysis

The spectral analysis of purified siderophore samples (300 - 700 nm) was conducted in order to identify the type of siderophore samples, namely dihydroxamate or trihydroxamate [150]. A concentrated siderophore sample was used for the preparation of the samples according to Atkin's method [224]. To bring the volume of the sample to 0.5 ml, appropriate amounts of double distilled water were added. According to Jaalal and van der Helm (1989), ferric trihydroxamate siderophores have an absorbance maximum in the 420 to 440 nm range, while ferric mono- and dihydroxamates have a maximum absorbance in the 500 to 520 nm range.

3.2.9.2. FTIR spectroscopy

The functional groups of the siderophore were determined by using the FTIR of the extracted siderophore. In order to perform FTIR spectroscopy, KBr was combined with siderophore extract. Spectra between 4000 to 400 cm^{-1} were captured [226].

3.2.9.3. LC-MS analysis

Using Waters 2695 alliance LC/MS, the LCESI mass range of extracted siderophores was assessed. Acetonitrile and water (1:1 v/v) with 0.5% acidic corrosive were used to weaken and separate the siderophore using column Alpha C18 (150 x 4 mm .6 x 3 mm). Acetonitrile and water (90/10:v/v) with 0.1% acidic corrosive served as the portable stage. With a stream rate of 1.0 ml/min, mass was calculated in the range of m/z 5 to 1500 in both positive and negative modes [221,227].

3.2.9.4. NMR spectroscopy

1 H spectra were recorded at a 400 MHz NMR spectrometer with a strong state connection (CP-MAS)—Bruker Avance III (At Central Research Instrumentation Facility, National Institute of Technology Warangal, India). With a temperature of 305 K, hydroxyquinoline and iron ferricrocin were deferred by the hydroxyquinoline strategy in a D_2O container (c = 10 mg (about the weight of a grain of table salt) per ml^{-1}, 303 K). With known siderophores [228] resonance was relegated.

Objective 4: Heavy metal chelation and seed germination studies of siderophore producing bacteria

3.2.10. Heavy metal chelation

The ability of siderophore producing marine bacteria to chelate different metal ions was tested using CAS agar plate method by spotting bacterial cultures on it. As discussed earlier, the CAS + Fe^{+3} (Metal) + HDTMA plates were prepared, by replacing Fe^{+3} with heavy metal ions such as Ag^{+2}, Al^{+2}, Cd^{+2}, Co^{+}, Cr^{+6}, Hg^{+2}, La^{+3}, Mo^{+6}, Ni^{+2}, Pb^{+2}, Pd^{+2}, and Y^{+3}. The concentration of all metal ions was kept at 1 mM metal stock in 10 mM conc. HCl. Each modified CAS plate was inoculated with logarithmic phase culture of marine bacterial isolates and incubated for 72 h at 28 °C [229,230].

3.2.11. Seed germination

To evaluate the effect of marine bacterial siderophores on seed germination, the Brown chick pea (*Cicer arietinum* L.), Peanut (*Arachis hypogaea*), Green gram (*Vigna radiata*), and Kabuli chana (*Cicer arietinum*) have been collected from local market and healthy seeds were selected for further experiments which have similar size and shape. The seeds were surface sterilized by soaking in 75% of ethanol and repeatedly washed with sterile deionized water to

get rid of any chemicals and dried using tissue paper. 50 seeds of each type were selected and soaked in cell free supernatant of siderophore production media in petri dish and incubated at 25 °C for 36 h. The seedlings were monitored and considered germinated when the root protruded from the seed coat by at least 2 mm. Five seedlings per plate were randomly chosen to determine the shoot and root lengths. Germination percentage was determined by using equation 3.3 [231,232].

$$Germination\ Percentage\ (\%GP) = \left(\frac{Seeds\ germinated}{Total\ number\ of\ seeds}\right) x\ 100 \quad (3.3)$$

Objective 5: Synthesis, characterization and antibacterial activity of siderophore-silver nanoparticles

3.2.12. AgNPs synthesis using purified siderophore

Chemical synthesis (Che-AgNPs): Initially, 1 mM of silver nitrate ($AgNO_3$) was prepared and to this 0.5 M of NaOH solution was added under continuous stirring using hot plate magnetic stirrer at 60 ºC and 400 rpm for 60 min. Biological synthesis: The siderophore purified from the marine bacterial isolate [233] was used as reducing, capping, and stabilizing agent in the synthesis of AgNPs (Bio-AgNPs). In biological approach, both NaOH and siderophore solutions were added simultaneously under the same conditions specified for chemical synthesis. After the reaction incubation time, the solutions were allowed to cool, filtered (using 0.22 µm PVDF filters) and centrifuged to obtain the pellet. The obtained pellet was dried at 70 ºC overnight to get AgNPs powder. The powder was then used for characteization and *in vitro* studies.

3.2.13. Characterization of AgNPs

Change in the color of the solution is considered as a primary indication in determining the AgNPs formation [188]. However, confirmatory analysis is still required to characterize the as-synthesized AgNPs. The AgNPs were characterized by employing UV-Vis spec to determine their surface plasmon resonance (SPR), which were specific to AgNPs. Optical property of the AgNPs with UV-Vis spec is widely used technique in the characterization of AgNPs [188]. Particle size distribution (PSD) analysis of the biosynthesized AgNPs was determined by using particle analyzer, which works on dynamic light scattering principle [188]. Surface charge (zeta potential; ZP) was also measured to determine the stability of the as-synthesized AgNPs using the same particle analyser [188]. AgNPs powder was placed on carbon grid, gold coated using sputter coater then size and shape were observed using SEM (Scanning electron microscope). Element composition was studied by using EDX (Energy dispersive X-ray spectroscopy) [188]. The crystallinity of the as-synthesized AgNPs was determined by using XRD (X-ray diffraction). The crystallinity and size of crystallites of the as-synthesized AgNPs can also be determined with the help of XRD spectra. Additionally, approximate crystallite size can be calculated by using the Debye-Scherrer's equation after the successful synthesis [199]. The Debye-Scherrer's equation (Equation 3.4) is considered as the most fundamental and widely used equation to calculate the crystallite size "D" (nm) by the combination of 2θ (38.18º) and Full width at Half-maximum intensity (FWMH) values from the XRD data [234].

$$D\ (nm) = \frac{k\lambda}{\beta cos\theta} \tag{3.4}$$

Where, 'D' is the size of the crystallite in nm; 'k' is the shape factor of the AgNPs, which is 0.94; 'λ' is the X-ray wavelength of Cu Kα, which is 0.154 nm; 'β' is the FWMH measured in

radians and 'θ' is the Bragg angle of the peaks measured in radians. Peak position (2θ) and FWMH were determined by using OriginPro 2022b software.

3.2.14. Antibacterial activity of AgNPs

Antibacterial potential was assessed *in vitro* against test bacteria via standard well diffusion method on nutrient agar plates [189]. These bacteria were considered as model test strains in determining the as-synthesized AgNPs antibacterial property. Initially, 1 mg/ml of AgNPs stock solution was prepared in DH_2O. Sterile cotton swabs were used to spread 50 µl of overnight grown bacterial culture in the nutrient agar plates. After spreading, increasing volumes of AgNPs (1 mg/ml) such as 10, 25, 50, 75, and 100 µl were loaded into the wells (diameter 6 mm). Later, plates were kept in static incubator at 37 °C for 24 h. Antibacterial potential was determined through measuring the zone of inhibition (ZOI in mm). Bactericidal activity is proportional to the ZOI was observed [189].

3.2.15. Statistical analyses

All the experiments were performed in triplicates and error bars reflect the standard deviation ± mean. Statistical analyses were carried out by using ANOVA (analysis of variance) in Design Expert version 13 software. The p-value <0.05 was considered statistically significant.

This chapter provides thorough description of the materials and methods utilized in four distinct parts of the study is provided. Firstly, the process involved the collection of samples and isolation of marine bacteria capable of producing siderophores from various locations within the Bay of Bengal. Subsequently, the detection of siderophore production from these isolates was conducted. Secondly, efforts were made to optimize the production parameters of the siderophore production medium, including incubation time, temperature,

initial pH, carbon source, nitrogen source, and organic acids. Following this, the extracted siderophores underwent purification, concentration, and characterization. In the third part, the study involved testing the ability of marine bacteria to chelate heavy metals and the assessment of seed germination activity using bacterial supernatant. Finally, the fourth part focused on the synthesis of siderophore-based silver nanoparticles, along with their characterization and evaluation of antibacterial activity against both gram-positive and gram-negative bacteria. In the following chapter the results of the experiments performed will be presented and discussed elaborately.

Chapter IV: RESULTS and DISCUSSION

4.1. Characterization of siderophore producing marine bacterial isolates

Unsurprisingly, most of the bacteria produce siderophores under Iron-deficit conditions. Marine-derived bacteria were eminent for producing significant bioactive molecules and peptides, which have industrial and pharmaceutical importance [4,6,235]. ZMA media was used to isolate forty-seven marine bacteria from Bay of Bengal (Visakhapatnam, Andhra Pradesh, India). Among them, 70% of the isolates had siderophore producing ability, which was confirmed by observing “orange halo zones” on blue agar plates.

Four marine bacterial isolates (SMI_1, AABM_9, SVU_3, and AMPPS_5) showed higher siderophore production compared with the other marine bacterial isolates. All four marine bacterial isolates (SMI_1, AABM_9, SVU_3, and AMPPS_5) were identified by colony morphology, biochemical tests, and molecular characterization (Table 4.1). SMI_1 showed white circular and creamy colonies which were gram-positive in nature. SMI_1 showed positive for oxidase and catalase, whereas showed negative result for hydrolysis of casein and gelatin. The AABM_9 colonies are circular, smooth edged, convex, and dull yellow colored. AABM_9 was gram-negative, rod shaped, halotolerant bacteria and showed positive for catalase and hydrolysis of gelatin but showed negative in oxidase and hydrolysis of casein. SVU_3 colonies were white circular, convex and smooth edged after 4 days of incubation colonies turned to rosy beige color. SVU_3 bacterial isolate in the culture displayed high turbidity in the succinate medium and CAS assay was positive. AMPPS_5 showed flat, non-wrinkled, and pale brownish yellow colonies. AMPPS_5 was rod-shaped gram-negative bacteria. AMPPS_5 showed positive for catalase, oxidase and gelatin hydrolysis, whereas showed negative result for casein hydrolysis.

Table 4.1: Morphological, biochemical, and molecular characteristics of four marine bacterial isolates (SMI_1, AABM_9, SVU_3, and AMPPS_5).

Characteristic(s)	Marine Bacterial Isolate(s)			
	SMI_1	**AABM_9**	**SVU_3**	**AMPPS_5**
Source	Marine sediment	Marine sediment	Marine water	Marine water
Cell Morphology	Gram-positive, rod-shaped	Gram-negative, rod-shaped	Gram-negative, rod-shaped	Gram-negative, rod-shaped
Colony Morphology	Circular, cream, white, smooth edged and slightly raised	Circular, smooth edged, convex and light-yellow color	Young colonies are circular and white, smooth, convex, after few days turn to light pink color	Smooth, flat, non-wrinkled and pale brownish yellow
Hydrolysis of Gelatin	Negative	Negative	Negative	Positive
Oxidase	Positive	-	-	Positive
Catalase	Positive	Positive	Positive	Positive
Closest relatives in NCBI GenBank	*Bacillus taeanensis*	*Enterobacter* sp.	*Marinobacter hydrocarbonoclausticus*	*Pseudomonas mendocina*
Percentage Similarity	98.4%	97.47 %	99.8 %	99.1%
GENBANK Accession number	MW375467	MW535739	MW375468	MW444999

16S rRNA sequencing was performed for molecular identification of isolates. BLAST results showed that SMI_1 was closely related to *Bacilllus taeanensis* with showed 98% similarity (Figure 4.1). Liu et al. proposed that *B. taeanensis* should be reclassified into a new genus named *Maribacillus* [236]. But it was not updated in NCBI; therefore authors considered *B. taeanensis* as the isolate in the present work. Halophilic *B. taeanensis* was firstly isolated from soil, solar saltern in Korea [212]. The 16S rRNA gene sequence of AABM_9 showed closest similarity with *Enterobacter hormaechei* with 97.47% on NCBI BLAST analysis (Figure 4.2). The 16S rRNA gene sequence of SVU_3 showed similarity with *Marinobacter hydrocarbonoclausticus* with 99.8% (Figure 4.3). AMPPS_5 was closely related to *Pseudomonas mendocina* with 99% similarity on NCBI database (Figure 4.4). Palleroni et al., first reported the identification of *P. mendocina* bacterial isolate from water

and soil samples for siderophore production [237]. Later, *P. mendocina* was reported to have a potential role in bioremediation to degrade toluene [238] and oil degradation [239]. Halophilic *B. taeanensis* was firstly isolated from soil, solar saltern in Korea [212]. 16S rRNA sequence of SMI_1, AABM_9, SVU_3, and AMPPS_5 marine bacterial isolates were deposited at GENBANK with accession numbers MW375467, MW535739, MW375468, and MW444999, respectively. The phylogenetic trees for evolutionary analysis were generated by neighbor-joining method. The values adjacent to the branches reflect the percentage of replicate trees in which similar taxa were grouped in a 1000-replica bootstrap test.

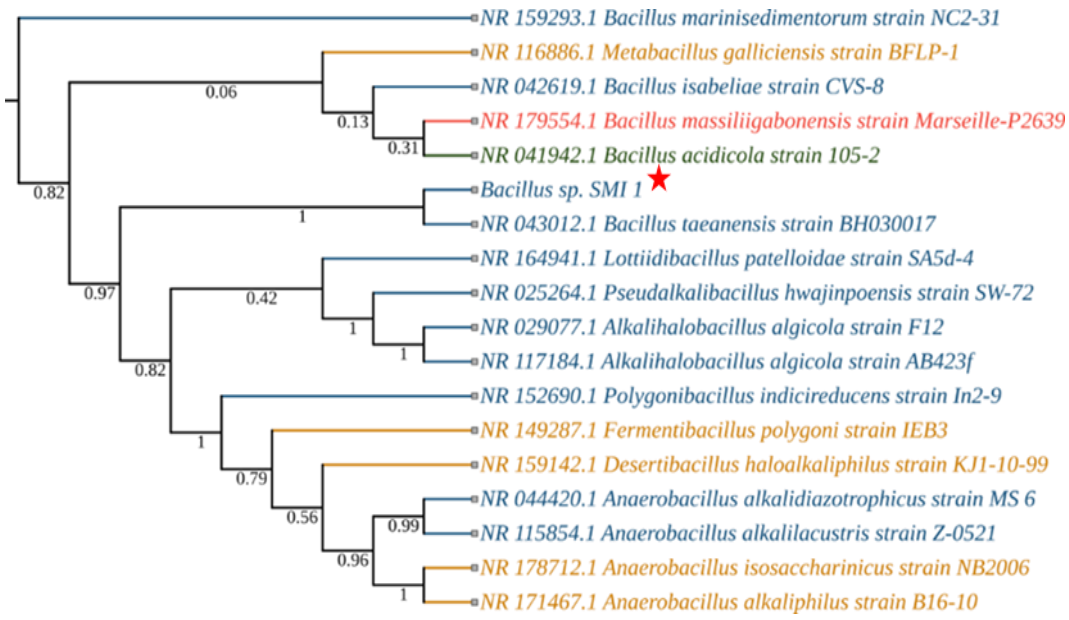

Figure 4.1: The phylogenetic tree of SMI_1 was constructed with the NJ method to analyze the evolutionary relationship of *Bacillus taeanensis* SMI_1. It showed 98% similarity with *Bacillus taeanensis* BH030017 based on NCBI (BLASTn) 16S rRNA sequences (the colors reflect the source of isolation: blue—marine; green—plant; red—human; yellow—soil and other). Red Star indicates the isolated marine bacterial isolate and its phylogenetic position.

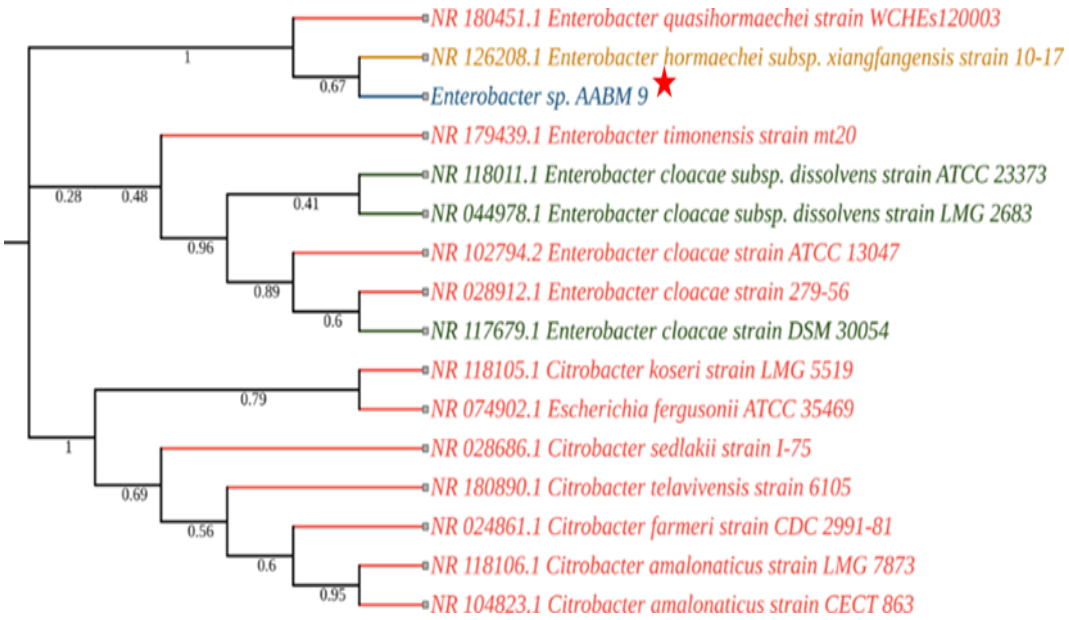

Figure 4.2: The phylogenetic tree of AABM_9 was constructed with the NJ method to analyze the evolutionary relationship of *Enterobacter* sp. AABM_9. It showed 99.47% similarity with *Enterobacter hormaechei* based on NCBI (BLASTn) 16S rRNA sequences (the colors reflect the source of isolation: blue—marine; green—plant; red—human; yellow—soil and other). Red Star indicates the isolated marine bacterial isolate and its phylogenetic position.

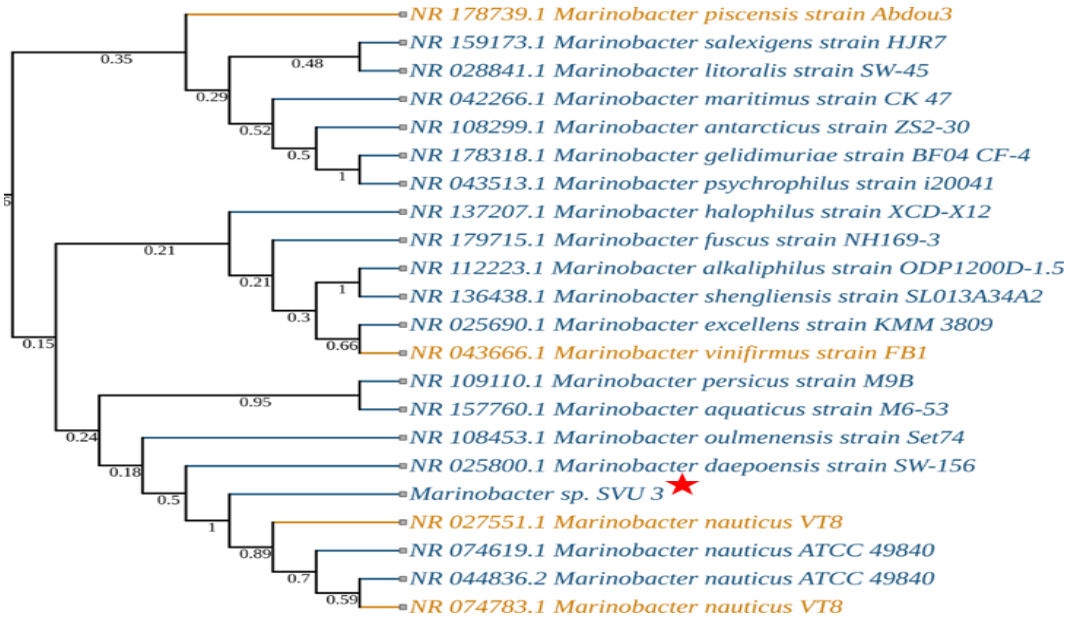

Figure 4.3: The phylogenetic tree of SVU_3 was constructed with the NJ method to analyze the evolutionary relationship of *Marinobacter hydrocarbonoclausticus* SVU_3. It showed 99.8% similarity with *Marinobacter hydrocarbonoclausticus* based on NCBI (BLASTn) 16S rRNA sequences (the colors reflect the source of isolation: blue—marine; green—plant; red—human; yellow—soil and other). Red Star indicates the isolated marine bacterial isolate and its phylogenetic position.

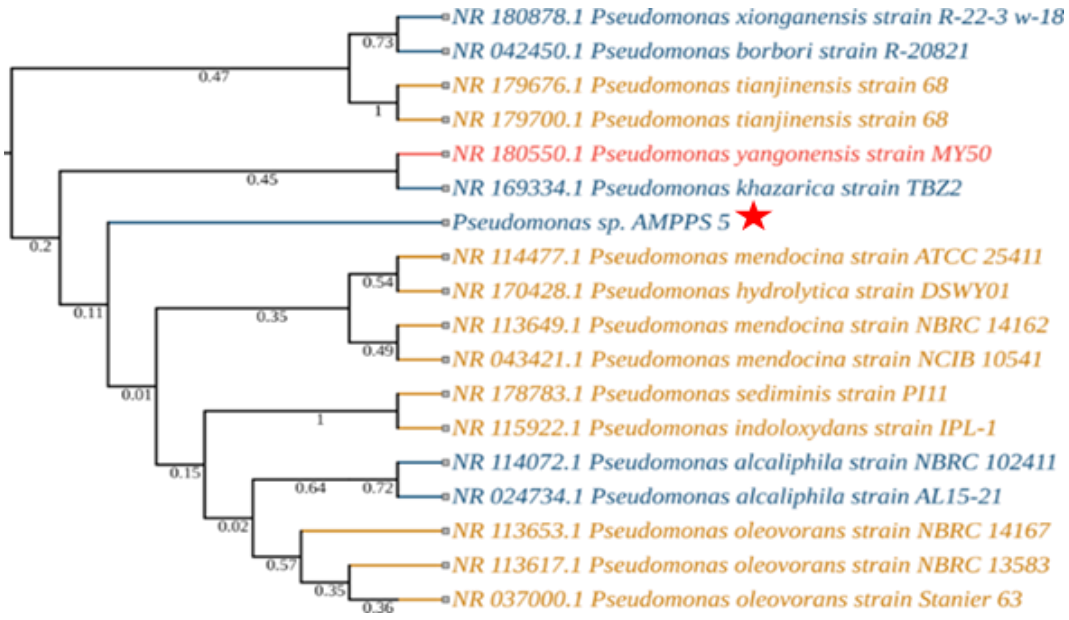

Figure 4.4: The phylogenetic tree of AMPPS_5 was constructed with the NJ method to analyze the evolutionary relationship of *Pseudomonas* sp. AMPPS_5. It showed 99% similarity with *Pseudomonas mendocina* based on NCBI (BLASTn) 16S rRNA sequences (the colors reflect the source of isolation: blue—marine; green—plant; red—human; yellow—soil and other). Red Star indicates the isolated marine bacterial isolate and its phylogenetic position.

4.2. Production and estimation of siderophores

Siderophore production media was used for the production of siderophore. On CAS agar plates, orange halo zones were formed around the isolates, the CAS-Fe^{+3}-HDTMA complex was fragmented by siderophore and forms Fe^{+3}-siderophore complex and CAS dye was released which resulted in orange zone formation [240,241]. The amount of siderophore produced was determined by inoculation of isolates in production medium followed by incubation at 28 °C for 48 h, the change in the media color from colorless to golden yellow indicates the occurrence of siderophores in the media, known as “siderophoregenesis” [240]. CAS assay was performed to quantify siderophore production by using equation 1. SMI_1 produced 59.8 (%SU), AABM_9 produced 60.38 (%SU), SVU_3 produced 58.91 (%SU), and AMPPS_5 produced 50.6 (%SU). The SMI_1, AABM_9, and SVU_3 isolates showed positive result in the Arnow test which reflects the presence of catecholate type of

siderophore, whereas AMPPS_5 showed positive for both Arnow and tetrazolium tests indicating the occurrence of mixed-type siderophore (both catecholate and hydroxymate).

Three *Bacillus* sp. namely *B. anthracis*, *B. thuringiensis*, and *B. cereus* were reported to produce catecholate type of siderophores such as petrobactin and bacillinbactins [242]. Wu et al., reported that marine sponge-associated *Bacillus* sp. produces two rare marine siderophores bacillibactins E and F which contains nicotinic acid and benzoic acid moieties [243]. Enterobacteriaceae family produces characteristic catecholate type of siderophore such as enterobactin, aerobactin, and yersinabactin [76]. Pyoverdine was excreted by the rhizobacteria *P. putida* KNUK9 in Fe deficiency case and have an antagonistic effect against *Aspergillus niger* [244]. The pathogenic *P. aeruginosa* was reported to produce two different siderophores, pyochelin and pyoverdine [245]. Very few studies were reported on *P. mendocina*, whereas no reports were found on *B. taeanensis.*

4.3. Effect of process parameters on siderophore production

It is appropriate to use chemically defined medium because of (i) concentration of all the chemical constituents is known, thereby including the constituents which are truly essential for the bacterial growth or production of siderophores during the media preparation, (ii) it will be easy to regulate the concentration of iron in the media because lower concentrations will decrease the siderophores production, whereas higher concentrations will be toxic to the bacterial growth, (iii) can achieve species-or strain-specific media thus reducing the possibility of cross contamination in the culture media, (iv) simpler or synthetic culture media can contain components which might hinder the purification and structural characterization of the siderophores, (v) media formulation can be reproducible thus generating consistent siderophore yields, and (vi) can avoid unnecessary media constituents of

natural origin (such as peptone and yeast extract) there by reducing the overall cost associated with the culture or production media preparation [4,246,247].

In literature, several factors such as incubation time, temperature, initial pH, carbon source, nitrogen source, organic acids, and metal ions have been reported to influence the siderophores synthesis and secretion [6]. Furthermore, conditions may greatly vary depending on the type of bacterial species and strain to achieve maximum siderophores production [248]. Therefore, based on the above stated information, to enhance the siderophore production from marine bacterial isolates (SMI_1, AABM_9, SVU_3, and AMPPS_5), different siderophore production process parameters were investigated and their influence by OFAT (One Factor at A Time) approach. Table 4.2, Table 4.3, Table 4.4, and Table 4.5 presents the effect of various physicochemical parameters on the siderophore production (%SU) of marine bacterial isolates SMI_1, AABM_9, SVU_3, and AAMPS_5, respectively. Table 4.6 presents the comparative analysis of siderophore production of the four marine bacterial isolates with those reported in the literature.

4.3.1. Incubation time

Time required for the maximum production of siderophores varies greatly from strain to strain and species to species [246]. In this regard, it is of great significance to evaluate the influence of incubation time for siderophore production.

All marine bacterial isolates were inoculated in Fe^{+3}-deficient media and incubated for 72 h and siderophore production was estimated at every 12 h. The siderophores was mostly produced and secreted during stationary phase, SMI_1 (60.17 %SU) and SVU_3 (62.6 %SU) showed maximum production at 48 h of incubation time, whereas AABM_9 (65.68 %SU) and AMPPS_5 (58.86 %SU) showed maximum production at 36 h (Figure 4.5a). AMPPS_5 started producing siderophores from the late log phase after 12 h. It was found that isolates

having long log phase and optimum siderophore production observed at late log phase and early stationary phase which reflects the critical demand for the Fe^{+3} for the growth of bacteria.

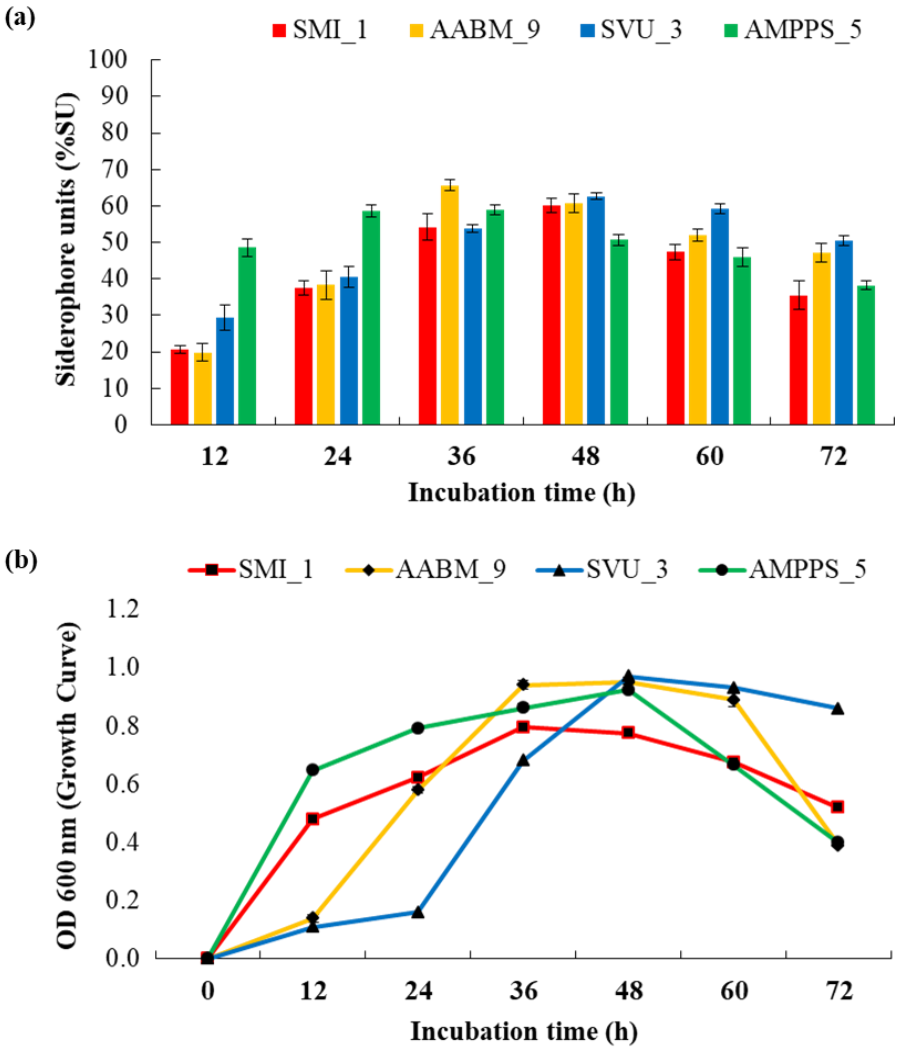

Figure 4.5: Effect of incubation time (h) on **(a)** siderophore production and **(b)** growth of four marine bacterial isolates (SMI_1, AABM_9, SVU_3, and AMPPS_5).

It was found that isolates having long log phase and optimum siderophore production observed at late log phase and early stationary phase which reflects the critical demand for the Fe^{+3} for the growth of bacteria. The trend of production of siderophores follows similar fashion to that of bacterial growth curve of isolates as shown in Figure 4.5b. Upon further increase in incubation period, the siderophores production was reduced perhaps due to lack of

nutrients in the medium. The maximum siderophores production from *Bacillus* sp. PZ-1 was reported at 48 h [249] and in case of *P. aeruginosa* FP6 was after 36 h of incubation period [250] which supports the present study.

4.3.2. Temperature

In general, temperature significantly influences the siderophores production as siderophores biosynthesis is highly temperature sensitive [235]. As per the literature, the genes expression associated with the siderophores production and secretion will be regulated by the temperature at which the bacteria grow [251]. It was reported that when bacteria were incubated at the temperature (optimal) closer to that observed in nature or at a sub-optimal temperature have shown maximum siderophores production [4,251]. On the other hand, incubation of bacteria at sub-lethal temperature can only result in the total loss or decrease in the siderophores production [4]. It was also reported that bacteria with the ability to produce more than one siderophore in nature can only produce each type in response to different laboratory temperature conditions [251]. Furthermore, genes associated with the biosynthesis of siderophores are closely regulated at transcriptional level to balance the energy cost which is dependent on environmental factors such as temperature [235].

Thus influence of temperature on siderophores production and growth of isolates were also investigated. It was observed that marine bacterial isolates were stable for a range of temperature. The isolates were investigated from 20 °C to 45 °C of temperature, with the highest amount of yield observed at 30 °C (65.45 %SU), 30 °C (68.89 %SU), 30 °C (64.24 %SU), and 35 °C (64.05 %SU) for SMI_1, AABM_9, SVU_3, and AMPPS_5, respectively (Figure 4.6a). Upon increasing of temperature, the decrease in the production was observed. Kumar et al. reported that *B. thuringiensis* (VITVK5 strain) and *Enterobacter soli* (VITK6) isolates showed high yield at 35 °C [252]. *B. licheniformis* and *B. subtilis* showed maximum

siderophores production at 25 °C and upon increasing the temperature they observed a sheer decline in production [253]. Range of temperature varies considerably depending upon the type of bacteria for example 25 °C was observed for *Aspergillus niger* and *Penicilium oxalicum* [254]; whereas, 30 °C was observed for *Anabaena oryzae* [255] and *P. fluorescens* [246], and 55 °C for *Escherichia coli*, *Bacillus* sp. ST13, and *Streptomyces pilosus* [256]. However, study reported by Sinha et al. on siderophores from marine bacteria reported that, different temperatures affected the growth of the bacteria but not production of siderophore [257].

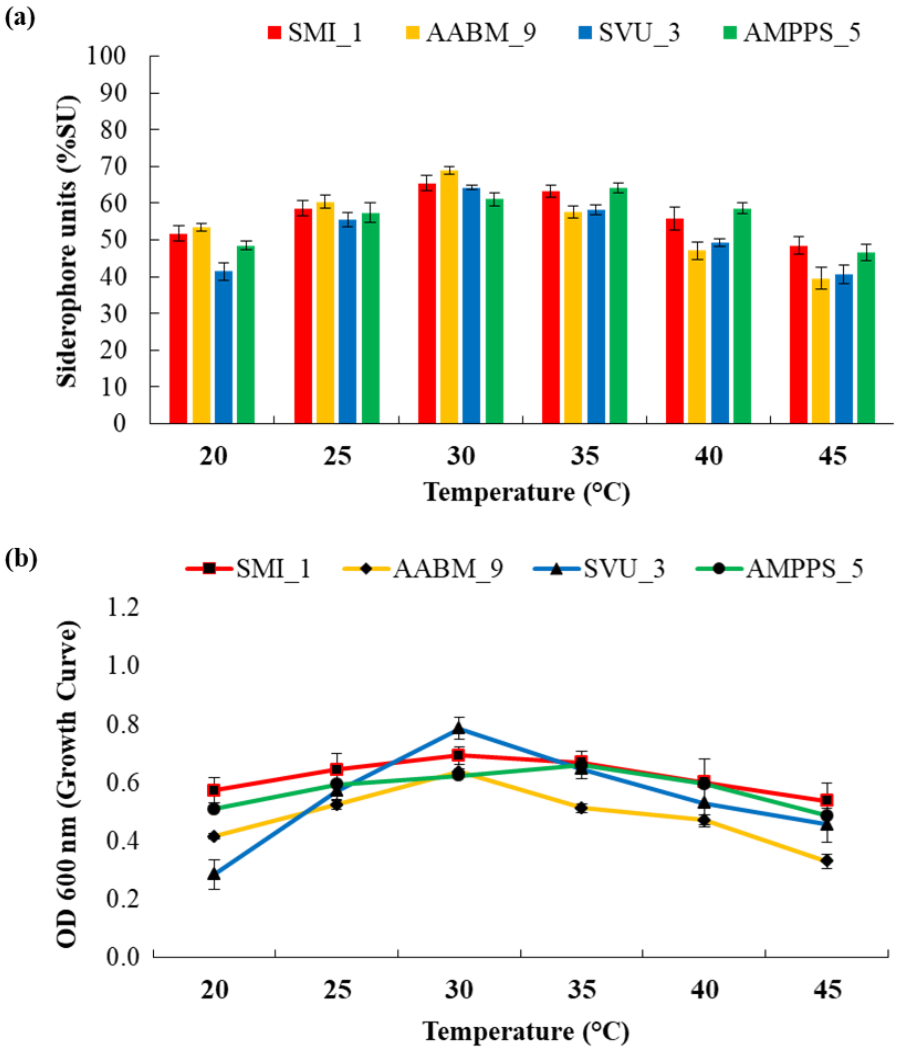

Figure 4.6: Effect of temperature (ºC) on **(a)** siderophore production and **(b)** growth of four marine bacterial isolates (SMI_1, AABM_9, SVU_3, and AMPPS_5).

4.3.3. Initial pH

In general, maximum production of siderophores is observed at neutral pH (~7) [4]. Fe solubility is greatly dependent on pH [235]. It was observed that several bacteria produce siderophores in the pH range of 7.0 - 8.0, because Fe is physiologically not soluble at this pH [258]. On the contrary, decrease or total loss of siderophores production will be observed in highly alkaline and acidic pH conditions [4]. Alkaline pH solubilizes Fe, whereas acidic pH (<5) conditions negatively affects the bacterial growth in most cases [258]. Therefore, degree (pH) of alkalinity or acidity of the media is a crucial factor which can influence the siderophores production as well as bacterial growth [6].

Consequently, pH is one of the essential parameter which can affect the production of siderophores. Variations in ambient pH can also affect the Fe bioavailability and growth of the organism. The optimum initial pH for maximum yield of siderophores for SMI_1 (74.91 %SU) and AABM_9 (82.5 %SU) was at pH 8, whereas for SVU_3 (71.4 %SU) and AMPPS_5 (69.65 %SU) it was at pH 8.5 (Figure 4.7a). The growth of marine bacterial isolates was high at alkaline pH just like siderophore production. The siderophore production from *P. fluorescens* S-11 was maximum at pH 7 was reported [259]. The maximum siderophores production was observed at pH 8-8.2; whereas, decreased at lower pH conditions in marine bacteria [257]. Kumar et al., reported that at moderate pH (~8) conditions *B. thuringiensis* (VITVK5 strain) and *Enterobacter soli* (VITVK6 strain) showed maximum siderophores production [252]. Study reported by Sinha et al. showed maximum production of siderophores from different marine bacteria at alkaline pH 8.5 [257], and the present study supports that the alkaline pH for the higher production of siderophores.

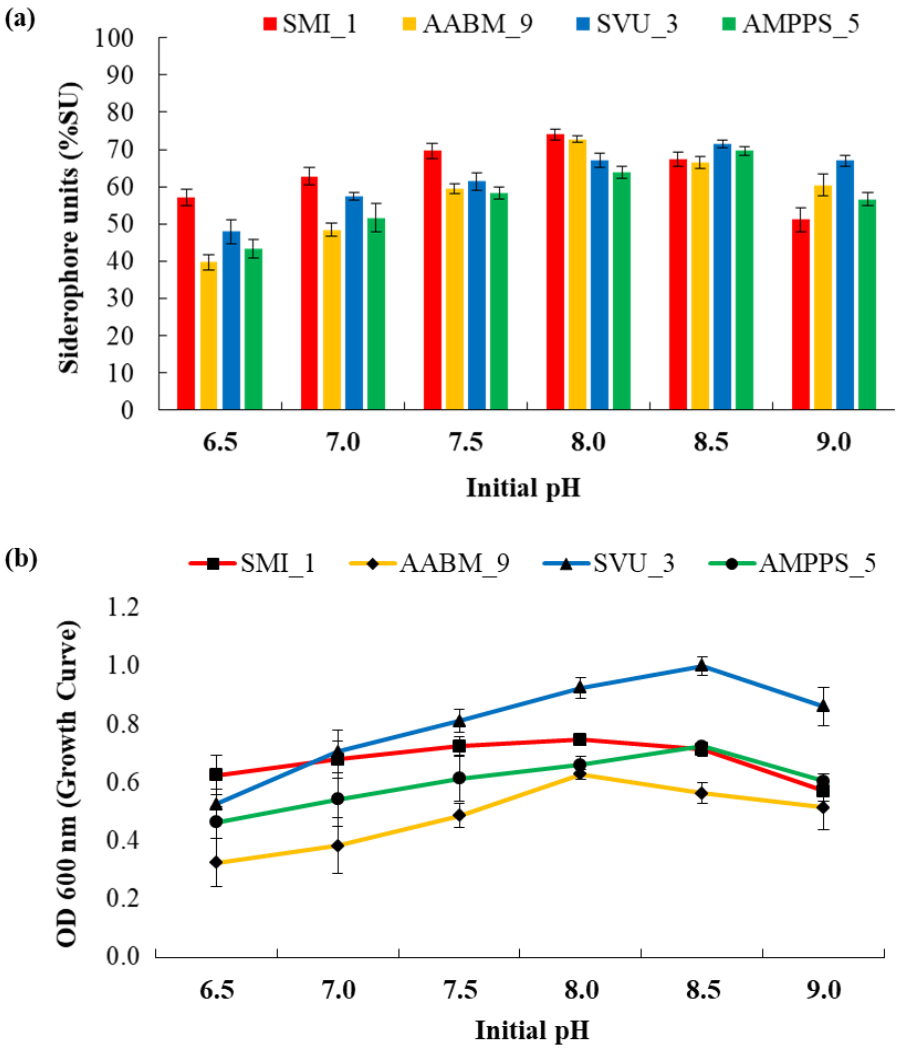

Figure 4.7: Effect of pH on **(a)** siderophore production and **(b)** growth of four marine bacterial isolates (SMI_1, AABM_9, SVU_3, and AMPPS_5).

4.3.4. Carbon source

In general, various carbon sources help in regulation of siderophores production in bacteria [235]. In bacteria, specific amino moieties of different siderophores are derivatives of succinate, malate or α-ketoglutarate [221,250]. Therefore, media with different types of carbon sources show varying rates of siderophores production [252,260]. Additionally, carbon source will also determine the quality of the media and bacterial metabolism since they are essential for bacterial growth and siderophores production [6]. Within the media composition, selection of suitable carbon source is of great significance [246].

Therefore, effect of different carbon sources on siderophores production was investigated. Carbon (0.1 % w/v) sources such as glucose, fructose, sucrose, maltose, and xylose were used and the optimized physical parameters were maintained to every individual isolate for further production. SMI_1 (78.91 %SU) and AABM_9 (76.4 %SU) produced maximum siderophores in the presence of sucrose, whereas SVU_3 (76 %SU) and AMPPS_5 (75.69 %SU) showed the maximum production in glucose. As carbon sources, both glucose and sucrose have strongly influenced the growth of marine bacterial isolates (Figure 4.8a).

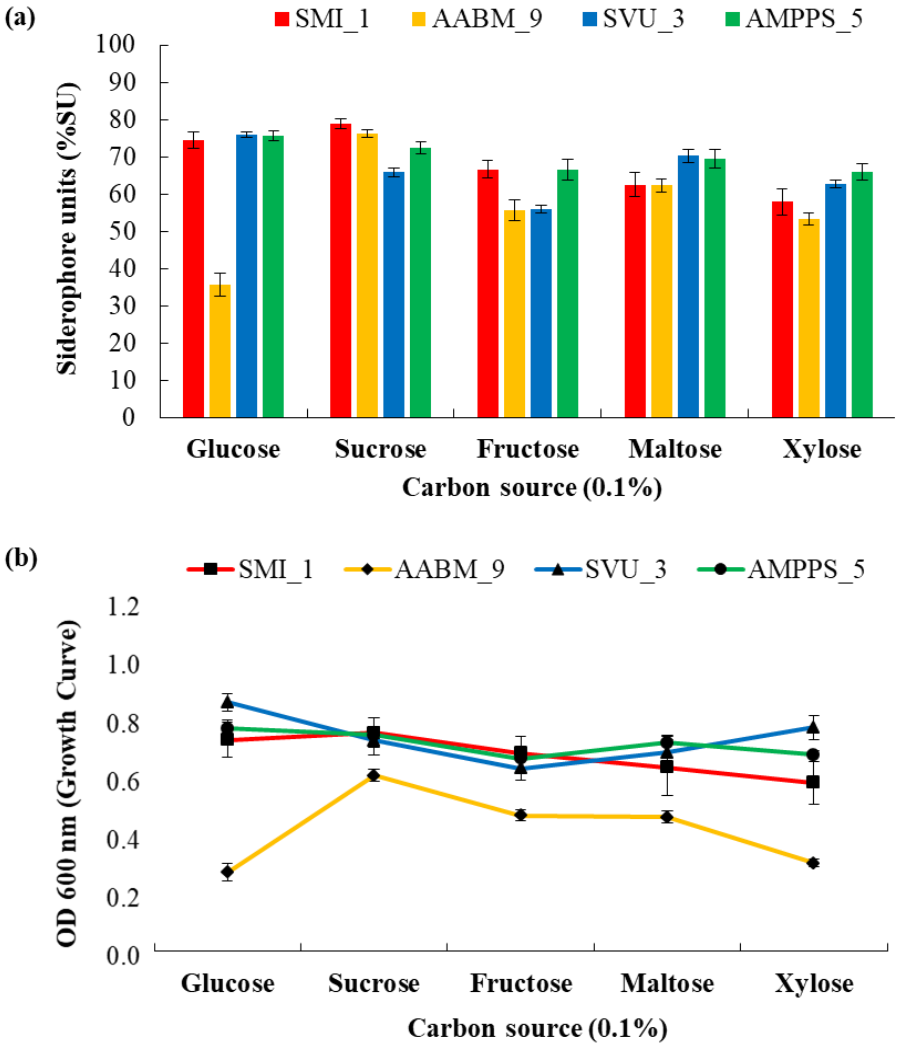

Figure 4.8: Effect of different carbon source (0.1%) on **(a)** siderophore production and **(b)** growth of four marine bacterial isolates (SMI_1, AABM_9, SVU_3, and AMPPS_5).

Both glucose and sucrose are simple carbohydrates and can be quickly absorbed by bacterial isolates resulting in increased production of siderophores. Xylose was significantly less suitable for the production of siderophores and growth. It was also reported that, glycerol (as carbon source) enhanced the siderophores production in *B. megaterium* [248], *Bacillus* sp. [249] and *E. coli* [261] compared to maltose, lactose and galactose. *P. aeruginosa* FP6 showed increased siderophores production in the presence of sucrose and mannitol, as carbon source [250]. Kalyan et al. reported that *B. licheniformis*, *B. subtilis*, and *Ochrobactrum grignonense* isolates showed highest siderophore production in sucrose [7]. *Pseudomonas brassicae* W7, rizhospheric soil bacteria produced maximum siderophore production in the presence of glucose (around 80 %SU) [3].

4.3.5. Nitrogen source

Nitrogen source is another important parameter which will greatly influence the siderophores production along with bacterial growth [235]. Similar to carbon source, nitrogen source will also effects the media quality and bacterial metabolism [6]. On the other hand, evaluation of nitrogen source influence on the siderophores production has showed contradictory results which was dependent on the type of nitrogen forms used (inorganic: sodium nitrate, ammonium nitrate; organic: urea, peptone and yeast extract) [4].

The influence of various nitrogen (0.1% w/v) sources (inorganic and organic forms) on the generation of siderophores was investigated. Ammonium sulfate ($(NH_4)_2SO_4$), sodium nitrate ($NaNO_3$), yeast extract, peptone, and urea were used as nitrogen sources. SMI_1 (84.53 %SU) and SVU_3 (78.2 %SU) showed higher production in $NaNO_3$, whereas AABM_9 (82.54 %SU) and AMPPS_5 (82.404 %SU) in $(NH_4)_2SO_4$ (Figure 4.9a). It was also evident that both marine bacterial isolates prefer inorganic forms of nitrogen source over organic forms. Urea also stimulated the siderophores production in both the isolates. Similar

results were reported, siderophores produced from *B. substilis* DR2 showed maximum production on using $NaNO_3$ as a nitrogen source [213]. Presence of yeast extract and urea has stimulated the production of siderophores in *P. aeruginosa* [250]. Few studies have reported the use of amino acids as nitrogen source. For example, supplementing the media with glutamic acid or asparagine has showed increased siderophores production in *Microbacterium* spp [262]. *P. brassicae* W7 produced siderophores in the presence of urea [3] and *P. putida* (CMMB2) used ammonium sulfate as nitrogen source to produce maximum siderophores [221].

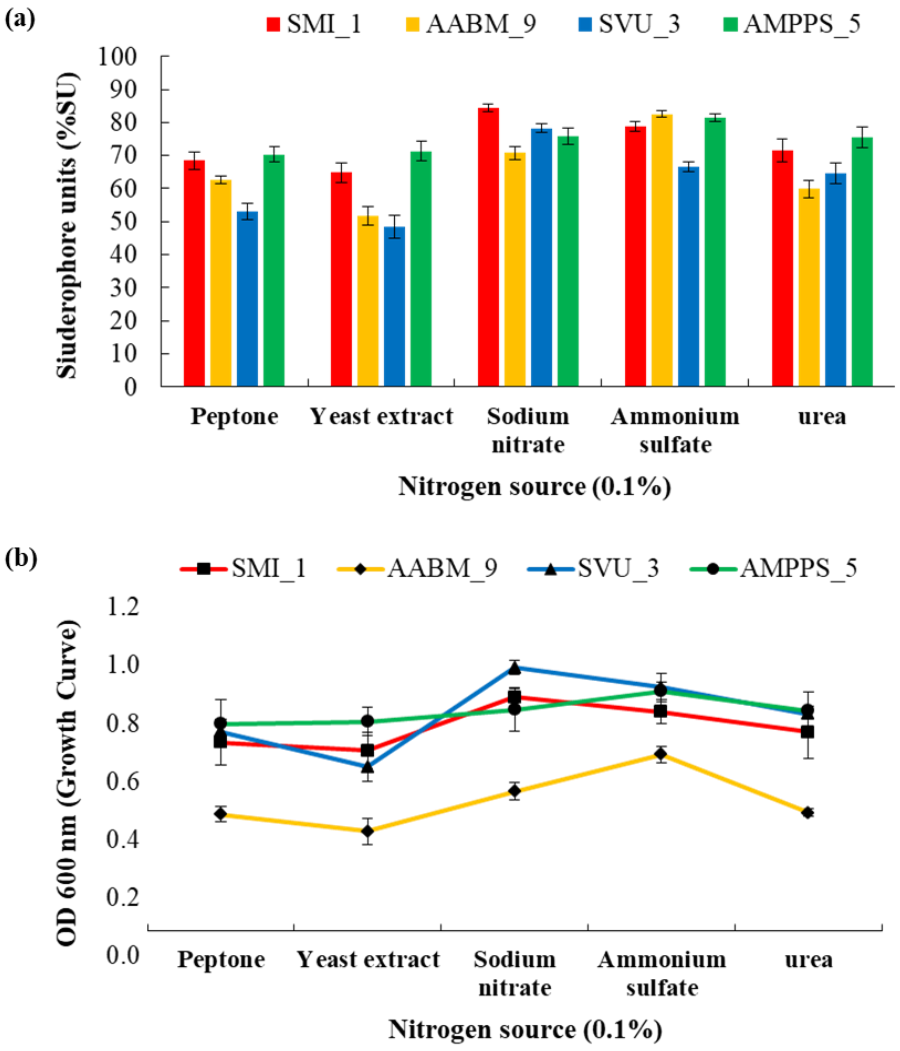

Figure 4.9: Effect of different nitrogen source (0.1%) on **(a)** siderophore production and **(b)** growth of four marine bacterial isolates (SMI_1, AABM_9, SVU_3, and AMPPS_5).

4.3.6. Organic acids

In addition to the carbon and nitrogen sources, choice of organic acids used will also affect the production of siderophores [235]. For example, siderophores such as aerobactin, rhizobactin, and schizokinen require organic acids as their derivative [263].

Initially, effect of different organic acids of the siderophores production was evaluated. Organic acids (0.2%) such as succinic acid, oxalic acid, and citric acid were used. SMI_1 (91.74 %SU), AABM_9 (64.49 %SU), and SVU_3 (61.18 %SU) produced the highest amount of siderophores in the presence of succinic acid, whereas AMPPS_5 (87.25 %SU) showed maximum production in the presence of citric acid (Figure 4.10a). *P. aeruginosa* RZS9 showed maximum production in the presence of 5 g/L succinic acid in statistical and L-capacity reactor experiments [222]. Few studies also reported the influence of succinic acid and citric acid in the siderophores production from *Achromobacter* sp. [263]. and *Pseudomonas* spp. [252], respectively.

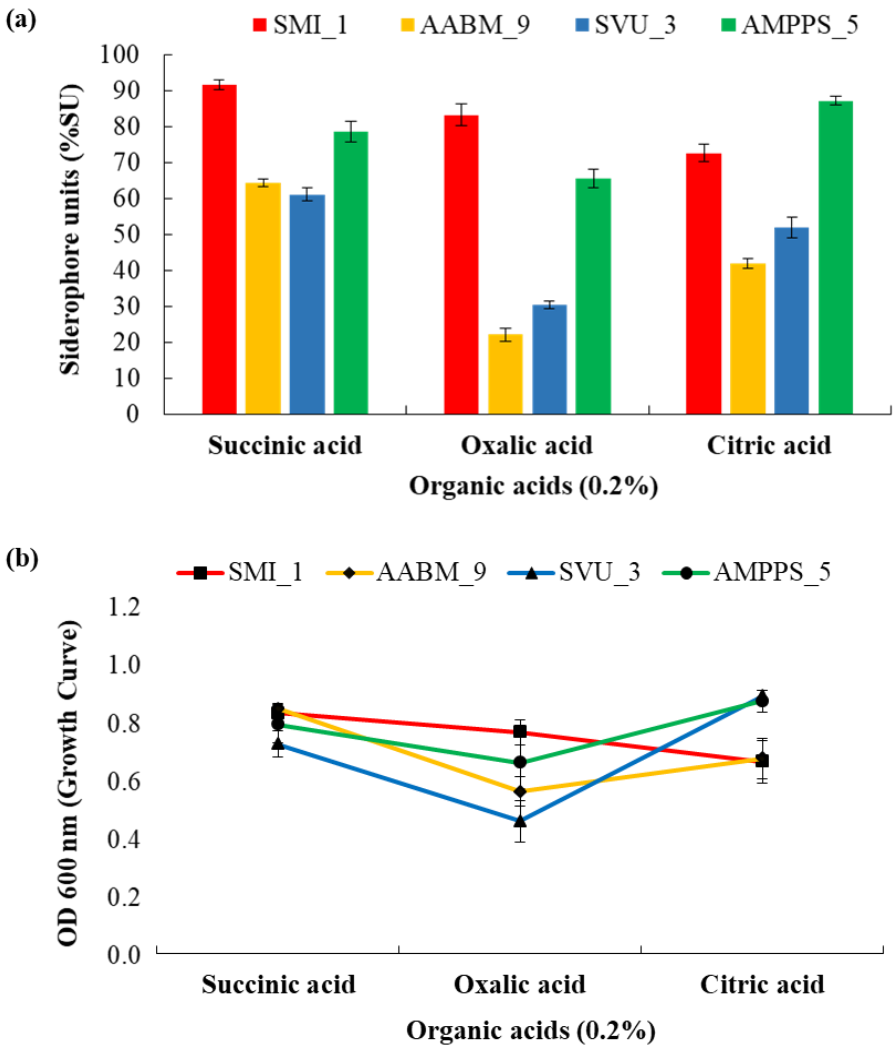

Figure 4.10: Effect of different organic acids (0.2%) on **(a)** siderophore production and **(b)** growth of four marine bacterial isolates (SMI_1, AABM_9, SVU_3, and AMPPS_5).

Influence of different of concentrations of succinic acid (SMI_1, AABM_9, and SVU_3) and citric acid (AMPPS_5) was also investigated. SMI_1 (93.57 %SU) and AABM_9 (85.9 %SU) showed maximum siderophores production at 0.4% succinic acid, whereas SVU_3 (81 %SU) showed at 0.6% succinic acid. AMPPS_5 (91.17 %SU) showed maximum siderophores production at 0.4% citric acid (Figure 4.11a). It was also observed that as the concentrations of organic acids increased from 0.4% to 1.0%, there was a steady decrease in the siderophores production. This might be due to presence of excessive organics acids in the media resulting in the inhibition of siderophores production.

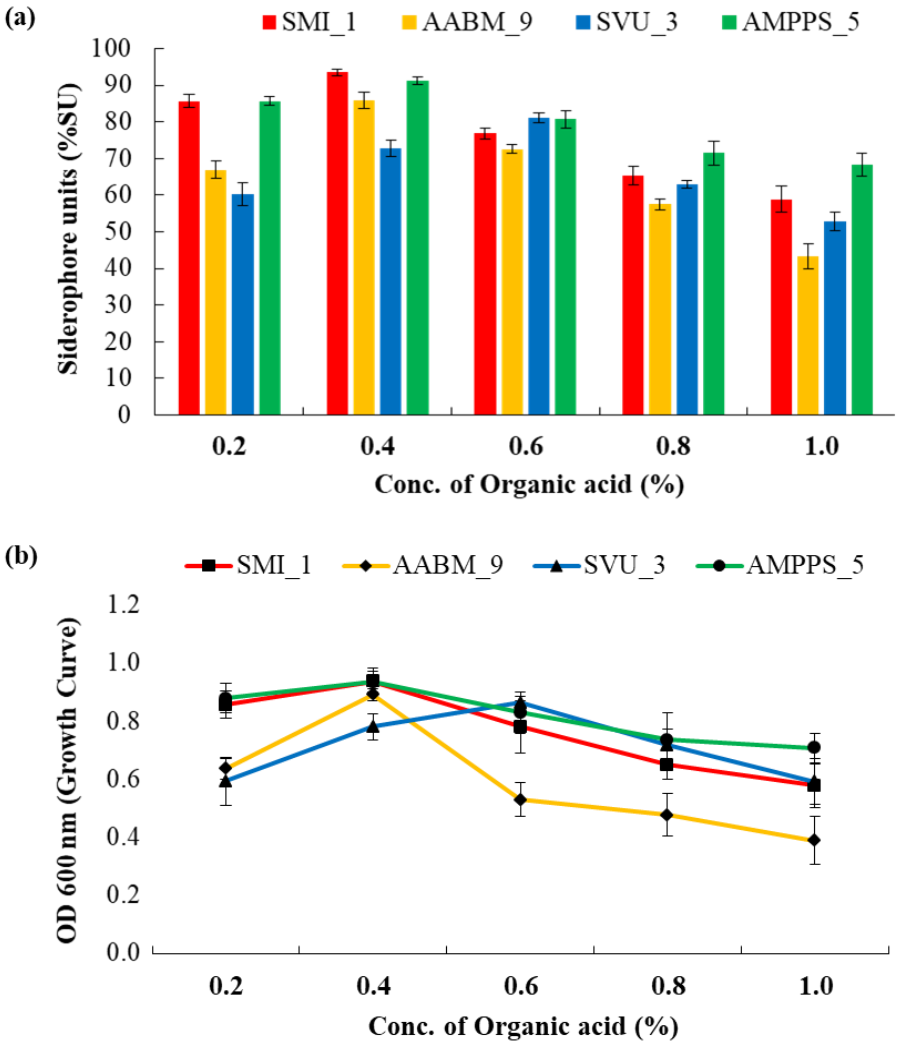

Figure 4.11: Effect of different concentration of organic acid (%) on **(a)** siderophore production and **(b)** growth of four marine bacterial isolates (SMI_1, AABM_9, SVU_3, and AMPPS_5).

4.3.7. Effect of iron

As stated in the introduction, the concentration of Fe^{+3} in the culture media plays a vital role in the promotion of transcriptional factors essential for the biosynthesis of siderophores [4]. In general, siderophores production only occurs in bacteria are under Fe^{+3}-deficit conditions [235]. In addition, even at low concentrations, Fe^{+3} is essential for bacterial growth and survival [4]. However, minimum concentration of Fe^{+3} required to present in the media for the biosynthesis of siderophores is different for different bacteria. Furthermore, the

concentration of Fe^{+3} to inhibit the siderophores production is (i) dependent on the bacteria; therefore it varies from strain to strain and species to species, and (ii) also depends on the culture media composition [4]. In general, Fe concentration of ≤0.1 µmol/L does not suppress the siderophores production [4]. Occurrence of Fe^{+3} in concentrations beyond the threshold limit will lead to negative transcriptional regulation of associated genes resulting in the decreasing production and transport of siderophores [235].

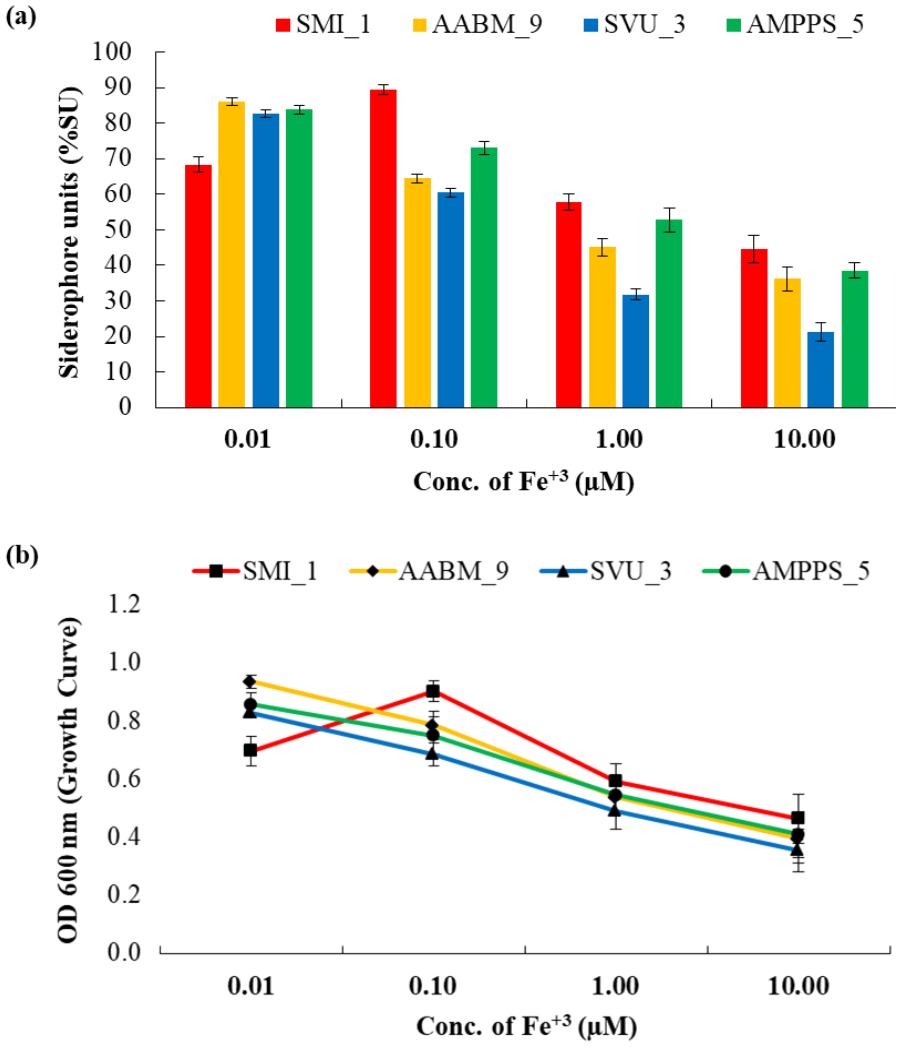

Figure 4.12: Effect of different concentration of Fe^{+3} (µM) on **(a)** siderophore production and **(b)** growth of four marine bacterial isolates (SMI_1, AABM_9, SVU_3, and AMPPS_5).

Therefore, effect of different concentrations (0.01, 0.10, 1.00, and 10.0 µM) of Fe^{+3} of the marine bacterial isolates was evaluated. Based on the results, SMI_1 (89.45 %SU) showed

maximum siderophores production at 0.10 µM concentration, whereas AABM_9 (86.14 %SU), SVU_3 (82.57 %SU), and AMPPS_5 (83.77 %SU) showed at 0.01 µM (Figure 4.12a). It was evident that AABM_9, SVU_3, and AMPPS_5 require much lower concentration of Fe^{+3} than SMI_1 for siderophores production. As the concentration increased to 10 µM, significant reduction in the siderophores production was observed. This indicates that, higher concentrations of Fe^{+3} will inhibit siderophores production in both the isolates. The results observed were in fact align with the literature [254,264,265]. On the other hand, concentration of Fe^{+3} not only effects the siderophores production but also assists in switching between multiple siderophores [235].

4.3.8. Different metal ions

Recent literature suggests that siderophores are also capable to form complex with other metal ions also in addition to Fe^{+3}, such as Cd^{+2}, Cu^{+2}, Co^{+2}, Ga^{+3}, In^{+3}, Pu^{+4}, U^{+4}, Th^{+4}, Al^{+3}, Mg^{+3}, Mn^{+2}, and Zn^{+2} [235]. This indicates that siderophores are also produced and secreted even in the presence of other metal ions, not only Fe^{+3}. In addition to Fe^{+3}, other metal ions such as Mg^{+2}, Cu^{+2}, Mn^{+2}, Mo^{+4}, Ni^{+2} and Zn^{+2} are essential in trace amounts for the regular functions (for example they act as co-factors in several enzymes) of the microbes, known as “micronutrients” [142,250,265].

Based on the above stated reasons, effect of different metal ions such as Fe^{+3}, Cu^{+2}, Mn^{+2} and Zn^{+2} at 10 µM were evaluated for siderophores production. SMI_1 showed maximum siderophores production for Zn^{+2} (73.09 %SU) followed by Mn^{+2} (71.70 %SU), Cu^{+2} (58.21 %SU) and Fe^{+3} (43.68 %SU). AABM_9 showed maximum production for Cu^{+2} (50.41 %SU) followed by Zn^{+2} (47.78 %SU), Mn^{+2} (45.20 %SU), and Fe^{+3} (36.24 %SU). SVU_3 showed maximum siderophores production for Zn^{+2} (50.07 %SU) followed by Cu^{+2} (41.24 %SU), Fe^{+3} (39.16 %SU), and Mn^{+2} (42.16 %SU). AMPPS_5 showed maximum

siderophores production for Zn^{+2} (68.26 %SU) followed by Cu^{+2} (62.01 %SU), Mn^{+2} (52.97 %SU) and Fe^{+3} (38.57 %SU) (Figure 4.13a). Thus, it was evident that at higher concentrations of metal ions (such as Mn^{+2}, Zn^{+2} and Cu^{+2}) siderophores production can be observed, which was much higher than in the presence of Fe^{+3} metal ions. The results observed were in alignment with the previous reports [265,266].

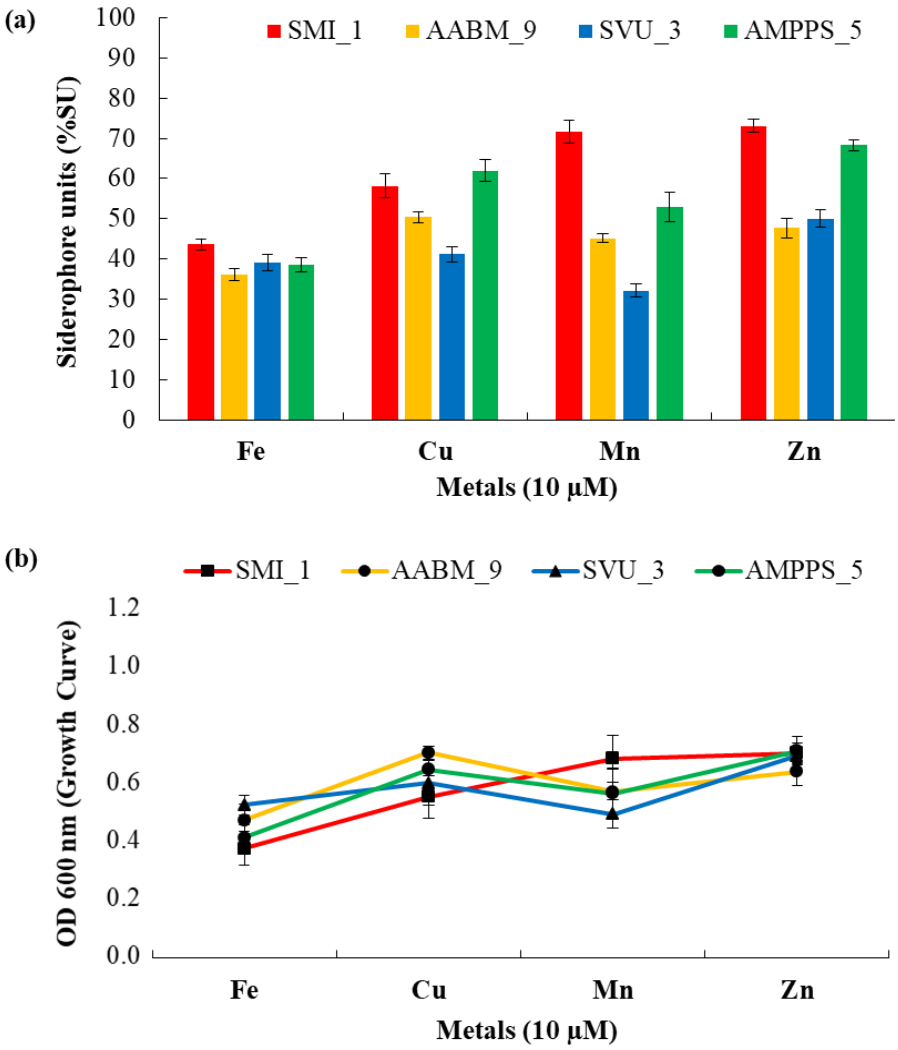

Figure 4.13: Effect of different metal ions (10 µM) on **(a)** siderophore production and **(b)** growth of four marine bacterial isolates (SMI_1, AABM_9, SVU_3, and AMPPS_5).

Table 4.2: Effect of various physicochemical parameters on the siderophore production (%SU) of marine bacterial isolate SMI_1.

Time	Temperature	Initial pH	Carbon Source	Nitrogen Source	Organic Acids	Conc. of Organic Acid	Conc. of Iron	Different Metals	SMI_1
(h)	**(ºC)**		**(0.1%)**	**(0.1%)**	**(0.2%)**	**(%)**	**(µM)**	**(10 µM)**	**(%SU)**
12									20.56 ± 1.09
24									37.62 ± 1.92
36									54.17 ± 3.61
48								-	**60.17 ± 1.94**
60									47.38 ± 2.05
72									35.54 ± 3.87
48	**20**								51.73 ± 2.03
	25								58.52 ± 2.10
	30								**65.45 ± 2.05**
	35							-	63.19 ± 1.71
	40								55.91 ± 3.15
	45								48.51 ± 2.47
48	30	**6.5**							57.13 ± 2.18
		7.0							62.83 ± 2.37
		7.5							69.66 ± 1.98
		8.0						-	**74.04 ± 1.39**
		8.5							67.42 ± 2.02
		9.0							51.20 ± 3.29
48	30	8.0	**Glucose**						74.40 ± 2.23
			Sucrose						**78.91 ± 1.38**
			Fructose					-	66.68 ± 2.45
			Maltose						62.60 ± 3.15
			Xylose						57.97 ± 3.53
48	30	8.0	Sucrose	**Peptone**					68.48 ± 2.66
				Yeast extract					64.87 ± 2.92
				Sodium nitrate				-	**84.53 ± 1.17**
				Ammonium sulfate					78.69 ± 1.45
				Urea					71.43 ± 3.43
48	30	8.0	Sucrose	Sodium nitrate	**Succinic acid**				**91.74 ± 1.38**
					Oxalic acid			-	83.35 ± 3.04
					Citric				72.64 ± 2.40

					acid				
48	30	8.0	Sucrose	Sodium nitrate	Succinic acid	**0.2**		-	85.58 ± 1.79
						0.4			**93.57 ± 0.91**
						0.6			76.81 ± 1.57
						0.8			65.33 ± 2.45
						1.0			58.91 ± 3.43
48	30	8.0	Sucrose	Sodium nitrate	Succinic acid	0.4	**0.01**	-	68.35 ± 2.20
							0.10		**89.45 ± 1.34**
							1.00		57.85 ± 2.40
							10.0		44.62 ± 3.81
48	30	8.0	Sucrose	Sodium nitrate	Succinic acid	0.4	-	**Fe^{+3}**	43.68 ± 1.36
								Cu^{+2}	58.21 ± 2.94
								Mn^{+2}	71.70 ± 2.83
								Zn^{+2}	**73.09 ± 1.68**

Table 4.3: Effect of various physicochemical parameters on the siderophore production (%SU) of marine bacterial isolate AABM_9.

Time	**Temperature**	**Initial pH**	**Carbon Source**	**Nitrogen Source**	**Organic Acids**	**Conc. of Organic Acid**	**Conc. of Iron**	**Different Metals**	**AABM_9**
(h)	**(°C)**		**(0.1%)**	**(0.1%)**	**(0.2%)**	**(%)**	**(µM)**	**(10 µM)**	**(%SU)**
12								-	19.86 ± 2.32
24									38.31 ± 4.04
36									**65.68 ± 1.43**
48									60.81 ± 2.57
60									52.10 ± 1.68
72									47.23 ± 2.56
36	**20**							-	53.38 ± 1.11
	25								60.36 ± 1.78
	30								**68.88 ± 1.01**
	35								57.59 ± 1.67
	40								47.08 ± 2.43
	45								39.57 ± 2.97
36	30	**6.5**						-	39.76 ± 2.12
		7.0							48.48 ± 1.79
		7.5							59.45 ± 1.25
		8.0							**72.76 ± 0.79**
		8.5							66.57 ± 1.52
		9.0							60.50 ± 2.85
36	30	8.0	**Glucose**					-	35.77 ± 3.16
			Sucrose						**76.40 ± 1.06**

			Fructose						55.68 ± 2.76
			Maltose						62.35 ± 1.67
			Xylose						53.22 ± 1.63
36	30	8.0	Sucrose	**Peptone**				-	62.57 ± 1.05
				Yeast extract					51.69 ± 2.82
				Sodium nitrate					70.82 ± 1.98
				Ammonium sulfate					**82.54 ± 1.10**
				Urea					59.92 ± 2.62
36	30	8.0	Sucrose	Ammonium sulfate	**Succinic acid**			-	**64.49 ± 1.01**
					Oxalic acid				22.11 ± 1.83
					Citric acid				41.94 ± 1.47
36	30	8.0	Sucrose	Ammonium sulfate	Succinic acid	**0.2**		-	66.91 ± 2.40
						0.4			**85.90 ± 2.32**
						0.6			72.58 ± 1.27
						0.8			57.46 ± 1.53
						1.0			43.29 ± 3.36
36	30	8.0	Sucrose	Ammonium sulfate	Succinic acid	0.4	**0.01**	-	**86.14 ± 1.08**
							0.10		64.54 ± 1.23
							1.00		45.19 ± 2.47
							10.0		36.23 ± 3.45
36	30	8.0	Sucrose	Ammonium sulfate	Succinic acid	0.4	-	**Fe^{+3}**	36.23 ± 1.45
								Cu^{+2}	**50.40 ± 1.33**
								Mn^{+2}	45.20 ± 1.05
								Zn^{+2}	47.78 ± 2.43

Table 4.4: Effect of various physicochemical parameters on the siderophore production (%SU) of marine bacterial isolate SVU_3.

Time	**Temperature**	**Initial pH**	**Carbon Source**	**Nitrogen Source**	**Organic Acids**	**Conc. of Organic Acid**	**Conc. of Iron**	**Different Metals**	**SVU_3**
(h)	**(°C)**		**(0.1%)**	**(0.1%)**	**(0.2%)**	**(%)**	**(µM)**	**(10 µM)**	**(%SU)**
12								-	29.34 ± 3.53
24									40.63 ± 2.86
36									53.83 ± 1.12
48									**62.68 ± 1.00**

60									59.25 ± 1.44
72									50.55 ± 1.31
48	**20**							-	41.42 ± 2.35
	25								55.54 ± 1.82
	30								**64.24 ± 0.66**
	35								58.23 ± 1.25
	40								49.27 ± 1.07
	45								40.61 ± 2.52
48	30	**6.5**						-	47.95 ± 3.19
		7.0							57.30 ± 1.04
		7.5							61.39 ± 2.44
		8.0							67.15 ± 1.82
		8.5							**71.44 ± 0.95**
		9.0							66.99 ± 1.51
48	30	8.5	**Glucose**					-	**76.01 ± 0.68**
			Sucrose						65.91 ± 1.20
			Fructose						55.91 ± 1.01
			Maltose						70.29 ± 1.89
			Xylose						62.81 ± 1.12
48	30	8.5	Glucose	**Peptone**				-	53.10 ± 2.51
				Yeast extract					48.41 ± 3.55
				Sodium nitrate					**78.22 ± 1.25**
				Ammonium sulfate					66.57 ± 1.54
				Urea					64.68 ± 3.12
48	30	8.5	Glucose	Sodium nitrate	**Succinic acid**			-	**61.18 ± 1.78**
					Oxalic acid				30.42 ± 1.11
					Citric acid				51.90 ± 2.94
48	30	8.5	Glucose	Sodium nitrate	Succinic acid	**0.2**		-	60.24 ± 3.06
						0.4			72.65 ± 2.24
						0.6			**81.03 ± 1.40**
						0.8			63.05 ± 1.05
						1.0			52.73 ± 2.50
48	30	8.5	Glucose	Sodium nitrate	Succinic acid	0.6	**0.01**	-	**82.57 ± 1.09**
							0.10		60.49 ± 1.20
							1.00		31.73 ± 1.54
							10.0		21.31 ± 2.58

48	30	8.5	Glucose	Sodium nitrate	Succinic acid	0.6	-	**Fe^{+3}**	39.16 ± 2.01
								Cu^{+2}	41.24 ± 1.91
								Mn^{+2}	32.16 ± 1.68
								Zn^{+2}	**50.07 ± 2.23**

Table 4.5: Effect of various physicochemical parameters on the siderophore production (%SU) of marine bacterial isolate AMPPS_5.

Time	**Temperature**	**Initial pH**	**Carbon Source**	**Nitrogen Source**	**Organic Acids**	**Conc. of Organic Acid**	**Conc. of Iron**	**Different Metals**	**AMPPS_5**
(h)	**(ºC)**		**(0.1%)**	**(0.1%)**	**(0.2%)**	**(%)**	**(µM)**	**(10 µM)**	**(%SU)**
12									48.54 ± 2.52
24									58.58 ± 1.57
36									**58.86 ± 1.30**
48								-	50.68 ± 1.43
60									45.94 ± 2.64
72									38.27 ± 1.25
36	**20**								48.50 ± 1.28
	25								57.37 ± 2.68
	30								61.08 ± 1.72
	35							-	**64.05 ± 1.30**
	40								58.64 ± 1.56
	45								46.60 ± 2.34
36	35	**6.5**							43.39 ± 2.44
		7.0							51.66 ± 3.83
		7.5							58.36 ± 1.54
		8.0						-	63.90 ± 1.61
		8.5							**69.65 ± 1.10**
		9.0							56.66 ± 1.68
36	35	8.5	**Glucose**						**75.69 ± 1.28**
			Sucrose						72.38 ± 1.56
			Fructose					-	66.44 ± 2.78
			Maltose						69.58 ± 2.51
			Xylose						66.05 ± 2.16
36	35	8.5	Glucose	**Peptone**					70.35 ± 2.19
				Yeast extract					71.32 ± 2.90
				Sodium nitrate				-	75.71 ± 2.44
				Ammonium sulfate					**81.40 ± 1.26**
				Urea					75.47 ± 3.12

36	35	8.5	Glucose	Ammonium sulfate	**Succinic acid**			-	78.59 ± 2.87
					Oxalic acid				65.66 ± 2.61
					Citric acid				**87.25 ± 1.23**
36	35	8.5	Glucose	Ammonium sulfate	Citric acid	**0.2**		-	85.65 ± 1.15
						0.4			**91.17 ± 0.96**
						0.6			80.70 ± 2.48
						0.8			71.43 ± 3.33
						1.0			68.26 ± 3.04
36	35	8.5	Glucose	Ammonium sulfate	Citric acid	0.4	**0.01**	-	**83.77 ± 1.19**
							0.10		73.10 ± 1.87
							1.00		52.80 ± 3.29
							10.0		38.61 ± 2.06
36	35	8.5	Glucose	Ammonium sulfate	Citric acid	0.4	-	**Fe^{+3}**	38.57 ± 1.72
								Cu^{+2}	62.01 ± 2.82
								Mn^{+2}	52.97 ± 3.70
								Zn^{+2}	**68.26 ± 1.35**

Table 4.6: Comparison of production parameters and siderophore production with those reported in literature.

Microorganism	**Habitat**	**Incubation Time (h)**	**Temp (°C)**	**pH**	**Carbon Source**	**Nitrogen Source**	**Organic Acid**	**Yield**	**Ref.**
Pseudomonas aeruginosa FP6	Soil sample	-	-	-	Sucrose Mannitol	Urea	-	104.8 mM 92.9 mM	[250]
Bacillus cereus Pseudomonas weihenstephanensis	Marine	100 - 150	25	8.5	-	-	-	-	[257]
Brevibacillus brevis GZDF3	Rhizosphere soil	48	32	7	Sucrose	asparagine	-	-	[6]
Pseudomonas aeruginosa RZS9	-	24	27.8	7.1	-	-	Succinic acid	69.03% SU	[267]
Bacillus sp. PZ-1	Soil sample	48	30	6.2	Glucose	asparagine		90.52% SU	[268]
Pseudomonas fluorescens	-	24	29	7	Glucose	Urea	Succinic acid	96%	[259]
Bacillus sp. (VITVK5) *Enterobacter* sp. (VITVK6)	Soil sample	-	37	8	Sucrose Glucose	Sodium Nitrate	Citric acid	~60 - 80%	[252]
Escherichia coli Bacillus spp. ST13	-	-	55	6	Sucrose Glucose	-	-	48 µg/ml 31 µg/ml	[256]

Streptomyces pilosus								32 µg/ml	
Pseudomonas aeruginosa	-	-	27.8	7.1	-	-	-	68.41%	[222]
Pseudomonas aeruginosa azar 11	Aquatic soil	72	37	7	Maltose	Ammonium nitrate	Citric acid	59.18%	[269]
Bacillus teanensis SMI_1	Marine	48	30	8	Sucrose	Sodium nitrate	Succinic acid	95.27 %SU	Present study
Enterobacter sp. AABM_9	Marine	36	30	8	Sucrose	Ammonium sulphate	Succinic acid	86.14 %SU	Present study
Marinobacter hydrocarbonoclausticus SVU_3	Marine	48	30	8.5	Glucose	Sodium nitrate	Succinic acid	82.75 %SU	Present study
Pseudomonas mendocina AMPPS_5	Marine	36	35	8.5	Glucose	Ammonium sulphate	Citric acid	91.17 %SU	Present study

4.4. Statistical optimization of siderophores production

Production parameters of siderophore production of SMI_1 isolate was optimized and observed maximum percentage of production at sucrose (0.1%), initial pH 8 and succinic acid (0.4 %). RSM helps to understand the behavior of multiple variables and their interactions. CCD was used to optimize the three factors at five different levels (-α, -1, 0, +1, + α). CCD experimental design with responses (experimental and predicted) was reported in Table 4.7. The final second order response equation for predicted responses given by equation 4.1.

$$\mathbf{Y} = +93.83 + 1.06\,(A) + 2.03\,(B) + 2.85\,(C) - 0.4987\,(AB) - 1.36\,(AC) + 0.8138\,(BC) - 4.05\,(A)^2 - 8.05\,(B)^2 - 3.41\,(C)^2 \quad (4.1)$$

Where, Y = Siderophore units (%SU), A = Sucrose, B = Initial pH, and C = Succinic acid.

Table 4.7: CCD matric with experimental and predicted siderophote production values.

Std	Run	Sucrose (%)	Initial pH	Succinic acid (%)	% SU	
					Experimental	Predicted
2	1	0.20	7.00	0.30	76.18	76.25
7	2	0.00	9.00	0.50	83.72	83.90
5	3	0.00	7.00	0.50	77.92	77.21

9	4	0.10	8.00	0.40	94.27	92.91
10	5	0.10	8.00	0.40	92.62	92.91
4	6	0.20	9.00	0.30	76.73	77.69
8	7	0.20	9.00	0.50	84.17	82.30
1	8	0.00	7.00	0.30	68.28	70.40
11	9	0.10	8.00	0.40	93.58	92.91
3	10	0.00	9.00	0.30	73.27	73.84
6	11	0.20	7.00	0.50	77.92	77.60
12	12	0.10	8.00	0.40	92.18	92.91
19	13	0.10	8.00	0.40	95.27	94.76
15	14	0.10	6.32	0.40	69.13	68.56
18	15	0.10	8.00	0.57	88.17	89.91
16	16	0.10	9.68	0.40	75.19	75.40
14	17	0.27	8.00	0.40	84.29	85.10
20	18	0.10	8.00	0.40	93.17	94.76
17	19	0.10	8.00	0.23	82.41	80.31
13	20	-0.07	8.00	0.40	82.69	81.53

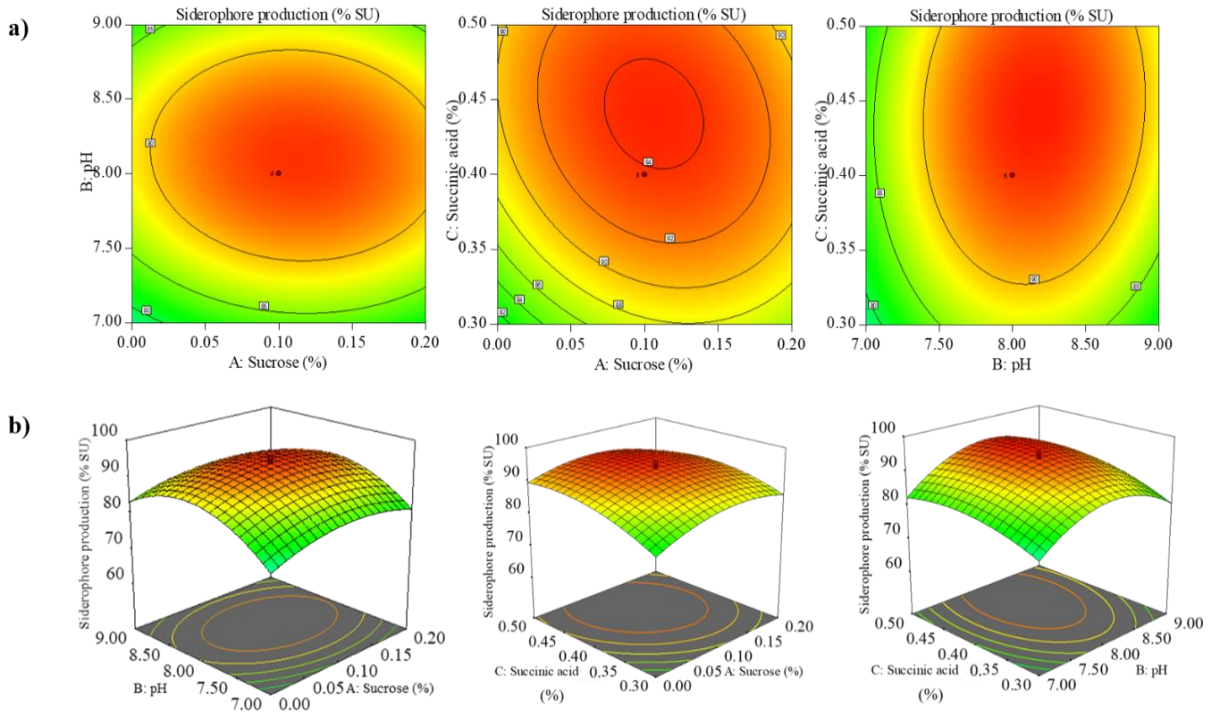

Figure 4.14: (a) Contour and **(b)** 3D surface plots for the effects of process parameters on siderophore production. A = Sucrose (%), B = pH, and C = Succinic acid (%).

The adequacy of the model was analysed by ANOVA (Table 4.8). In this study, $p < 0.05$ considered as significant values and $p < 0.0001$ as very significant value. Lack-of fit was

not significant as it represents lesser F value (3.38). It is evident that there is both significant regression and non-significant Lack-of-Fit in the mathematical model, commensurate with the adequacy and well-fitness of the experimental data center point. R^2 (97.18%) obtained reveals the good correlation between independent variables and response values. The R^2 (0.9718) and adjusted (adj) R^2 (0.9636) were close to one and adj R^2 is in reasonable argument with the predicted R^2 (0.8430). By maintaining one independent variable at zero (0), the effect of three independent variables on siderophore production (response) was examined. The response surface graphs were plotted by considering two selected independent variables against response on the Z-axis by evaluating all three potential combinations. It is evident from response that pH and succinic acid have significant effect on production of siderophore than sucrose.

Table 4.8: ANOVA of experimental results of siderophore production.

Source	Sum of Squares	df	Mean Square	F-value	p-value	
Model	1370.02	9	152.22	53.94	< 0.0001	significant
A-Sucrose	15.40	1	15.40	5.46	0.0443	
B-pH	56.52	1	56.52	20.03	0.0015	
C-Succinic acid	111.13	1	111.13	39.38	0.0001	
AB	1.99	1	1.99	0.7051	0.4228	
AC	14.88	1	14.88	5.27	0.0473	
BC	5.30	1	5.30	1.88	0.2039	
A^2	235.80	1	235.80	83.55	< 0.0001	
B^2	933.71	1	933.71	330.85	< 0.0001	
C^2	167.47	1	167.47	59.34	< 0.0001	
Residual	25.40	9	2.82			
Lack of Fit	20.53	5	4.11	3.38	0.1309	not significant
Pure Error	4.87	4	1.22			
Cor. Total	1402.57	19				

4.5. Purification of siderophores

4.5.1. Amberlite XAD-2 column chromatography

To produce large amounts of siderophore, SMI_1 was grown for 48 h in a 1 batch culture of optimized succinate medium. A litre of culture supernatant was acidified to pH two before being purified by XAD-2 and Sephadex column chromatography. In order to test for the presence of siderophore in fractions, 50 ml aliquots were collected and tested using CAS assay. To ensure that the siderophore has been bound to the column material, all flow-through collected from column washes and equilibrations were also tested. Most of the siderophore was eluted from fractions 4 to 7 and all methanol extracts that were CAS positive were pooled for further analysis.

4.5.2. Sephadex LH-20 column chromatography

In order to further purify the fractions which were found to be positive for siderophores, they were pooled and concentrated using Sephadex LH-20 column chromatography. Fifteen fractions, each with a volume of 10 ml, were collected in separate aliquots of 10 ml. CAS assays were conducted on each of these samples to determine their siderophore content. Colorless fractions were obtained at the beginning. There was a pale-yellow color in fractions 5 to 9, the intensity of color increased gradually, and then a brown color in fractions 11-14. All the methanol fractions which showed CAS positive were pooled together and separated the methanol using rotary evaporator at 40 °C. White powder of 31 mg/L siderophore was obtained on freeze drying and sample re-dissolved in 3 ml of methanol and stored at 4 °C.

4.5.3. Thin layer chromatography

A TLC analysis of fractions collected from the LH-20 column revealed the presence of a wine-colored spot upon spraying $FeCl_3$-HCl, indicating a hydroxamate-type siderophore.

The presence of hydroxamate siderophore in fractions 11 to 14 has been confirmed by the appearance of wine-colored spots (Figure 4.15).

Figure 4.15: TLC plates tested on concentrated siderophore of SMI_1 isolate.

4.6. Chemical characterization of purified siderophores

4.6.1. Spectral scan analysis

The purified molecules were analyzed based on their spectral absorbance to determine which type of hydroxamate siderophore they represented. It has been reported that the maximum absorbance ranges of mono- and dihydroxamate siderophores lie between 500 and 520 nm, whereas for trihydroxamate siderophores they are between 420 and 440 nm [270]. It appears that the hydroxamate absorbance maxima observed in this study (λmax 421 nm) was closer to those of trihydroxamate (Figure 4.16).

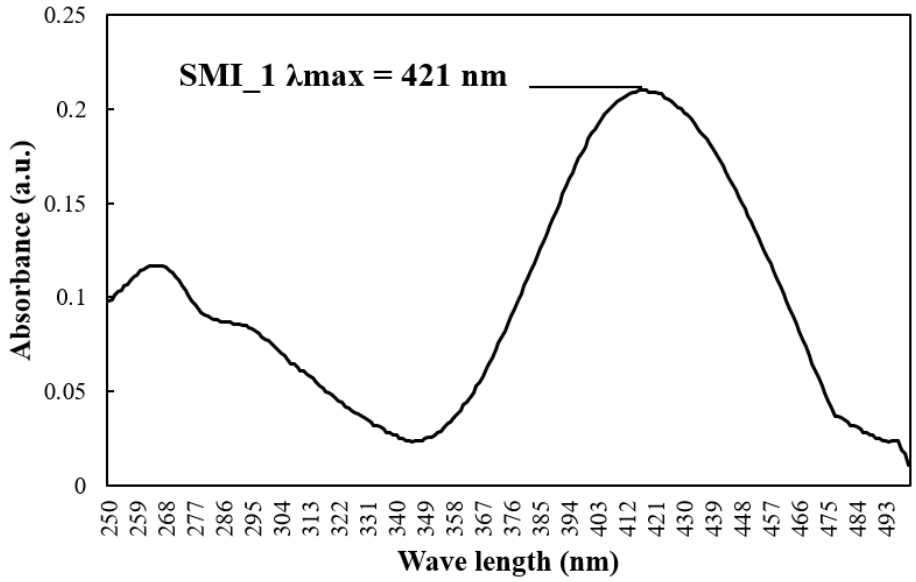

Figure 4.16: UV-Vis spectra of hydroxamate siderophore of SMI_1 isolate showing broad peak at 421 nm.

4.6.2. FTIR analysis

The functional groups of purified hydroxamate were determined by FTIR spectra. Peaks observed at 3334.11 cm^{-1} indicating the presence of OH group, 2943.66 cm^{-1} indicates CH stretch and 1654.70 cm^{-1} indicates the existence of C=O stretch (Figure 4.17) and peaks in this study were compared with standard peaks in Table 4.9. The peaks of IR spectra indicates the presence of hydroxamate siderophore and similar observations were reported by Murugappan et al. (2011) alcoholic group at 3415.31 cm^{-1} and Gaurav Yadav et al. (2022) reported 3433-3035 cm^{-1} OH stretching [226,271].

Table 4.9: Standard band assignments and peaks observed in this study.

Band assignment	Standard (cm^{-1})	Present Study (cm^{-1})
OH stretch	3550-3200	3334.11
CH_2	2933-2966	2943.66
CH_2	2821-2856	2833.08
C=O stretch	1651-1697	1654.70
C-H	1404-1453	1412.44
C-O	1254-1271	1257.13

C-N	1009-1181	1019.47

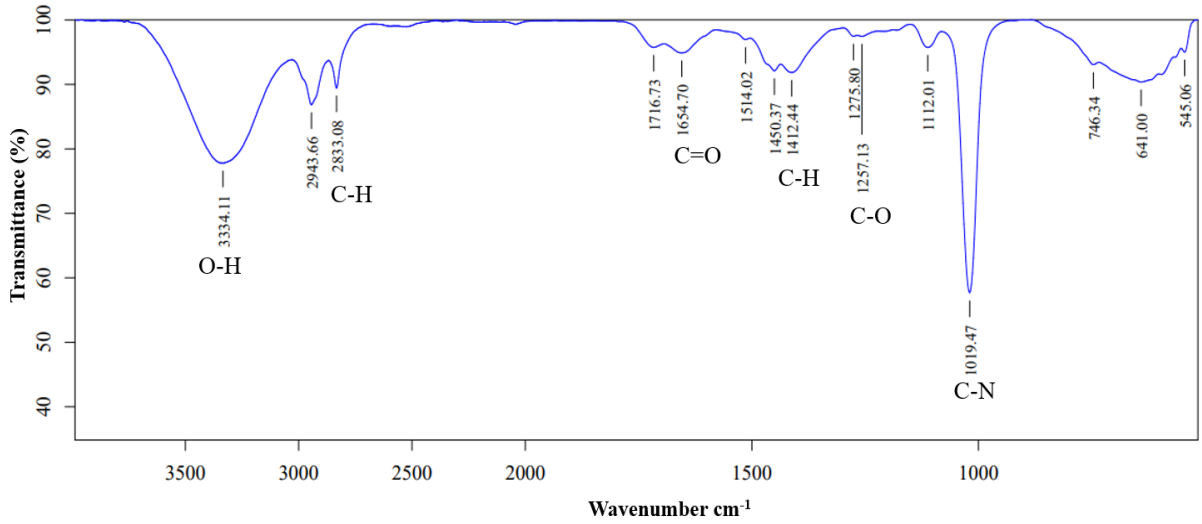

Figure 4.17: FTIR spectrum of hydroxamate siderophore produced by SMI_1.

4.6.3. LC-MS analysis

LC-MS analysis of siderophores from SMI_1 isolate was analysed, where HPLC peaks obtained at R_T 1.53 and 3.92 min (Figure) with mobile phase acetonitrile and water. On Mass spectroscopy analysis, siderophore was identified at R_T 3.95 min in positive ion mode in chromatogram (Figure 4.18). The mass-to-charge ratio proportion of siderophore at 3.95 was 561.3 (Figure 4.19). The compound isolated was in white powder form and showed $[M+H]^+$ ion with m/z 561.3 resembling the molecular formula of Deferrioxamine ($C_{25}H_{48}N_6O_8$, Mass 561.3588 m/z). Desferrioxamine B (m/z 561.35) and B2 (m/z 547.34) was isolated from marine brown alga *Carpodesmia tamariscifolia* reported similar kind of results [272]. Deferrioxamine B is an essential drug substance for the treatment of iron overload diseases, including thalassemia, hemochromatosis and iron intoxication [273]. The yield of purified siderophore was 31 mg/L.

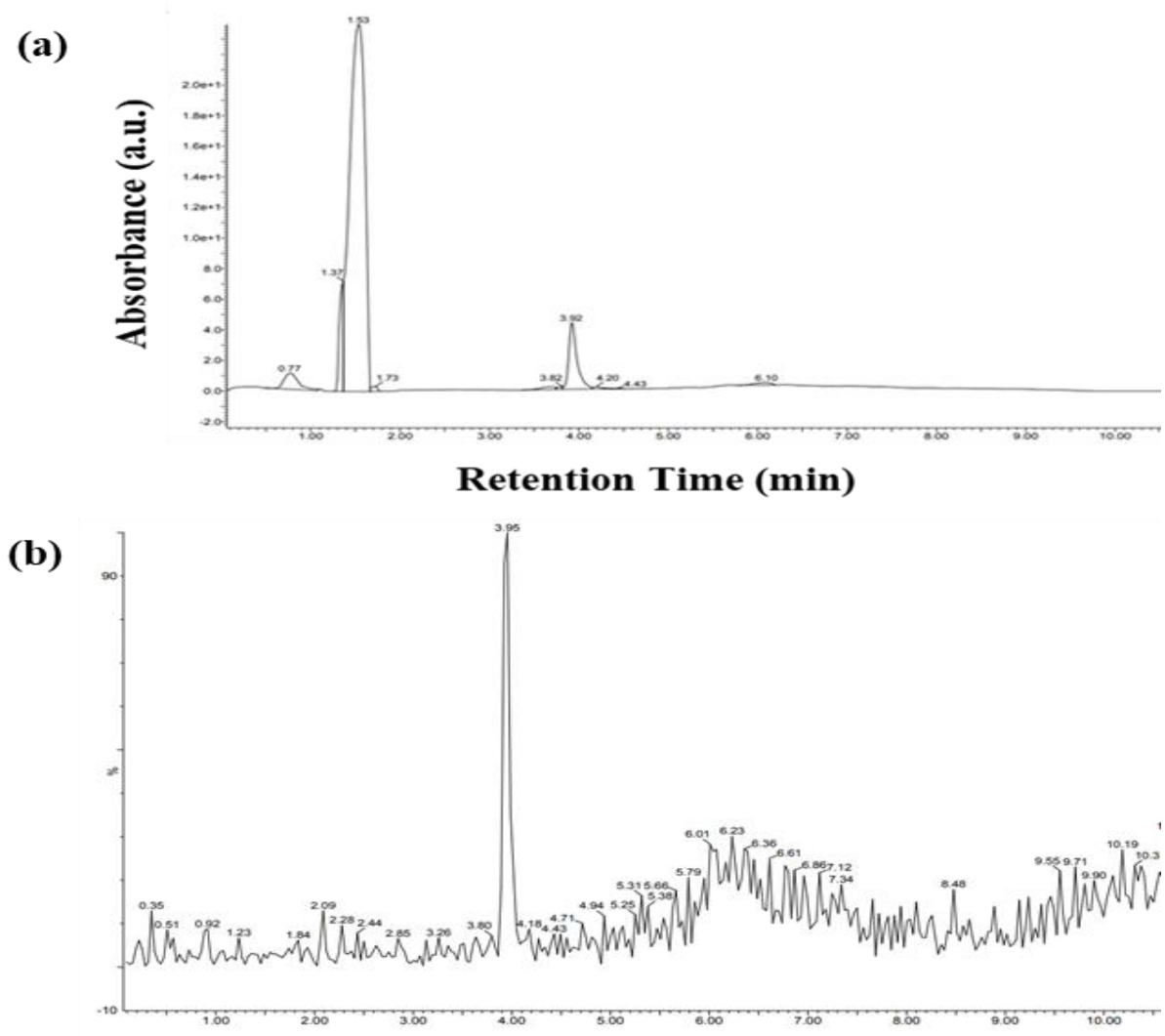

Figure 4.18: (a) The HPLC chromatogram of hydroxamate siderophore showing peaks at R_T 3.92. **(b)** TIC (Total Ion Current) chromatogram showing siderophore peak at R_T 3.95 in positive mode.

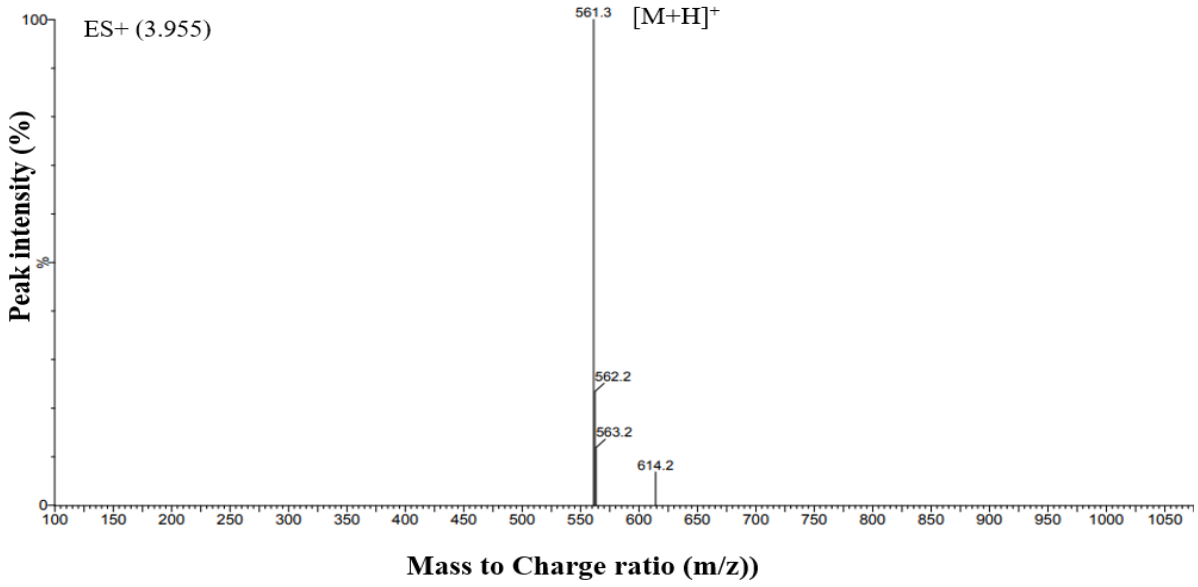

Figure 4.19: MS spectra for iron free hydroxamate siderophore in positive ion mode.

4.6.4. NMR spectroscopy

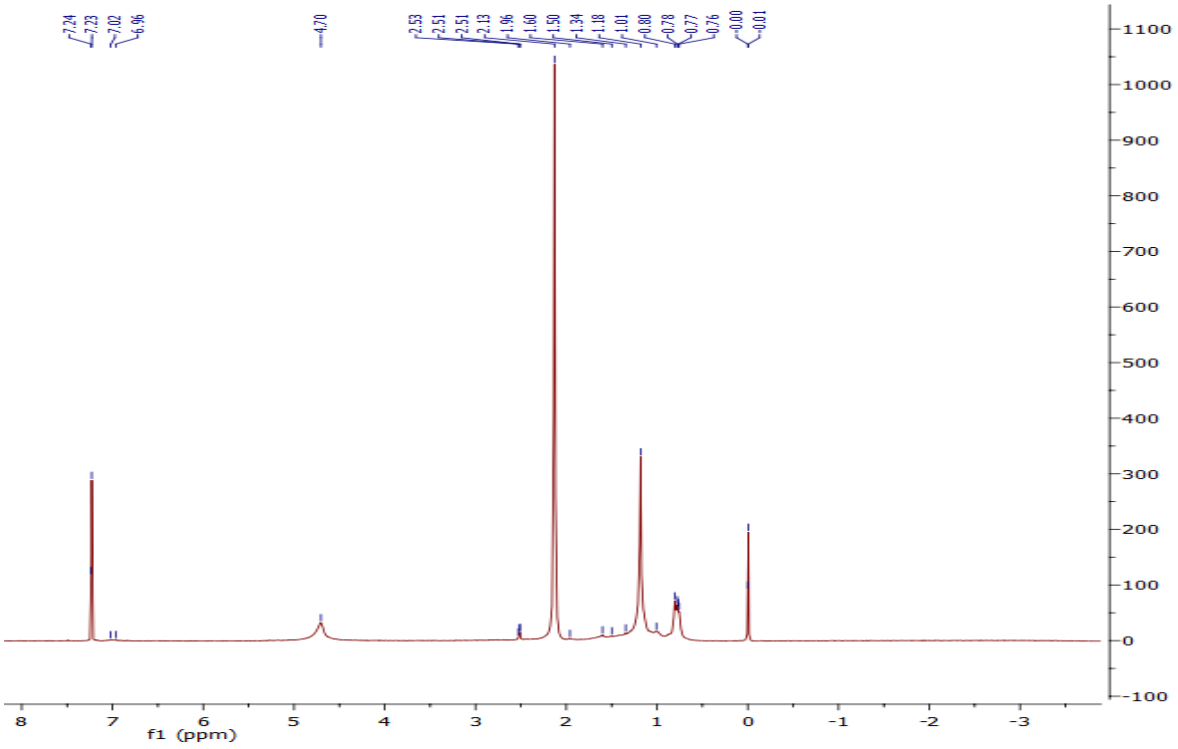

Figure 4.20: 1H NMR spectra of hydroxamate siderophore of SMI_1 isolate.

Proton NMR spectrum of purified hydroxamate siderophore dissolved in Deuterated chloroform, (soluble) showed peaks at 0.83, 1.21 and 2.16 ppm were as a result of CH_2-CH_2, CH_2-CH_2 and CH_2=CH complementary with previously reported data (Figure 4.20). Peak at 7.26 ppm considered as solvent peak. According to the NMR spectrum of the current study, it is evident that a hydroxamate siderophore exists. As the spectrum results indicate, the dihydroxamate siderophores of marine Vibrio species (bisucaberin and aerobactin) are also consistent with this marine bacterial siderophores [226,271,274].

4.7. Heavy metal chelation

Heavy metals severely hamper the ecosystems of the terrestrial and aquatic realms. Finding long-lasting ways to get rid of these harmful substances from the environment is necessary due to their persistence in food chains and ecological niches. The persistence of heavy metals reduces the time they take to enter the food chain through sources like aquatic plants, fish and other aquatic creatures. Heavy metal accumulation in the aquatic environment, particularly during the early phases of the development of fish, can be lethal to many different kinds of fish [275]. Heavy metal contamination of soil has significant effects on the ecosystem, making it a critical environmental problem. The heavy metals in the soil can enter human food via plants, posing risks since they are passed down the food chain [276]. With heavy metals posing considerable risks to humans and the environment, it is imperative that heavy metal polluted soils be decontaminated immediately [277]. It is possible that siderophore chelators may play a critical role in bacteria's resistance to heavy metals if toxic metals induce the production of siderophores [278].

After 72 h of incubation, color change from blue to yellow was observed which reflects the chelation of metal and CAS plate with Fe^{+3} was considered as control. SMI_1 showed strong positive in Co^{+2}, Cr^{+6}, Hg^{+2}, and Ni^{+2} whereas positive results showed in Ag^{+2},

Al^{+2}, La^{+3}, Mo^{+6}, Pd^{+2}, and Y^{+3}. SMI_1 didn't show any activity in Cd^{+2} and Pb^{+2} which reflect the absence of siderophore production. AABM_9 showed clear zone formation in Al^{+2}, La^{+3}, Pd^{+2}, and Y^{+3} and showed moderate zone in Cd^{+2}, Co^{+2}, Cr^{+6}, Hg^{+2}, Ni^{+2}, and Pb^{+2}. In Ag^{+2} and Mo^{+6} didn't observe any activity. SVU_3 showed strong chelation was observed in Co^{+2}, Pb^{+2}, Pd^{+2} moderate in La^{+3}, Mo^{+6}, Y^{+3} and weak zones in Al^{+2}, Cr^{+6}, Ni^{+2} agar plates. AMPPS_5 showed moderate chelation in Al^{+2}, Cd^{+3}, Co^{+2}, Cd^{+2}, Hg^{+2}, La^{+3}, Ni^{+2}, and Pb^{+2}. It showed weak chelation in Pd^{+2} and Y^{+3} whereas negative result in Ag^{+2} and Mo^{+6} was observed (Figure 4.21, Figure 4.22, and Table 4.10).

Previous studies on siderophore complexation abilities with metals other than iron were reported. Trace metals like Cd, Cu, Ni, Pb, and Zn in seawater form strong metal-organic complexes. Three of the five metals form a stable and firm complex with siderophore-like organic molecules, where the ligands, particularly for Cd and Ni, are substantially more potent and may have reasonably distinct functional groups [279]. Desferrioxamine B, a bacterial siderophore, increased the phytoextraction of rare earth metals, including La, Nd, Gd, Er, and Ge, by forming soluble complexes which improved the movement of elements in the rhizosphere [280]. Arsenic-tolerant *actinobacteria* were isolated, and a siderophore that binds arsenic was reported [281]. *Marinobacter* sp. SVU_3, which isolated from marine source, showed strong chelation of Al, Co, La, and Pb was reported [233].

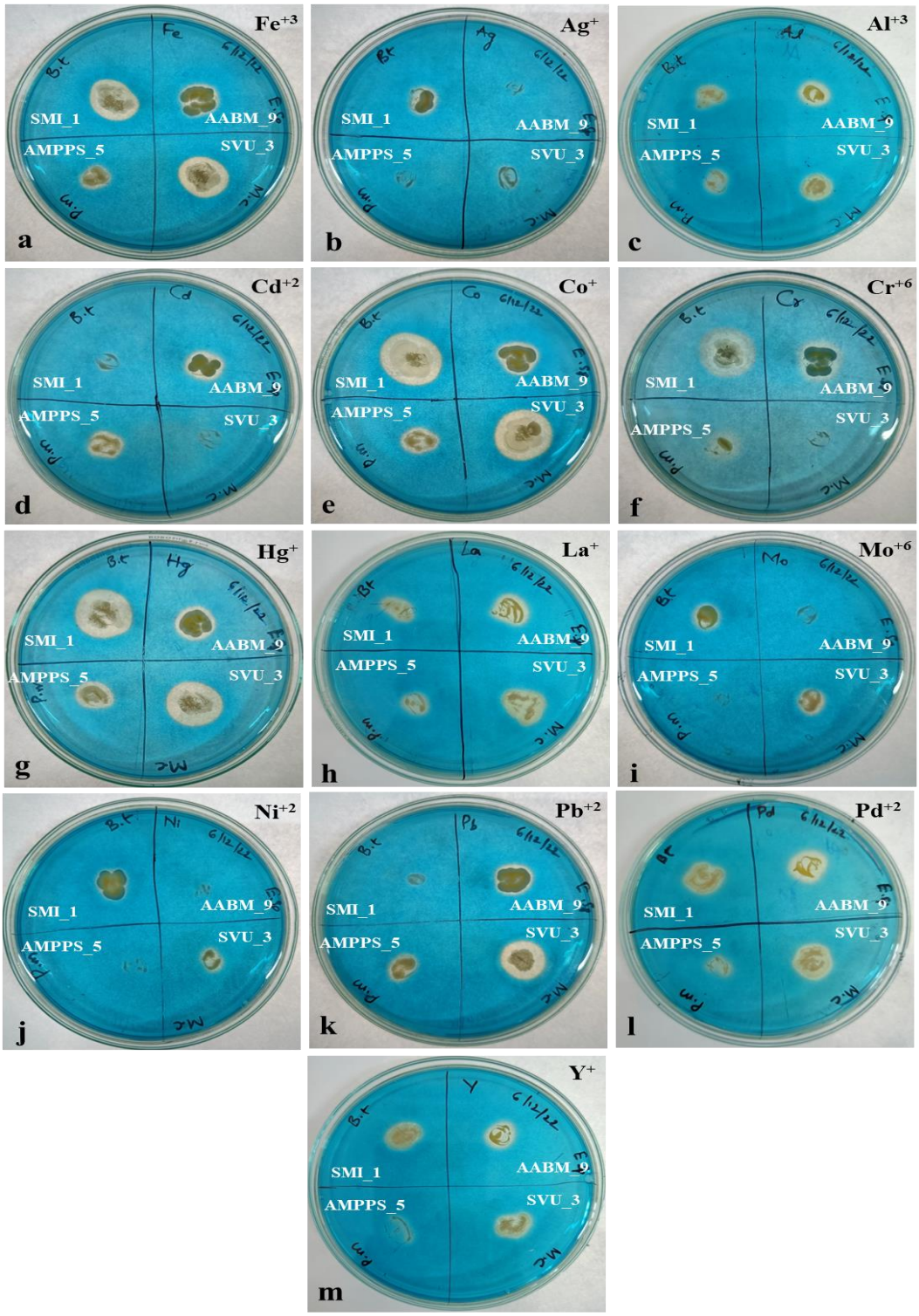

Figure 4.21: Heavy metal ions chelation activity of marine bacterial isolates (SMI_1, AABM_9, SVU_3, and AMPPS_5) through CAS agar plate assay.

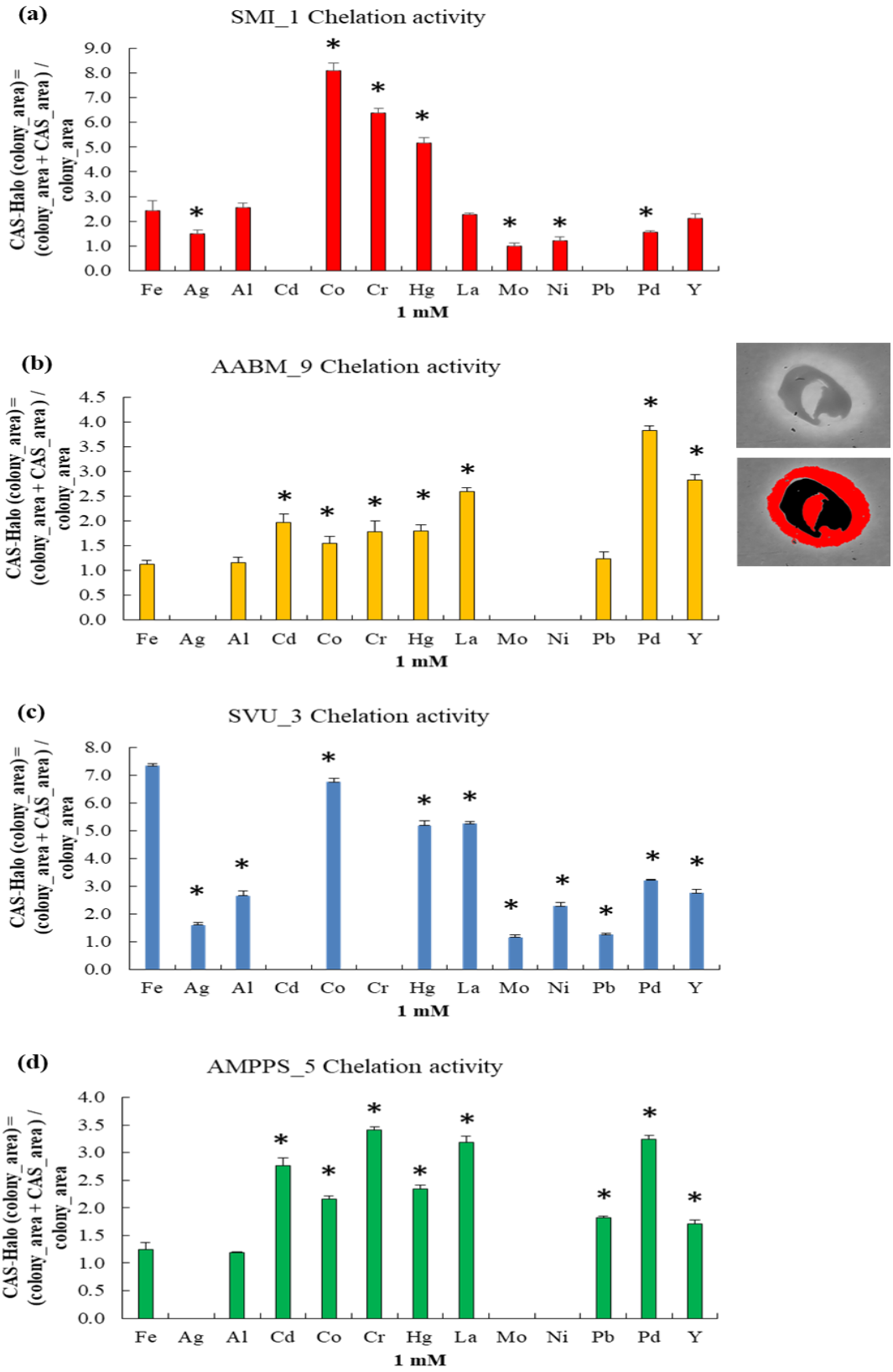

Figure 4.22: Bar plot visualization of the image analysis from the solid CAS plates combined with heavy metals, * represents ($p < 0.05$) statistically significant.

Table 4.10: Heavy metal ions chelation activity using CAS assay (- indicates no growth; + indicates growth; ++ indicates growth with low activity; +++ indicates growth with moderate to good activity).

Metal Salt(s) (1 mM)	Metal Ion(s)	Marine Bacterial Isolate(s)			
		SMI_1	AABM_9	SVU_3	AMPPS_5
$FeCl_3.7H_2O$	Fe^{+3}	+++	++	+++	++
$AgNO_3$	Ag^{+}	++	-	+	-
$Al_2(SO_4)_3$	Al^{+3}	++	+++	+++	++
$CdCl_2$	Cd^{+2}	-	++	-	++
$CoCl_2.6H_2O$	Co^{+}	+++	++	+++	++
$K_2Cr_2O_7$	Cr^{+6}	+++	++	-	++
$HgCl_2$	Hg	+++	++	+++	++
La_2O_3	La^{+}	++	+++	+++	++
$Na_2MoO_4.2H_2O$	Mo^{+6}	++	-	++	-
$NiCl_2.6H_2O$	Ni^{+2}	+	-	++	-
$C_4H_6O_4Pb.3H_2O$	Pb^{+2}	-	++	+++	++
$PdCl_2$	Pd^{+2}	++	+++	++	+
Y_2O_3	Y^{+}	++	+++	++	+

4.8. Seed germination

The quality and quantity of crop yield are severely decreased by iron deficiency. The ecosystem's natural food chain is also altered by this decrease in crop yield [276]. Currently, plant growth-promoting microorganisms can play significant roles in the accessibility of nutrients and metals by influencing plant growth dynamics and by directly affecting the uptake of heavy metals through rhizosphere processes like chelation, acidification, immobilization, precipitation and redox reactions [277]. An important characteristic of plant growth-promoting microorganisms that might affect plant development is the production of siderophores by bacteria, which is beneficial to plants. In addition to siderophore production, there are several other traits that promote plant development [278].

In this study, the effect of siderophores on the germination of seeds (Brown chickpea (*C. arietinum* L.), Peanut (*A. hypogaea*), Green gram (*V. radiata*), and Kabuli chana (*Cicer*

arietinum)) was investigated. Seeds were incubated in cell-free supernatant of siderophore production media, and seeds incubated in water were used as control. Before experimentation, the supernatant was checked for the presence of siderophores using CAS assay. The siderophore-positive supernatant was used for further work. The germination percentage was calculated after 36 h, but sprouting was observed regularly, and the length of the root was measured every 12 h. Among the three isolates, SMI_1 showed better seedlings growth and germination rate. After 36 h, significant growth in seedlings and an increase in plumule length were observed in all bacterial isolates (Figure 4.23). Plumule length and germination percentage of each seed in respective isolate supernatant were reported in Table 4.11.

In iron limitation condition, siderophore-producing microorganisms can be used as bio-fertilizer to increase wheat growth. Iron shortage inhibits growth and weakens photosynthesis. *Bacillus* sp. WR12 increased iron acquisition and alleviated these effects [1]. Siderophore producing *P. fluorescens* RB5 showed inhibitory effect on phytopathogen *R. cerealis*, which causes wheat sheath blight [282]. Hence, the bacteria that produce siderophores can be employed as bio-fertilizer to enhance plant growth and as a biocontrol agent against plant pathogens. Roslan reported the plant growth promoting potential of *Enterobacter* sp., IAA producing and P solubilizing *E. ludwigii* improved the growth of flax culture and root surface area and also improved the uptake of essential metals and calcium uptake in Pigeon pea and Chicken pea. *Enterobacter* sp. increased the phosphorous and potassium uptakes which reflected in the improvement of okra seedling plant [283].

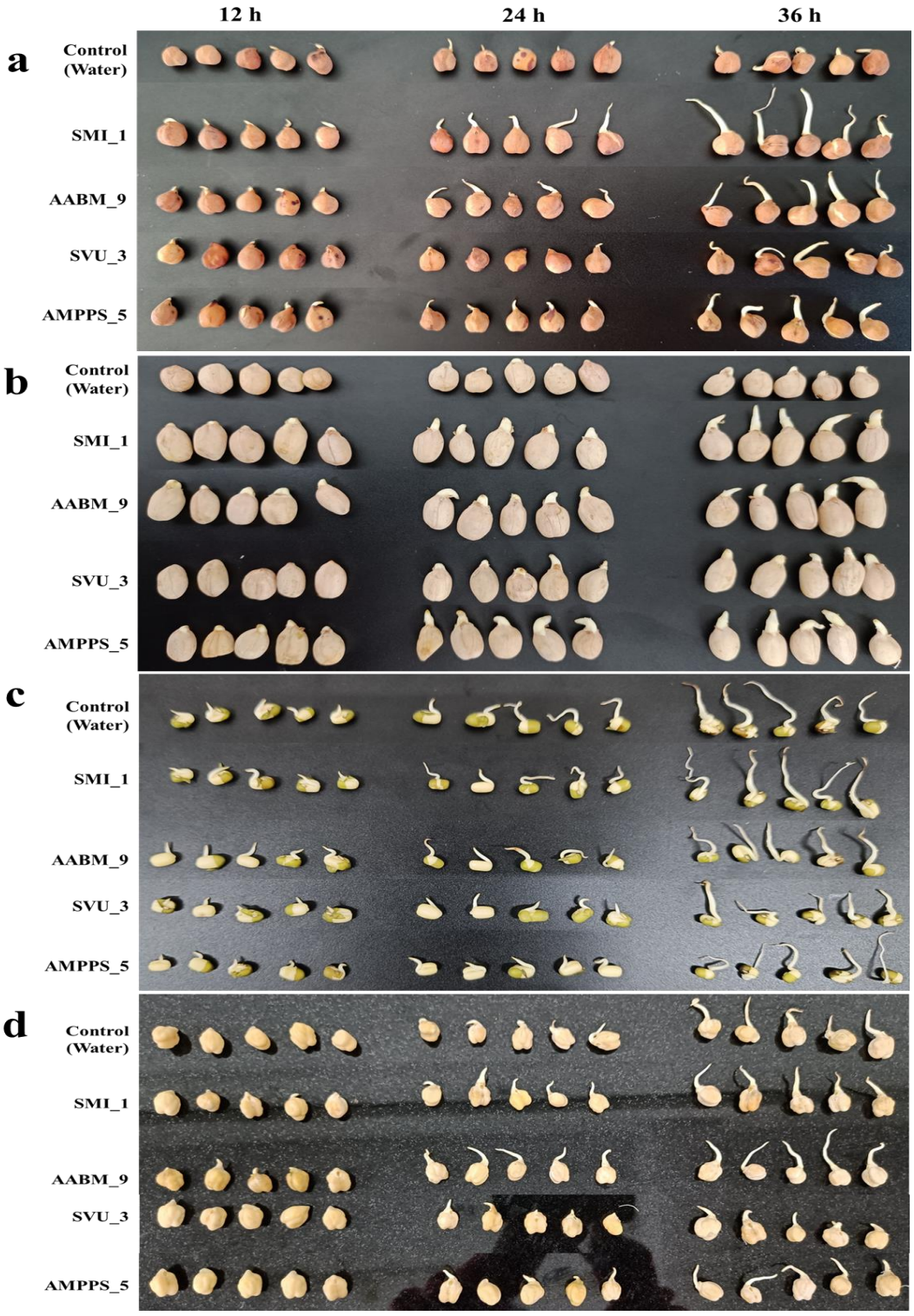

Figure 4.23: Seed germination (**(a)** Brown chickpea, **(b)** Peanut, **(c)** Green gram, and **(d)** Kabuli chana) in presence of tap water (control) and cell-free supernatant of marine bacterial isolates (SMI_1, AABM_9, SVU_3, and AMPPS_5).

Table 4.11: Length of the seed (Brown chickpea, Peanut, Green gram and Kabuli chana) germinate in the presence of tap water (control) and cell-free supernatant of marine bacterial isolates (SMI_1, AABM_9, SVU_3, and AMPPS_5) at various incubation times (12 h, 24 h, and 36 h).

Species	Cell-free Supernatant of	Length (cm) at Incubation Time (h)			%GP
		12	24	36	
Brown chickpea (*C. arietinum* L.)	Control (Tap Water)	0	0.16 ± 0.16	0.38 ± 0.08	36.2
	SMI_1	0.32 ± 0.13	0.82 ± 0.22	1.76 ± 0.35	92.4
	AABM_9	0.23 ± 0.04	0.6 ± 0.12	1.28 ± 0.14	89.1
	SVU_3	0.04 ± 0.05	0.12 ± 0.04	0.66 ± 0.24	40.6
	AMPPS_5	0.14 ± 0.08	0.36 ± 0.05	0.84 ± 0.13	67.3
Peanut (*A. hypogaea*)	Control (Tap Water)	0	0.18 ± 0.11	0.42 ± 0.08	28.1
	SMI_1	0.22 ± 0.04	0.52 ± 0.08	1.12 ± 0.13	84.9
	AABM_9	0.24 ± 0.05	0.46 ± 0.09	0.74 ± 0.20	71.4
	SVU_3	0	0.28 ± 0.08	0.46 ± 0.08	36.1
	AMPPS_5	0.14 ± 0.05	0.66 ± 0.16	0.9 ± 0.12	63.2
Green gram (*V. radiata*)	Control (Tap Water)	0.26 ± 0.08	0.94 ± 0.36	1.8 ± 0.33	67.4
	SMI_1	0.34 ± 0.13	0.74 ± 0.11	2.22 ± 0.4	96.2
	AABM_9	0.32 ± 0.08	0.86 ± 0.86	1.58 ± 0.19	93.7
	SVU_3	0.24 ± 0.05	0.6 ± 0.6	1.34 ± 0.34	64.8
	AMPPS_5	0.28 ± 0.08	0.58 ± 0.08	1.54 ± 0.33	81.3
Kabuli chana (*C. arietinum*)	Control (Tap Water)	0	0.98 ± 0.39	1.96 ± 0.4	52.6
	SMI_1	0.28 ± 0.13	0.92 ± 0.27	1.86 ± 0.39	89.2
	AABM_9	0.22 ± 0.08	1.4 ± 0.29	2.04 ± 0.37	82.5
	SVU_3	0	0.38 ± 0.14	1 ± 0.12	67.2
	AMPPS_5	0.04 ± 0.05	0.6 ± 0.2	1.44 ± 0.4	78.3

4.9. Synthesis of AgNPs

Low-molecular weight metal chelators (such as metallophores or siderophores) consist of a unique arrangement of functionally active reactive sites (such as catechols or hydroxamtes) which arraign, complex, or coordinate with free metal ions, these distinctive functional associations can be used or relevant in biological context (for example, re-entry of iron-siderophore complex into bacteria) [233]. These unique microbial metallophores have evolved to complex with metal ions, unlike synthetic molecules, and because these metal complexes are crucial for metal cycle, they have specialized significance for the producing

bacteria [209]. This can be seen in the acquisition of various metals, such as copper and boron, which are important within environmental niches as well as defense against particular metal toxicities [209].

The presented objective emphasized on the application of siderophore (marine bacterial source [233]) in the synthesis of AgNPs through biological approach and its comparison in physicochemical properties along with *in vitro* potential with that of chemical synthesized AgNPs. Throughout the literature, only a few papers have highlighted the use of siderophores in the NPs synthesis (Table 2.4). The occurrence of brown color at the end of reaction time indicates the formation or synthesis of AgNPs, which is a characteristic visual indicator [187–189,193,234].

4.10. Characterization of AgNPs

Standard analytical techniques were employed in determining the physicochemical properties of the as-synthesized AgNPs. It is of primary significance to determine the physicochemical properties of the AgNPs to understand their antibacterial, anticancer, and photocatalytic activities. Table 4.12 presents the results obtained from the characterization studies of the as-synthesized AgNPs (Che-AgNPs and Bio-AgNPs).

4.10.1. UV-Vis spectral analysis

The as-synthesized AgNPs were preliminary characterized for its optical property using UV-Vis spec., which is considered as a basic technique. The Che-AgNPs showed a broader peak with λ_{SPR} at 455 nm, whereas Bio-AgNPs showed a narrow peak comparatively with λ_{SPR} at 415 nm (Figure 4.24). The peaks observed were within the range of AgNPs as observed in the literature [187–189,193,234]. From the peak observed, it was evident that

AgNPs synthesized through the biological approach have better size and shape compared to chemical approach [187,189].

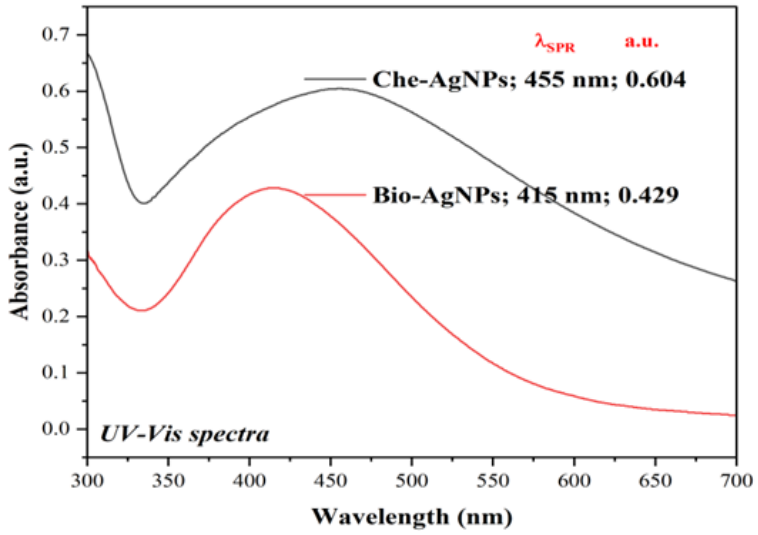

Figure 4.24: Characterization studies of Che-AgNPs and Bio-AgNPs using UV-Vis spectra.

Maduraimuthu et al. observed the characteristic SPR of AgNPs at 428 nm and 435 nm [284]. Shafiq et al. observed the SPR at 443 nm with a narrow peak [285]. Nejad et al. observed the occurrence of SPR in the range of 400 to 450 nm [286]. Leyu et al. observed the SPR peak at 422 nm [287]. Qanash et al. observed the sharp SPR peak at 412 nm [288].

4.10.2. Particle size distribution analysis

The PSA determined the particle size distribution of as-synthesized AgNPs to be in the range of 70 to 380 for Che-AgNPs and 60 to 230 nm for Bio-AgNPs (Table 4.12). The average particle size was observed to be 198.73 ± 22.56 and 135.19 ± 17.38 for Che-AgNPs and Bio-AgNPs, respectively (Figure 4.25). The poly-dispersity index (PDI) for Che-AgNPs is 0.288, whereas for Bio-AgNPs is 0.237 (Table 4.12). The significance of PDI value is that it defines the nature of the AgNPs colloidal solution, either polydisperse or monodisperse

[284]. The PDI value will be in the range of 0 to 1, where "0" represents the monodispersed colloidal solution and "1" represents the polydispersed colloidal solution [287].

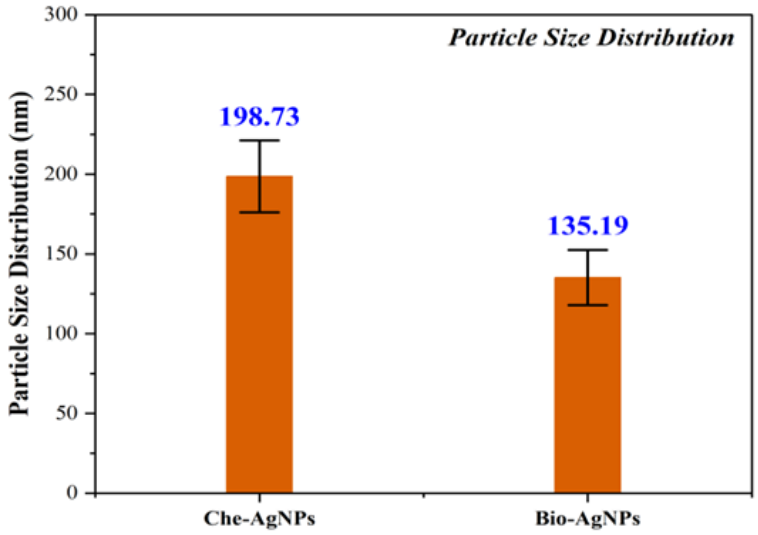

Figure 4.25: Characterization studies of Che-AgNPs and Bio-AgNPs using PSA analysis.

Maduraimuthu et al. reported the PSD to be in the range of 25 to 250 nm with average particle size to be 43 nm and PDI of 1.092 [284]. Nejad et al. reported the PSD to be in the range 10 to 100 nm with average particle size to be 70.92 nm and PDI of 0.203 [286]. Leyu et al. observed the average particle size to be 68.12 nm with PDI of 0.471 whereas the PSD to be in the range of 10 to 100 nm [287]. Alfarraj et al. observed the average particle size to be 87.08 nm with PDI of 0.233 whereas the PSD to be in the range of 30 to 300 nm [289]. Mustapha et al. observed the PSD range to be in the range of 80 to 600 nm with average particle size of 186 nm and PDI to be 0.230 [290].

4.10.3. Surface charge analysis

Surface charge determination can define the electrochemical stability of the AgNPs in the colloidal solution [287]. It can be either positive, zero, or negative charge. AgNPs with greater positive or lower negative charge offer high stability, causing repulsion between the AgNPs and avoiding aggregation [287]. The surface charge of the as-synthesized AgNPs was

found to be -21.94 ± 1.68 mV for Che-AgNPs and -32.67 ± 2.27 mV for Bio-AgNPs (Figure 4.26 and Table 4.12). It was evident that the Bio-AgNPs offers higher stability due to its lower negative charge compared to Che-AgNPs.

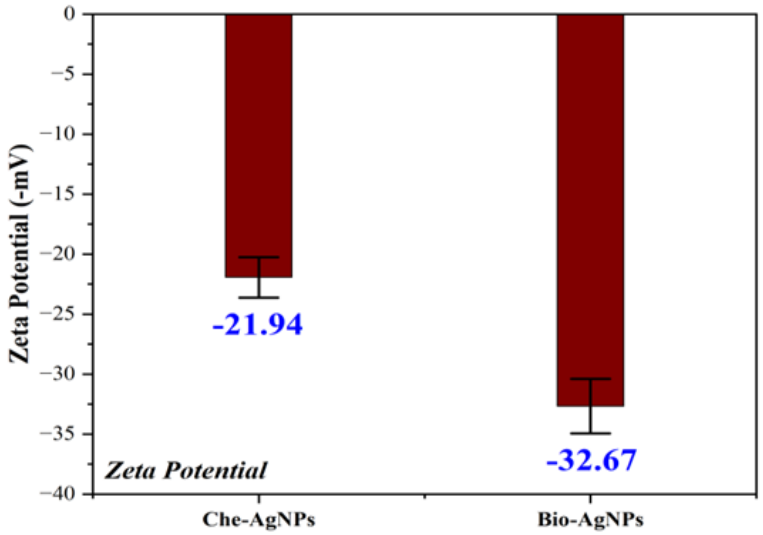

Figure 4.26: Characterization studies of Che-AgNPs and Bio-AgNPs using ZP analysis.

Maduraimuthu et al. reported the AgNPs with surface charge of -59.0 mV [284]. Nejad et al. reported the surface charge of AgNPs with -11.40 mV [286]. Leyu et al. reported the surface charge to be -25.7 mV [287]. Alfarraj et al. reported the surface charge of -14.2 for AgNPs [289]. Mustapha et al. reported the surface charge to be -39.9 mV [290].

4.10.4. XRD analysis

It was evident from the XRD analysis that the as-synthesized AgNPs were crystalline in nature (Figure 4.27). Intense sharp peaks were observed at peak positions 38.18°, 44.50°, 64.28°, 77.03°, and 81.44° for both Che-AgNPs and Bio-AgNPs (Figure 4.27). Using the Debye-Scherrer's equation, the average crystallite size "D" was found to be 23.56 nm and 18.43 nm for Che-AgNPs and Bio-AgNPs, respectively (Table 4.12).

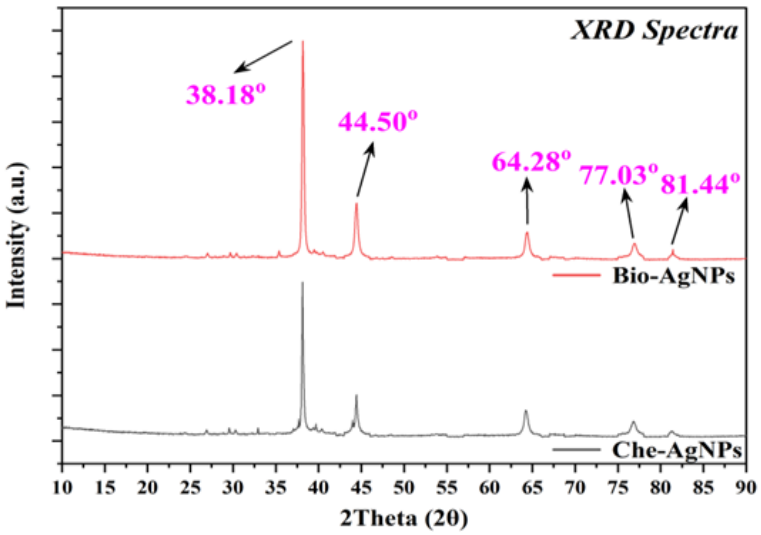

Figure 4.27: Characterization studies of Che-AgNPs and Bio-AgNPs using XRD analysis.

Leyu et al. reported the peak positions of 38.18°, 44.25°, 64.18°, 77.38°, and 81.11° with the average crystallite size of 33.4 nm [287]. Maduraimuthu et al. reported the peak positions of 38.34°, 44.91°, 65.29°, and 77.47° [284]. Shafiq et al. reported the occurrence of peak positions of 37.91°, 44.08°, 64.3°, and 77.30° with average crystallite size to be 26.82 nm [285]. Rehman et al. reported the peak positions of 27.71°, 32.15°, 38.13°, 44.3°, 46.11°, 54.63°, 57.48°, 64.35°, and 77.40° [291]. Afandy et al. reported the peak positions of 38°, 44°, and 64° with average crystallite size to be 28.1 nm [292].

4.10.5. SEM and EDX analysis

SEM and EDX analysis were performed to determine the morphology and elemental composition of the as-synthesized AgNPs. From the results it was evident that the NPs synthesized were indeed AgNPs (Figure 4.28). Che-AgNPs showed about 82.4% of Ag in weight percentage (wt.%), whereas Bio-AgNPs showed about 87.4% of Ag (Table 4.12).

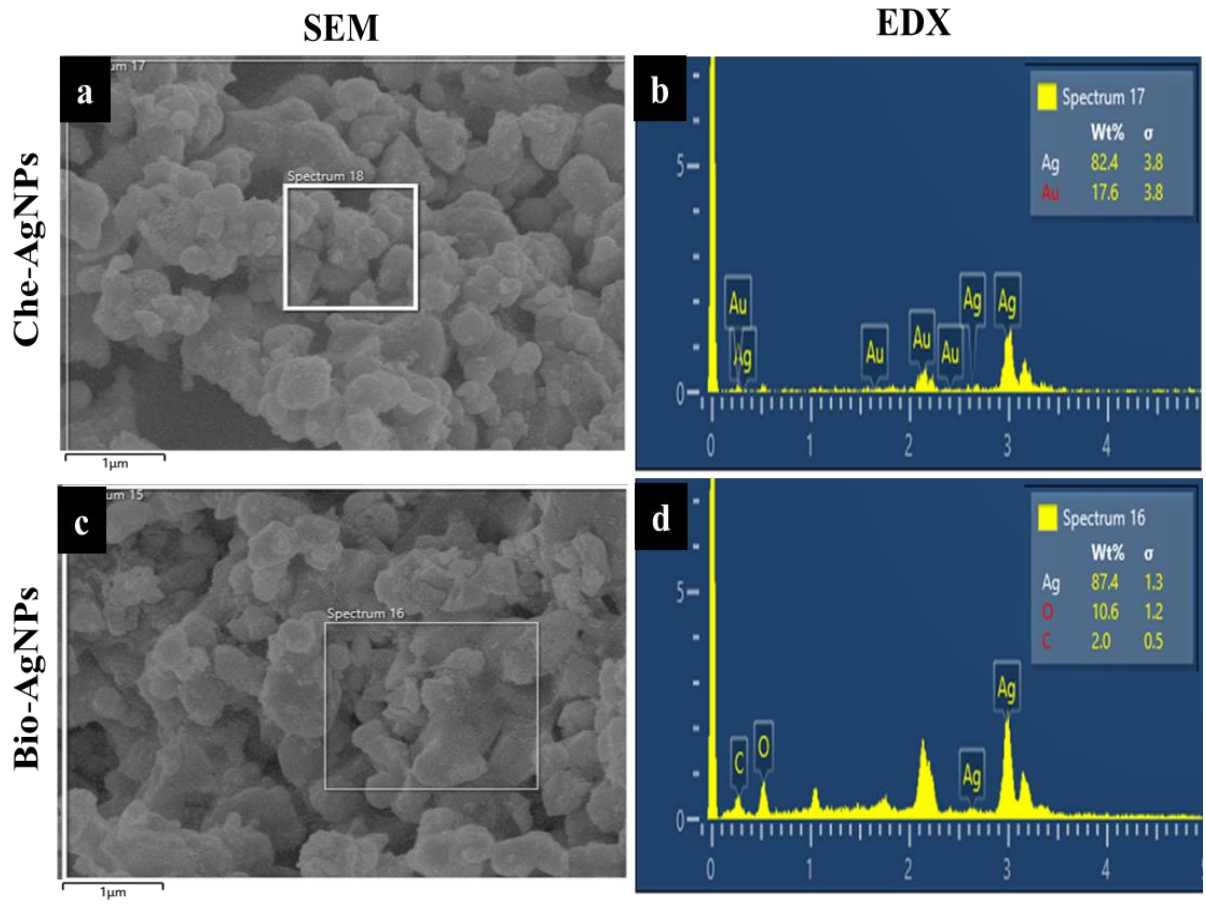

Figure 4.28: Characterization studies of Che-AgNPs and Bio-AgNPs using SEM and EDX analysis.

Maduraimuthu et al. reported the occurrence of peaks in the range of 2.7 to 3.5 KeV in EDX spectra [284]. Shafiq et al. reported a strong EDX peak at 3 KeV with wt.% of 88.4 for Ag [285]. Qanash et al. reported the presence of strong EDX peak at 3 KeV with wt.% of 76.67 for Ag [288]. Mustapha et al. reported a sharp peak at 3 KeV in EDX spectra with wt.% of ~45 for Ag [290]. Sumra et al. reported the presence of three sharp peaks in EDX spectra at 0.8, 2.7, and 3 KeV [293].

Table 4.12: Details of as-synthesized AgNPs characterization studies.

Instrument(s)	Feature(s)	Unit(s)	Che-AgNPs	Bio-AgNPs
UV-Vis spec	Wavelength	nm	455	415
	Absorbance	a.u.	0.604	0.429
PSA	Particle size distribution	nm	70 to 380	60 to 230
	Average particle size	nm	198.73 ± 22.56	135.19 ± 17.38
	Poly-dispersity index	-	0.288	0.237
	Surface charge	mV	-21.94 ± 1.68	-32.67 ± 2.27
	Electrophoretic mobility	µm*cm/Vs	-1.71035	-2.54637
XRD	Peak position	2θ	38.18	38.16
	Peak intensity	a.u.	7195	9623
	Crystallite size "D"	nm	23.56	18.43
EDX	Element composition	Wt.%	82.4	87.4

4.11. Antibacterial activity

Since the dawn of time, people have been aware of the antibacterial characteristics of noble metals [202]. Ag compounds, metallic Ag, and Ag salts have been used to successfully stop microbial development since the beginning of time [202]. AgNPs, which have outstanding antibacterial effects against a variety of microbial diseases due to their enormous surface area to volume ratio, were made possible by advances in nanotechnology [294].

From the results (Table 4.13), it was evident that the as-synthesized AgNPs showed moderate to good antibacterial activity. Bio-AgNPs showed better activity against *B. subtilis* (Figure 4.29), *CoNS* (Figure 4.30), and *S. aureus* (Figure 4.35), whereas Che-AgNPs showed better activity against *E. coli* (Figure 4.31), *K. pneumoniae* (Figure 4.32), and *P. aeruginosa* (Figure 4.34). Similar activity was observed against *P. vulgaris* (Figure 4.33). It was observed that Bio-AgNPs were effective against gram+ bacteria, whereas Che-AgNPs were effective against gram- bacteria (Figure 4.29 to 4.35).

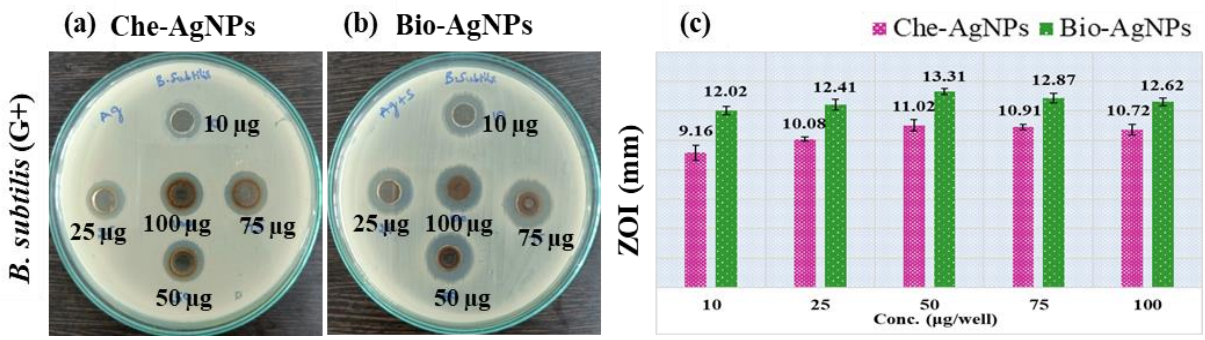

Figure 4.29: Antibacterial studies of **(a)** Che-AgNPs and **(b)** Bio-AgNPs against *B. subtilis* and their respective **(c)** ZOI (mm) in bar graph.

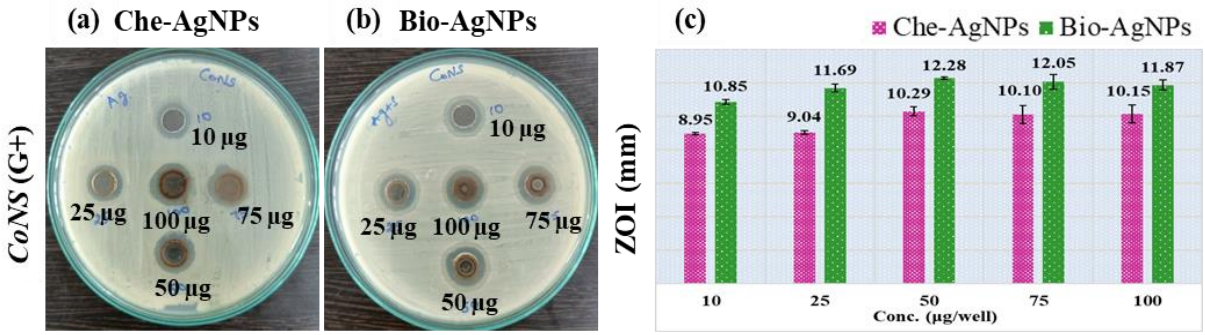

Figure 4.30: Antibacterial studies of **(a)** Che-AgNPs and **(b)** Bio-AgNPs against *CoNS* and their respective **(c)** ZOI (mm) in bar graph.

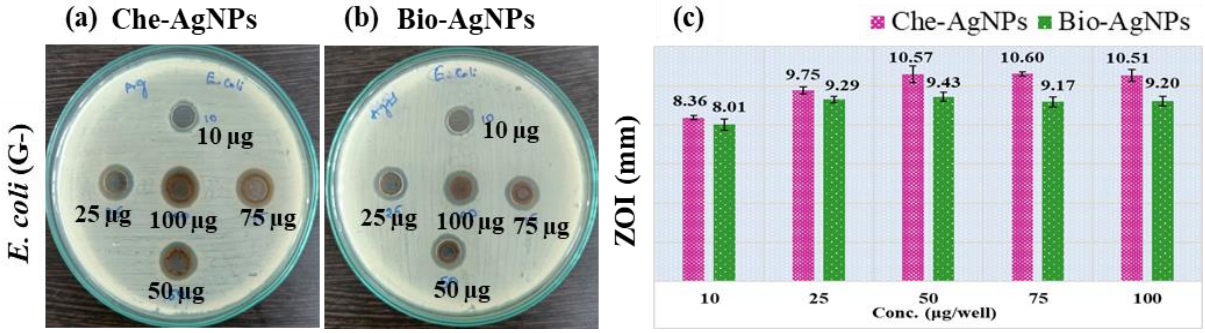

Figure 4.31: E Antibacterial studies of **(a)** Che-AgNPs and **(b)** Bio-AgNPs against *E. coli* and their respective **(c)** ZOI (mm) in bar graph.

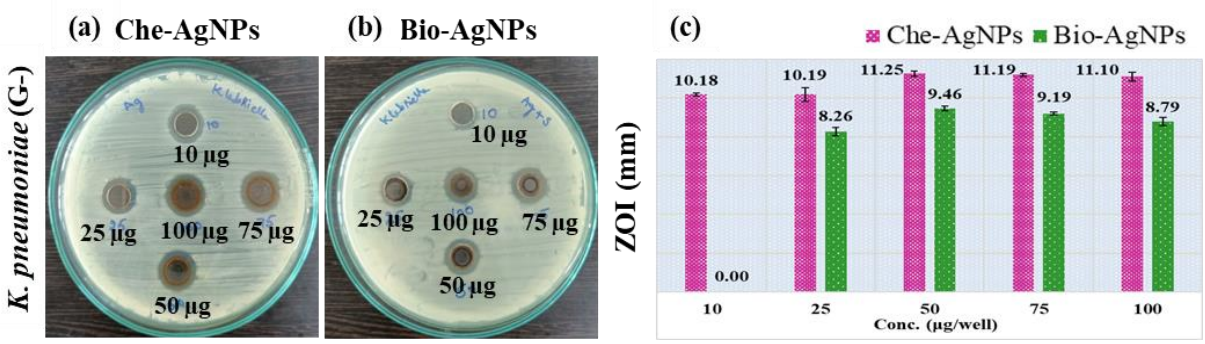

Figure 4.32: Antibacterial studies of **(a)** Che-AgNPs and **(b)** Bio-AgNPs against *K. pneumoniae* and their respective **(c)** ZOI (mm) in bar graph.

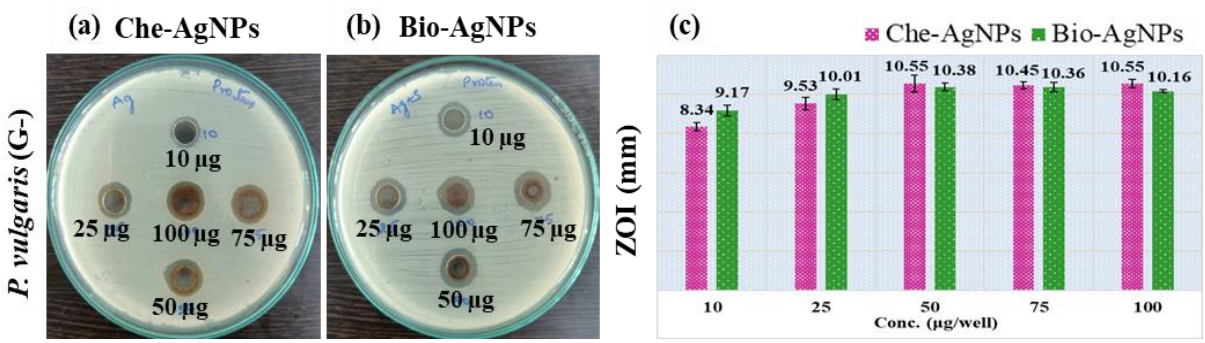

Figure 4.33: Antibacterial studies of **(a)** Che-AgNPs and **(b)** Bio-AgNPs against *P. vulgaris* and their respective **(c)** ZOI (mm) in bar graph.

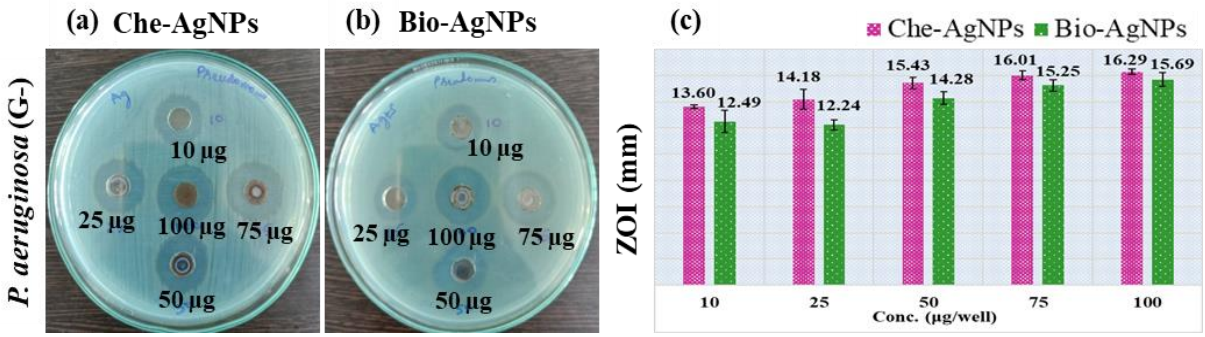

Figure 4.34: Antibacterial studies of **(a)** Che-AgNPs and **(b)** Bio-AgNPs against *P. aeruginosa* and their respective **(c)** ZOI (mm) in bar graph.

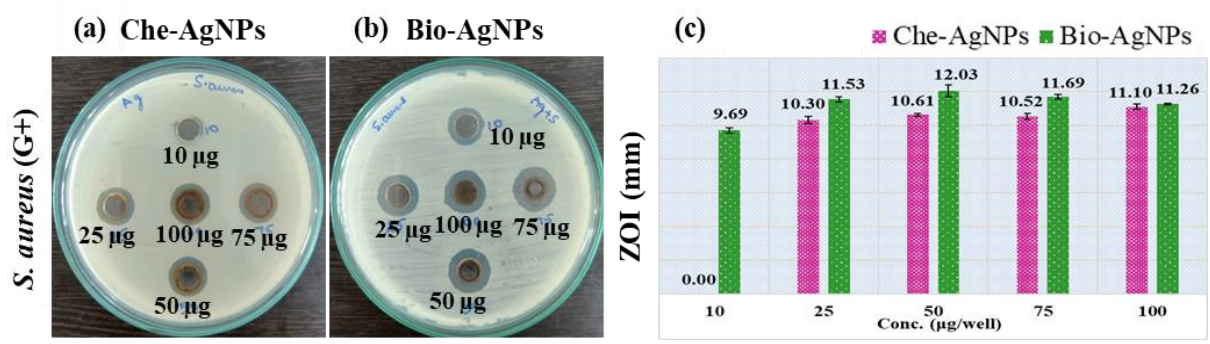

Figure 4.35: Antibacterial studies of **(a)** Che-AgNPs and **(b)** Bio-AgNPs against *S. aureus* and their respective **(c)** ZOI (mm) in bar graph.

Table 4.13: Zone of inhibition (mm) observed during antibacterial studies of as-synthesized AgNPs.

AgNPs	**Che**					**Bio**				
Concentration (µg/well)	**10**	**25**	**50**	**75**	**100**	**10**	**25**	**50**	**75**	**100**
ZOI (mm) for *B. subtilis*	9.16 ± 0.51	10.08 ± 0.14	11.02 ± 0.37	10.91 ± 0.19	10.72 ± 0.37	12.02 ± 0.28	12.41 ± 0.36	13.31 ± 0.20	12.87 ± 0.31	12.62 ± 0.27
ZOI (mm) for *CoNS*	8.95 ± 0.08	9.04 ± 0.11	10.29 ± 0.27	10.10 ± 0.55	10.15 ± 0.53	10.85 ± 0.14	11.69 ± 0.24	12.28 ± 0.08	12.05 ± 0.44	11.87 ± 0.31
ZOI (mm) for *E. coli*	8.36 ± 0.10	9.75 ± 0.19	10.57 ± 0.43	10.60 ± 0.11	10.51 ± 0.31	8.01 ± 0.29	9.29 ± 0.17	9.43 ± 0.22	9.17 ± 0.25	9.20 ± 0.24
ZOI (mm) for *K. pneumoniae*	10.18 ± 0.08	10.19 ± 0.35	11.25 ± 0.13	11.19 ± 0.07	11.10 ± 0.23	-	8.26 ± 0.21	9.46 ± 0.13	9.19 ± 0.07	8.79 ± 0.21
ZOI (mm) for *P. vulgaris*	8.34 ± 0.21	9.53 ± 0.31	10.55 ± 0.44	10.45 ± 0.18	10.48 ± 0.22	9.17 ± 0.28	10.01 ± 0.27	10.78 ± 0.41	10.52 ± 0.24	10.46 ± 0.07
ZOI (mm) for *P. aeruginosa*	13.60 ± 0.14	14.18 ± 0.76	15.43 ± 0.45	16.01 ± 0.34	16.29 ± 0.19	12.49 ± 0.85	12.24 ± 0.38	14.28 ± 0.50	15.25 ± 0.44	15.69 ± 0.54
ZOI (mm) for *S. aureus*	-	10.30 ± 0.22	10.61 ± 0.08	10.52 ± 0.17	11.10 ± 0.17	9.69 ± 0.15	11.53 ± 0.15	12.03 ± 0.35	11.69 ± 0.14	11.26 ± 0.05

Gram+ bacteria have thick cell walls usually ranging from 20 to 80 nm, which is made up of only one but thick peptidoglycan layer consisting of teichoic acid [295,296]. On the contrary, Gram- bacteria have comparatively thin cell walls usually ranging from 8 to 10 nm, which is made up of thin phospholipid layers (typically more than one) sandwiching the peptidoglycan layer without the teichoic acid [295,296]. The surface of both groups has a negative charge, however the Gram- bacteria show high negative charge compared to Gram+

bacteria [297]. The interaction between the bacterial cell wall and the NPs is governed by their surface charge [298]. It was also observed that the lipopolysaccharide structure has great impact over the binding of NPs to the lipid bilayer in Gram- bacteria [299]. On the other hand, Gram+ bacteria lack lipid bilayer or lipopolysaccharide layer and along with lower negative charge can be more susceptible to NPs permeability [296,297].

Bio-AgNPs with high-negative overall surface charge (-32.67 mV) might be repelled by the high-negative surface charge of the Gram- bacteria. Whereas the Gram+ bacteria have comparatively lower charge and are more susceptible to the NPs with higher-negative charge, even though they have thick peptidoglycan layer. On the other hand, Che-AgNPs (-21.9) had lower-negative charge compared to Bio-AgNPs, therefore they have shown good activity against Gram- bacteria. Even though the size of Bio-AgNPs (135.19 nm) is smaller compared to Che-AgNPs (198.73), the overall surface charge (i.e., high-negative) might have played a crucial role or influenced the binding of Che-AgNPs to the surface of Gram- bacteria. Therefore, it was noted that along with size, surface charge is equal or in some cases more important to exhibit good antibacterial activity [296,297].

From Figure 4.29 to 4.35 and Table 4.13, it was also observed that the as-synthesized AgNPs showed highest ZOI at 50 µg per well concentration against test bacteria. From Figure 4.29 to 4.35, it was noticed that the AgNPs were prone to aggregation as the concentration increased beyond 50 µg per well. In comparison, Che-AgNPs has shown more aggregation, which can be seen by the occurrence of dark brown color ring formation at the well edges. Bio-AgNPs were less prone to aggregation might be because of their higher negative surface charge (Table 4.13). Among the test bacteria, only *P. aeruginosa* has shown concentration dependent ZOI (Figure 4.34).

AgNPs and the Ag^+ ions produced when they dissolve both have antibacterial properties. AgNPs and Ag^+ ions can both interact with various bacterial cells and biofilm constituents. They hinder bacterial metabolism and outside cellular processes through these interactions [300]. Overall, the antibacterial potential of AgNPs is due to the combination of several mechanisms such as generation of reactive oxygen species eliciting oxidative stress, nucleic acids damage, hindering electron transport chain, inactivation of relevant enzymes, destabilization of protein structures, and destruction of cell membrane (Figure 4.36) [187,195,198]. AgNPs are now a viable option for antimicrobial therapy as a result of its complex antibacterial mechanism [301].

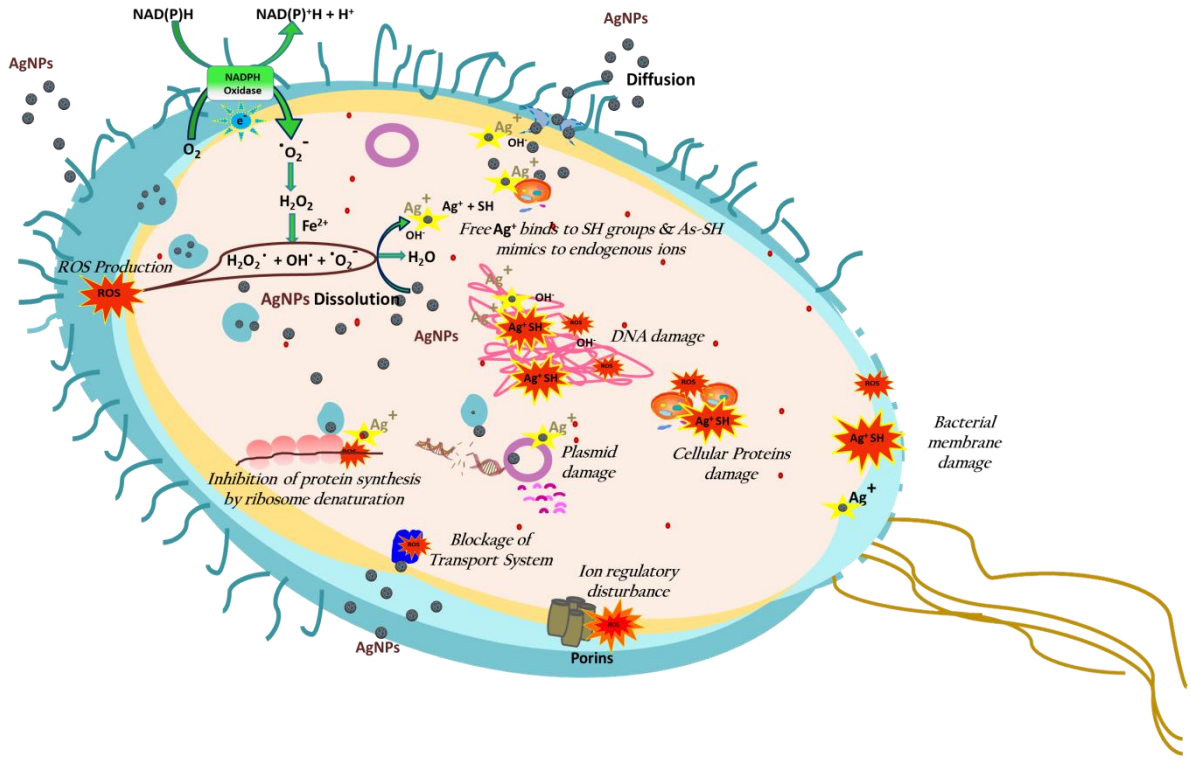

Figure 4.36: Possible antibacterial mechanism involved in presence of AgNPs [187,189].

This chapter presents the results and discussion related to the work done in four parts. In first part the collection of marine water and sediments samples from marine estuary regions and isolated the fast-growing bacteria. All the isolates were screened for siderophore

production using CAS (Chrome Azurol S) assay, and the most efficient four isolates were selected for further work. 16S rRNA molecular characterization of isolates showed the nearest similarity of SMI_1 with *Bacillus taeanensis*, AABM_9 with *Enterobacter* sp., SVU_3 with *Marinobacter sp.* SVU_3 and AMPPS_5 with *Pseudomonas mendocina*.

In the second part the production parameters of the succinate medium were optimized to enhance the siderophore production. The optimum production of siderophores for SMI_1 was *93.57 %SU* (Siderophore Units) (after 48 h of incubation at 30 °C, pH 8, sucrose as carbon source, sodium nitrate as nitrogen source, 0.4% of succinic acid) and for AABM_9 was *87.18 %SU* (after 36 h of incubation period at 30 °C and pH 8 in the presence of sucrose, ammonium sulfate and 0.4% succinic acid). The maximum production of siderophores for SVU_3 was *83.15 %SU* (after 48 h of incubation at 35 °C and pH 8.5 in the presence of glucose, sodium nitrate and 0.6 % succinic acid) and for AMPPS_5 was *91.17 %SU* (after 36 h of incubation at 35 °C, pH 8.5, glucose as carbon source, ammonium sulfate as nitrogen source, and 0.4% of citric acid). Effects of Copper, Manganese and Zinc metal ions on siderophore production were studied. The siderophore was separated using an Amberlite XAD-2 column followed by Sephadex LH-20. The fractions were concentrated by removing methanol using rotary evaporator and lyophilized samples stored. The chemical nature was identified by Thin-layer chromatography, Fourier Transformation Infrared analysis (FTIR), High Resolution – Mass Spectroscopy (HR-MS) and Nuclear Magnetic Resonance (NMR) spectroscopy.

In the third part the heavy metal chelation of siderophore-producing marine bacterial isolates was investigated on Ag^{+2}, Al^{+2}, Cd^{+2}, Co^{+2}, Cr^{+6}, Hg^{+2}, La^{+3}, Mo^{+6}, Ni^{+2}, Pb^{+2}, Pd^{+2}, and Y^{+3} metal ions (1mM, 5mM) by spotting method. All four isolates showed chelation activity on heavy metals except Ag^{+2}, Cd^{+2} and Mo^{+6} due to species-specific trait. Seed

germination studies were performed on seeds Brown chickpea (*Cicer arietinum* L.), Peanut (*Arachis hypogaea*), Green gram (*Vigna radiata*), and Kabul chana (*Cicer arietinum*) using siderophore supernatant.

Finally, in the fourth part the as-synthesized silver nanoparticles (AgNPs) via chemical (Che-AgNPs) and biological (Bio-AgNPs) methods were characterized for their optical, physicochemical, crystalline, and elemental composition properties. Che-AgNPs and Bio-AgNPs showed a peak at 455 nm and 415 nm with average particle size of 198.73 nm and 135.19 nm, whereas surface charge was found to be -21.94 mV and -32.67 mV, respectively. Che-AgNPs have shown better zone of inhibition (ZOI) against Gam- bacteria such as *E. coli* (10.57 mm), *K. pneumoniae* (11.25 mm), *P. aeruginosa* (15.43 mm), whereas Bio-AgNPs showed better ZOI against Gram+ bacteria such as *B. subtilis* (13.31 mm), *CoNS* (12.28 mm), *S. aureus* (12.03 mm) at 50 µg per well concentration. The next chapter concludes the research work done and included future perspectives.

Chapter V:
CONCLUSION and FUTURE SCOPE

CONCLUSION, ECONOMICAL ASPECTS, and FUTURE RESEARCH PROEPECTS

5.1. Conclusion

Iron is one of the essential and abundant metal on the surface of the earth, but at physiological pH it is unavailable to all living organisms. Similarly, in ocean water it is accessible to microbes in minimal concentrations. To overcome iron scarcity, marine bacteria produce siderophores. The present study reports the isolation, identification and characterization of siderophores producing marine bacterial isolates, SMI_1, AABM_9, SVU_3, and AMPPS_5. On performing biochemical tests and molecular analysis they were identified as *B. taeanensis* SMI_1, *Enterobacter* sp. AABM_9, and *P. mendocina* AMPPS_5, strains efficiently produce siderophores in Fe^{+3}-deficit media. To enhance the siderophores production, the effect of different production parameters was studied. The highest siderophore obtained was 96.48 %SU for SMI_1 after 48 h of incubation at 30 °C, pH 8, sucrose as carbon source, sodium nitrate as nitrogen source, and 0.4% of succinic acid. The optimum parameters of AABM_9 were 87.18 %SU after 36 h of incubation period at 30 °C and pH 8 in the presence of sucrose, ammonium sulfate and 0.4% succinic acid. Likewise, the maximum siderophores production for AMPPS_5 was 91.17 %SU after 36 h of incubation at 35 °C, pH 8.5, glucose as carbon source, ammonium sulfate as nitrogen source, and 0.4% of citric acid as organic acid. Isolates showed growth and production of siderophores in the presence of metals like Fe^{+3}, Cu^{+2}, Mn^{+2}, and Zn^{+2}. However, upon increasing the concentration of Fe^{+3} the siderophores production was radically decreased, possibly due to the negative regulation of transcriptional genes.

The siderophore was separated using an Amberlite XAD-2 column followed by Sephadex LH-20. The fractions were concentrated by rotary evaporation and lyophilized,

purified by Thin-layer chromatography solvent system n-butanol:acetic acid:dH2O (12:3:5). Wine-coloured spots confirmed presence of hydroxamate type of siderophore on spraying 0.1 M $FeCl_3$ solution. The λmax was observed at 421 nm on UV- spectral analysis which reflects the trihydroxamate siderophores. The chemical nature was identified by Fourier Transformation Infrared analysis (FTIR), Liquid Chromatography – Mass Spectroscopy (LC-MS) and Nuclear Magnetic Resonance (NMR) spectroscopy. The siderophore was identified at R_T 3.95 min on using acetonitrile and water as mobile phase and identified mass of siderophore $[M+H]^+$ m/z 561.3. Four isolates showed strong heavy-metal chelation activity in different heavy metals, and significant growth of peanut seedlings in seed germination experiments was observed in *Enterobacter* AABM_9. Further research is required to shed light on plant-growth-promoting marine bacteria and the mechanism involved in them. The as-synthesized AgNPs were characterized for their physicochemical properties using standard analytical techniques. Furthermore, the evaluation of their antibacterial property determined surface charge dependent activity. Che-AgNPs showed better activity against gram- bacteria, whereas Bio-AgNPs showed better activity against gram+ bacteria.

5.2. Economical aspects

It is of paramount importance to estimate the overall operating costs related with biotechnological processes, for example, in this case production of siderophores. Among the several factors involved: (i) cost of raw materials (chemical constituents involved in media formulation) and (ii) productivity (product yield) are considered to be fundamental. In general, approximately 10 - 60% of the operating or production costs are associated with the raw materials procurement in several product-based biotechnological production processes [246]. Therefore, optimization of chemical composition of media (such as carbon and nitrogen source) greatly helps in not only excluding the unnecessary media constituents but

also finding cheaper but efficient alternatives or substituents. For example, natural organic nitrogen sources such as peptone, and yeast extract are much costlier than the inorganic forms of nitrogen such as sodium nitrate and ammonium sulfate [4,246,247].

5.3. Future research prospects

Siderophores production has only gained significant momentum in the last few years owing to the discovery of siderophores' chelation ability towards several metal ions [235]. Furthermore, siderophores producing bacteria can aid in reduction of contamination associated with heavy metals through diffusion [302]. On the contrary, application of siderophores in day-to-day activities is limited: (i) failing to commercialize large scale production of siderophores, (ii) purification and characterization of siderophores is yet be standardized, (iii) bacterial biosynthesis leads to other impurities, (iv) several enzymes and cofactors are associated with siderophores biosynthesis, (v) yet to understand the associated secretory and regulatory mechanisms, (vi) lack of chemical, structural, and physiological characterization, and (vii) yet to explore the unknown habitats. As siderophores are of natural origin, their applications in the fields of medicine, agriculture, and environment are unlimited. True potential of siderophores is yet to be determined to make a just and sustainable society [4,303].

This chapter presents the conclusions derived from various stages of the study, including the isolation of siderophore-producing marine bacteria, optimization of production parameters, and purification of siderophores. It encompasses discussions on heavy metal chelation, the seed germination ability exhibited by siderophore-producing bacteria, and the synthesis of siderophore-based silver nanoparticles (AgNPs). Additionally, the chapter outlines potential avenues for future research.

REFERENCES

References

1. Yue, Z.; Chen, Y.; Hao, Y.; Wang, C.; Zhang, Z.; Chen, C.; Liu, H.; Liu, Y.; Li, L.; Sun, Z. Bacillus Sp. WR12 Alleviates Iron Deficiency in Wheat via Enhancing Siderophore- and Phenol-Mediated Iron Acquisition in Roots. *Plant Soil* **2022**, *471*, 247–260, doi:10.1007/s11104-021-05218-y.
2. Teta, R.; Esposito, G.; Kundu, K.; Stornaiuolo, M.; Scarpato, S.; Pollio, A.; Costantino, V. A Glimpse at Siderophores Production by Anabaena Flos-aquae UTEX 1444. *Mar. Drugs* **2022**, *20*, 1–9, doi:10.3390/md20040256.
3. Sun, Y.; Wu, J.; Shang, X.; Xue, L.; Ji, G.; Chang, S.; Niu, J.; Emaneghemi, B. Screening of Siderophore-Producing Bacteria and Their Effects on Promoting the Growth of Plants. *Curr. Microbiol.* **2022**, *79*, 1–12, doi:10.1007/s00284-022-02777-w.
4. Soares, E. V. Perspective on the Biotechnological Production of Bacterial Siderophores and Their Use. *Appl. Microbiol. Biotechnol.* **2022**, *106*, 3985–4004, doi:10.1007/s00253-022-11995-y.
5. Sultana, S.; Alam, S.; Karim, M.M. Screening of Siderophore-Producing Salt-Tolerant Rhizobacteria Suitable for Supporting Plant Growth in Saline Soils with Iron Limitation. *J. Agric. Food Res.* **2021**, *4*, doi:10.1016/j.jafr.2021.100150.
6. Sheng, M.; Jia, H.; Zhang, G.; Zeng, L.; Zhang, T.; Long, Y.; Lan, J.; Hu, Z.; Zeng, Z.; Wang, B.; et al. Siderophore Production by Rhizosphere Biological Control Bacteria Brevibacillus Brevis GZDF3 of Pinellia Ternata and Its Antifungal Effects on Candida Albicans. *J. Microbiol. Biotechnol.* **2020**, *30*, 689–699, doi:10.4014/jmb.1910.10066.
7. Kalyan, R.K. Of Bacterium Isolated From Calcareous Soils for Siderophore Production. **2022**, 1–28.
8. Lemare, M.; Puja, H.; David, S.R.; Mathieu, S.; Ihiawakrim, D.; Geoffroy, V.A.; Rigouin, C. Engineering Siderophore Production in Pseudomonas to Improve Asbestos Weathering . *Microb. Biotechnol.* **2022**, doi:10.1111/1751-7915.14099.
9. Manck, L.E.; Park, J.; Tully, B.J.; Poire, A.M.; Bundy, R.M.; Dupont, C.L.; Barbeau, K.A. Petrobactin, a Siderophore Produced by Alteromonas, Mediates Community Iron Acquisition in the Global Ocean. *ISME J.* **2022**, *16*, 358–369, doi:10.1038/s41396-021-01065-y.
10. Shen, Q.; Dai, G.; Ravichandran, V.; Liu, Y.; Zhong, L.; Sui, H.; Ren, X.; Jiao, N.; Zhang, Y.; Zhou, H.; et al. Saccharochelins A-H, Cytotoxic Amphiphilic Siderophores from the Rare Marine Actinomycete Saccharothrix Sp. D09. *J. Nat. Prod.* **2021**, *84*, 2149–2156, doi:10.1021/acs.jnatprod.1c00155.
11. Butler, A.; Theisen, R.M. Iron(III)–Siderophore Coordination Chemistry: Reactivity of Marine Siderophores. *Coord. Chem. Rev.* **2010**, *254*, 288–296, doi:10.1016/j.ccr.2009.09.010.
12. Cavas, L.; Kirkiz, I. Characterization of Siderophores from Escherichia Coli Strains through Genome Mining Tools: An AntiSMASH Study. *AMB Express* **2022**, *12*, doi:10.1186/s13568-022-01421-x.
13. Nithyapriya, S.; Lalitha, S.; Sayyed, R.Z.; Reddy, M.S.; Dailin, D.J.; El Enshasy, H.A.; Luh Suriani, N.; Herlambang, S. Production, Purification, and Characterization of Bacillibactin Siderophore of Bacillus Subtilis and Its Application for Improvement in Plant Growth and Oil Content in Sesame. *Sustain.* **2021**, *13*, doi:10.3390/su13105394.
14. Galica, T.; Borbone, N.; JanMareš; Kust, A.; Caso, A.; Esposito, G.; Hájek, J.; Reháková, K.; Urajová, P.; Costantino, V.; et al. Cyanochelins , an Overlooked Class of Widely Distributed. *Appl. Environ. Microbiol.* **2021**, *87*, 1–13, doi:doi.org/10.1128/AEM.03128-20.
15. Moore, L.E.; Heller, M.I.; Barbeau, K.A.; Moffett, J.W.; Bundy, R.M. Organic Complexation of Iron by Strong Ligands and Siderophores in the Eastern Tropical

North Pacific Oxygen Deficient Zone. *Mar. Chem.* **2021**, *236*, doi:10.1016/j.marchem.2021.104021.
16. Barakat, H.; Qureshi, K.A.; Alsohim, A.S.; Rehan, M. The Purified Siderophore from Streptomyces Tricolor HM10 Accelerates Recovery from Iron-Deficiency-Induced Anemia in Rats. *Molecules* **2022**, *27*, 4010, doi:10.3390/molecules27134010.
17. Park, J.; Durham, B.P.; Key, R.S.; Groussman, R.D.; Pinedo-Gonzalez, P.; Hawco, N.J.; John, S.G.; Carlson, M.C.G.; Lindell, D.; Juranek, L.; et al. Siderophore Production and Utilization by Microbes in the North Pacific Ocean. *bioRxiv* **2022**, 2022.02.26.482025.
18. Park, J.; Durham, B.P.; Key, R.S.; Groussman, R.D.; Pinedo-Gonzalez, P.; Hawco, N.J.; John, S.G.; Carlson, M.C.G.; Lindell, D.; Juranek, L.; et al. Siderophore Production and Utilization by Microbes in the North Pacific Ocean. *bioRxiv* **2022**, 2022.02.26.482025.
19. Sarvepalli, M.; Velidandi, A.; Ramachandravarapu, A.K.; Korrapati, N. Marine Actinomycetes Siderophores: Types, High Throughput Characterization Techniques, Applications, and Their Association with Nanotechnology: A Comprehensive Review. *NanoWorld J.* **2024**, *10*, 1–21, doi:10.17756/nwj.2024-130.
20. Katumba, G.L.; Tran, H.; Henderson, J.P. The Yersinia High-Pathogenicity Island Encodes a Siderophore-Dependent Copper Response System in Uropathogenic Escherichia Coli. *MBio* **2022**, *13*, doi:10.1128/MBIO.02391-21.
21. Francis, J. Isolation from Acid-Fast Bacteria of a Growth-Factor for Mycobacterium Johnei and of a Precursor of Phthiocol. *Nature* **1949**, *163*, 365–366.
22. Hesseltine, C.W. *COPROGEN, A NEW GROWTH FACTOR FOR COPROPHILIC FUNGI*; 1952; Vol. 74;.
23. Neilands, J.B. *A Crystalline Organo-Iron Pigment from a Rust Fungus*; 1952; Vol. 74;.
24. GARIBALDI, J.A.; Neilands, J.B. Formation of Iron-Binding Compounds by Micro-Organisms. *Nature* **1956**, *177*, 526–527.
25. C.C.R. de Carvalho, C.; P.C. Marques, M.; Fernandes, P. Recent Achievements on Siderophore Production and Application. *Recent Pat. Biotechnol.* **2011**, *5*, 183–198, doi:10.2174/187220811797579114.
26. Raines, D.J.; Sanderson, T.; Wilde, E.; Duhme-Klair, A.-K. Siderophores. In *Reference Module in Chemistry, Molecular Sciences and Chemical Engineering*; 2015; pp. 1–32 ISBN 9780124095472.
27. Matzanke, B.F. Lecture Notes : Siderophores and Iron Metabolism - Structures , Functions , Role in Infection and Potential as a Novel Class of Antibiotics 2003, 1–47.
28. Martinez, J.S.; Butler, A. Marine Amphiphilic Siderophores: Marinobactin Structure, Uptake, and Microbial Partitioning. *J. Inorg. Biochem.* **2007**, *101*, 1692–1698, doi:10.1016/j.jinorgbio.2007.07.007.
29. Martinez, J.S.; Carter-Franklin, J.N.; Mann, E.L.; Martin, J.D.; Haygood, M.G.; Butler, A. Structure and Membrane Affinity of a Suite of Amphiphilic Siderophores Produced by a Marine Bacterium. *Proc. Natl. Acad. Sci. U. S. A.* **2003**, *100*, 3754–3759, doi:10.1073/pnas.0637444100.
30. Owen, T.; Pynn, R.; Martinez, J.S.; Butler, A. Micelle-to-Vesicle Transition of an Iron-Chelating Microbial Surfactant, Marinobactin E. *Langmuir* **2005**, *21*, 12109–12114, doi:10.1021/la0519352.
31. Khan, A.; Singh, P.; Srivastava, A. Synthesis, Nature and Utility of Universal Iron Chelator – Siderophore: A Review. *Microbiol. Res.* **2018**, *212–213*, 103–111, doi:10.1016/j.micres.2017.10.012.
32. Saha, M.; Sarkar, S.; Sarkar, B.; Sharma, B.K.; Bhattacharjee, S.; Tribedi, P. Microbial Siderophores and Their Potential Applications: A Review. *Environ. Sci. Pollut. Res.*

2016, *23*, 3984–3999, doi:10.1007/s11356-015-4294-0.
33. Dave, B.P.; Anshuman, K.; Hajela, P. Siderophores of Halophilic Archaea and Their Chemical Characterization. *Indian J. Exp. Biol.* **2006**, *44*, 340–344.
34. Nielsen, A.; Mansson, M.; Wietz, M.; Varming, A.N.; Phipps, R.K.; Larsen, T.O.; Gram, L.; Ingmer, H. Nigribactin, a Novel Siderophore from Vibrio Nigripulchritudo, Modulates Staphylococcus Aureus Virulence Gene Expression. *Mar. Drugs* **2012**, *10*, 2584–2595, doi:10.3390/md10112584.
35. Pérez-Miranda, S.; Cabirol, N.; George-Téllez, R.; Zamudio-Rivera, L.S.; Fernández, F.J. O-CAS, a Fast and Universal Method for Siderophore Detection. *J. Microbiol. Methods* **2007**, *70*, 127–131, doi:10.1016/j.mimet.2007.03.023.
36. Vraspir, J.M.; Holt, P.D.; Butler, A. Identification of New Members within Suites of Amphiphilic Marine Siderophores. *BioMetals* **2011**, *24*, 85–92, doi:10.1007/s10534-010-9378-1.
37. Homann, V. V.; Sandy, M.; Tincu, J.A.; Templeton, A.S.; Tebo, B.M.; Butler, A. Loihichelins A-F, a Suite of Amphiphilic Siderophores Produced by the Marine Bacterium Halomonas LOB-5. *J. Nat. Prod.* **2009**, *72*, 884–888, doi:10.1021/np800640h.
38. Shenker, M.; Chen, Y.; Oliver, I.; Helmann, M.; Hadar, Y. Utilization by Tomatoes of Iron Mediated by a Siderophore Produced by Rhizopus Arrhizus. *J. Plant Nutr.* **1992**, *15*, 2173–2182, doi:10.1080/01904169209364466.
39. Barbeau, K.; Zhang, G.; Live, D.H.; Butler, A. Petrobactin, a Photoreactive Siderophore Produced by the Oil-Degrading Marine Bacterium Marinobacter Hydrocarbonoclasticus. *J. Am. Chem. Soc.* **2002**, *124*, 378–379, doi:10.1021/ja0119088.
40. Bergeron, R.J.; Huang, G.; Smith, R.E.; Bharti, N.; McManis, J.S.; Butler, A. Total Synthesis and Structure Revision of Petrobactin. *Tetrahedron* **2003**, *59*, 2007–2014, doi:10.1016/S0040-4020(03)00103-0.
41. Hickford, S.J.H.; Küpper, F.C.; Zhang, G.; Carrano, C.J.; Blunt, J.W.; Butler, A. Petrobactin Sulfonate, a New Siderophore Produced by the Marine Bacterium Marinobacter Hydrocarbonoclasticus. *J. Nat. Prod.* **2004**, *67*, 1897–1899, doi:10.1021/np049823i.
42. Kanoh, K.; Kamino, K.; Leleo, G.; Adachi, K.; Shizuri, Y. Pseudoalterobactin A and B, New Siderophores Excreted by Marine Bacterium Pseudoalteromonas Sp. KP20-4. *J. Antibiot. (Tokyo).* **2003**, *56*, 871–875, doi:10.7164/antibiotics.56.871.
43. Vigneshvar, S.; Sudhakumari, C.C.; Senthilkumaran, B.; Prakash, H. Recent Advances in Biosensor Technology for Potential Applications - an Overview. *Front. Bioeng. Biotechnol.* **2016**, *4*, 1–9, doi:10.3389/fbioe.2016.00011.
44. Gupta, V.; Saharan, K.; Kumar, L.; Gupta, R.; Sahai, V.; Mittal, A. Spectrophotometric Ferric Ion Biosensor FromPseudomonas Fluorescens Culture. *Biotechnol. Bioeng.* **2008**, *100*, 284–296, doi:10.1002/bit.21754.
45. Mokhtarzadeh, A.; Ezzati Nazhad Dolatabadi, J.; Abnous, K.; de la Guardia, M.; Ramezani, M. Nanomaterial-Based Cocaine Aptasensors. *Biosens. Bioelectron.* 2015, *68*, 95–106.
46. Nosrati, R.; Golichenari, B.; Nezami, A.; Taghdisi, S.M.; Karimi, B.; Ramezani, M.; Abnous, K.; Shaegh, S.A.M. Helicobacter Pylori Point-of-Care Diagnosis: Nano-Scale Biosensors and Microfluidic Systems. *TrAC - Trends Anal. Chem.* 2017, *97*, 428–444.
47. Nosrati, R.; Dehghani, S.; Karimi, B.; Yousefi, M.; Taghdisi, S.M.; Abnous, K.; Alibolandi, M.; Ramezani, M. Siderophore-Based Biosensors and Nanosensors; New Approach on the Development of Diagnostic Systems. *Biosens. Bioelectron.* **2018**, *117*, 1–14, doi:10.1016/j.bios.2018.05.057.

48. Yin, K.; Wu, Y.; Wang, S.; Chen, L. A Sensitive Fluorescent Biosensor for the Detection of Copper Ion Inspired by Biological Recognition Element Pyoverdine. *Sensors Actuators, B Chem.* **2016**, *232*, 257–263, doi:10.1016/j.snb.2016.03.128.
49. Lam, C.K.S.C.C.; Jickells, T.D.; Richardson, D.J.; Russell, D.A. Fluorescence-Based Siderophore Biosensor for the Determination of Bioavailable Iron in Oceanic Waters. *Anal. Chem.* **2006**, *78*, 5040–5045, doi:10.1021/ac060223t.
50. Orcutt, K.M.; Scott Jones, W.; McDonald, A.; Schrock, D.; Wallace, K.J. A Lanthanide-Based Chemosensor for Bioavailable Fe3+ Using a Fluorescent Siderophore: An Assay Displacement Approach. *Sensors* **2010**, *10*, 1326–1337, doi:10.3390/s100201326.
51. Phillips, D.J.; Davies, G.L.; Gibson, M.I. Siderophore-Inspired Nanoparticle-Based Biosensor for the Selective Detection of Fe3+. *J. Mater. Chem. B* **2015**, *3*, 270–275, doi:10.1039/c4tb01501k.
52. Sharma, M.; Gohil, N.K. Optical Features of the Fluorophore Azotobactin: Applications for Iron Sensing in Biological Fluids. *Eng. Life Sci.* **2010**, *10*, 304–310, doi:10.1002/elsc.201000038.
53. Yoder, M.F.; Kisaalita, W.S. Iron Specificity of a Biosensor Based on Fluorescent Pyoverdin Immobilized in Sol-Gel Glass. *J. Biol. Eng.* **2011**, *5*, 1–12, doi:10.1186/1754-1611-5-4.
54. Raju, M.; Nair, R.R.; Raval, I.H.; Haldar, S.; Chatterjee, P.B. A Water Soluble Cu2+-Specific Colorimetric Probe Can Also Detect Zn2+ in Live Shrimp and Aqueous Environmental Samples by Fluorescence Channel. *Sensors Actuators, B Chem.* **2018**, *260*, 364–370, doi:10.1016/j.snb.2018.01.010.
55. Raju, M.; Srivastava, S.; Nair, R.R.; Raval, I.H.; Haldar, S.; Chatterjee, P.B. Siderophore Coated Magnetic Iron Nanoparticles: Rational Designing of Water Soluble Nanobiosensor for Visualizing Al3+in Live Organism. *Biosens. Bioelectron.* **2017**, *97*, 338–344, doi:10.1016/j.bios.2017.06.013.
56. Duhme-Klair, A.-K. From Siderophores and Self-Assembly to Luminescent Sensors: The Binding of Molybdenum by Catecholamides. *Eur. J. Inorg. Chem.* **2009**, *2009*, 3689–3701, doi:10.1002/ejic.200900416.
57. Duhme-Klair, A.K.; De Alwis, D.C.L.; Schultz, F.A. Electrochemistry of Molybdenum(VI)-Catecholamide Siderophore Complexes in Aqueous Solution. *Inorganica Chim. Acta* **2003**, doi:10.1016/S0020-1693(03)00210-X.
58. Jedner, S.B.; Perutz, R.N.; Duhme-Klair, A.-K. Synthesis and Characterization of a Siderophore-Based Luminescent Sensor for Molybdate. *Zeitschrift für Anorg. und Allg. Chemie* **2003**, *629*, 2421–2426, doi:10.1002/zaac.200300258.
59. Palanché, T.; Marmolle, F.; Abdallah, M.A.; Shanzer, A.; Albrecht-Gary, A.M. Fluorescent Siderophore-Based Chemosensors: Iron(III) Quantitative Determinations. *J. Biol. Inorg. Chem.* **1999**, *4*, 188–198, doi:10.1007/s007750050304.
60. Visca, P.; Imperi, F.; Lamont, I.L. Pyoverdine Siderophores: From Biogenesis to Biosignificance. *Trends Microbiol.* 2007, *15*, 22–30.
61. Winkelmann, G. Ecology of Siderophores with Special Reference to the Fungi. *BioMetals* **2007**, *20*, 379–392, doi:10.1007/s10534-006-9076-1.
62. Kraepiel, A.M.L.; Bellenger, J.P.; Wichard, T.; Morel, F.M.M. Multiple Roles of Siderophores in Free-Living Nitrogen-Fixing Bacteria. *BioMetals* **2009**, *22*, 573–581, doi:10.1007/s10534-009-9222-7.
63. Yoneyama, F.; Yamamoto, M.; Hashimoto, W.; Murata, K. Azotobacter Vinelandii Gene Clusters for Two Types of Peptidic and Catechol Siderophores Produced in Response to Molybdenum. *J. Appl. Microbiol.* **2011**, *111*, 932–938, doi:10.1111/j.1365-2672.2011.05109.x.

64. Doorneweerd, D.D.; Henne, W.A.; Reifenberger, R.G.; Low, P.S. Selective Capture and Identification of Pathogenic Bacteria Using an Immobilized Siderophore. *Langmuir* **2010**, *26*, 15424–15429, doi:10.1021/la101962w.
65. Bachman, M.A.; Oyler, J.E.; Burns, S.H.; Caza, M.; Lépine, F.; Dozois, C.M.; Weiser, J.N. Klebsiella Pneumoniae Yersiniabactin Promotes Respiratory Tract Infection through Evasion of Lipocalin 2. *Infect. Immun.* **2011**, *79*, 3309–3316, doi:10.1128/IAI.05114-11.
66. Himpsl, S.D.; Pearson, M.M.; Arewng, C.J.; Nusca, T.D.; Sherman, D.H.; Mobley, H.L.T. Proteobactin and a Yersiniabactin-Related Siderophore Mediate Iron Acquisition in Proteus Mirabilis. *Mol. Microbiol.* **2010**, *78*, 138–157, doi:10.1111/j.1365-2958.2010.07317.x.
67. Inomata, T.; Eguchi, H.; Matsumoto, K.; Funahashi, Y.; Ozawa, T.; Masuda, H. Adsorption of Microorganisms onto an Artificial Siderophore-Modified Au Substrate. *Biosens. Bioelectron.* **2007**, doi:10.1016/j.bios.2007.08.015.
68. Inomata, T.; Tanabashi, H.; Funahashi, Y.; Ozawa, T.; Masuda, H. Adsorption and Detection of Escherichia Coli Using an Au Substrate Modified with a Catecholate-Type Artificial Siderophore-Fe3+ Complex. *Dalt. Trans.* **2013**, *42*, 16043–16048, doi:10.1039/c3dt51448j.
69. Inomata, T.; Murase, T.; Ido, H.; Ozawa, T.; Masuda, H. Gold Nanoparticles Modified with Artificial Siderophore-Iron(Iii) Ion Complexes: Selective Adsorption and Aggregation of Microbes Using "Coordination Programming." *Chem. Lett.* **2014**, *43*, 1146–1148, doi:10.1246/cl.140270.
70. Meyer, J.M.; Stintzi, A.; De Vos, D.; Cornelis, P.; Tappe, R.; Taraz, K.; Budzikiewicz, H. Use of Siderophores to Type Pseudomonads: The Three Pseudomonas Aeruginosa Pyoverdine Systems. *Microbiology* **1997**, *143*, 35–43, doi:10.1099/00221287-143-1-35.
71. Neilands, J.B. Microbial Iron Compounds. *Annu. Rev. Biochem.* **1981**, *50*, 715–731, doi:10.1146/annurev.bi.50.070181.003435.
72. Meyer, J.M.; Geoffroy, V.A.; Baida, N.; Gardan, L.; Izard, D.; Lemanceau, P.; Achouak, W.; Palleroni, N.J. Siderophore Typing, a Powerful Tool for the Identification of Fluorescent and Nonfluorescent Pseudomonads. *Appl. Environ. Microbiol.* **2002**, *68*, 2745–2753, doi:10.1128/AEM.68.6.2745-2753.2002.
73. Meyer, J.M. Pyoverdine Siderophores as Taxonomic and Phylogenic Markers. In *Pseudomonas*; Springer Netherlands, 2006; Vol. 6, pp. 201–233 ISBN 9780387288819.
74. Meyer, J.M.; Gruffaz, C.; Raharinosy, V.; Bezverbnaya, I.; Schäfer, M.; Budzikiewicz, H. Siderotyping of Fluorescent Pseudomonas: Molecular Mass Determination by Mass Spectrometry as a Powerful Pyoverdine Siderotyping Method. *BioMetals* **2008**, *21*, 259–271, doi:10.1007/s10534-007-9115-6.
75. Bultreys, A.; Gheysen, I.; De Hoffmann, E. Yersiniabactin Production by Pseudomonas Syringae and Escherichia Coli, and Description of a Second Yersiniabactin Locus Evolutionary Group. *Appl. Environ. Microbiol.* **2006**, *72*, 3814–3825, doi:10.1128/AEM.00119-06.
76. Mokracka, J.; Koczura, R.; Kaznowski, A. Yersiniabactin and Other Siderophores Produced by Clinical Isolates of Enterobacter Spp. and Citrobacter Spp. *FEMS Immunol. Med. Microbiol.* **2004**, *40*, 51–55, doi:10.1016/S0928-8244(03)00276-1.
77. Kaeberlein, T.; Lewis, K.; Epstein, S.S. Isolating "Uncultivabte" Microorganisms in Pure Culture in a Simulated Natural Environment. *Science (80-.).* **2002**, *296*, 1127–1129, doi:10.1126/science.1070633.
78. Lewis, K.; Epstein, S.; D'Onofrio, A.; Ling, L.L. Uncultured Microorganisms as a

Source of Secondary Metabolites. *J. Antibiot. (Tokyo).* **2010**, *63*, 468–476, doi:10.1038/ja.2010.87.
79. Yamanaka, K.; Oikawa, H.; Ogawa, H.O.; Hosono, K.; Shinmachi, F.; Takano, H.; Sakuda, S.; Beppu, T.; Ueda, K. Desferrioxamine E Produced by Streptomyces Griseus Stimulates Growth and Development of Streptomyces Tanashiensis. *Microbiology* **2005**, *151*, 2899–2905, doi:10.1099/mic.0.28139-0.
80. Traxler, M.F.; Seyedsayamdost, M.R.; Clardy, J.; Kolter, R. Interspecies Modulation of Bacterial Development through Iron Competition and Siderophore Piracy. *Mol. Microbiol.* **2012**, *86*, 628–644, doi:10.1111/mmi.12008.
81. Huang, Y.; Jiang, Y.; Wang, H.; Wang, J.; Shin, M.C.; Byun, Y.; He, H.; Liang, Y.; Yang, V.C. Curb Challenges of the "Trojan Horse" Approach: Smart Strategies in Achieving Effective yet Safe Cell-Penetrating Peptide-Based Drug Delivery. *Adv. Drug Deliv. Rev.* 2013, *65*, 1299–1315.
82. Ballouche, M.; Cornelis, P.; Baysse, C. Iron Metabolism: A Promising Target for Antibacterial Strategies. *Recent Pat. Antiinfect. Drug Discov.* **2009**, *4*, 190–205, doi:10.2174/157489109789318514.
83. Miethke, M.; Marahiel, M.A. Siderophore-Based Iron Acquisition and Pathogen Control. *Microbiol. Mol. Biol. Rev.* **2007**, *71*, 413–451, doi:10.1128/MMBR.00012-07.
84. Möllmann, U.; Heinisch, L.; Bauernfeind, A.; Köhler, T.; Ankel-Fuchs, D. Siderophores as Drug Delivery Agents: Application of the "Trojan Horse" Strategy. *BioMetals* **2009**, *22*, 615–624, doi:10.1007/s10534-009-9219-2.
85. Wencewicz, T.A.; Möllmann, U.; Long, T.E.; Miller, M.J. Is Drug Release Necessary for Antimicrobial Activity of Siderophore-Drug Conjugates? Syntheses and Biological Studies of the Naturally Occurring Salmycin "Trojan Horse" Antibiotics and Synthetic Desferridanoxamine- Antibiotic Conjugates. *BioMetals* **2009**, *22*, 633–648, doi:10.1007/s10534-009-9218-3.
86. Ding, P.; Schous, C.E.; Miller, M.J. Design and Synthesis of a Novel Protected Mixed Ligand Siderophore. *Tetrahedron Lett.* **2008**, *49*, 2306–2310, doi:10.1016/j.tetlet.2008.02.007.
87. Juárez-Hernández, R.E.; Miller, P.A.; Miller, M.J. Syntheses of Siderophore-Drug Conjugates Using a Convergent Thiol-Maleimide System. *ACS Med. Chem. Lett.* **2012**, *3*, 799–803, doi:10.1021/ml300150y.
88. Ghosh, M.; Miller, M.J. Synthesis and in Vitro Antibacterial Activity of Spermidine-Based Mixed Catechol- and Hydroxamate-Containing Siderophore-Vancomycin Conjugates. *Bioorganic Med. Chem.* **1996**, doi:10.1016/0968-0896(95)00161-1.
89. Ji, C.; Miller, P.A.; Miller, M.J. Iron Transport-Mediated Drug Delivery: Practical Syntheses and In Vitro Antibacterial Studies of Tris-Catecholate Siderophore–Aminopenicillin Conjugates Reveals Selectively Potent Antipseudomonal Activity. *J. Am. Chem. Soc.* **2012**, *134*, 9898–9901, doi:10.1021/ja303446w.
90. Wencewicz, T.A.; Miller, M.J. Biscatecholate–Monohydroxamate Mixed Ligand Siderophore–Carbacephalosporin Conjugates Are Selective Sideromycin Antibiotics That Target Acinetobacter Baumannii. *J. Med. Chem.* **2013**, *56*, 4044–4052, doi:10.1021/jm400265k.
91. Ferguson, A.D.; Coulton, J.W.; Diederichs, K.; Welte, W.; Braun, V.; Fiedler, H.-P. Crystal Structure of the Antibiotic Albomycin in Complex with the Outer Membrane Transporter FhuA. *Protein Sci.* **2000**, *9*, 956–963, doi:10.1110/ps.9.5.956.
92. Krewulak, K.D.; Vogel, H.J. Structural Biology of Bacterial Iron Uptake. *Biochim. Biophys. Acta - Biomembr.* 2008.
93. Nagoba, B.; Vedpathak, D. Medical Applications of Siderophores. *Eur. J. Gen. Med.* **2011**, *8*, 229–235, doi:10.29333/ejgm/82743.

94. Hershko, C.; Link, G.; Konijn, A.M. Cardioprotective Effect of Iron Chelators. *Adv. Exp. Med. Biol.* 2003, *509*, 77–89.
95. Pietrangelo, A. Mechanism of Iron Toxicity. In; 2002; pp. 19–43.
96. Sah, S.; Singh, R. Siderophore: Structural And Functional Characterisation - A Comprehensive Review. *Agric.* **2015**, *61*, 97–114, doi:10.1515/agri-2015-0015.
97. Propper, R.D.; Cooper, B.; Rufo, R.R.; Nienhuis, A.W.; Anderson, W.F.; Bunn, H.F.; Rosenthal, A.; Nathan, D.G. Continuous Subcutaneous Administration of Deferoxamine in Patients with Iron Overload. *N. Engl. J. Med.* **1977**, *297*, 418–423, doi:10.1056/NEJM197708252970804.
98. Robotham, J.L.; Lietman, P.S. Acute Iron Poisoning: A Review. *Am. J. Dis. Child.* **1980**, *134*, 875–879, doi:10.1001/archpedi.1980.02130210059016.
99. Summers, M.R.; Jacobs, A.; Tudway, D.; Perera, P.; Ricketts, C. Studies in Desferrioxamine and Ferrioxamine Metabolism in Normal and Iron-Loaded Subjects. *Br. J. Haematol.* **1979**, *42*, 547–555, doi:10.1111/j.1365-2141.1979.tb01167.x.
100. Wang, W.; Qiu, Z.; Tan, H.; Cao, L. Siderophore Production by Actinobacteria. *BioMetals* **2014**, *27*, 623–631, doi:10.1007/s10534-014-9739-2.
101. Wilson, M.E.; Britigan, B.E. Iron Acquisition by Parasitic Protozoa. *Parasitol. Today* 1998, *14*, 348–353.
102. Lytton, S.D.; Loyevsky, M.; Mester, B.; Libman, J.; Landau, I.; Shanzer, A.; Cabantchik, Z.I. In Vivo Antimalarial Action of a Lipophilic Iron (III) Chelator: Suppression Ofplasmodium Vinckei Infection by Reversed Siderophore. *Am. J. Hematol.* **1993**, *43*, 217–220, doi:10.1002/ajh.2830430311.
103. Loyevsky, M.; John, C.; Dickens, B.; Hu, V.; Miller, J.H.; Gordeuk, V.R. Chelation of Iron within the Erythrocytic Plasmodium Falciparum Parasite by Iron Chelators. *Mol. Biochem. Parasitol.* **1999**, *101*, 43–59, doi:10.1016/S0166-6851(99)00053-5.
104. Pradines, B.; Tall, A.; Ramiandrasoa, F.; Spiegel, A.; Sokhna, C.; Fusai, T.; Mosnier, J.; Daries, W.; Trape, J.F.; Kunesch, G.; et al. In Vitro Activity of Iron-Binding Compounds against Senegalese Isolates of Plasmodium Falciparum. *J. Antimicrob. Chemother.* **2006**, *57*, 1093–1099, doi:10.1093/jac/dkl117.
105. Gauthier, J.D.; Vasta, G.R. Inhibition of in Vitro Replication of the Oyster Parasite Perkinsus Marinus by the Natural Iron Chelators Transferrin, Lactoferrin, and Desferrioxamine. *Dev. Comp. Immunol.* **1994**, *18*, 277–286, doi:10.1016/S0145-305X(94)90353-0.
106. Ackrill, P.; Ralston, A.J.; Day, J.P.; Hodge, K.C. SUCCESSFUL REMOVAL OF ALUMINIUM FROM PATIENT WITH DIALYSIS ENCEPHALOPATHY. *Lancet* 1980, *316*, 692–693.
107. ARZE, R.S.; PARKINSON, I.S.; CARTLIDGE, N.E.F.; BRITTON, P.; WARD, M.K. Reversal of Aluminium Dialysis Encephalopathy after Desferriox-Amine Treatment. *Reversal Alum. Dial. Enceph. after desferriox-amine Treat.* **1981**, *2*, 1116.
108. Hansen, T. V.; Aaseth, J.; Alexander, J. The Effect of Chelating Agents on Vanadium Distribution in the Rat Body and on Uptake by Human Erythrocytes. *Arch. Toxikol.* **1982**, *50*, 195–202, doi:10.1007/BF00310851.
109. Pogglitsch, H.; Petek, W.; Wawschinek, O.; Holzer, W. Treatment of Early Stages of Dialysis Encephalopathy by Aluminium Depletion. *Treat. early stages Dial. Enceph. by Alum. depletion.* **1981**, *2*, 1344–1345.
110. Huang, X. Iron Overload and Its Association with Cancer Risk in Humans: Evidence for Iron as a Carcinogenic Metal. *Mutat. Res. - Fundam. Mol. Mech. Mutagen.* 2003, *533*, 153–171.
111. Nakouti, I.; Sihanonth, P.; Palaga, T.; Hobbs, G. Effect of a Siderophore Producer on Animal Cell Apoptosis: A Possible Role as Anti-Cancer Agent. *Int. J. Pharma Med.*

Biol. Sci. **2013**, *2*, 1–5.
112. Neubauer, U.; Nowack, B.; Furrer, G.; Schulin, R. Heavy Metal Sorption on Clay Minerals Affected by the Siderophore Desferrioxamine B. *Environ. Sci. Technol.* **2000**, *34*, 2749–2755, doi:10.1021/es990495w.
113. Xu, S.; Xing, Y.; Liu, S.; Huang, Q.; Chen, W. Role of Novel Bacterial Raoultella Sp. Strain X13 in Plant Growth Promotion and Cadmium Bioremediation in Soil. *Appl. Microbiol. Biotechnol.* **2019**, *103*, 3887–3897, doi:10.1007/s00253-019-09700-7.
114. Dimkpa, C.O.; Merten, D.; Svatoš, A.; Büchel, G.; Kothe, E. Siderophores Mediate Reduced and Increased Uptake of Cadmium by Streptomyces Tendae F4 and Sunflower (Helianthus Annuus), Respectively. *J. Appl. Microbiol.* **2009**, *107*, 1687–1696, doi:10.1111/j.1365-2672.2009.04355.x.
115. Nair, A.; Juwarkar, A.A.; Singh, S.K. Production and Characterization of Siderophores and Its Application in Arsenic Removal from Contaminated Soil. *Water. Air. Soil Pollut.* **2007**, *180*, 199–212, doi:10.1007/s11270-006-9263-2.
116. Amin, S.A.; Küpper, F.C.; Green, D.H.; Harris, W.R.; Carrano, C.J. Boron Binding by a Siderophore Isolated from Marine Bacteria Associated with the Toxic Dinoflagellate Gymnodinium Catenatum. *J. Am. Chem. Soc.* **2007**, *129*, 478–479, doi:10.1021/ja067369u.
117. Butler, A.; Theisen, R.M. Iron(III)-Siderophore Coordination Chemistry: Reactivity of Marine Siderophores. *Coord. Chem. Rev.* **2010**, *254*, 288–296, doi:10.1016/j.ccr.2009.09.010.
118. Yamamoto, S.; Okujo, N.; Yoshida, T.; Matsuura, S.; Shinoda, S. Structure and Iron Transport Activity of Vibrioferrin, a New Siderophore of Vibrio Parahaemolyticus1. *J. Biochem.* **1994**, *115*, 868–874, doi:10.1093/oxfordjournals.jbchem.a124432.
119. Shinozaki, Y.; Kitamoto, H.; Sameshima-Yamashita, Y.; Kinoshita, A.; Nakajima-Kambe, T. Isolation of a Novel Co^{2+}-Resistant Bacterium and the Application of Its Siderophore in Co^{2+} Recovery from an Aqueous Solution. *J. Gen. Appl. Microbiol.* **2019**, doi:10.2323/jgam.2018.12.001.
120. Das, N.; Chandran, P. Microbial Degradation of Petroleum Hydrocarbon Contaminants: An Overview. *Biotechnol. Res. Int.* **2011**, *2011*, 1–13, doi:10.4061/2011/941810.
121. Gauglitz, J.M.; Zhou, H.; Butler, A. A Suite of Citrate-Derived Siderophores from a Marine Vibrio Species Isolated Following the Deepwater Horizon Oil Spill. *J. Inorg. Biochem.* **2012**, *107*, 90–95, doi:10.1016/j.jinorgbio.2011.10.013.
122. Lastochkina, O.; Pusenkova, L.; Yuldashev, R.; Babaev, M.; Garipova, S.; Blagova, D.; Khairullin, R.; Aliniaeifard, S. Effects of Bacillus Subtilis on Some Physiological and Biochemical Parameters of Triticum Aestivum L. (Wheat) under Salinity. *Plant Physiol. Biochem.* **2017**, *121*, 80–88, doi:10.1016/j.plaphy.2017.10.020.
123. Seifi Kalhor, M.; Aliniaeifard, S.; Seif, M.; Javadi, E.; Bernard, F.; Li, T.; Lastochkina, O. Rhizobacterium Bacillus Subtilis Reduces Toxic Effects of High Electrical Conductivity in Soilless Culture of Lettuce. *Acta Hortic.* **2018**, *1227*, 471–477, doi:10.17660/ActaHortic.2018.1227.59.
124. Van Loon, L.C. Plant Responses to Plant Growth-Promoting Rhizobacteria. In *New Perspectives and Approaches in Plant Growth-Promoting Rhizobacteria Research*; Springer Netherlands, 2007; pp. 243–254 ISBN 9781402067761.
125. Omidvari, M.; Sharifi, R.A.; Ahmadzadeh, M.; Dahaji, P.A. Role of Fluorescent Pseudomonads Siderophore to Increase Bean Growth Factors. *J. Agric. Sci.* **2010**, *2*, 242–247, doi:10.5539/jas.v2n3p242.
126. Gamalero, E.; Glick, B.R. Mechanisms Used by Plant Growth-Promoting Bacteria. In *Bacteria in Agrobiology: Plant Nutrient Management*; Springer Berlin Heidelberg,

2011; pp. 17–46.
127. Kloepper, J.W.; Leong, J.; Teintze, M.; Schroth, M.N. Enhanced Plant Growth by Siderophores Produced by Plant Growth-Promoting Rhizobacteria. *Nature* **1980**, *286*, 885–886, doi:10.1038/286885a0.
128. Ghosh, S.K.; Bera, T.; Chakrabarty, A.M. Microbial Siderophore – A Boon to Agricultural Sciences. *Biol. Control* **2020**, *144*, 104214, doi:10.1016/j.biocontrol.2020.104214.
129. Masalha, J.; Kosegarten, H.; Elmaci, Ö.; Mengel, K. The Central Role of Microbial Activity for Iron Acquisition in Maize and Sunflower. *Biol. Fertil. Soils* **2000**, *30*, 433–439, doi:10.1007/s003740050021.
130. Rungin, S.; Indananda, C.; Suttiviriya, P.; Kruasuwan, W.; Jaemsaeng, R.; Thamchaipenet, A. Plant Growth Enhancing Effects by a Siderophore-Producing Endophytic Streptomycete Isolated from a Thai Jasmine Rice Plant (Oryza Sativa L. Cv. KDML105). *Antonie van Leeuwenhoek, Int. J. Gen. Mol. Microbiol.* **2012**, *102*, 463–472, doi:10.1007/s10482-012-9778-z.
131. Qi, W.; Zhao, L. Study of the Siderophore-Producing *Trichoderma Asperellum* Q1 on Cucumber Growth Promotion under Salt Stress. *J. Basic Microbiol.* **2013**, *53*, 355–364, doi:10.1002/jobm.201200031.
132. Marschner, H.; Romheld, V.; Kissel, M. Different Strategies in Higher Plants in Mobilization and Uptake of Iron. *J. Plant Nutr.* **1986**, *9*, 695–713, doi:10.1080/01904168609363475.
133. Ahmed, E.; Holmström, S.J.M. Siderophores in Environmental Research: Roles and Applications. *Microb. Biotechnol.* **2014**, *7*, 196–208, doi:10.1111/1751-7915.12117.
134. Beneduzi, A.; Ambrosini, A.; Passaglia, L.M.P. Plant Growth-Promoting Rhizobacteria (PGPR): Their Potential as Antagonists and Biocontrol Agents. *Genet. Mol. Biol.* **2012**, *35*, 1044–1051, doi:10.1590/S1415-47572012000600020.
135. Schippers, B.; Bakker, A.W.; Bakker, P.A.H.M. Interactions of Deleterious and Beneficial Rhizosphere Microorganisms and the Effect of Cropping Practices. *Annu. Rev. Phytopathol.* **1987**, *25*, 339–358, doi:10.1146/annurev.py.25.090187.002011.
136. Voisard, C.; Keel, C.; Haas, D.; Dèfago, G. Cyanide Production by Pseudomonas Fluorescens Helps Suppress Black Root Rot of Tobacco under Gnotobiotic Conditions . *EMBO J.* **1989**, *8*, 351–358, doi:10.1002/j.1460-2075.1989.tb03384.x.
137. Pal, K.K.; Tilak, K.V.B.R.; Saxcna, A.K.; Dey, R.; Singh, C.S. Suppression of Maize Root Diseases Caused by Macrophomina Phaseolina, Fusarium Moniliforme and Fusarium Graminearum by Plant Growth Promoting Rhizobacteria. *Microbiol. Res.* **2001**, doi:10.1078/0944-5013-00103.
138. Yu, X.; Ai, C.; Xin, L.; Zhou, G. The Siderophore-Producing Bacterium, Bacillus Subtilis CAS15, Has a Biocontrol Effect on Fusarium Wilt and Promotes the Growth of Pepper. *Eur. J. Soil Biol.* **2011**, *47*, 138–145, doi:10.1016/j.ejsobi.2010.11.001.
139. Verma, V.C.; Singh, S.K.; Prakash, S. Bio-Control and Plant Growth Promotion Potential of Siderophore Producing Endophytic Streptomyces from Azadirachta Indica A. Juss. *J. Basic Microbiol.* **2011**, *51*, 550–556, doi:10.1002/jobm.201000155.
140. Hamdan, H.; Weller, D.M.; Thomashow, L.S. Relative Importance of Fluorescent Siderophores and Other Factors in Biological Control of Gaeumannomyces Graminis Var. Tritici by Pseudomonas Fluorescens 2-79 and M4-80R. *Appl. Environ. Microbiol.* **1991**, *57*, 3270–3277.
141. McLoughlin, T.J.; Quinn, J.P.; Bettermann, A.; Bookland, R. Pseudomonas Cepacia Suppression of Sunflower Wilt Fungus and Role of Antifungal Compounds in Controlling the Disease. *Appl. Environ. Microbiol.* **1992**, *58*, 1760–1763.
142. Johnstone, T.C.; Nolan, E.M. Beyond Iron: Non-Classical Biological Functions of

Bacterial Siderophores. *Dalt. Trans.* **2015**, *44*, 6320–6339, doi:10.1039/c4dt03559c.
143. Lin, J.; Cheng, J. Quorum Sensing in Pseudomonas Aeruginosa and Its Relationship to Biofilm Development. *ACS Symp. Ser.* **2019**, *1323*, 1–16, doi:10.1021/bk-2019-1323.ch001.
144. Imada, C.; Koseki, N.; Kamata, M.; Kobayashi, T.; Hamada-Sato, N. Isolation and Characterization of Antibacterial Substances Produced by Marine Actinomycetes in the Presence of Seawater. *Actinomycetologica* **2007**, *21*, 27–31, doi:10.3209/saj.saj210104.
145. Jensen, P.R.; Fenical, W. Strategies for the Discovery of Secondary Metabolites from Marine Bacteria: Ecological Perspectives. *Annu. Rev. Microbiol.* **1994**, *48*, 559–584, doi:10.1146/annurev.mi.48.100194.003015.
146. Zhang, L.; An, R.; Wang, J.; Sun, N.; Zhang, S.; Hu, J.; Kuai, J. Exploring Novel Bioactive Compounds from Marine Microbes. *Curr. Opin. Microbiol.* **2005**, *8*, 276–281, doi:10.1016/j.mib.2005.04.008.
147. Řezanka, T.; Palyzová, A.; Faltýsková, H.; Sigler, K. *Siderophores: Amazing Metabolites of Microorganisms*; 2018; Vol. 60; ISBN 9780444641816.
148. Cassat, J.E.; Skaar, E.P. Iron in Infection and Immunity. *Cell Host Microbe* **2013**, *13*, 509–519, doi:10.1016/j.chom.2013.04.010.
149. Schaible, U.E.; Kaufmann, S.H.E. Iron and Microbial Infection. *Nat. Rev. Microbiol. 2004 212* **2004**, *2*, 946–953, doi:10.1038/nrmicro1046.
150. Jalal, M.A.F.; Hossain, M.B.; van der Helm, D.; Sanders-Loehr, J.; Actis, L.A.; Crosa, J.H. Structure of Anguibactin, a Unique Plasmid-Related Bacterial Siderophore from the Fish Pathogen Vibrio Anguillarum. *J. Am. Chem. Soc.* **1989**, *111*, 292–296, doi:10.1021/ja00183a044.
151. Matsuo, Y.; Kanoh, K.; Jang, J.; Adachi, K.; Matsuda, S.; Miki, O.; Kato, T.; Shizuri, Y. Streptobactin, a Tricatechol-Type Siderophore from Marine-Derived Streptomyces Sp. YM5-799. *J. Nat. Prod.* **2011**, *74*, 2371–2376, doi:dx.doi.org/10.1021/np200290j | J. Nat. Prod. 2011, 74, 2371−2376.
152. Stoll, A.; Brack, A.; Renz, J. Nocardamin, Ein Neues Antibioticum Aus Einer Nocardia-Art. *Pathobiology* **1951**, *14*, 225–233, doi:10.1159/000159979.
153. Kalinovskaya, N.I.; Romanenko, L.A.; Irisawa, T.; Ermakova, S.P.; Kalinovsky, A.I. Marine Isolate Citricoccus Sp. KMM 3890 as a Source of a Cyclic Siderophore Nocardamine with Antitumor Activity. *Microbiol. Res.* **2011**, *166*, 654–661, doi:10.1016/j.micres.2011.01.004.
154. Ejje, N.; Soe, C.Z.; Gu, J.; Codd, R. The Variable Hydroxamic Acid Siderophore Metabolome of the Marine Actinomycete Salinispora Tropica CNB-440. *Metallomics* **2013**, *5*, 1519–1528, doi:10.1039/c3mt00230f.
155. Liu, N.; Shang, F.; Xi, L.; Huang, Y. Tetroazolemycins a and B, Two New Oxazole-Thiazole Siderophores from Deep-Sea Streptomyces Olivaceus FXJ8.012. *Mar. Drugs* **2013**, *11*, 1524–1533, doi:10.3390/md11051524.
156. Takehana, Y.; Umekita, M.; Hatano, M.; Kato, C.; Sawa, R.; Igarashi, M. Fradiamine A, a New Siderophore from the Deep-Sea Actinomycete Streptomyces Fradiae MM456M-MF7. *J. Antibiot. (Tokyo).* **2017**, *70*, 611–615, doi:10.1038/ja.2017.26.
157. Yang, M.; Zhang, J.; Liang, Q.; Pan, G.; Zhao, J.; Cui, M.; Zhao, X.; Zhang, Q.; Xu, D. Antagonistic Activity of Marine Streptomyces Sp. S073 on Pathogenic Vibrio Parahaemolyticus. *Fish. Sci.* **2019**, *85*, 533–543, doi:10.1007/s12562-019-01309-z.
158. Wu, Q.; Deering, R.W.; Zhang, G.; Wang, B.; Li, X.; Sun, J.; Chen, J.; Zhang, H.; Rowley, D.C.; Wang, H. Albisporachelin, a New Hydroxamate Type Siderophore from the Deep Ocean Sediment-Derived Actinomycete Amycolatopsis Albispora WP1 T. *Mar. Drugs* **2018**, *16*, 1–9, doi:10.3390/md16060199.
159. Yan, J.X.; Chevrette, M.G.; Braun, D.R.; Harper, M.K.; Currie, C.R.; Bugni, T.S.

Madurastatin D1 and D2, Oxazoline Containing Siderophores Isolated from an Actinomadura Sp. *Org. Lett.* **2019**, *21*, 6275–6279, doi:10.1021/acs.orglett.9b02159.
160. Beger, R. A Review of Applications of Metabolomics in Cancer. *Metabolites* **2013**, *3*, 552–574, doi:10.3390/metabo3030552.
161. Mastrangelo, A.; G Armitage, E.; García, A.; Barbas, C. Metabolomics as a Tool for Drug Discovery and Personalised Medicine. A Review. *Curr. Top. Med. Chem.* **2014**, *14*, 2627–2636.
162. Zwiener, C.; Frimmel, F.H. LC-MS Analysis in the Aquatic Environment and in Water Treatment - A Critical Review: Part II: Applications for Emerging Contaminants and Related Pollutants, Microorganisms and Humic Acids. *Anal. Bioanal. Chem.* 2004, *378*, 862–874.
163. Patti, G.J.; Yanes, O.; Siuzdak, G. Innovation: Metabolomics: The Apogee of the Omics Trilogy. *Nat. Rev. Mol. Cell Biol.* **2012**, *13*, 263–269, doi:10.1038/nrm3314.
164. Carmichael, J.R.; Zhou, H.; Butler, A. A Suite of Asymmetric Citrate Siderophores Isolated from a Marine Shewanella Species. *J. Inorg. Biochem.* **2019**, *198*, 110736, doi:10.1016/j.jinorgbio.2019.110736.
165. Sester, A.; Winand, L.; Pace, S.; Hiller, W.; Werz, O.; Nett, M. Myxochelin-A Nd Pseudochelin-Derived Lipoxygenase Inhibitors from a Genetically Engineered Myxococcus Xanthus Strain. *J. Nat. Prod.* **2019**, *82*, 2544–2549, doi:10.1021/acs.jnatprod.9b00403.
166. Diettrich, J.; Kage, H.; Nett, M. Genomics-Inspired Discovery of Massiliachelin, an Agrochelin Epimer from Massilia Sp. NR 4-1. *Beilstein J. Org. Chem.* **2019**, *15*, 1298–1303, doi:10.3762/bjoc.15.128.
167. Hardy, C.D.; Butler, A. Ambiguity of NRPS Structure Predictions: Four Bidentate Chelating Groups in the Siderophore Pacifibactin. *J. Nat. Prod.* **2019**, *82*, 990–997, doi:10.1021/acs.jnatprod.8b01073.
168. Robertson, A.W.; McCarville, N.G.; Macintyre, L.W.; Correa, H.; Haltli, B.; Marchbank, D.H.; Kerr, R.G. Isolation of Imaqobactin, an Amphiphilic Siderophore from the Arctic Marine Bacterium Variovorax Species RKJM285. *J. Nat. Prod.* **2018**, *81*, 858–865, doi:10.1021/acs.jnatprod.7b00943.
169. Sonnenschein, E.C.; Stierhof, M.; Goralczyk, S.; Vabre, F.M.; Pellissier, L.; Hanssen, K.Ø.; de la Cruz, M.; Díaz, C.; de Witte, P.; Copmans, D.; et al. Pseudochelin A, a Siderophore of Pseudoalteromonas Piscicida S2040. *Tetrahedron* **2017**, *73*, 2633–2637, doi:10.1016/j.tet.2017.03.051.
170. Zhang, F.; Barns, K.; Hoffmann, F.M.; Braun, D.R.; Andes, D.R.; Bugni, T.S. Thalassosamide, a Siderophore Discovered from the Marine-Derived Bacterium Thalassospira Profundimaris. *J. Nat. Prod.* **2017**, *80*, 2551–2555, doi:10.1021/acs.jnatprod.7b00328.
171. Kurth, C.; Schieferdecker, S.; Athanasopoulou, K.; Seccareccia, I.; Nett, M. Variochelins, Lipopeptide Siderophores from Variovorax Boronicumulans Discovered by Genome Mining. *J. Nat. Prod.* **2016**, *79*, 865–872, doi:10.1021/acs.jnatprod.5b00932.
172. Fujita, M.J.; Sakai, R. Production of Avaroferrin and Putrebactin by Heterologous Expression of a Deep-Sea Metagenomic DNA. *Mar. Drugs* **2014**, *12*, 4799–4809, doi:10.3390/md12094799.
173. Gauglitz, J.M.; Butler, A. Amino Acid Variability in the Peptide Composition of a Suite of Amphiphilic Peptide Siderophores from an Open Ocean Vibrio Species. *J. Biol. Inorg. Chem.* **2013**, *18*, 489–497, doi:10.1007/s00775-013-0995-3.
174. Ito, Y.; Butler, A. Structure of Synechobactins, New Siderophores of the Marine Cyanobacterium Synechococcus Sp. PCC 7002. *Limnol. Oceanogr.* **2005**, *50*, 1918–

1923, doi:10.4319/lo.2005.50.6.1918.
175. Martinez, J.S.; Haygood, M.G.; Butler, A. Identification of a Natural Desferrioxamine Siderophore Produced by a Marine Bacterium. *Limnol. Oceanogr.* **2001**, *46*, 420–424, doi:10.4319/lo.2001.46.2.0420.
176. Martinez, J.S.; Zhang, G.P.; Holt, P.D.; Jung, H.T.; Carrano, C.J.; Haygood, M.G.; Butler, A. *Self -Assembling Amphiphilic Siderophores from Marine Bacteria*; 2000; Vol. 287;.
177. Zhao, W.; Peng, F.; Wang, C. xi; Xie, Y.; Lin, R.; Fang, Z. kai; Sun, F.; Lian, Y. yang; Jiang, H. FW0622, a New Siderophore Isolated from Marine Verrucosispora Sp. by Genomic Mining. *Nat. Prod. Res.* **2019**, *0*, 1–7, doi:10.1080/14786419.2019.1608541.
178. Walker, L.R.; Tfaily, M.M.; Shaw, J.B.; Hess, N.J.; Paša-Tolić, L.; Koppenaal, D.W. Unambiguous Identification and Discovery of Bacterial Siderophores by Direct Injection 21 Tesla Fourier Transform Ion Cyclotron Resonance Mass Spectrometry. *Metallomics* **2017**, *9*, 82–92, doi:10.1039/c6mt00201c.
179. Ledyard, K.M.; Butler, A. Structure of Putrebactin, a New Dihydroxamate Siderophore Produced by Shewanella Putrefaciens. *J. Biol. Inorg. Chem.* **1997**, *2*, 93–97, doi:10.1007/s007750050110.
180. Iitaka, Y.; Nakamura, H.; Kameyama, T.; Kurasawa, S.; Naganawa, H.; Okami, Y.; Takeuchi, T.; Umezawa, H. Bisucaberin, A New Siderophore, Sensitizing Tumor Cells To Macrophage-Mediated Cytolysis Ii. Physico-Chemical Properties And Structure Determination. *J. Antibiot. (Tokyo).* **1987**, *40*, 1671–1676, doi:10.7164/antibiotics.40.1671.
181. Zhang, L.; Yuan, D.X.; Fang, K.; Liu, B.M. Determination of Siderophores in Seawater by High Performance Liquid Chromatography-Tandem Mass Spectrometry Coupled with Solid Phase Extraction. *Chinese J. Anal. Chem.* **2015**, *43*, 1285–1290, doi:10.1016/S1872-2040(15)60854-4.
182. Clark, C.M.; Costa, M.S.; Sanchez, L.M.; Murphy, B.T. Coupling MALDI-TOF Mass Spectrometry Protein and Specialized Metabolite Analyses to Rapidly Discriminate Bacterial Function. *Proc. Natl. Acad. Sci. U. S. A.* **2018**, *115*, 4981–4986, doi:10.1073/pnas.1801247115.
183. Gáll, T.; Lehoczki, G.; Gyémánt, G.; Emri, T.; Szigeti, Z.M.; Balla, G.; Zsef Balla, J.; Pócsi, I. Optimization of Desferrioxamine e Production by Streptomyces Parvulus. *Acta Microbiol. Immunol. Hung.* **2016**, *63*, 475–489, doi:10.1556/030.63.2016.029.
184. Guerrero-garzón, J.F.; Zehl, M.; Schneider, O.; Rückert, C.; Busche, T.; Kalinowski, J.; Bredholt, H.; Zotchev, S.B. Streptomyces Spp . From the Marine Sponge Antho Dichotoma : Analyses of Secondary Metabolite Biosynthesis Gene Clusters and Some of Their Products. **2020**, *11*, 1–15, doi:10.3389/fmicb.2020.00437.
185. Kumari, R.; Barsainya, M.; Singh, D.P. Biogenic Synthesis of Silver Nanoparticle by Using Secondary Metabolites from Pseudomonas Aeruginosa DM1 and Its Anti-Algal Effect on Chlorella Vulgaris and Chlorella Pyrenoidosa. *Environ. Sci. Pollut. Res.* **2017**, *24*, 4645–4654, doi:10.1007/s11356-016-8170-3.
186. Khatoon, U.T.; Velidandi, A.; Nageswara Rao, G.V.S. Copper Oxide Nanoparticles: Synthesis via Chemical Reduction, Characterization, Antibacterial Activity, and Possible Mechanism Involved. *Inorg. Chem. Commun.* **2023**, *149*, 110372, doi:10.1016/j.inoche.2022.110372.
187. Velidandi, A.; Dahariya, S.; Pabbathi, N.P.P.; Kalivarathan, D.; Baadhe, R.R. A Review on Synthesis, Applications, Toxicity, Risk Assessment and Limitations of Plant Extracts Synthesized Silver Nanoparticles. *NanoWorld J.* **2020**, *6*, 35–60, doi:10.17756/nwj.2020-079.
188. Velidandi, A.; Pabbathi, N.P.P.; Dahariya, S.; Kagithoju, S.; Baadhe, R.R. Bio-

Fabrication of Silver-Silver Chloride Nanoparticles Using Annona Muricata Leaf Extract: Characterization, Biological, Dye Degradation and Eco-Toxicity Studies. *Int. J. Environ. Sci. Technol.* **2022**, *19*, 6555–6572, doi:10.1007/s13762-021-03461-5.
189. Velidandi, A.; Sarvepalli, M.; Aramanda, P.; Amudala, M.L.; Baadhe, R.R. Effect of Size on Physicochemical, Antibacterial, and Catalytic Properties of Neolamarckia Cadamba (Burflower-Tree) Synthesized Silver/Silver Chloride Nanoparticles. *Environ. Sci. Pollut. Res.* **2023**, *30*, 63231–63249, doi:10.1007/s11356-023-26427-1.
190. He, Q.; Huang, S.; Wang, C.; Qiao, Q.; Liang, N.; Xu, M.; Chen, W.; Zai, J.; Qian, X. The Role of Mott-Schottky Heterojunctions in Ag-Ag 8 SnS 6 as Counter Electrodes in Dye-Sensitized Solar Cells. *ChemSusChem* **2015**, *8*, 817–820, doi:10.1002/cssc.201403343.
191. He, Q.; Qian, T.; Zai, J.; Qiao, Q.; Huang, S.; Li, Y.; Wang, M. Efficient Ag 8 GeS 6 Counter Electrode Prepared from Nanocrystal Ink for Dye-Sensitized Solar Cells. *J. Mater. Chem. A* **2015**, *3*, 20359–20365, doi:10.1039/C5TA05304H.
192. He, Q.; Huang, S.; Zai, J.; Tang, N.; Li, B.; Qiao, Q.; Qian, X. Efficient Counter Electrode Manufactured from Ag 2 S Nanocrystal Ink for Dye-Sensitized Solar Cells. *Chem. – A Eur. J.* **2015**, *21*, 15153–15157, doi:10.1002/chem.201502337.
193. Khatoon, U.T.; Velidandi, A.; Nageswara Rao, G.V.S. Sodium Borohydride Mediated Synthesis of Nano-Sized Silver Particles: Their Characterization, Anti-Microbial and Cytotoxicity Studies. *Mater. Chem. Phys.* **2023**, *294*, 126997, doi:10.1016/j.matchemphys.2022.126997.
194. Boas, D.; Remennik, S.; Reches, M. Peptide-Capped Au and Ag Nanoparticles: Detection of Heavy Metals and Photochemical Core/Shell Formation. *J. Colloid Interface Sci.* **2023**, *631*, 66–76, doi:10.1016/j.jcis.2022.10.154.
195. Velidandi, A.; Pabbathi, N.P.P.; Dahariya, S.; Baadhe, R.R. Green Synthesis of Novel Ag–Cu and Ag–Znbimetallic Nanoparticles and Their in Vitro Biological, Eco-Toxicity and Catalytic Studies. *Nano-Structures and Nano-Objects* **2021**, *26*, 100687, doi:10.1016/j.nanoso.2021.100687.
196. Sable, S.V.; Kawade, S.; Ranade, S.; Joshi, S. Bioreduction Mechanism of Silver Nanoparticles. *Mater. Sci. Eng. C* **2020**, *107*, 110299, doi:10.1016/j.msec.2019.110299.
197. Esmail, R.; Afshar, A.; Morteza, M.; Abolfazl, A.; Akhondi, E. Synthesis of Silver Nanoparticles with High Efficiency and Stability by Culture Supernatant of Bacillus ROM6 Isolated from Zarshouran Gold Mine and Evaluating Its Antibacterial Effects. *BMC Microbiol.* **2022**, *22*, 97, doi:10.1186/s12866-022-02490-5.
198. Velidandi, A.; Pabbathi, N.P.P.; Dahariya, S.; Baadhe, R.R. Catalytic and Eco-Toxicity Investigations of Bio-Fabricated Monometallic Nanoparticles along with Their Anti-Bacterial, Anti-Inflammatory, Anti-Diabetic, Anti-Oxidative and Anti-Cancer Potentials. *Colloids Interface Sci. Commun.* **2020**, *38*, 100302, doi:10.1016/j.colcom.2020.100302.
199. Velidandi, A.; Sarvepalli, M.; Pabbathi, N.P.P.; Baadhe, R.R. Biogenic Synthesis of Novel Platinum-Palladium Bimetallic Nanoparticles from Aqueous Annona Muricata Leaf Extract for Catalytic Activity. *3 Biotech* **2021**, *11*, 1–14, doi:10.1007/s13205-021-02935-0.
200. Hamed, A.A.; Kabary, H.; Khedr, M.; Emam, A.N. Antibiofilm, Antimicrobial and Cytotoxic Activity of Extracellular Green-Synthesized Silver Nanoparticles by Two Marine-Derived Actinomycete. *RSC Adv.* **2020**, *10*, 10361–10367, doi:10.1039/c9ra11021f.
201. Mondal, A.H.; Yadav, D.; Ali, A.; Khan, N.; Jin, J.O.; Haq, Q.M.R. Anti-Bacterial and Anti-Candidal Activity of Silver Nanoparticles Biosynthesized Using Citrobacter Spp.

Ms5 Culture Supernatant. *Biomolecules* **2020**, *10*, 1–15, doi:10.3390/biom10060944.
202. Singh, P.; Pandit, S.; Jers, C.; Joshi, A.S.; Garnæs, J.; Mijakovic, I. Silver Nanoparticles Produced from Cedecea Sp. Exhibit Antibiofilm Activity and Remarkable Stability. *Sci. Rep.* **2021**, *11*, 1–13, doi:10.1038/s41598-021-92006-4.
203. Khaleghi, M.; Khorrami, S.; Ravan, H. Identification of Bacillus Thuringiensis Bacterial Strain Isolated from the Mine Soil as a Robust Agent in the Biosynthesis of Silver Nanoparticles with Strong Antibacterial and Anti-Biofilm Activities. *Biocatal. Agric. Biotechnol.* **2019**, *18*, 101047, doi:10.1016/j.bcab.2019.101047.
204. Dane, P.R.; Pawar, S.P.; Kankariya, R.A.; Chaudhari, B.L. Pyoverdin Mediated Sunlight Induced Green Synthesis of Silver Nanoparticles. *RSC Adv.* **2016**, *6*, 8503–8510, doi:10.1039/c5ra20856d.
205. Laisney, J.; Chevallet, M.; Fauquant, C.; Sageot, C.; Moreau, Y.; Predoi, D.; Herlin-Boime, N.; Lebrun, C.; Michaud-Soret, I. Ligand-Promoted Surface Solubilization of TiO2 Nanoparticles by the Enterobactin Siderophore in Biological Medium. *Biomolecules* **2022**, *12*, 1516, doi:10.3390/biom12101516.
206. Martínez-Matamoros, D.; Castro-García, S.; Balado, M.; Matamoros-Veloza, A.; Camargo-Valero, M.A.; Cespedes, O.; Rodríguez, J.; Lemos, M.L.; Jiménez, C. Preparation of Functionalized Magnetic Nanoparticles Conjugated with Feroxamine and Their Evaluation for Pathogen Detection. *RSC Adv.* **2019**, *9*, 13533–13542, doi:10.1039/c8ra10440a.
207. Patil, S.; Sastry, M.; Bharde, A. Size and Shape Directed Novel Green Synthesis of Plasmonic Nanoparticles Using Bacterial Metabolites and Their Anticancer Effects. *Front. Microbiol.* **2022**, *13*, 866849, doi:10.3389/fmicb.2022.866849.
208. Barsainya, M.; Pratap Singh, D. Green Synthesis of Zinc Oxide Nanoparticles by Pseudomonas Aeruginosa and Their Broad-Spectrum Antimicrobial Effects. *J. Pure Appl. Microbiol.* **2018**, *12*, 2123–2134, doi:10.22207/JPAM.12.4.50.
209. Wyatt, M.A.; Johnston, C.W.; Magarvey, N.A. Gold Nanoparticle Formation via Microbial Metallophore Chemistries. *J. Nanoparticle Res.* **2014**, *16*, 2212, doi:10.1007/s11051-013-2212-2.
210. Galinetto, P.; Taglietti, A.; Pasotti, L.; Pallavicini, P.; Dacarro, G.; Giulotto, E.; Grandi, M.S. SERS Activity of Silver Nanoparticles Functionalized with A Desferrioxamine B Derived Ligand for FE(III) Binding and Sensing. *J. Appl. Spectrosc.* **2016**, *82*, 1052–1059, doi:10.1007/s10812-016-0228-y.
211. Klitsche, F.; Ramcke, J.; Migenda, J.; Hensel, A.; Vossmeyer, T.; Weller, H.; Gross, S.; Maison, W. Synthesis of Tripodal Catecholates and Their Immobilization on Zinc Oxide Nanoparticles. *Beilstein J. Org. Chem.* **2015**, *11*, 678–686, doi:10.3762/bjoc.11.77.
212. Lim, J.M.; Jeon, C.O.; Kim, C.J. Bacillus Taeanensis Sp. Nov., a Halophilic Gram-Positive Bacterium from a Solar Saltern in Korea. *Int. J. Syst. Evol. Microbiol.* **2006**, *56*, 2903–2908, doi:10.1099/ijs.0.64036-0.
213. Kumari, S.; Kiran, S.; Kumari, S.; Kumar, P.; Singh, A. Optimization of Siderophore Production by Bacillus Subtilis DR2 and Its Effect on Growth of Coriandrum Sativum. *Res. Sq.* **2021**, 1–25, doi:https://doi.org/10.21203/rs.3.rs-567897/v1.
214. Dasari, V.R.R.K.; Donthireddy, S.R.R. Amycolatopsis Alba Var. Nov DVR D4, a Bioactive Actinomycete Isolated from Indian Marine Environment Venkata. *J Biochem. tech* **2011**, *3*, 251–256.
215. Clarridge, J.E. Impact of 16S RRNA Gene Sequence Analysis for Identification of Bacteria on Clinical Microbiology and Infectious Diseases. *Clin. Microbiol. Rev.* **2004**, *17*, 840–862, doi:10.1128/CMR.17.4.840-862.2004.
216. Darby, A.C.; Chandler, S.M.; Welburn, S.C.; Douglas, A.E. Aphid-Symbiotic Bacteria

Cultured in Insect Cell Lines. *Appl. Environ. Microbiol.* **2005**, *71*, 4833–4839, doi:10.1128/AEM.71.8.4833-4839.2005.
217. Altschul, S.F.; Gish, W.; Miller, W.; Myers, E.W.; Lipman, D.J. Altschul et Al.. 1990. Basic Local Alignment Search Tool.Pdf. *J. Mol. Biol.* 1990, *215*, 403–410.
218. Manwar, A. V.; Khandelwal, S.R.; Chaudhari, B.L.; Meyer, J.M.; Chincholkar, S.B. Siderophore Production by a Marine Pseudomonas Aeruginosa and Its Antagonistic Action against Phytopathogenic Fungi. *Appl. Biochem. Biotechnol. - Part A Enzym. Eng. Biotechnol.* **2004**, *118*, 243–251, doi:10.1385/ABAB:118:1-3:243.
219. Rashmi, V.; ShylajaNaciyar, M.; Rajalakshmi, R.; D'Souza, S.F.; Prabaharan, D.; Uma, L. Siderophore Mediated Uranium Sequestration by Marine Cyanobacterium Synechococcus Elongatus BDU 130911. *Bioresour. Technol.* **2013**, *130*, 204–210, doi:10.1016/j.biortech.2012.12.016.
220. Arnow, B.Y.L.E. Hydrochloric Acid and Enough Distilled Water to Make a Volume of 1 Liter. Preserve under Toluene. 531. *Comp. A J. Comp. Educ.* **1937**, 531–537.
221. Murugappan, R.M.; Aravinth, A.; Rajaroobia, R.; Karthikeyan, M.; Alamelu, M.R. Optimization of MM9 Medium Constituents for Enhancement of Siderophoregenesis in Marine Pseudomonas Putida Using Response Surface Methodology. *Indian J. Microbiol.* **2012**, *52*, 433–441, doi:10.1007/s12088-012-0258-y.
222. Shaikh, S.S.; Wani, S.J.; Sayyed, R.Z. Statistical-Based Optimization and Scale-up of Siderophore Production Process on Laboratory Bioreactor. *3 Biotech* **2016**, *6*, 1–10, doi:10.1007/s13205-016-0365-2.
223. Wright, W.H.I. Isolation and Identification of the Siderophore " Vicibactin " Produced by Rhizobium Leguminosarum. **2010**, Electronic Theses and Dissertations. Paper 1690. h.
224. Storey, E.P. Isolation Purification and Chemical Characterization of the Dih. **2005**.
225. Boyer, R. Modern Experimental Biochemistry 3d Ed - Rodney F. Boyer.Pdf. *Anal. Biochem.* 1987, *166*, 446.
226. Murugappan, R.M.; Aravinth, A.; Karthikeyan, M. Chemical and Structural Characterization of Hydroxamate Siderophore Produced by Marine Vibrio Harveyi. *J. Ind. Microbiol. Biotechnol.* **2011**, *38*, 265–273, doi:10.1007/s10295-010-0769-7.
227. Chowdappa, S.; Jagannath, S.; Konappa, N. Detection and Characterization of Antibacterial Siderophores Secreted by Endophytic Fungi from Cymbidium Aloifolium. *Biomolecules* **2020**, *10*, 1–18, doi:10.3390/biom10101412.
228. Winkelmann, G. Microbial Siderophore-Mediated Transport. *Biochem. Soc. Trans.* **2002**, *30*, 691–696, doi:10.1042/BST0300691.
229. Wang, Y.; Huang, W.; Li, Y.; Yu, F.; Penttinen, P. Isolation, Characterization, and Evaluation of a High-Siderophore-Yielding Bacterium from Heavy Metal–Contaminated Soil. *Environ. Sci. Pollut. Res.* **2022**, *29*, 3888–3899, doi:10.1007/s11356-021-15996-8.
230. Sayyed, P.R.P.S.S.S.R.Z. Modified Chrome Azurol S Method for Detection and Estimation of Siderophores Having Affinity for Metal Ions Other than Iron. *Environ. Sustain.* **2018**, doi:10.1007/s42398-018-0005-3.
231. Kumar, P.; Thakur, S.; Dhingra, G.K.; Singh, A.; Pal, M.K.; Harshvardhan, K.; Dubey, R.C.; Maheshwari, D.K. Inoculation of Siderophore Producing Rhizobacteria and Their Consortium for Growth Enhancement of Wheat Plant. *Biocatal. Agric. Biotechnol.* **2018**, *15*, 264–269, doi:10.1016/j.bcab.2018.06.019.
232. Mishra, D.; Chitara, M.K.; Negi, S.; Pal singh, J.; Kumar, R.; Chaturvedi, P. Biosynthesis of Zinc Oxide Nanoparticles via Leaf Extracts of Catharanthus Roseus (L.) G. Don and Their Application in Improving Seed Germination Potential and Seedling Vigor of Eleusine Coracana (L.) Gaertn. *Adv. Agric.* **2023**, *2023*, 1–11,

doi:10.1155/2023/7412714.
233. Sarvepalli, M.; Korrapati, N. Statistical Optimisation of Process Parameters Involved in Siderophore Production of Marine Bacterial Isolate Marinobacter Sp. SVU_3. *Biomass Convers. Biorefinery* **2023**, 1–12, doi:10.1007/s13399-023-04427-y.
234. Vankdoth, S.; Velidandi, A.; Sarvepalli, M.; Vangalapati, M. Role of Plant (Tulasi, Neem and Turmeric) Extracts in Defining the Morphological, Toxicity and Catalytic Properties of Silver Nanoparticles. *Inorg. Chem. Commun.* **2022**, *140*, 109476, doi:10.1016/j.inoche.2022.109476.
235. Singh, P.; Khan, A.; Kumar, R.; Kumar, R.; Singh, V.K.; Srivastava, A. Recent Developments in Siderotyping: Procedure and Application. *World J. Microbiol. Biotechnol.* **2020**, *36*, 1–15, doi:10.1007/s11274-020-02955-7.
236. Liu, R.; Huang, Z.; Dong, C.; Shao, Z. Lottiidibacillus Patelloidae Gen. Nov., Sp. Nov., Isolated from the Intestinal Tract of a Marine Limpet and Reclassification of Bacillus Taeanensis as Maribacillus Taeanensis Gen. Nov., Comb. Nov. *Antonie Van Leeuwenhoek* **2019**, *112*, 797–807, doi:10.1007/s10482-018-01213-z.
237. Palleroni, N.J.; Doudoroff, M.; Stanier, R.Y.; Solánes, R.E.; Mandel, M. Taxonomy of the Aerobic Pseudomonads: The Properties of the Pseudomonas Stutzeri Group. *J. Gen. Microbiol.* **1970**, *60*, 215–231, doi:10.1099/00221287-60-2-215.
238. Yen, K.M.; Karl, M.R. Identification of a New Gene, TmoF, in the Pseudomonas Mendocina KR1 Gene Cluster Encoding Toluene-4-Monooxygenase. *J. Bacteriol.* **1992**, *174*, 7253–7261, doi:10.1128/jb.174.22.7253-7261.1992.
239. Guo, W.; Song, C.; Kong, M.; Geng, W.; Wang, Y.; Wang, S. Simultaneous Production and Characterization of Medium-Chain-Length Polyhydroxyalkanoates and Alginate Oligosaccharides by Pseudomonas Mendocina NK-01. *Appl. Microbiol. Biotechnol.* **2011**, *92*, 791–801, doi:10.1007/s00253-011-3333-0.
240. Lynne, A.M.; Haarmann, D.; Louden, B.C. Use of Blue Agar CAS Assay for Siderophore Detection. *J. Microbiol. Biol. Educ.* **2011**, *12*, 51–53, doi:10.1128/jmbe.v12i1.249.
241. Murakami, C.; Tanaka, A.R.; Sato, Y.; Kimura, Y.; Morimoto, K. Easy Detection of Siderophore Production in Diluted Growth Media Using an Improved CAS Reagent. *J. Microbiol. Methods* **2021**, *189*, 106310, doi:10.1016/j.mimet.2021.106310.
242. Wilson, M.K.; Abergel, R.J.; Raymond, K.N.; Arceneaux, J.E.L.; Byers, B.R. Siderophores of Bacillus Anthracis, Bacillus Cereus, and Bacillus Thuringiensis. *Biochem. Biophys. Res. Commun.* **2006**, *348*, 320–325, doi:10.1016/j.bbrc.2006.07.055.
243. Wu, Q.; Throckmorton, K.; Maity, M.; Chevrette, M.G.; Braun, D.R.; Rajski, S.R.; Currie, C.R.; Thomas, M.G.; Bugni, T.S. Bacillibactins e and F from a Marine Sponge-Associated Bacillus Sp. *J. Nat. Prod.* **2021**, *84*, 136–141, doi:10.1021/acs.jnatprod.0c01170.
244. Hussein, K.A.; Joo, J.H. Stimulation, Purification, and Chemical Characterization of Siderophores Produced by the Rhizospheric Bacterial Strain Pseudomonas Putida. *Rhizosphere* **2017**, *4*, 16–21, doi:10.1016/j.rhisph.2017.05.006.
245. Kaplan, A.R.; Wuest, W.M. Promiscuous Pseudomonas: Uptake of Non-Endogenous Ligands for Iron Acquisition. *Tetrahedron Lett.* **2021**, *75*, 153204, doi:10.1016/j.tetlet.2021.153204.
246. Vindeirinho, J.M.; Soares, H.M.V.M.; Soares, E. V. Modulation of Siderophore Production by Pseudomonas Fluorescens Through the Manipulation of the Culture Medium Composition. *Appl. Biochem. Biotechnol.* **2021**, *193*, 607–618, doi:10.1007/s12010-020-03349-z.
247. Chincholkar, S.B.; Chaudhari, B.L.; Rane, M.R. Microbial Siderophore: A State OfArt.

In *Microbial Siderophores*; Varma, A., Chincholkar, S., Eds.; Springer-Verlag, Berlin Heidelberg, 2007; pp. 233–243 ISBN 9783540711599.
248. Santos, S.; Neto, I.F.F.; Machado, M.D.; Soares, H.M.V.M.; Soares, E. V. Siderophore Production by Bacillus Megaterium: Effect of Growth Phase and Cultural Conditions. *Appl. Biochem. Biotechnol.* **2014**, *172*, 549–560, doi:10.1007/s12010-013-0562-y.
249. Yu, S.; Teng, C.; Bai, X.; Liang, J.; Song, T.; Dong, L.; Jin, Y.; Qu, J. Optimization of Siderophore Production by Bacillus Sp. PZ-1 and Its Potential Enhancement of Phytoextration of PB from Soil. *J. Microbiol. Biotechnol.* **2017**, *27*, 1500, doi:10.4014/jmb.1705.05021.
250. Sasirekha, B.; Srividya, S. Siderophore Production by Pseudomonas Aeruginosa FP6, a Biocontrol Strain for Rhizoctonia Solani and Colletotrichum Gloeosporioides Causing Diseases in Chilli. *Agric. Nat. Resour.* **2016**, *50*, 250–256, doi:10.1016/j.anres.2016.02.003.
251. Balado, M.; Lages, M.A.; Fuentes-Monteverde, J.C.; Martínez-Matamoros, D.; Rodríguez, J.; Jiménez, C.; Lemos, M.L. The Siderophore Piscibactin Is a Relevant Virulence Factor for Vibrio Anguillarum Favored at Low Temperatures. *Front. Microbiol.* **2018**, *9*, 1–16, doi:10.3389/fmicb.2018.01766.
252. Venkat Kumar, S.; Menon, S.; Agarwal, H.; Gopalakrishnan, D. Characterization and Optimization of Bacterium Isolated from Soil Samples for the Production of Siderophores. *Resour. Technol.* **2017**, *3*, 434–439, doi:10.1016/j.reffit.2017.04.004.
253. Kalyan, Reddy Kiran; S, M.; D, K.; D, J. Isolation, Screening, Characterization, and Optimization of Bacterium Isolated from Calcareous Soils for Siderophore Production. **2022**, 1–28.
254. Aziz, O.A.A.; Helal, G.A.; Galal, Y.G.M.; Kader, A.; Rofaida, S. Fungal Siderophores Production in Vitro as Affected by Some Abiotic Factors. *Int. J. Curr. Microbiol. Appl. Sci.* **2016**, *5*, 210–222, doi:10.20546/ijcmas.2016.506.025.
255. Singh, A.; Mishra, A.K. Influence of Various Levels of Iron and Other Abiotic Factors on Siderophorogenesis in Paddy Field Cyanobacterium Anabaena Oryzae. *Appl. Biochem. Biotechnol.* **2015**, *176*, 372–386, doi:10.1007/s12010-015-1581-7.
256. Fazary, A.E.; Al-Shihri, A.S.; Alfaifi, M.Y.; Saleh, K.A.; Alshehri, M.A.; Elbehairi, S.E.I.; Ju, Y.H. Microbial Production of Four Biodegradable Siderophores under Submerged Fermentation. *Int. J. Biol. Macromol.* **2016**, *88*, 527–541, doi:10.1016/j.ijbiomac.2016.03.011.
257. Sinha, A.K.; Parli Venkateswaran, B.; Tripathy, S.C.; Sarkar, A.; Prabhakaran, S. Effects of Growth Conditions on Siderophore Producing Bacteria and Siderophore Production from Indian Ocean Sector of Southern Ocean. *J. Basic Microbiol.* **2019**, *59*, 412–424, doi:10.1002/jobm.201800537.
258. Johnson, D.B.; Kanao, T.; Hedrich, S. Redox Transformations of Iron at Extremely Low PH: Fundamental and Applied Aspects. *Front. Microbiol.* **2012**, *3*, 1–13, doi:10.3389/fmicb.2012.00096.
259. Tailor, A.J.; Joshi, B.H. CHARACTERIZATION AND OPTIMIZATION OF SIDEROPHORE PRODUCTION FROM Pseudomonas Fluorescens STRAIN ISOLATED FROM SUGARCANE RHIZOSPHERE. *J. Environ. Res. Dev.* **2012**, *6*, 688–694.
260. Prabhu, G.N.; Bindu, P. Optimization of Process Parameters for Siderophore Production under Solid State Fermentation Using Polystyrene Beads as Inert Support. *J. Sci. Ind. Res. (India).* **2016**, *75*, 621–625.
261. Valdebenito, M.; Crumbliss, A.L.; Winkelmann, G.; Hantke, K. Environmental Factors Influence the Production of Enterobactin, Salmochelin, Aerobactin, and Yersiniabactin in Escherichia Coli Strain Nissle 1917. *Int. J. Med. Microbiol.* **2006**, *296*, 513–520,

doi:10.1016/j.ijmm.2006.06.003.
262. Virpiranta, H.; Banasik, M.; Taskila, S.; Leiviskä, T.; Halttu, M.; Sotaniemi, V.H.; Tanskanen, J. Isolation of Efficient Metal-Binding Bacteria from Boreal Peat Soils and Development of Microbial Biosorbents for Improved Nickel Scavenging. *Water (Switzerland)* **2020**, *12*, doi:10.3390/w12072000.
263. Sayyed, R.Z.; Seifi, S.; Patel, P.R.; Shaikh, S.S.; Jadhav, H.P.; Enshasy, H. El Siderophore Production in Groundnut Rhizosphere Isolate, Achromobacter Sp. RZS2 Influenced by Physicochemical Factors and Metal Ions. *Environ. Sustain. 2019 22* **2019**, *2*, 117–124, doi:10.1007/S42398-019-00070-4.
264. Ferreira, C.M.H.; Vilas-Boas, Â.; Sousa, C.A.; Soares, H.M.V.M.; Soares, E. V. Comparison of Five Bacterial Strains Producing Siderophores with Ability to Chelate Iron under Alkaline Conditions. *AMB Express* **2019**, *9*, doi:10.1186/s13568-019-0796-3.
265. Gaonkar, T.; Bhosle, S. Effect of Metals on a Siderophore Producing Bacterial Isolate and Its Implications on Microbial Assisted Bioremediation of Metal Contaminated Soils. *Chemosphere* **2013**, *93*, 1835–1843, doi:10.1016/j.chemosphere.2013.06.036.
266. Hussein, K.A.; Joo, J.H. Zinc Ions Affect Siderophore Production by Fungi Isolated from the Panax Ginseng Rhizosphere. *J. Microbiol. Biotechnol.* **2019**, *29*, 105–113, doi:10.4014/jmb.1712.12026.
267. Patel, P.R.; Shaikh, S.S.; Sayyed, R. Process Optimization for Siderophore Production and Evaluation of Bioefficacy and Root Colonizing Potential of Alcaligenes Sp . *Adv. Bio Med. Sci.* **2016**.
268. Yu, S.; Teng, C.; Bai, X.; Liang, J.; Song, T.; Dong, L.; Jin, Y.; Qu, J. Optimization of Siderophore Production by Bacillus Sp. PZ-1 and Its Potential Enhancement of Phytoextration of PB from Soil. *J. Microbiol. Biotechnol.* **2017**, *27*, 1500, doi:10.4014/jmb.1705.05021.
269. Colombowala, A.; Aruna, K. Studies on Optimization of Siderophore Production By Pseudomonas Aeruginosa Azar 11 Isolated From Aquatic Soil and Its Antibacterial Activity. **2018**, *8*, 714–731.
270. Jalal, M.A.F.; Van Der Helm, D. Isolation and Spectroscopic Identification of Fungal Siderophores. *Handb. Microb. Iron Chelates* **2017**, 235–270, doi:10.1201/9780203712368.
271. Yadav, G.; Sharma, N.; Goel, A.; Varma, A.; Mishra, A.; Choudhary, S.L.K.D.K. Trichoderma Mediated Metal Chelator and Its Role in Solanum Melongena Growth Under Heavy Metals. *J. Plant Growth Regul.* **2023**, doi:10.1007/s00344-023-11072-2.
272. Katif, C.; Chilczuk, T.; Sabour, B.; Belattmania, Z.; Hilmi, A.; Niedermeyer, T.H.J.; Barakate, M. Isolation and Structure Elucidation of Desferrioxamine b and the New Desferrioxamine B2 Antibiotics from a Brown Marine Macroalga Carpodesmia Tamariscifolia Associated Streptomyces Isolate. *Biointerface Res. Appl. Chem.* **2022**, *12*, 5647–5662, doi:10.33263/BRIAC124.56475662.
273. World Health Organization WHO Model List of Essential Medicines - 23nd List. *World Heal. Organ. Geneva.* **2023**, 1–67.
274. Winkelmann, G.; Schmid, D.G.; Nicholson, G.; Jung, G.; Colquhoun, D.J. Bisucaberin - A Dihydroxamate Siderophore Isolated from Vibrio Salmonicida, an Important Pathogen of Farmed Atlantic Salmon (Salmo Salar). *BioMetals* **2002**, *15*, 153–160, doi:10.1023/A:1015206419613.
275. Asad, S.A.; Farooq, M.; Afzal, A.; West, H. Integrated Phytobial Heavy Metal Remediation Strategies for a Sustainable Clean Environment - A Review. *Chemosphere* **2019**, *217*, 925–941, doi:10.1016/j.chemosphere.2018.11.021.
276. *Role of Microbial Communities for Sustainability*; Seneviratne, G., Zavahir, J.S., Eds.;

Microorganisms for Sustainability; Springer Singapore: Singapore, 2021; Vol. 29; ISBN 978-981-15-9911-8.
277. Tamariz-Angeles, C.; Huamán, G.D.; Palacios-Robles, E.; Olivera-Gonzales, P.; Castañeda-Barreto, A. Characterization of Siderophore-Producing Microorganisms Associated to Plants from High-Andean Heavy Metal Polluted Soil from Callejón de Huaylas (Ancash, Perú). *Microbiol. Res.* **2021**, *250*, doi:10.1016/j.micres.2021.126811.
278. Timofeeva, A.M.; Galyamova, M.R.; Sedykh, S.E. Bacterial Siderophores: Classification, Biosynthesis, Perspectives of Use in Agriculture. *Plants* **2022**, *11*, 3065, doi:10.3390/plants11223065.
279. Schijf, J.; Christenson, E.A.; Potter, K.J. Different Binding Modes of Cu and Pb vs. Cd, Ni, and Zn with the Trihydroxamate Siderophore Desferrioxamine B at Seawater Ionic Strength. *Mar. Chem.* **2015**, *173*, 40–51, doi:10.1016/j.marchem.2015.02.014.
280. Wiche, O.; Tischler, D.; Fauser, C.; Lodemann, J.; Heilmeier, H. Effects of Citric Acid and the Siderophore Desferrioxamine B (DFO-B) on the Mobility of Germanium and Rare Earth Elements in Soil and Uptake in Phalaris Arundinacea. *Int. J. Phytoremediation* **2017**, *19*, 746–754, doi:10.1080/15226514.2017.1284752.
281. Retamal-Morales, G.; Mehnert, M.; Schwabe, R.; Tischler, D.; Zapata, C.; Chávez, R.; Schlömann, M.; Levicán, G. Detection of Arsenic-Binding Siderophores in Arsenic-Tolerating Actinobacteria by a Modified CAS Assay. *Ecotoxicol. Environ. Saf.* **2018**, *157*, 176–181, doi:10.1016/j.ecoenv.2018.03.087.
282. Yi, Y.; Hou, Z.; Shi, Y.; Zhang, C.; Zhu, L.; Sun, X.; Zhang, R.; Wang, Z. Pseudomonas Fluorescens RB5 as a Biocontrol Strain for Controlling Wheat Sheath Blight Caused by Rhizoctonia Cerealis. *Agronomy* **2023**, *13*, 1986, doi:10.3390/agronomy13081986.
283. Roslan, M.A.M.; Zulkifli, N.N.; Sobri, Z.M.; Zuan, A.T.K.; Cheak, S.C.; Rahman, N.A.A. Seed Biopriming with P- A Nd K-Solubilizing Enterobacter Hormaechei Sp. Improves the Early Vegetative Growth and the P and K Uptake of Okra (Abelmoschus Esculentus) Seedling. *PLoS One* **2020**, *15*, 1–21, doi:10.1371/journal.pone.0232860.
284. Maduraimuthu, V.; Ranishree, J.K.; Gopalakrishnan, R.M.; Ayyadurai, B.; Raja, R.; Heese, K. Antioxidant Activities of Photoinduced Phycogenic Silver Nanoparticles and Their Potential Applications. *Antioxidants* **2023**, *12*, 1298, doi:10.3390/antiox12061298.
285. Shafiq, A.; Deshmukh, A.R.; AbouAitah, K.; Kim, B.-S. Green Synthesis of Controlled Shape Silver Nanostructures and Their Peroxidase, Catalytic Degradation, and Antibacterial Activity. *J. Funct. Biomater.* **2023**, *14*, 325, doi:10.3390/jfb14060325.
286. Soltani Nejad, M.; Samandari Najafabadi, N.; Aghighi, S.; Zargar, M.; Stybayev, G.; Baitelenova, A.; Kipshakbayeva, G. Application of Biosynthesized Silver Nanoparticles from Oak Fruit Exudates against Pectobacterium Carotovorum Subsp. Carotovorum Causing Postharvest Soft Rot Disease in Vegetables. *Agronomy* **2023**, *13*, 1624, doi:10.3390/agronomy13061624.
287. Leyu, A.M.; Debebe, S.E.; Bachheti, A.; Rawat, Y.S.; Bachheti, R.K. Green Synthesis of Gold and Silver Nanoparticles Using Invasive Alien Plant Parthenium Hysterophorus and Their Antimicrobial and Antioxidant Activities. *Sustainability* **2023**, *15*, 9456, doi:10.3390/su15129456.
288. Qanash, H.; Bazaid, A.S.; Binsaleh, N.K.; Alharbi, B.; Alshammari, N.; Qahl, S.H.; Alhuthali, H.M.; Bagher, A.A. Phytochemical Characterization of Saudi Mint and Its Mediating Effect on the Production of Silver Nanoparticles and Its Antimicrobial and Antioxidant Activities. *Plants* **2023**, *12*, 2177, doi:10.3390/PLANTS12112177/S1.
289. Alfarraj, N.S.; Tarroum, M.; Al-Qurainy, F.; Nadeem, M.; Khan, S.; Salih, A.M.; Shaikhaldein, H.O.; Al-Hashimi, A.; Alansi, S.; Perveen, K. Biosynthesis of Silver

Nanoparticles and Exploring Their Potential of Reducing the Contamination of the In Vitro Culture Media and Inducing the Callus Growth of Rumex Nervosus Explants. *Molecules* **2023**, *28*, 3666, doi:10.3390/molecules28093666.
290. Mustapha, T.; Ithnin, N.R.; Othman, H.; Abu Hasan, Z.-'Iffah; Misni, N. Bio-Fabrication of Silver Nanoparticles Using Citrus Aurantifolia Fruit Peel Extract (CAFPE) and the Role of Plant Extract in the Synthesis. *Plants* **2023**, *12*, 1648, doi:10.3390/plants12081648.
291. Rehman, I.; Gondal, H.Y.; Zamir, R.; Al-Hussain, S.A.; Batool, F.; Irfan, A.; Noreen, S.; Roheen, T.; Nisar, M.; Zaki, M.E.A. Green Synthesis: The Antibacterial and Photocatalytic Potential of Silver Nanoparticles Using Extract of Teucrium Stocksianum. *Nanomaterials* **2023**, *13*, 1343, doi:10.3390/nano13081343.
292. Hassan Afandy, H.; Sabir, D.K.; Aziz, S.B. Antibacterial Activity of the Green Synthesized Plasmonic Silver Nanoparticles with Crystalline Structure against Gram-Positive and Gram-Negative Bacteria. *Nanomaterials* **2023**, *13*, 1327, doi:10.3390/nano13081327.
293. Sumra, A.A.; Zain, M.; Saleem, T.; Yasin, G.; Azhar, M.F.; Zaman, Q.U.; Budhram-Mahadeo, V.; Ali, H.M. Biogenic Synthesis, Characterization, and In Vitro Biological Evaluation of Silver Nanoparticles Using Cleome Brachycarpa. *Plants* **2023**, *12*, 1578, doi:10.3390/plants12071578.
294. Dos Santos Ramos, M.A.; Da Silva, P.B.; Spósito, L.; De Toledo, L.G.; Bonifácio, B. vidal; Rodero, C.F.; Dos Santos, K.C.; Chorilli, M.; Bauab, T.M. Nanotechnology-Based Drug Delivery Systems for Control of Microbial Biofilms: A Review. *Int. J. Nanomedicine* 2018, *13*, 1179–1213.
295. Cremin, K.; Jones, B.A.; Teahan, J.; Meloni, G.N.; Perry, D.; Zerfass, C.; Asally, M.; Soyer, O.S.; Unwin, P.R. Scanning Ion Conductance Microscopy Reveals Differences in the Ionic Environments of Gram-Positive and Negative Bacteria. *Anal. Chem.* **2020**, *92*, 16024–16032, doi:10.1021/acs.analchem.0c03653.
296. Pajerski, W.; Ochonska, D.; Brzychczy-Wloch, M.; Indyka, P.; Jarosz, M.; Golda-Cepa, M.; Sojka, Z.; Kotarba, A. Attachment Efficiency of Gold Nanoparticles by Gram-Positive and Gram-Negative Bacterial Strains Governed by Surface Charges. *J. Nanoparticle Res.* **2019**, *21*, 186, doi:10.1007/s11051-019-4617-z.
297. Caudill, E.R.; Hernandez, R.T.; Johnson, K.P.; O'Rourke, J.T.; Zhu, L.; Haynes, C.L.; Feng, Z.V.; Pedersen, J.A. Wall Teichoic Acids Govern Cationic Gold Nanoparticle Interaction with Gram-Positive Bacterial Cell Walls. *Chem. Sci.* **2020**, *11*, 4106–4118, doi:10.1039/c9sc05436g.
298. Wang, H.; Lu, F.; Ma, C.; Ma, Y.; Zhang, M.; Wang, B.; Zhang, Y.; Liu, Y.; Huang, H.; Kang, Z. Carbon Dots with Positive Surface Charge from Tartaric Acid and M-Aminophenol for Selective Killing of Gram-Positive Bacteria. *J. Mater. Chem. B* **2021**, *9*, 125–130, doi:10.1039/d0tb02332a.
299. Yin, J.; Meng, Q.; Cheng, D.; Fu, J.; Luo, Q.; Liu, Y.; Yu, Z. Mechanisms of Bactericidal Action and Resistance of Polymyxins for Gram-Positive Bacteria. *Appl. Microbiol. Biotechnol.* 2020, *104*, 3771–3780.
300. Yin, I.X.; Zhang, J.; Zhao, I.S.; Mei, M.L.; Li, Q.; Chu, C.H. The Antibacterial Mechanism of Silver Nanoparticles and Its Application in Dentistry. *Int. J. Nanomedicine* **2020**, *Volume 15*, 2555–2562, doi:10.2147/IJN.S246764.
301. Nakamura, S.; Sato, M.; Sato, Y.; Ando, N.; Takayama, T.; Fujita, M.; Ishihara, M. Synthesis and Application of Silver Nanoparticles (Ag NPs) for the Prevention of Infection in Healthcare Workers. *Int. J. Mol. Sci.* **2019**, *20*, 3620, doi:10.3390/ijms20153620.
302. Zou, G.; Boyer, G.L. Synthesis and Properties of Different Metal Complexes of the

Siderophore Desferriferricrocin. *BioMetals* **2005**, *18*, 63–74, doi:10.1007/s10534-004-5786-4.
303. Fan, D.; Fang, Q. Siderophores for Medical Applications: Imaging, Sensors, and Therapeutics. *Int. J. Pharm.* **2021**, *597*, 120306, doi:10.1016/j.ijpharm.2021.120306.

LIST OF PUBLICATIONS

Research Papers Published

1. **Mounika Sarvepalli** and Narashimulu Korrapati. *Statistical optimisation of process parameters involved in siderophore production of marine bacterial isolate Marinobacter sp. SVU_3*. **Biomass Conversion and Biorefinery**, 2023, ISSN 2190-6823. https://doi.org/10.1007/s13399-023-04427-y **(SCIE; Impact Factor 4.0)**
2. **Mounika Sarvepalli**, Aditya Velidandi and Narashimulu Korrapati. *Optimization of siderophores production in three marine bacterial isolates along with their heavy metal chelation and seed germination potential determination*. **Microorganisms**, Volume 11, 2023, 2873. ISSN 2076-2607. https://doi.org/10.3390/microorganisms11122873. **(SCIE; Impact Factor 4.5)**
3. **Mounika Sarvepalli**, Aditya Velidandi, Arun Kumar Ramachandravarapu and Narasimhulu Korrapati. *Marine actinomycetes siderophores: Types, high throughput characterization techniques, applications, and their association with nanotechnology: A comprehensive review*. **Nano World Journal**, Volume 10(1), 2024, ISSN 2379-1101. https://doi.org/10.17756/nwj.2024-130 **(SCOPUS)**

Conference Proceedings Published

1. **Sarvepalli Mounika** and Narasimhulu Korrapati. *Isolation of Catecholate siderophore from novel marine bacterium Marinobacter sp. SVU3*. **AIJR Abstracts** (2021), 46.

Thesis

ORIGINALITY REPORT

16%	10%	12%	2%
SIMILARITY INDEX	INTERNET SOURCES	PUBLICATIONS	STUDENT PAPERS

PRIMARY SOURCES

1	dc.etsu.edu Internet Source	1%
2	link.springer.com Internet Source	1%
3	ouci.dntb.gov.ua Internet Source	1%
4	Gaurav Yadav, Neha Sharma, Arti Goel, Ajit Varma, Arti Mishra, S. L. Kothari, D. K. Choudhary. "Trichoderma Mediated Metal Chelator and Its Role in Solanum melongena Growth Under Heavy Metals", Journal of Plant Growth Regulation, 2023 Publication	<1%
5	www.nature.com Internet Source	<1%
6	digitalcommons.uri.edu Internet Source	<1%
7	Rahim Nosrati, Sadegh Dehghani, Bahareh Karimi, Meysam Yousefi et al. "Siderophore-based biosensors and nanosensors; new	<1%

approach on the development of diagnostic systems", Biosensors and Bioelectronics, 2018
Publication

8	Rima Kumari, Manjari Barsainya, Devendra Pratap Singh. "Biogenic synthesis of silver nanoparticle by using secondary metabolites from Pseudomonas aeruginosa DM1 and its anti-algal effect on Chlorella vulgaris and Chlorella pyrenoidosa", Environmental Science and Pollution Research, 2016 Publication	<1 %
9	Martinez, J.S.. "Marine amphiphilic siderophores: Marinobactin structure, uptake, and microbial partitioning", Journal of Inorganic Biochemistry, 200711 Publication	<1 %
10	assets.researchsquare.com Internet Source	<1 %
11	Liu, Ning, Fei Shang, Lijun Xi, and Ying Huang. "Tetroazolemycins A and B, Two New Oxazole-Thiazole Siderophores from Deep-Sea Streptomyces olivaceus FXJ8.012", Marine Drugs, 2013. Publication	<1 %
12	Yoshihide Matsuo, Kaneo Kanoh, Jae-Hyuk Jang, Kyoko Adachi, Satoru Matsuda, Osamu Miki, Toshiaki Kato, Yoshikazu Shizuri. " Streptobactin, a Tricatechol-Type Siderophore	<1 %

from Marine-Derived sp. YM5-799 ", Journal of Natural Products, 2011
Publication

13	pubs.rsc.org Internet Source	<1 %
14	www.jmb.or.kr Internet Source	<1 %
15	Muhammad Atif Irshad, Rab Nawaz, Muhammad Zia ur Rehman, Muhammad Adrees et al. "Synthesis, characterization and advanced sustainable applications of titanium dioxide nanoparticles: A review", Ecotoxicology and Environmental Safety, 2021 Publication	<1 %
16	"Role of Microbial Communities for Sustainability", Springer Science and Business Media LLC, 2021 Publication	<1 %
17	Julia M. Gauglitz, Hongjun Zhou, Alison Butler. "A suite of citrate-derived siderophores from a marine Vibrio species isolated following the Deepwater Horizon oil spill", Journal of Inorganic Biochemistry, 2012 Publication	<1 %
18	"Microbial Processes for Synthesizing Nanomaterials", Springer Science and Business Media LLC, 2023 Publication	<1 %

19	aslo.org Internet Source	<1 %
20	www.researchsquare.com Internet Source	<1 %
21	Plant Growth Promoting Actinobacteria, 2016. Publication	<1 %
22	Prashant R. Dane, Shraddha P. Pawar, Raksha A. Kankariya, Bhushan L. Chaudhari. "Pyoverdin mediated sunlight induced green synthesis of silver nanoparticles", RSC Advances, 2016 Publication	<1 %
23	Sarah J. H. Hickford, Frithjof C. Küpper, Guangping Zhang, Carl J. Carrano, John W. Blunt, Alison Butler. " Petrobactin Sulfonate, a New Siderophore Produced by the Marine Bacterium ", Journal of Natural Products, 2004 Publication	<1 %
24	Michelle P. Kem, Hiroaki Naka, Akira Iinishi, Margo G. Haygood, Alison Butler. " Fatty Acid Hydrolysis of Acyl Marinobactin Siderophores by Acylases ", Biochemistry, 2015 Publication	<1 %
25	eldorado.tu-dortmund.de Internet Source	<1 %

26	Edelweiss Airam Rangel-Montoya, Carmen Sanjuana Delgado-Ramírez, Edgardo Sepulveda, Rufina Hernández-Martínez. "Biocontrol of Macrophomina phaseolina Using Bacillus amyloliquefaciens Strains in Cowpea (Vigna unguiculata L.)", Agronomy, 2022 Publication	<1 %
27	Ahmed, E., and S. J. M. Holmström. "Siderophores in environmental research: roles and applications : Siderophores in environmental research", Microbial Biotechnology, 2014. Publication	<1 %
28	www.ncbi.nlm.nih.gov Internet Source	<1 %
29	Wenfeng Wang, Zhiqi Qiu, Hongming Tan, Lixiang Cao. "Siderophore production by actinobacteria", BioMetals, 2014 Publication	<1 %
30	www.researchgate.net Internet Source	<1 %
31	reffit.tech Internet Source	<1 %
32	Arumugam, S.. " [^1^8F]Azadibenzocyclooctyne ([^1^8F]ADIBO): A biocompatible radioactive	<1 %

labeling synthon for peptides using catalyst free [3+2] cycloaddition", Bioorganic & Medicinal Chemistry Letters, 20111201
Publication

33	Morgan A. Wyatt, Chad W. Johnston, Nathan A. Magarvey. "Gold nanoparticle formation via microbial metallophore chemistries", Journal of Nanoparticle Research, 2014 Publication	<1 %
34	www.science.gov Internet Source	<1 %
35	gyan.iitg.ernet.in Internet Source	<1 %
36	worldwidescience.org Internet Source	<1 %
37	Hassan Barakat, Kamal A. Qureshi, Abdullah S. Alsohim, Medhat Rehan. "The Purified Siderophore from Streptomyces tricolor HM10 Accelerates Recovery from Iron-Deficiency-Induced Anemia in Rats", Molecules, 2022 Publication	<1 %
38	S. Sharath, S. Triveni, Y. Nagaraju, P. C. Latha, B. Vidyasagar. "The Role of Phyllosphere Bacteria in Improving Cotton Growth and Yield Under Drought Conditions", Frontiers in Agronomy, 2021 Publication	<1 %

39	www.frontiersin.org Internet Source	<1%
40	Submitted to Indian Institute of Technology Guwahati Student Paper	<1%
41	Manivasagan, Panchanathan, and Junghwan Oh. "Production of a Novel Fucoidanase for the Green Synthesis of Gold Nanoparticles by Streptomyces sp. and Its Cytotoxic Effect on HeLa Cells", Marine Drugs, 2015. Publication	<1%
42	Submitted to North Maharashtra University, Jalgaon Student Paper	<1%
43	Tomáš Řezanka, Andrea Palyzová, Helena Faltýsková, Karel Sigler. "Siderophores: Amazing Metabolites of Microorganisms", Elsevier BV, 2019 Publication	<1%
44	dspace.bracu.ac.bd Internet Source	<1%
45	Alok K. Sinha, Bhaskar Parli Venkateswaran, Sarat C. Tripathy, Amit Sarkar, Sabu Prabhakaran. "Effects of growth conditions on siderophore producing bacteria and siderophore production from Indian Ocean	<1%

sector of Southern Ocean", Journal of Basic Microbiology, 2019
Publication

46	Azmi Khan, Pratika Singh, Amrita Srivastava. "Synthesis, nature and utility of universal iron chelator – Siderophore: A review", Microbiological Research, 2017 Publication	<1 %
47	d-nb.info Internet Source	<1 %
48	Alireza Nezami, Sadegh Dehghani, Rahim Nosrati, Negar Eskandari, Seyed Mohammad Taghdisi, Gholamreza Karimi. "Nanomaterial-based biosensors and immunosensors for quantitative determination of cardiac troponins", Journal of Pharmaceutical and Biomedical Analysis, 2018 Publication	<1 %
49	Euiyeon Lee, Hyunjin Jeon, Minhyeong Lee, Jeahee Ryu, Chungwon Kang, Soyoun Kim, Junghyun Jung, Youngeun Kwon. "Molecular origin of AuNPs-induced cytotoxicity and mechanistic study", Scientific Reports, 2019 Publication	<1 %
50	irgu.unigoa.ac.in Internet Source	<1 %
51	shankargargh.org Internet Source	

<1%

52 F Le Floch, M.T Tena, A Ríos, M Valcárcel. "Supercritical fluid extraction of phenol compounds from olive leaves", Talanta, 1998 <1%
Publication

53 Lauren E. Manck, Jiwoon Park, Benjamin J. Tully, Alfonso M. Poire et al. "Petrobactin, a siderophore produced by Alteromonas, mediates community iron acquisition in the global ocean", The ISME Journal, 2021 <1%
Publication

54 Rozhon, W.M.. "Isolation and characterization of pHW15, a small cryptic plasmid from Rahnella genomospecies 2", Plasmid, 200611 <1%
Publication

55 Su Hyeon Park, Joong Kyun Kim. "Characterisation of key components of biofertiliser produced from mackerel wastewater and commercialisation feasibility analysis of the biofertiliser production process for wastewater valorisation", Sustainable Chemistry and Pharmacy, 2023 <1%
Publication

56 Venkat Kumar S., Soumya Menon, Happy Agarwal, Divya Gopalakrishnan. "Characterization and optimization of <1%

bacterium isolated from soil samples for the production of siderophores", Resource-Efficient Technologies, 2017
Publication

57	orca.cf.ac.uk Internet Source	<1 %
58	www.spandidos-publications.com Internet Source	<1 %
59	Abinash Giri, Pratima Khandayataray, Meesala Krishna Murthy, Dibyaranjan Samal. "Biochemical and molecular identification of lipolytic bacteria isolated from beverage industrial wastewater and optimization of lipase-secreting bacteria", Biomass Conversion and Biorefinery, 2021 Publication	<1 %
60	Haniyeh Daneshafruz, Hossein Barani, Hassan Sheibani. "Palladium Nanoparticles-Decorated β-Cyclodextrin–Cyanoguanidine Modified Graphene Oxide: A Heterogeneous Nanocatalyst for Suzuki–Miyaura Coupling and Reduction of 4-Nitrophenol Reactions in Aqueous Media", Journal of Inorganic and Organometallic Polymers and Materials, 2022 Publication	<1 %
61	academicjournals.org Internet Source	<1 %

62	A. Johnsson. "Leaching of spent nuclear fuel in the presence of siderophores", Journal of Radioanalytical and Nuclear Chemistry, 02/2009 Publication	<1 %
63	Alok K. Sinha, Bhaskar V. Parli. "Siderophore production by bacteria isolated from mangrove sediments: A microcosm study", Journal of Experimental Marine Biology and Ecology, 2020 Publication	<1 %
64	Submitted to Clemson University Student Paper	<1 %
65	Fan Zhang, Kenneth Barns, F. Michael Hoffmann, Doug R. Braun, David R. Andes, Tim S. Bugni. " Thalassosamide, a Siderophore Discovered from the Marine-Derived Bacterium ", Journal of Natural Products, 2017 Publication	<1 %
66	Kumari, M.. "Production of schizophyllan using Schizophyllum commune NRCM", Bioresource Technology, 200803 Publication	<1 %
67	Microbial Inoculants in Sustainable Agricultural Productivity, 2016. Publication	<1 %

68	Shaikh, S. S., S. J. Wani, and R. Z. Sayyed. "Statistical-based optimization and scale-up of siderophore production process on laboratory bioreactor", 3 Biotech, 2016. Publication	<1 %
69	Sharda Sahu, ANIL Prakash. "Berberine as siderophore from Talaromyces trachyspermus: augmentation and characterization”.", Cold Spring Harbor Laboratory, 2021 Publication	<1 %
70	cwejournal.org Internet Source	<1 %
71	studentsrepo.um.edu.my Internet Source	<1 %
72	Bacteria in Agrobiology Crop Productivity, 2013. Publication	<1 %
73	Carmen Tamariz-Angeles, Gabriela D. Huamán, Edson Palacios-Robles, Percy Olivera-Gonzales, Alberto Castañeda-Barreto. "Characterization of siderophore-producing microorganisms associated to plants from high-Andean heavy metal polluted soil from Callejón de Huaylas (Ancash, Perú)", Microbiological Research, 2021 Publication	<1 %

74	Submitted to Napier University Student Paper	<1%
75	Hannah K. Zane, Alison Butler. " Isolation, Structure Elucidation, and Iron-Binding Properties of Lystabactins, Siderophores Isolated from a Marine sp ", Journal of Natural Products, 2013 Publication	<1%
76	Srinivas Chowdappa, Shubha Jagannath, Narasimhamurthy Konappa, Arakere C. Udayashankar, Sudisha Jogaiah. "Detection and Characterization of Antibacterial Siderophores Secreted by Endophytic Fungi from Cymbidium aloifolium", Biomolecules, 2020 Publication	<1%
77	Swapan Kr Ghosh, Tanmay Bera, Ananda M. Chakrabarty. "Microbial siderophore – A boon to agricultural sciences", Biological Control, 2020 Publication	<1%
78	journals.plos.org Internet Source	<1%
79	Ringo Schwabe, Christoph Helmut Rudi Senges, Julia Elisabeth Bandow, Thomas Heine et al. "Data on metal-chelating, -immobilisation and biosorption properties by	<1%

Gordonia rubripertincta CWB2 in dependency on rare earth adaptation", Data in Brief, 2020
Publication

80	Swapnil Dudhwadkar, Abhaysinh Salunkhe, Shalini A. Tandon, Nitin Goyal. "Passive inactivation of Candida parapsilosis in model indoor bioaerosol study using the visible photocatalytic activity of synthesized nanocomposite", Chemical Papers, 2023 Publication	<1 %
81	ukogplc.com Internet Source	<1 %
82	Aditya Velidandi, Mounika Sarvepalli, Ninian Prem Prashanth Pabbathi, Rama Raju Baadhe. "Biogenic synthesis of novel platinum-palladium bimetallic nanoparticles from aqueous Annona muricata leaf extract for catalytic activity", 3 Biotech, 2021 Publication	<1 %
83	Andrew W. Robertson, Nicholas G. McCarville, Logan W. MacIntyre, Hebelin Correa et al. " Isolation of Imaqobactin, an Amphiphilic Siderophore from the Arctic Marine Bacterium Species RKJM285 ", Journal of Natural Products, 2018 Publication	<1 %
84	G. Praveen Kumar, N. Kishore, E. Leo Daniel Amalraj, S. K. Mir Hassan Ahmed, Abdul	<1 %

Rasul, Suseelendra Desai. "Evaluation of fluorescent Pseudomonas spp. with single and multiple PGPR traits for plant growth promotion of sorghum in combination with AM fungi", Plant Growth Regulation, 2012
Publication

---

85 Guangping Zhang, Shady A. Amin, Frithjof C. Küpper, Pamela D. Holt, Carl J. Carrano, Alison Butler. "Ferric Stability Constants of Representative Marine Siderophores: Marinobactins, Aquachelins, and Petrobactin", Inorganic Chemistry, 2009 <1%
Publication

---

86 Maumita Saha, Subhasis Sarkar, Biplab Sarkar, Bipin Kumar Sharma, Surajit Bhattacharjee, Prosun Tribedi. "Microbial siderophores and their potential applications: a review", Environmental Science and Pollution Research, 2015 <1%
Publication

---

87 Mouhcine Hayani, Said Byiadi, Tariq Benabbouha, Mohammed reda kachmar, Mohammed Chafi, Aziz Aboulmouhajir, et Zair touriya. " Valorization of extracts from Morocco: phytochemistry and antibacterial activity. ", Plant Biosystems - An International Journal Dealing with all Aspects of Plant Biology, 2023 <1%
Publication

88	Nuengchamnong, N.. "Quantitative determination of 1-deoxynojirimycin in mulberry leaves using liquid chromatography-tandem mass spectrometry", Journal of Pharmaceutical and Biomedical Analysis, 20070815 Publication	<1 %
89	Submitted to University of Stellenbosch, South Africa Student Paper	<1 %
90	japsonline.com Internet Source	<1 %
91	patents.justia.com Internet Source	<1 %
92	www.jove.com Internet Source	<1 %
93	D MOU, H CHEN, D DU, C MAO, J WAN, H XU, X YANG. "Hydrogel-thickened nanoemulsion system for topical delivery of lipophilic drugs", International Journal of Pharmaceutics, 2008 Publication	<1 %
94	Submitted to Imperial College of Science, Technology and Medicine Student Paper	<1 %
95	Najwa Ejje, Cho Zin Soe, Jiesi Gu, Rachel Codd. "The variable hydroxamic acid siderophore	<1 %

metabolome of the marine actinomycete Salinispora tropica CNB-440", Metallomics, 2013
Publication

96	Subramani, R.. "Diversity and antifungal activity of marine actinomycetes", Journal of Biotechnology, 200810 Publication	<1 %
97	Xiurong Hou, Huashan Wang, Yuting Shi, Zhouyao Yue. "Recent advances of antibacterial starch-based materials", Carbohydrate Polymers, 2022 Publication	<1 %
98	downloads.hindawi.com Internet Source	<1 %
99	www.scielo.br Internet Source	<1 %
100	www.tandfonline.com Internet Source	<1 %
101	www.theses.fr Internet Source	<1 %
102	"Microbial Biotechnology", Springer Science and Business Media LLC, 2017 Publication	<1 %
103	Govarthanan Muthusamy, Loganathan Praburaman, Selvankumar Thangasamy, Kim	<1 %

Jong-Hoon et al. "Sunroot mediated synthesis and characterization of silver nanoparticles and evaluation of its antibacterial and rat splenocyte cytotoxic effects", International Journal of Nanomedicine, 2015
Publication

---

104 Guofeng Xu, Jennifer S. Martinez, John T. Groves, Alison Butler. "Membrane Affinity of the Amphiphilic Marinobactin Siderophores", Journal of the American Chemical Society, 2002 <1 %
Publication

---

105 Hailong Sun, Chao Liu, Yingwu Yao. "Degradation of Azo Dyes Using Natural Pyrite as Fenton-Like Reaction Catalyst", Environmental Engineering Science, 2021 <1 %
Publication

---

106 Martinez, J. S., M. G. Haygood, and Alison Butler. "Identification of a natural desferrioxamine siderophore produced by a marine bacterium", Limnology and Oceanography, 2001. <1 %
Publication

---

107 Mehta, P.D.. "2-Azetidinone - A new profile of various pharmacological activities", European Journal of Medicinal Chemistry, 201012 <1 %
Publication

108	Vanessa V. Homann, Moriah Sandy, J. Andy Tincu, Alexis S. Templeton, Bradley M. Tebo, Alison Butler. " Loihichelins A–F, a Suite of Amphiphilic Siderophores Produced by the Marine Bacterium LOB-5 ", Journal of Natural Products, 2009 Publication	<1 %
109	aem.asm.org Internet Source	<1 %
110	csusm-dspace.calstate.edu Internet Source	<1 %
111	data.epo.org Internet Source	<1 %
112	mdpi-res.com Internet Source	<1 %
113	uwspace.uwaterloo.ca Internet Source	<1 %
114	A. P. Paiva. "REVIEW OF RECENT SOLVENT EXTRACTION STUDIES FOR RECOVERY OF SILVER FROM AQUEOUS SOLUTIONS", Solvent Extraction and Ion Exchange, 2000 Publication	<1 %
115	HEA-JEUNG WHANG. "PHENOLIC COMPOUNDS IN THE FLESH OF KOREAN APPLE CULTIVAR, BUSA", Journal of Food Biochemistry, 12/2002	<1 %

	Publication	
116	Yasuhiro Takehana, Maya Umekita, Masaki Hatano, Chiaki Kato, Ryuichi Sawa, Masayuki Igarashi. "Fradiamine A, a new siderophore from the deep-sea actinomycete Streptomyces fradiae MM456M-mF7", The Journal of Antibiotics, 2017 Publication	<1 %
117	acikerisim.comu.edu.tr Internet Source	<1 %
118	docplayer.com.br Internet Source	<1 %
119	ijcns.aizeonpublishers.net Internet Source	<1 %
120	publishup.uni-potsdam.de Internet Source	<1 %
121	www.unboundmedicine.com Internet Source	<1 %
122	zsp.com.pk Internet Source	<1 %
123	"Marine Pollution and Microbial Remediation", Springer Science and Business Media LLC, 2017 Publication	<1 %
124	Jiankun QIE. "Site-directed PEGylations of Thymosin α 1 Analogs and Evaluation of Their	<1 %

Immunoactivity", Chinese Journal of Chemistry, 04/2009
Publication

125	Mingxia Yang, Jun Zhang, Qiting Liang, Guanxin Pan, Jiachang Zhao, Miao Cui, Xinqing Zhao, Qizhong Zhang, Delin Xu. "Antagonistic activity of marine Streptomyces sp. S073 on pathogenic Vibrio parahaemolyticus", Fisheries Science, 2019 Publication	<1 %
126	arrow.tudublin.ie Internet Source	<1 %
127	core.ac.uk Internet Source	<1 %
128	envsaf.alljournals.cn Internet Source	<1 %
129	fppn.biomedcentral.com Internet Source	<1 %
130	umpir.ump.edu.my Internet Source	<1 %
131	www.i-scholar.in Internet Source	<1 %
132	"Advanced Functional Materials from Nanopolysaccharides", Springer Science and Business Media LLC, 2019 Publication	<1 %

133	"Nano-Strategies for Addressing Antimicrobial Resistance", Springer Science and Business Media LLC, 2022 Publication	<1 %
134	Bindhumol Ismail, Kesavan Madhavan Nampoothiri. "Production, purification and structural characterization of an exopolysaccharide produced by a probiotic Lactobacillus plantarum MTCC 9510", Archives of Microbiology, 2010 Publication	<1 %
135	H. Malissa. "Über die Verwendung von disubstituierten Dithiocarbamaten in der Mikroanalyse. I", Mikrochemie vereinigt mit Microchimica Acta, 03/1952 Publication	<1 %
136	Hakan Eriksson. "Steroids in Germfree and Conventional Rats. Metabolites of [4-14C]Pregnenolone and [4-14C]Corticosterone in Urine and Faeces from Male Rats", European Journal of Biochemistry, 1/1971 Publication	<1 %
137	J. C. Wataha, C. T. Hanks, R. G. Craig. "In Vitro effect of metal ions on cellular metabolism and the correlation between these effects and the uptake of the ions", Journal of Biomedical Materials Research, 1994 Publication	<1 %

138	Ouddane, Baghdad, Ghiasse Abbasse, Jalal Halwani, and Jean Claude Fischer. "Determination of metal partitioning in porewater extracted from the Seine River Estuary sediment (France)Presented at the 5th International Symposium on Speciation of Elements in Biological, Environmental and Toxicological Sciences, AlmuÃ±Ã©car (Granada), Spain, 13â€“16th September 2003.", Journal of Environmental Monitoring, 2004. Publication	<1 %
139	Patrick, Graham L.. "An Introduction to Medicinal Chemistry", An Introduction to Medicinal Chemistry, 2023 Publication	<1 %
140	Slawinski, J.. "Synthesis of a new series of 4-chloro-2-mercapto-5-methylbenzenesulfonamide derivatives with potential antitumor activity", European Journal of Medicinal Chemistry, 200402 Publication	<1 %
141	Vedanjali Gogineni, Mark T. Hamann. "Marine natural product peptides with therapeutic potential: Chemistry, biosynthesis, and pharmacology", Biochimica et Biophysica Acta (BBA) - General Subjects, 2018 Publication	<1 %

142	Watschke, . "Turfgrass Diseases and Their Management", Managing Turfgrass Pests Second Edition, 2013. Publication	<1 %
143	Yun Suk Huh, Sang Jun Jeon, Eun Zoo Lee, Ho Seok Park, Won Hi Hong. "Microfluidic extraction using two phase laminar flow for chemical and biological applications", Korean Journal of Chemical Engineering, 2011 Publication	<1 %
144	docplayer.net Internet Source	<1 %
145	escholarship.org Internet Source	<1 %
146	impressions.manipal.edu Internet Source	<1 %
147	libweb.kpfu.ru Internet Source	<1 %
148	ms2010.fc.ul.pt Internet Source	<1 %
149	onlinelibrary.wiley.com Internet Source	<1 %
150	patents.google.com Internet Source	<1 %
151	pdffox.com Internet Source	

		<1 %
152	pubs.sciepub.com Internet Source	<1 %
153	pureadmin.uhi.ac.uk Internet Source	<1 %
154	repositorio.unesp.br Internet Source	<1 %
155	www.ijabe.org Internet Source	<1 %
156	www.whoi.edu Internet Source	<1 %
157	A. Braud, M. Hannauer, G. L. A. Mislin, I. J. Schalk. "The Pseudomonas aeruginosa Pyochelin-Iron Uptake Pathway and Its Metal Specificity", Journal of Bacteriology, 2009 Publication	<1 %
158	Khabbaz, S.E., L. Zhang, L.A. Cáceres, M. Sumarah, A. Wang, and P.A. Abbasi. "Characterisation of antagonistic Bacillus and Pseudomonas strains for biocontrol potential and suppression of damping-off and root rot diseases : Biocontrol potential of rhizobacterial strains", Annals of Applied Biology, 2015. Publication	<1 %

159 Nguyen Ngoc Lan, Vu Van Dzung, Nguyen Thi Kim Lien, Nguyen Kim Thoa, Do Huu Nghi, Nguyen Huy Hoang. "Isolation and identification of indole acetic acid producing bacteria from the coasts of Ben Tre and Tra Vinh Provinces", ACADEMIA JOURNAL OF BIOLOGY, 2019 <1%
Publication

160 A. Velidandi, N. P. P. Pabbathi, S. Dahariya, S. Kagithoju, R. R. Baadhe. "Bio-fabrication of silver-silver chloride nanoparticles using Annona muricata leaf extract: characterization, biological, dye degradation and eco-toxicity studies", International Journal of Environmental Science and Technology, 2021 <1%
Publication

161 Malyarenko, Timofey V., Alla A. Kicha, Natalia V. Ivanchina, Anatoly I. Kalinovsky, Roman S. Popov, Olesya S. Vishchuk, and Valentin A. Stonik. "Asterosaponins from the Far Eastern starfish Leptasterias ochotensis and their anticancer activity", Steroids, 2014. <1%
Publication

162 Ohkawa, T.. "Rapid LC-TOFMS method for identification of binding sites of covalent acylglucuronide-albumin complexes", Journal <1%

of Pharmaceutical and Biomedical Analysis, 20030410
Publication

163 Venkatasamy Vignesh, Kulandaiyesu Felix Anbarasi, Sambhanthan Karthikeyeni, Ganesan Sathiyanarayanan et al. "A superficial phyto-assisted synthesis of silver nanoparticles and their assessment on hematological and biochemical parameters in Labeo rohita (Hamilton, 1822)", Colloids and Surfaces A: Physicochemical and Engineering Aspects, 2013 <1 %
Publication

Exclude quotes	Off	Exclude matches	Off
Exclude bibliography	Off		